# Activation of microbial secondary metabolism toward production of novel bioactive natural products

## （新規生理活性天然化合物の生産に向けた微生物二次代謝の活性化）

2022 年 9 月

埼玉大学大学院理工学研究科（博士後期課程）

理工学専攻（主指導教員　高橋　俊二）

ISLAM ADEL ABDELHAKIM AMIN

# Doctoral Thesis

# Activation of microbial secondary metabolism toward production of novel bioactive natural products

Submitted to

## Graduate School of Science and Engineering

## Saitama University

**Supervisor:** Shunji Takahashi

**Presented By:**

Islam Adel Abdelhakim Amin

Student ID: 19DB010

September, 2022

# Acknowledgement

To the almighty ALLAH, who has bestowed upon me all of these blessings in order to complete my task, and who has sustained and blessed me throughout my life via his might and kindness, I express my profound gratitude.

Aside from my own efforts, the accomplishment of my thesis is largely dependent on the support and guidance provided by a huge number of others. I'd want to use this occasion to convey my appreciation to the individuals who have played a role in the successful completion of my thesis.

I would like to express my deepest gratitude to Prof. Hiroyuki Osada for believing in me and giving me the chance to be a member of his research group in an outstanding environment at RIKEN. Without his precious support, it would not be possible to conduct this research.

My enormous appreciation is addressed to Prof. Shunji Takahashi, as the thesis supervisor. I will never forget his continuous encouragement, helpful criticism, and indispensable support not only in science but also in my normal life.

I am greatly thankful to Dr. Takayuki Motoyama for mentoring and guiding me throughout my Ph.D. study. Without his guidance and valuable comments, this thesis would not have materialized.

*Islam Adel Abdelhakim Amin*

*June, 2022*

# Table of contents

# List of Abbreviations

| ACP | Acyl Carrier Protein |
|---|---|
| ADP | Adenosine Diphosphate |
| AT | Acyl Transferase |
| AU | Absorbance Unit |
| $[\alpha]_D$ | Specific rotation at the sodium D-line |
| BGC | Biosynthetic Gene Cluster |
| Brs | Broad singlet |
| $CDCl_3$ | Deuterated chloroform |
| $CD_3OD$ | Deuterated methanol |
| c | concentration |
| CoA | Coenzyme A |
| COSY | Correlation Spectroscopy |
| CV | Column Volume |
| d | doublet |
| dd | doublet of doublet |
| DEPT | Distortionless Enhancement by Polarization Transfer |
| DH | Dehydratase |
| DMSO | Dimethyl sulfoxide |
| DNA | Deoxyribonucleic Acid |
| ER | Enoyl Reductase |
| ESI | Electrospray Ionization |
| *et al.* | et altera (and others) |
| EtOAc | Ethyl acetate |
| FAS | Fatty Acid Synthase |
| FDA | Food and Drug Administration |
| HDAC | Histone Deacetylase |
| HiTES | High Throughput Elicitor Screening |
| HMBC | Heteronuclear Multiple-Bond Correlation |
| HSQC | Heteronuclear Single Quantum Coherence |
| HPLC | High Performance Liquid Chromatography |

| | |
|---|---|
| HR-ESITOFMS | High Resolution Electrospray Ionization Time of Flight Mass Spectrometry |
| HR-MS | High Resolution Mass |
| Hz | Hertz |
| $IC_{50}$ | half-maximal inhibitory concentration |
| i.d. | internal diameter |
| IR | Infra Red |
| *J* | Coupling constant |
| KR | Ketoreductase |
| KS | Ketoacyl Synthase |
| LC-MS | Liquid Chromatography Mass Spectrometry |
| LC-MS/MS | Liquid Chromatography - Tandem Mass Spectrometry |
| m | multiplet |
| MeCN | Acetonitrile |
| MeOH | Methanol |
| MHz | Mega Hertz |
| MPLC | Medium Pressure Liquid Chromatography |
| MT | Methyl Transferase |
| MS | Mass Spectrometry |
| *m/z* | mass per charge |
| NA | Not Assayed |
| NMR | Nuclear Magnetic Resonance |
| NOESY | Nuclear Overhauser Effect Spectroscopy |
| NPDepo | Natural Products Depository |
| NPs | Natural Products |
| NRPs | Non Ribosomal Peptides |
| NRPSs | Non Ribosomal Peptide Synthetases |
| ODS | Octadecyl-Silica |
| OSMAC | One Strain Many Compounds |
| PDA | Photodiode Array |
| PDB | Potato Dextrose Broth |
| PKS | Polyketide Synthase |
| PKS-NRPS | Polyketide Synthase-Non Ribosomal Peptide Synthetase |
| ppm | part per million |
| q | quartet |

| | |
|---|---|
| RNA | Ribonucleic Acid |
| RP-HPLC | Reversed Phase-High Performance Liquid Chromatography |
| s | singlet |
| SARPs | *Streptomyces* Antibiotic Regulatory Proteins |
| SMs | Secondary Metabolites |
| sp. | species |
| t | triplet |
| UPLC | Ultra-Performance Liquid Chromatography |
| UV | Ultra Violet |
| $UV_{max}$ | Ultraviolet absorption maximum |
| WT | Wild-Type |
| 1D-NMR | One Dimension-Nuclear Magnetic Resonance |
| 2D-NMR | Two Dimension-Nuclear Magnetic Resonance |
| $\delta_H$ | $^1$H chemical shift |
| $\delta_C$ | $^{13}$C chemical shift |
| $\lambda$ | Wavelength |

**Chapter 1**

**Introduction and Background**

## 1. Metabolism

Metabolism is a fundamental physiological process that describes all the chemical reactions involved in maintenance of the cell and the organism. It is divided into primary and secondary metabolism. The former type is known to be essential for life of the organism and involved in growth, development, and reproduction; and categorized into energy consuming processes (anabolism) and energy producing processes (catabolism). In contrast, secondary metabolism consists of biochemical pathways for production of metabolites that are not directly involved in the organism's growth, development or reproduction. However, secondary metabolites play a major role in the adaptation of organisms to their environment and represent an important source of valuable compounds in medicine, agriculture and beyond.

Most secondary metabolites originate from primary metabolite precursors, making it difficult to clearly delineate the boundaries between primary and secondary metabolism. Figure 1 depicts the correlation between them.
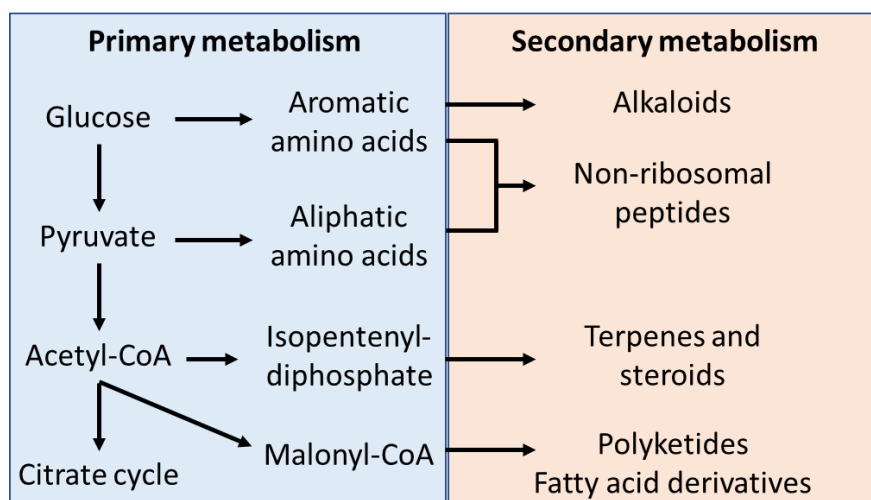
**Fig. 1.** The correlation between primary and secondary metabolism

## 2. Secondary metabolism

Secondary metabolites are also known as natural products as they are mainly obtained from natural origin such as plants, fungi, and bacteria. They are low molecular weight molecules that represent a wide range of chemical structures from simple fatty acids to complex scaffolds terpenoids, alkaloids, and polyketides. Despite this relatively wide distribution of secondary metabolites, it is still mysterious why plants and microorganisms accumulate them. However, many reports suggested that this arsenal of chemicals are the primary defense tool against invaders or a communication signaling machinery with the neighborhoods [1].

Besides this important ecological role of secondary metabolites, microbial natural products constitute a milestone in the field of drug discovery especially after the discovery

of penicillin from *Penicillium notatum* by Fleming in 1929 followed by streptomycin discovery in 1943 [2,3]. These discoveries dramatically changed the research of natural products and positioned microbial natural products as one of the most important and sustainable resources in drug discovery. During the golden age of antibiotics discovery (1940-1960), it was anticipated that humanity passed the risk of infectious diseases. However, microbial evolution and genetic jugglery have dispelled this notion, and number of resistant strains is in continuous increase without equal introduction of new antibiotics [4,5].

## 3. Classes of secondary metabolites

Secondary metabolites can be classified according to chemical structure, occurrence, biosynthesis, or function. Four of the biggest classes are described in the following sections: terpenes, alkaloids, nonribosomal peptides (NRPs), and polyketides.

### 3.1. Terpenes

Terpenes are a widely distributed class of naturally occurring hydrocarbons mainly produced by plants but also accumulated in microbial cultures. These compounds are biosynthesized through mevalonate pathway and resulted from assembly of several isoprene units ($C_5H_8$) to give different lengths of terpenes ($C_5H_8)_n$ namely mono, sesqui, di, tri, and tetraterpenes [6]. The backbone of terpenes can be linear, cyclic, branched,

saturated, or unsaturated and can be further modified mainly by oxidation to give

terpenoids. This class of compounds is responsible for the flavors and aromas of most

plants derived volatile oils (Fig. 2). So, it is widely used commercially in perfumery and

food industry [7]. In addition, terpenes have a wide range of medicinal uses among of

which antiplasmodial activity of popular sesquiterpene lactone artemisinin and its

derivatives (Fig. 2) [8]. Taxol is another natural diterpene that is widely used in cancer

treatment [9] (Fig. 2).



Limonene          Myrecene          Linalool          Menthol

Taxol          Artemesinin
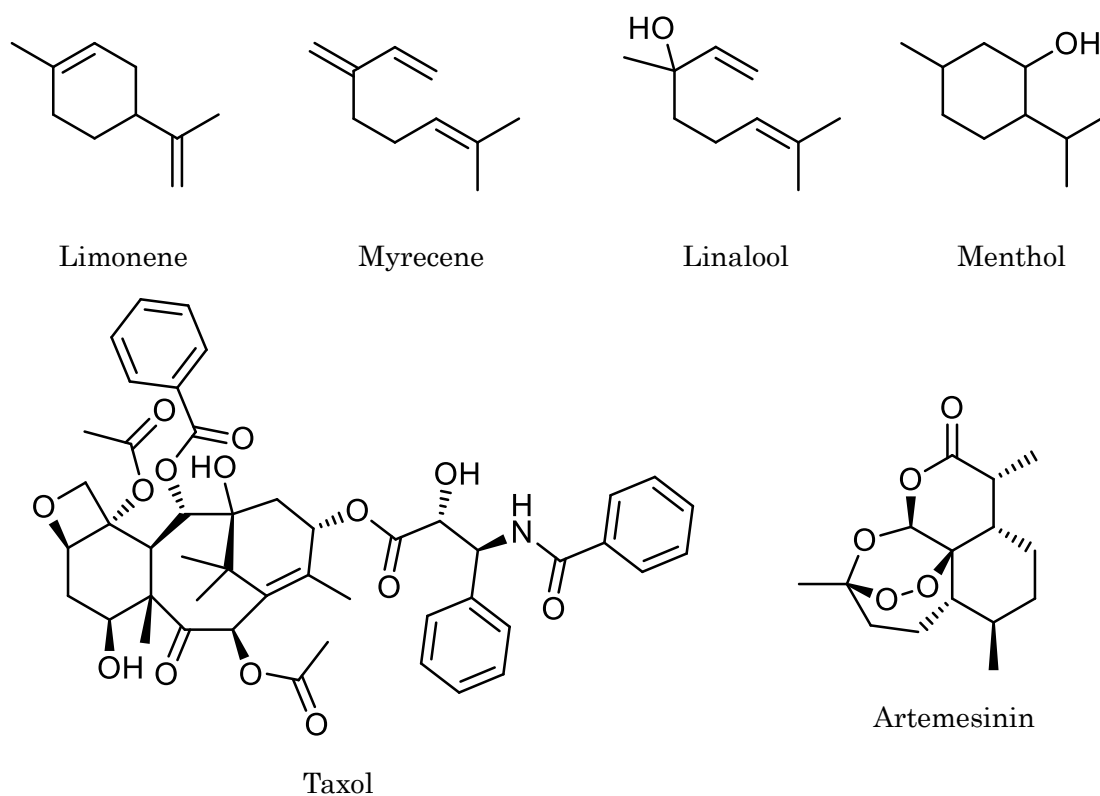
**Fig. 2.** Popular examples of terpenes and terpene derivatives

### 3.2. Alkaloids

Alkaloids are a large and structurally diverse group of natural products of microbial, plant and animal origin. They were primarily defined as basic organic nitrogenous compounds of plant origin that exert a pharmacological effect on mammals. However, this definition was extended after the discovery of alkaloids isolated from fungi and animals[10]. Alkaloids can be classified according to their occurrence, chemical structure, amino acid involved in its biosynthesis and physiological activity. Caffeine is a member of xanthine family alkaloids that comes on the top of the list of alkaloids used by humankind due to its central nervous system stimulant effect (Fig. 3). Tropane alkaloids are widely used in medicine as antispasmodic or local anesthetic medicines including atropine, hyoscine and cocaine. Phenanthrene alkaloids are very popular narcotic analgesics and antitussives isolated from opium such as morphine and codeine (Fig. 3). Indole alkaloids like those isolated from *Vinca* herb including vincristine and vinblastine are widely used anticancer agents [10] (Fig. 3).



Morphine

Vinblastine

Caffeine
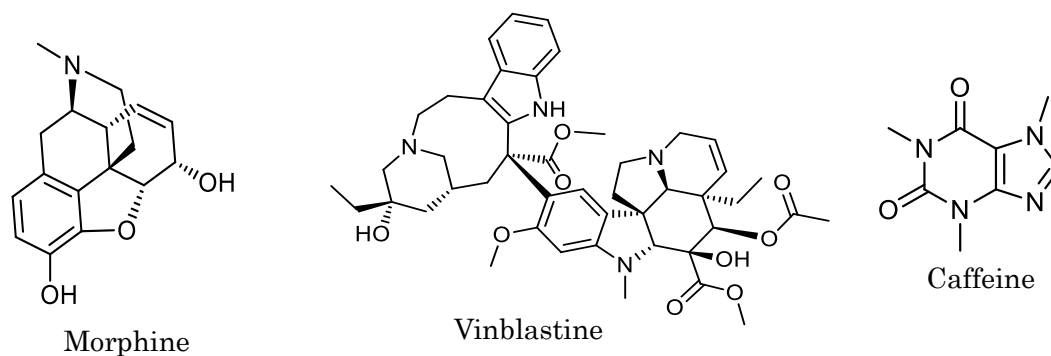
**Fig. 3.** Popular examples of alkaloids

### 3.3. Nonribosomal peptides (NRPs)

In contrast to ribosomal proteins, nonribosomal peptides can contain nonproteinogenic amino acids. Biosynthesis of these peptides is catalyzed by multidomain, multimodular enzyme called nonribosomal peptide synthetase (NRPS) [11]. Each module in an NRPS is dedicated to loading a single amino acid. The modules are further subdivided into domains, each of which catalyzes a single step. An adenylating domain recognizes amino acids and activates them via a pantothenylation/peptidyl carrier domain. The condensation/peptide-bond formation domain forms peptide bonds between the different amino acids, and the resulting peptides are released by a thioesterase domain. The incorporation of different amounts of amino acids, followed by cyclization or modifications such as acetylation or glycosylation, results in a wide range of NRP structures. β-lactam antibiotics, pigments, or siderophores are common examples of this class of secondary metabolites (Fig. 4).



Penicillin G

Indigoidine

Enterobactin
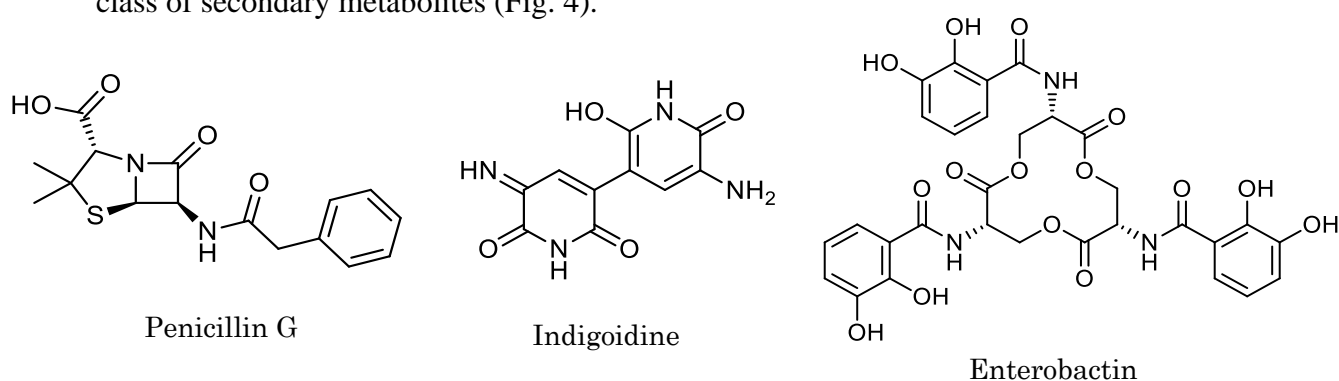
**Fig. 4.** Popular examples of nonribosomal peptides.

### 3.4. Polyketides

Polyketides are a structurally and functionally diverse group of bioactive natural chemicals that have been shown to be a rich source of pharmaceutical and agrochemical lead molecules. Polyketide synthase (PKS), a multi-enzyme complex that is very similar to fatty acid synthase (FAS), catalyzes the production of polyketides from acyl-CoA thioesters [12]. Polyketides are made up of CoA-activated starter units (mainly acetyl-CoA or malonyl-CoA) and go through a stepwise elongation process similar to fatty acid biosynthesis. Type I PKSs are multifunctional enzymes organized into modules, each of which harbors a set of distinct domains responsible for the catalysis of one cycle of polyketide chain elongation. Simplest PKS module must contain at least three biocatalytic domains, a ketoacyl synthase (KS) domain, an acyl transferase (AT) domain, and an acyl carrier protein (ACP) domain. They may also contain optional domains such as methyltransferases (MT), ketoreductases (KR), dehydratases (DH), or enoyl reductases (ER), which are the main reasons behind structure diversification of polyketides [11].

The biosynthesis involves the condensation of acetyl-CoA or propionyl-CoA with malonyl-CoA or methylmalonyl-CoA in a stepwise manner [11,13]. The condensation reaction is pursued by the decarboxylation of the extender unit, resulting in a β-keto functional group. The first condensation produces an acetoacetyl group, which is a

diketide. Subsequent condensations result in triketides, tetraketides, and so on [11].

Macrolides antibiotics, statins, tetracyclines, and anthraquinones are very popular

examples of this class of secondary metabolites that are biosynthesized by either modular

or iterative type I PKSs [14] (Fig. 5).


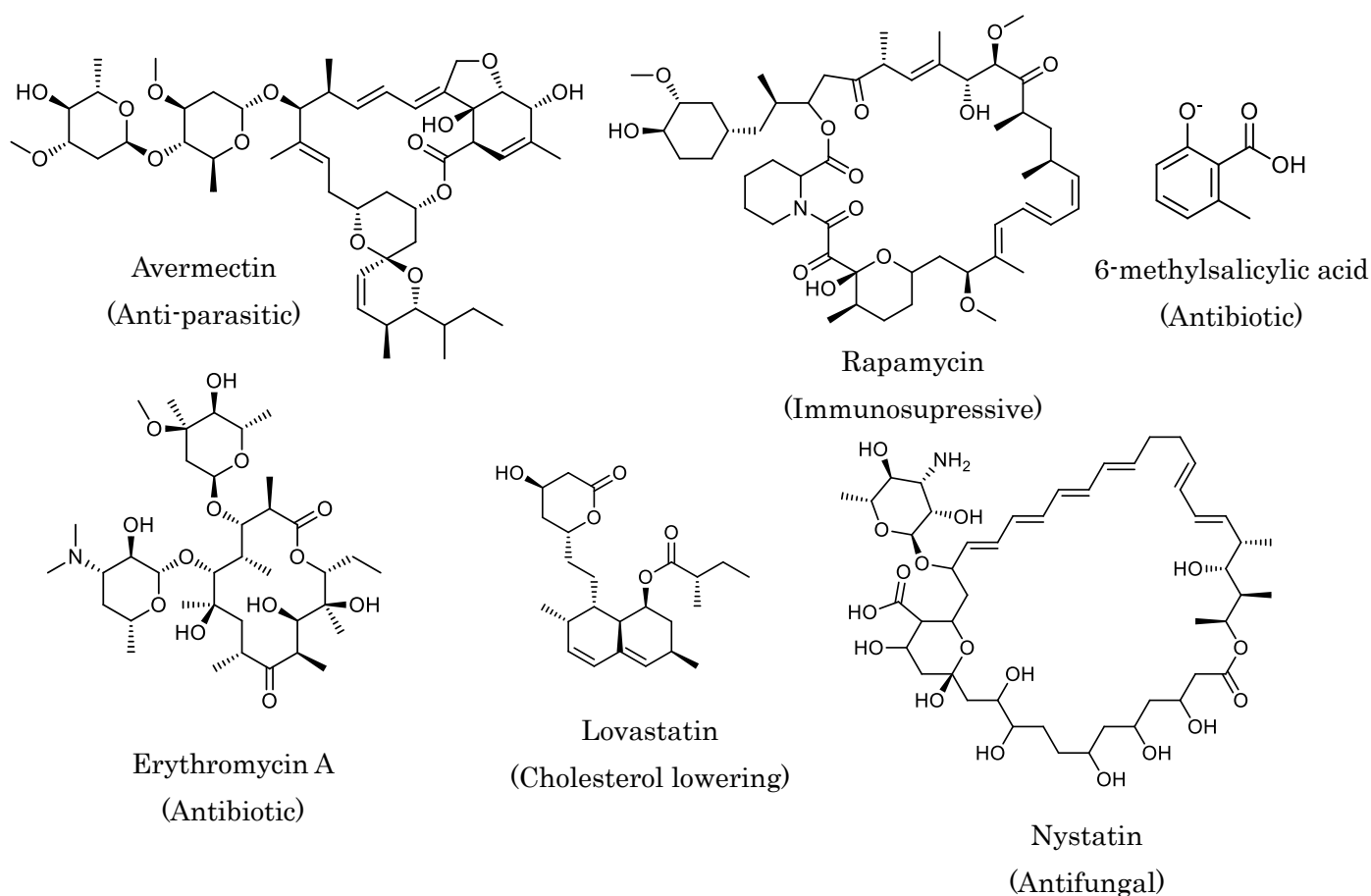
**Fig. 5.** Examples of polyketide natural products and their respective bioactivities

## 4. Impact of Natural Products on Drug Discovery

Natural products (NPs) have long been important in medication development,

particularly for cancer and infectious diseases [15,16], but also for other therapeutic areas

such as cardiovascular disease (statins) and multiple sclerosis (fingolimod) [17–19].

In a recent review published by D. J. Newman and G. M. Cragg, in 2020, the contribution of natural products or their derivatives in drug discovery for treatment of various kinds of diseases has been reported. It has been shown that about 34% (441) of all small molecules approved (1394) from January 1981 to September 2019 was obtained from natural products either directly or indirectly [17].

**4.1. Natural products as antibacterial agents:** Natural products are the main suppliers of small molecules for the antibacterial drug industry compared with biological macromolecules and synthetic approaches. Unaltered natural products and their derivatives represent about 57% of all approved antibacterial agents since 1981 to 2019. Earliest examples are antibacterial natural products / derivatives were penicillins, streptomycin, cephalosporins, and erythromycin. Recently, FDA has approved some natural products derived antibacterial agents including aminoglycoside derivative, plazomicin, tetracycline analogues, omadacycline, eravacycline, and sarecycline in addition to lefamulin [17].

**4.2. Natural products as antitumor agents:** Plant-derived medicines including vinblastine and vincristine, etoposide, paclitaxel (Taxol®), docetaxel, and topotecan are among the most effective cancer chemotherapeutics now available [20]. Chemical modifications of rapamycin firstly isolated from *Streptomyces hygroscopicus* have

yielded clinically approved drugs such as everolimus and temsirolimus [20]. Other antitumor agents were also approved for human use that are chemically modified from its lead compounds primarily isolated from marine organisms such as cytarabine, trabectedin, halichondrin B, and eribulin [20]. Since 1981-2019, about 25% (62) of all approved anticancer drugs (247) were obtained from natural products or their derivatives [17].

**4.3. Natural products as diverse therapeutics:** Artemisinin and ivermectin are two widely used unaltered natural medicines for treating malaria and worm infections, respectively [8,21]. Furthermore, nature-derived molecules accounted for 31% of anti-glucoma and anti-multiple sclerosis drugs. Latanoprost and its derivatives are popular glaucoma treatments; however, fingolimod HCl and fumarate derivatives are examples of multiple sclerosis treatments [17,18]. Natural products also account for 14% and 9% of approved anti-diabetic and antifungal drugs, respectively [17].

## 5. Biosynthetic gene clusters

In contrast to genes that are required for the synthesis of a primary metabolite that are dispersed throughout the fungal genome, the genes encoding the enzymatic activities to produce any secondary metabolite are arranged in a contiguous fashion as a biosynthetic gene cluster (BGC) [22]. It has been nearly 30 years since the discovery of the penicillin BGC [23]. The contiguous arrangement of genes dedicated to a single metabolite, which

was once thought to be a rare occurrence, is now proven to be a prevalent theme in the

microbial genome. Biosynthetic gene clusters can be defined as tightly linked groups of

mostly non-homologous genes that work together to form a single, discrete metabolic

pathway, where the genes are physically close to one another on the genome, and their

expression is frequently coregulated [24] (Fig. 6).
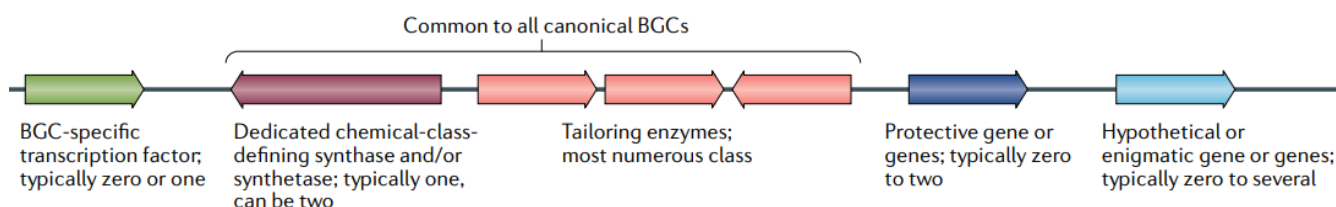


**Fig. 6.** A schematic overview of a typical biosynthetic gene cluster

The traditional method for discovering novel bioactive secondary metabolites

involves collecting and cultivating a microbial strain, then extracting and isolating

chemicals using bioassays. However, genomic investigations using whole-genome

sequencing techniques have revealed that the number of biosynthetic genes involved in

the biosynthesis of secondary metabolites in microorganisms vastly outnumbers the

known molecules [25]. This may be attributed to the fact that the well settled laboratory

culture conditions prevent any competition or life-threatening circumstances that would

trigger the production of SMs, leaving many gene clusters "silent" or "cryptic". Various

approaches have been taken in attempts to activate silent SM gene clusters and resulted

in the discovery new bioactive compounds [22,26]. This activation approaches can be achieved via manipulation of culture conditions, genetic based modifications, or chemical elicitation.

## 6.    Approaches for activation of silent biosynthetic gene clusters

## 6.1. Manipulation of culture conditions

## 6.1.1. <u>O</u>ne <u>S</u>train <u>MA</u>ny <u>C</u>ompounds approach (OSMAC)

This technique revealed that culturing of one strain in different culture media has resulted in altered metabolic profiles of the same strain and new SM were accumulated (Fig. 7). A well-known example of OSMAC is the production of 15 compounds originating from five different biosynthetic pathways by *Aspergillus ochraceus* DSM 7428 through the manipulation of media composition, aeration, shape of culturing flask or temperature culturing conditions [27]. Recently, a new siderophore glucuronide, nocardamin glucuronide, was isolated by applying the OSMAC approach to the ascamycin-producing strain, *Streptomyces* sp. 80H647 [28]. In addition, six new 11-mer peptaibols, zealpeptaibolins A – F, were isolated from the soil fungus, *Trichoderma* sp. RK10-F026, utilizing the same approach [29]. However, because the physiological conditions responsible for the activation of silent gene clusters are unknown, and it is

often impossible to predict the intricate regulatory circuits involved in pathway control, this technique is primarily empirical [30].

In addition to changing culture conditions, external influences like as UV radiation, enzyme inhibitors, and heat shock, may lead to the identification of novel bioactive secondary metabolites [30]. Indeed, adding the F-actin inhibitor jasplakinolide to the growth medium of the fungus *Phomopsis asparagi* resulted in the production of three novel chaetoglobosins that were not present in the fungus's axenic culture [31].

### 6.1.2. Co-cultivation approach

Fungi and bacteria live in complex communities in nature, sharing similar niches, using similar resources, and overcoming the same external cues for survival [32]. As a result, simulating the natural environment in the laboratory may result in direct contact involving competition for space or for limited nutrients, resulting in the induction of silent biosynthetic pathways and the production of novel bioactive compounds [25] (Fig. 7). *Streptomyces hygroscopicus* co-cultured with *Aspergillus nidulans* activated the gene cluster of a polyketide named orsellinic acid, demonstrating the potential of this approach [33]. Another example is *Streptomyces clavuligerus* co-cultured with a methicillin-resistant *Staphylococcus aureus* that activated holomycin biosynthesis [34]. However, like with the previous technique, the mechanism of activation of the cryptic gene clusters

is not fully understood, and it is difficult to predict which pathways will be activated in this manner.

## 6.2. Genetic-based activation approaches

## 6.2.1. Ribosome engineering

Ribosomal engineering is an effective technique for activating dormant genes in fungi [35]. This method involves modifying the ribosome through the insertion of mutations conferring resistance to anti-ribosomal medicines such as aminoglycosides antibiotics, gentamycin, streptomycin, spectinomycin, or neomycin (Fig. 7). When one of these medications is applied to the fungus, it develops mutant drug resistance through a point mutation in the ribosomal component [36]. Reculturing these mutant resistant strains showed different metabolic profiles indicating activation of dormant biosynthetic pathways.

This method has been used to isolate novel secondary metabolites from fungi with great success. As a result of gentamycin resistance being introduced into the marine-derived fungus *Penicillium purpurogenum*, anticancer natural compounds were isolated that were not present in the wild-type culture [37]. In another experiment, the development of hygromycin B-resistant mutants of *Monascus pilosus* NBRC 4520 resulted in an increase in the natural product of this fungus [38].

## 6.2.2. Chromatin remodeling

For the control of eukaryotic genome transcription, chromatin remodeling is a critical process [39]. Chromatin is made up of repeated nucleosome units, each of which contains two copies of histones H2A, H2B, H3, and H4 [39], which are then wrapped around chromosomal DNA and joined by a linker histone (H1) [40,41]. DNA packaging and accessibility are dynamically altered by histones in response to physiological and developmental stimuli (Fig. 7). These are accomplished through post-translational alterations to histone tails, such as deacetylation and methylation, which eventually influence gene expression [42].

It has been demonstrated that acetylation, methylation, phosphorylation, and ADP-ribosylation of DNA can influence gene expression in fungi [43,44]. For instance, deletion of the *hdaA* gene encoding an *Aspergillus nidulans* histone deacetylase (HDAC) resulted in the bioproduction of penicillin and sterigmatocystin [45], but loss of *sumO* resulted in an increase in asperthecin production [46]. These findings imply that any ligands capable of inducing epigenetic alterations may be used to activate dormant gene clusters and/or increase the biosynthesis of fungal metabolites produced constitutively. Additionally, this strategy avoids sophisticated genetic manipulations and culture-based procedures, emphasizing its potential for drug discovery [24].

### 6.2.3. Manipulation of global regulatory systems

Instead of trying to find environmental cues that influence the regulatory networks as in OSMAC approach, the engineering of global regulatory genes aims to affect the same regulatory systems, but at a more refined molecular level through over-expression or inactivation of the genes controlling the cellular response to these phenomena [26] (Fig. 7). Production of SMs in microorganisms is linked to morphological development and nutrient availability (carbon and nitrogen sources, phosphate starvation, amino acid and iron availability) [47]. Numerous global regulators have been successfully linked to its environmental cues, including PacC and pH [48]; the CCAAT-binding complex (CBC) and iron [49]; AreA and nitrogen [50]; the velvet complex and light [51]; and CreA and carbon [52].

PacC, the critical component for pH regulation in fungi, is one of the most researched global regulators. It promotes penicillin biosynthesis in *Aspergillus parasiticus* at alkaline pH [53], but inhibits aflatoxin biosynthesis [54]. LaeA, is a global protein of the velvet complex that responds to light, firstly discovered in *Aspergillus* sp. and strongly linked with secondary metabolism regulation. Increased transcription of the penicillin and lovastatin genes occurs when *laeA* is overexpressed. However, many metabolic gene

clusters, including sterigmatocystin, penicillin and lovastatin, were blocked by deletion of *laeA* [55].

### 6.2.4. Transcription factors and promoter exchange

Typically, BGC promoter sequences do not induce transcription under all growth conditions and are heavily affected by intracellular regulatory networks. Manipulation of promoter sequences by substituting functionally active promoters for native silent promoters directly in the generating organism has proven to be an effective technique for driving expression of silent genes [26]. The in-dependent introduction of *ermE*p* upstream of *ftdA* and *ftdB*, which encode putative desaturase and hybrid polyketide synthase-nonribosomal peptide synthase, respectively, activated a silent polycyclic tetramate macrolactam (PTM) gene cluster in *Streptomyces albus*, resulting in the identification of 6-epi-alteramides A and B [56]. Additionally, the manufacture of a blue pigment called 'indigoidine' was induced in *S. albus* by expressing the NRPS gene *bpsA* under the *ermE*p* promoter [56]. In *Aspergillus nidulans*, substituting the natural promoter of the non-ribosomalpeptide synthetase, *acvA*, with a promoter from the ethanol dehydrogenase, *alcA*p, from the same host led to a 30-fold increase in penicillin production [57].

17

### 6.2.5. Manipulation of pathway-specific regulators

Pathway-specific transcriptional regulatory genes are often identified within the BGCs and they may either suppress or promote the biosynthesis of the relevant SM (Fig. 7). The co-localization of pathway-specific regulatory genes gives an option for selective activation of the desired BGC either by inactivation of the repressor or over-expression of the activator genes [26]. TetR family repressors can tightly bind to DNA and prevent the transcription of the downstream genes. Inactivation of TetR family repressors have induced jadomycin [58,59], kinamycin [60], auricin [61], and ceoelimycin biosynthesis [62,63]. In contrast to the TerR family, most characterized SARPs and LuxR proteins are transcriptional activators, which facilitate the binding of RNA polymerase to initiate transcription [64,65]. Overexpression of the SARP-type regulator gene *papR2* from *Streptomyces pristinaespiralis* in *Streptomyces lividans* leads to the activation of the silent undecylprodigiosin (Red) gene cluster [66].

### 6.2.6. Heterologous expression of target BGC in a suitable host

Numerous microbes that have the potential of producing diverse natural products, such as *Cyanobacteria* strains and filamentous fungi, are genetically intractable [67]. Heterologous expression enables access to the genomic potential of these organisms in a genetically compatible host. *Escherichia coli* and *Saccharomyces cerevisiae* are ideal

hosts for the development of bacterial and fungal SMs (Fig. 7). *E. coli* appears to be well-suited for the development of *Cyanobacteria*-derived pathways that have difficulty in being genetically manipulated, as evidenced by the reported production of microcystin [68] and lyngbyatoxin [69]. In many cases, hosts that are evolutionarily close to the organism harboring the target pathway appear to be the ideal candidates for heterologous expression. Thus, numerous well-characterized *Streptomyces* species are highly adaptable and serve as effective alternative hosts for heterologous characterization of Actinobacteria genes. *S. albus* J1074 [70], *S. lividans* TK24 [71], *S. venezuelae* ATCC10712, and *S. coelicolor* A3(2) have all been extensively employed for cryptic pathway expression. In filamentous fungi, *Aspergillus* species have been routinely exploited as heterologous hosts. One early example is the transfer of the whole penicillin gene cluster to *A. nidulans*, while geodin has been generated heterologously in this host more recently [72–74].

## 6.3. Chemical activation of microbial metabolism

High-throughput elicitor screening (HiTES) represents an additional activation approach (Fig. 7), first utilized by Craney *et al*. in 2012. They screened over 30000 small molecules to discover potent secondary metabolism inducers and identified 19 candidate compounds that altered secondary metabolite profiles in *Streptomyces coelicolor* [75]. In

a related study, sublethal quantities of the antibiotic trimethoprim were demonstrated to

trigger the expression of many specialized metabolite BGCs in *Burkholderia*

*thailandensis* E264 in a high-throughput strategy for the discovery of chemical elicitors

that activate silent gene clusters [76]. Another example of chemical elicitation is the use

of ß-carboline compound (BR-1), which successfully induced reveromycin production in

*Streptomyces* sp. SN-593 [77]. This approach can be easily employed in any microbial

culture, does not require genetic manipulation, and is readily scalable to high-throughput,

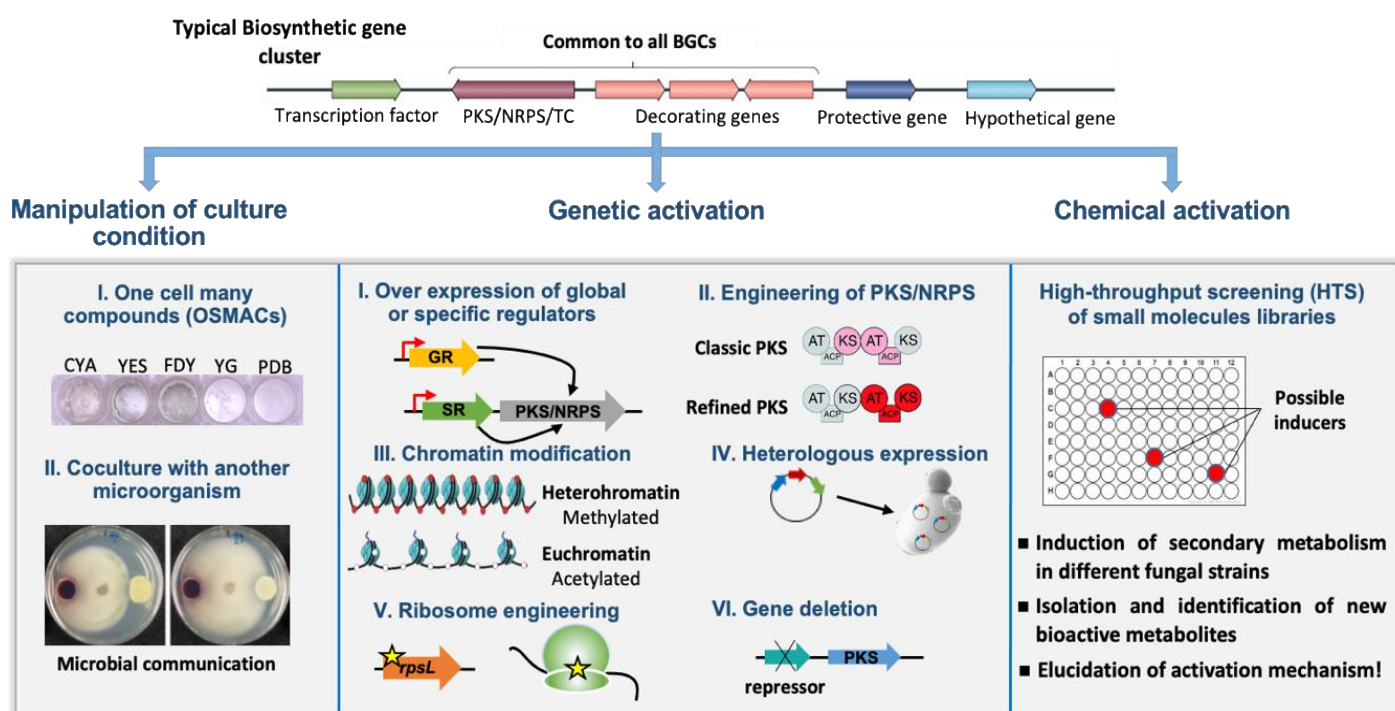all of which are advantages over the genetic approach.



**Fig. 7.** Different approaches of microbial secondary metabolism activation

### 7. NPD938 as a fungal secondary metabolism regulator

Tenuazonic acid is a fungal metabolite produced by *Pyricularia oryzae* and plays an important role in controlling the rice blast disease [78,79]. Experiments related to induction of tenuazonic acid for combating rice blast disease or identification of its biosynthetic gene cluster were performed by our group [80,81]. Recently, through elicitor screening of a pilot library of 376 small molecules [representing the chemical space of over 40,000 compounds available in the RIKEN Natural Products Depository (NPDepo) at RIKEN], NPD866 was identified as a tenuazonic acid inducer. Twenty-one compounds that were structurally similar to NPD866 were investigated for their potential to induce tenuazonic acid production (Fig. 8). NPD938 was shown to be the most powerful inducer among the 21 chemicals tested. NPD938 stimulated the formation of tenuazonic acid, terpendoles, and pyridoxatin in *Pyricularia oryzae*, as well as terpendoles and pyridoxatin in *Tolypocladium album* (RK99-F33) [80].
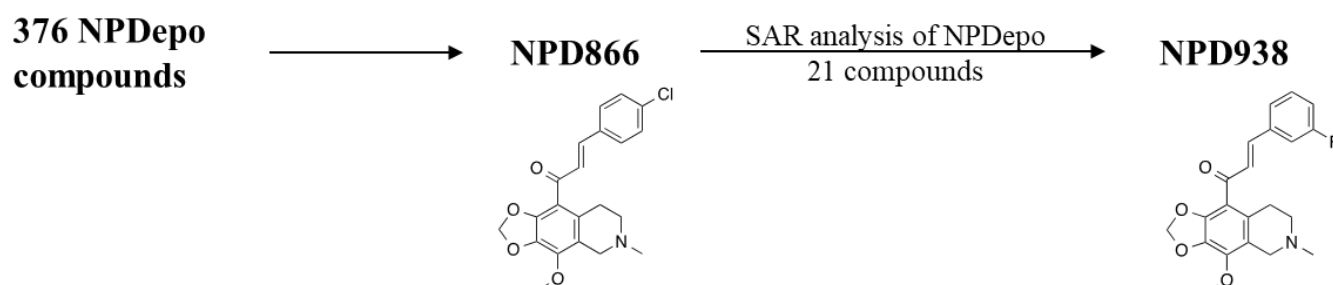


**Fig. 8.** Screening of Natural Products Depository database for induction of tenuazonic acid in *Pyricularia oryzae* and discovery of NPD938.

**Aim of this study**

The number of biosynthetic genes in many fungi, responsible for the production of secondary metabolites, greatly outnumbers the known compounds. This suggests that the biosynthetic potential of fungi is greatly unexplored and revealed that many potential bioactive metabolites are waiting to be discovered if these cryptic gene clusters become activated. Thus, we aim at chemical induction of fungal secondary metabolism for efficient utilization of the fungal biosynthetic machineries and production of novel bioactive natural products. This will be achieved using a recently discovered fungal secondary metabolism regulator namely NPD938.

**Chapter 2**

**Isolation, identification, and bioactivity evaluation of induced compounds from**

***Fusarium* sp. RK97-94 culture treated with NPD938**

In this chapter, we aimed at chemical induction of secondary metabolism in *Fusarium* sp. RK97-94 using NPD938. We have succeeded in purification and identification of three lucilactaene analogues, of which dihydroNG391 was strongly induced by NPD938 indirectly. Antimalarial potentials of the isolated compounds were determined and revealed that dihydrolucilactaene and 13α-hydroxylucilactaene are potent antimalarial compounds ($IC_{50}$ = 0.0015 and 0.68 µM, respectively). Structure-activity relationship of lucilactaene and its derivatives as antimalarial lead compounds was also demonstrated.

## 1. Introduction

The development of multi-drug-resistant diseases represents a major global threat to public health. Thus, the continuous discovery of novel drugs for the treatment of life-threatening diseases such as cancer, resistant bacterial infections, and malaria is of great importance. Natural products and their derivatives constitute over 50 percent of approved antibacterial drugs, and 25% of approved anticancer agents over the period of 1981–2019 [17]. Filamentous fungi are valuable microorganisms, known to produce a great variety of natural products with potential applications in the pharmaceutical industry and beyond [82]. Despite their great potential stemming from the production of diverse secondary metabolites, genome sequencing and bioinformatics tools recently revealed that the majority of secondary metabolite biosynthetic gene clusters are silent under usual laboratory conditions [83–85]. This suggests the existence of a great number of novel metabolites yet to be discovered via the activation of such silent gene clusters.

Manipulating the culture conditions of microorganisms has major impact on secondary metabolite profiles. One strain-many compounds (OSMAC) and co-culture approaches were successfully implemented to activate cryptic gene clusters resulting in the identification of new bioactive compounds [27–29,86]. A well-known example of OSMAC is the production of 15 compounds originating from five different biosynthetic

pathways by *Aspergillus ochraceus* DSM 7428 through the manipulation culturing conditions [27].

Genetic activation is another widely used approach, implemented by altering the expression of global or pathway-specific regulators, chromatin landscape modification, gene cluster refactoring, or the use of a heterologous host for target gene cluster overexpression [45,85,87–92]. For example, the overexpression of cluster-specific transcription factor GliZ resulted in a marked increase of gliotoxin levels, while its deletion suppressed gliotoxin production [93]. The earliest report on the epigenetic regulation of fungal secondary metabolites dates back to 2007, when histone deacetylase (*hda*) deletion was shown to result in the activation of multiple gene clusters in *Aspergillus nidulans* [45].

High-throughput elicitor screening (HiTES) represents an additional activation approach, first utilized by Craney *et al*. in 2012. They screened over 30000 small molecules to discover potent secondary metabolism inducers and identified 19 candidate compounds that altered secondary metabolite profiles in *Streptomyces coelicolor* [75]. Another example of chemical elicitation is the use of ß-carboline compound (BR-1), which successfully induced reveromycin production in *Streptomyces* sp. SN-593 [77,94]. This approach can be easily employed in any microbial culture, does not require genetic

manipulation, and is readily scalable to high-throughput, all of which are advantages over the genetic approach.

As a part of our fungal secondary metabolism activation project, our group recently identified NPD938 (Fig. S1) as a fungal secondary metabolism inducer via elicitor screening of a pilot library, which contains 376 small molecules [representing the chemical space of approximately 40,000 compounds available in RIKEN Natural Products Depository (NPDepo) at RIKEN] [95,96]. Compound identification was followed by structure-activity relationship analysis. NPD938 successfully induced the production of tenuazonic acid in *Pyricularia oryzae*, as well as that of terpendoles and pyridoxatin from *Tolypocladium album* (RK99-F33) [80].

Herein, we describe the purification, structural elucidation, and biological activity assessment of two new lucilactaene analogues named dihydroNG391 (**1**) and dihydrolucilactaene (**2**), as well as a known one, namely 13α-hydroxylucilactaene (**3**) [97], from *Fusarium* sp. RK97-94 (Fig. 9). DihydroNG391 (**1**) was strongly induced by NPD938. We also proposed that NPD938 facilitated the regiospecific reduction of the carbonyl group at C-12 in NG391/393 into corresponding alcohols via activating another reductase domain within or outside the gene cluster. In addition, we investigated the structure-activity relationship of lucilactaenes as antimalarial lead compounds.
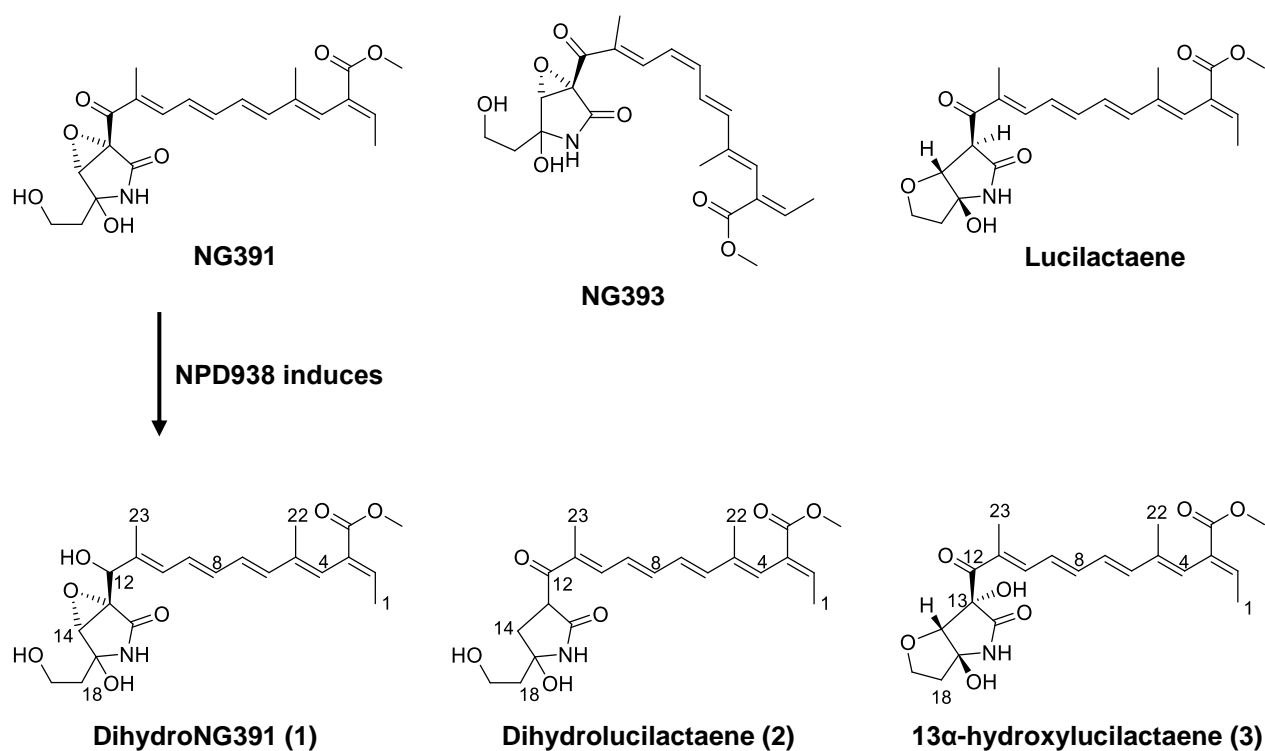
26

**Fig. 9.** Structures of lucilactaene and its derivatives, showing the new analogues identified in this study **1–3**.

## 2. Induction of new lucilactaene analogs in NPD938-treated *Fusarium* sp. RK97-94

Treatment of *Fusarium* sp. RK97-94 with different concentrations of NPD938 (Fig. 10A) resulted in the induction of a prominent peak with strong UV absorption at $\lambda_{max}$ 321 nm and an expected mass of 419, as revealed by LC-MS (Fig. 10B and 10C). Compound **1** accumulation was observed in two of the media used, namely YG, and to a lesser extent, PDB+0.1% agar. Out of the media assessed, these two were the only to co-produce previously identified cytotoxic, antimalarial, and mutagenic compounds (lucilactaene, NG391, and NG393) (Fig. 9), with a mass range similar to that of **1** [98,99]. Thus, we

speculated that this compound might be a lucilactaene analogue. This was confirmed after

culturing PKS-NRPS knockout strain (Δ*luc5*) lacking the core gene involved in *Fusarium*

sp. RK97-94 lucilactaene biosynthesis [99]. Lucilactaene, NG391, NG393, and induced

compound peaks consequently disappeared (Fig. S2).
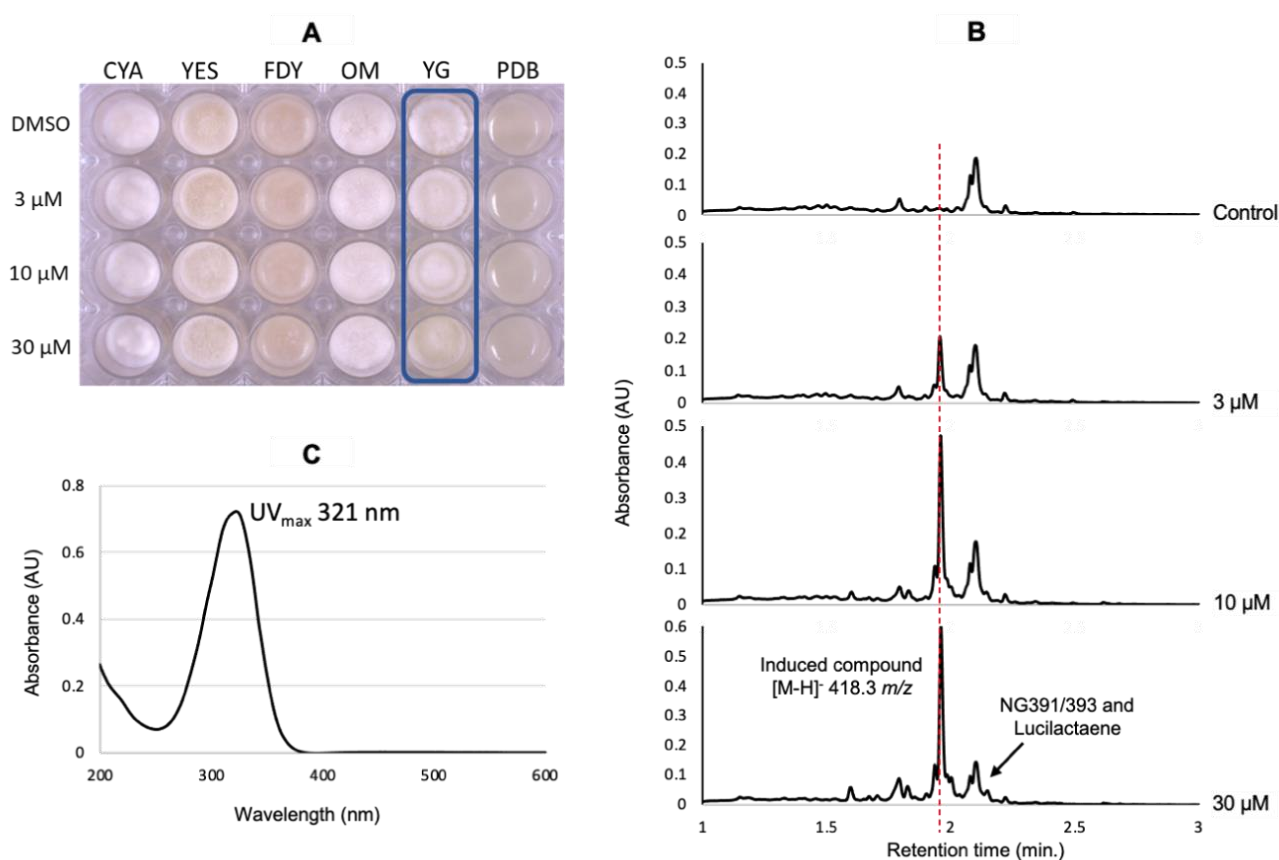


**Fig. 10. A)** 7-d culture of *Fusarium sp*. RK97-94 in a 24-well plate with different culture media under different concentrations of NPD938. **B)** UPLC chromatograms of methanolic extracts from YG culture media (Yeast extract 0.5 % and 2 % Glucose), showing strong induction at 1.9 min with [M-H]⁻ 418.3 *m/z*. **C)** UV$_{max}$ of induced peak.

Unlike known lucilactaene analogues that displayed UV$_{max}$ range from 350 – 375 nm [97,98], compound **1** exhibited an unusual UV absorption pattern and unique mass value that were never reported in literature, suggestive of a new lucilactaene analogue. Furthermore, normal-phase MPLC followed by RP-HPLC fractionation of the EtOAc extract of NPD938-treated *Fusarium* sp. RK97-94 culture revealed the presence of two additional unknown peaks, **2** and **3**, that overlapped with NG391/393 peaks in UPLC analysis (Fig. S3). Peak **2** exhibited UV$_{max}$ at 368 nm, as well as [M-H]$^-$ 402 *m/z* and [M+H]$^+$ 404 *m/z* in ESI-MS analysis, suggesting a molecular weight of 403 Da, which has never been reported for lucilactaene analogues [100,101]. Peak **3** displayed similar mass of NGs in ESI-MS ([M-H]$^-$ 416 *m/z*) but with different retention time (Fig. S3) and different UV$_{max}$ (360 nm) [102]. Literature and database search suggested a possible known hydroxylated lucilactaene derivative [97].

### 3. Purification of target metabolites

Lucilactaene-like compounds are characterized by a pentaene skeleton known for its instability [101]. Thus, all purification steps for **1–3** were conducted away from light, as much as possible, by collecting fractions in opaque, tightly closed vials dipped in ice to minimize the instability of these compounds due to light, high temperature, or atmospheric oxygen. The EtOAc extract (2.77 g) obtained from 7 L culture of *Fusarium*

sp. RK97-94 treated with 30 µM NPD938 (Fig. S4) was subjected to fractionation by normal-phase MPLC using gradient elution, as described above (Fig. S5). Target compound was detected in MPLC fraction tubes 64–72 (~ 400 mg), that was further fractionated into four subfractions (I, II, III, and IV) via preparative high-performance liquid chromatography (Fig. S3). Compound **1** was purified from subfraction I using open silica column chromatography with gradient elution of chloroform and methanol (0, 2.5, 5, 10, 50% methanol), followed by semipreparative RP-HPLC (isocratic, 35% acetonitrile in water, flow rate 4 mL/min) to afford 3.5 mg. Compound **2** (2.7 mg) was purified from subfraction IV via preparative RP-HPLC with isocratic elution of 55% acetonitrile in water at a flow rate of 8 mL/min. Compound **3** (8.5 mg) was purified from subfraction II through preparative RP-HPLC [Mobile phase, A ($H_2O$), B (acetonitrile); gradient elution, B 40 to 60% (0 to 40 min), B 60 to 100% (40 to 50 min), B 100% (50 to 60 min); flow rate of 8 mL/min].

## 4.    Structure elucidation for compounds 1-3

Compound **1** was isolated as pale yellow amorphous powder upon freeze drying, with an $UV_{max}$ of 324 nm. HR-ESI-TOF/MS analysis in both positive and negative modes yielded [M+Na]$^+$ 442.1842 *m/z* and [M-H]$^-$ 418.1850 *m/z*, respectively (Fig. S6), suggesting the molecular formula of $C_{22}H_{29}NO_7$ calculated for [M+Na]$^+$ 442.1836 *m/z*

and [M-H]$^-$ 418.1871. Considering the differences in molecular formula (+2H) between

**1** and NG391/393, the obvious decrease in UV$_{max}$ of **1** from that of NG391/393, and the

decrease in its unsaturation number by one bond, this reduction must decrease the length

of conjugation and afford compound with higher polarity at lower retention time using

RP-HPLC (Fig. 10B). To this end, we proposed a reduction of the carbonyl group at C-

12 to its corresponding alcohol. To verify this, compound **1** was subjected to 1D and 2D-

NMR spectroscopy (Table 1, Fig. S7–13), and the results were compared with previously

reported data for NG391/393 [101]. $^{13}$C-NMR data displayed 22 carbon signals,

comparable with the NGs skeleton. The only major difference was the disappearance of

the carbonyl signal of C-12 at $\delta_C$ 190.0 and the appearance of a new peak at $\delta_C$ 69.6,

proving the reduction of the ketonic carbonyl to its corresponding alcohol (Fig. 11A).

This result was further confirmed in $^1$H-NMR data by an additional peak formed at $\delta_H$

4.66 (1H, s), assigned for the oxymethine proton produced from the reduced carbonyl.

Heteronuclear Multiple Bond Correlation (HMBC) analysis revealed a strong correlation

from $\delta_H$ 4.66 (1H, s, H-12) to $\delta_C$ 12.2 (C-23), 61.9 (C-13), 128.9 (C-10), and 135.2 (C-

11), in addition to a strong correlation from $\delta_H$ 1.86 (3H, s, H-23) to $\delta_C$ 69.6 (C-12), which

is consistent with reduction of C-12 to its corresponding alcohol. The intact epoxide ring

was confirmed from the unsaturation number as well as the close chemical shift of its two

31

carbons, C-13 (61.9) and C-14 (61.1), similar to previously published data [101,103].

Large coupling constant values of 14.32 Hz between $J_{H6-H7}$ and $J_{H8-H9}$ combined with

strong NOESY correlation between H-9 and H-23, H-4 and H-6, and H-7 and H-22

indicate an *E* configuration of the polyene skeleton. HMBC, COSY, and HSQC data (Fig.

11A, S10–12) were consistent with 1D spectroscopic data and confirmed the presence of

the pentaene skeleton connected to the substituted pyrrolidone skeleton. Thus, compound

**1** was identified as a new lucilactaene derivative, named dihydroNG391 (**1**).
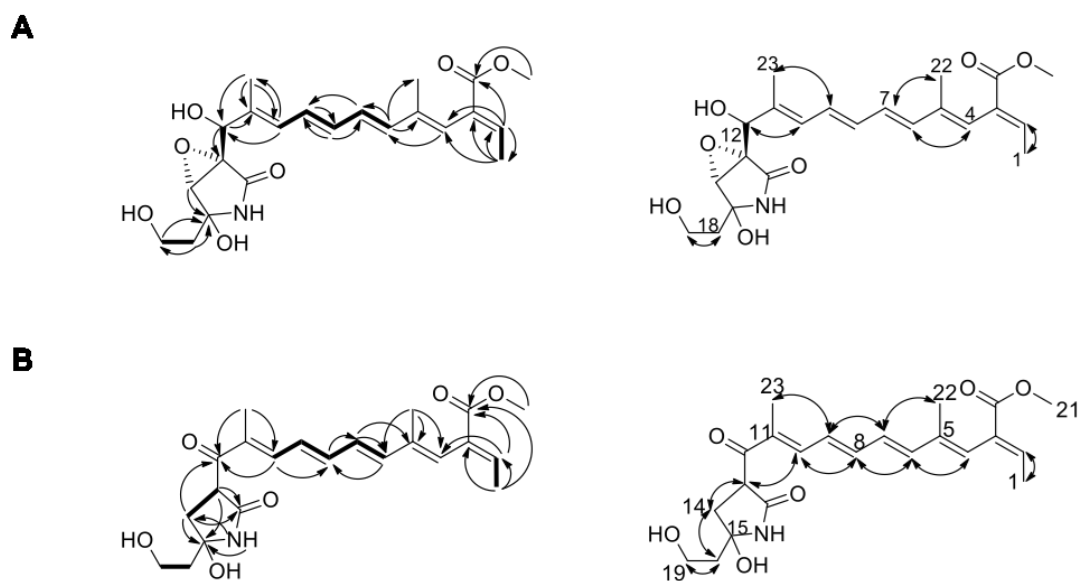


**Fig. 11.** 2D-NMR correlations of A) dihydroNG391 (**1**) and B) dihydrolucilactaene (**2**).
COSY: bold line, HMBC: one-sided arrows NOESY: two-sided arrows.

Compound **2** was isolated as yellow amorphous powder upon freeze drying. HR-ESI-

TOF/MS analysis in both positive and negative modes displayed [M-H]⁻ 402.1914 *m/z*,

(Fig. S14), with a molecular formula of $C_{22}H_{29}NO_6$ calculated for $[M-H]^-$ 402.1922 *m/z*, suggesting a reduced form of lucilactaene; thus, it was named dihydrolucilactaene (**2**). This compound did not show a marked decrease in $UV_{max}$ from that of lucilactaene (368 nm), which excluded the possibility of a polyene skeleton, and C-12 or C-17 reduction. Unsaturation number of **2** was lower than that of lucilactaene by one double bond, proving that the reduction must affect the fused furano-pyrrolidone rings through its opening. Based on full NMR analysis (Table 1, Fig. S15–21), we proposed an open tetrahydrofuran ring structure of lucilactaene (De-epoxyNG391). $^{13}$C-NMR data were in good agreement with NG391 data, except for the two carbon signals at $\delta_C$ 62.3 (C-13) and 64.3 (C-14) observed for NG391, which disappeared, followed by the appearance of two new signals at $\delta_C$ 49.2 (C-13) and 39.9 (C-14), which confirmed the de-epoxidation of NG391 and opening of the fused furan ring at C-14 position of lucilactaene. This was confirmed by $^1$H-NMR data, wherein two additional peaks to NG391 were detected at $\delta_H$ 4.37 (1H, dd, 6.87, 2.3 Hz) and $\delta_H$ 2.35 (2H, m), assigned for H-13 and H-14, attached to the same two new carbon peaks detected based on HSQC data. Further, $^1$H-COSY analysis revealed a strong correlation between these two additional protons's signals, proving the removal of the epoxide group from NG391's structure. Chemical shift of the hydroxylated methylene carbon (C-19) at $\delta_C$ 58.8 is identical to that of its corresponding carbon in NG391, but not

of lucilactaene ($\delta_C$ 68.0), providing additional evidence for the opening of lucilactaene's

tetrahydrofuran ring [101]. The *E* configuration of polyene-skeleton was confirmed by

NOESY correlations between H-4 to H-6, H-7 to H-9, and H-8 to H-10 and by high values

of coupling constants of protons from H6 to H-9 (Fig. 11B, Table 1). All ^{1}H-NMR signals

were assigned to corresponding carbons using HSQC data and connected based on COSY

and HMBC data (Fig. 11B) to confirm another new lucilactaene derivative named

dihydrolucilactaene (**2**).

Compound **3** was obtained as yellow amorphous powder upon freeze drying with

$UV_{max}$ of 360 nm. HR-ESI-TOF/MS analysis in both positive and negative modes

displayed [M-H][-] 416.1705 *m/z*, and [M+Cl][-] 452.1474 *m/z* (Fig. S22), suggesting a

molecular formula of $C_{22}H_{27}NO_7$ calculated for [M+H][+] 418.1860 *m/z*, similar to

NG391/393. ^{1}H and ^{13}C-NMR analysis yielded a different spectroscopic pattern from that

of NGs, and were almost identical to that of 13α-hydroxylucilactaene (Table S1) [97].

This was supported by full 2D-NMR analysis (Fig. S23-30) and [α]$_D$ measurement [97].

**Table. 1**. 500 MHz NMR spectroscopic data for DihydroNG391 (**1**) and Dihydrolucilactaene (**2**) in CD₃OD and CDCl₃, respectively).

| No. | DihydroNG391 (1) | | | | Dihydrolucilactaene (2) | | | |
|---|---|---|---|---|---|---|---|---|
| | $\delta_H$ (Multiplicity, *J* Hz) | $\delta_C$ | HMBC | NOESY | $\delta_H$ (Multiplicity, *J* Hz) | $\delta_C$ | HMBC | NOESY |
| 1 | 1.71 dd (6.87, 1.15) | 14.7 | 2, 3, 4 | 2 | 1.76 dd (7.45, 1.15) | 16.1 | 2, 3, 20 | 2 |
| 2 | 6.91 q (6.87) | 139.6 | 1, 4, 20 | 1 | 6.99 q (7.45) | 140.7 | 1, 4, 20 | 1 |
| 3 | - | 130.6 | | | - | 130.4 | | |
| 4 | 6.04 brs | 124.2 | 6, 22 | 6 | 6.22 brs | 128.1 | 6, 22 | 6 |
| 5 | - | 138.4 | | | - | 138.1 | | |
| 6 | 6.41 m | 136.4 | 4, 5, 7, 22 | 4 | 6.62 d (15.46) | 142.2 | 7, 8, 23 | 4, 8 |
| 7 | 6.34 dd (14.32, 9.17) | 134 | 9 | 22 | 6.44 dd (10.88, 14.89) | 128.5 | 5, 6 | 9, 22 |
| 8 | 6.42 m | 128.6 | 7, 9 | | 6.82 dd (10.88, 14.89) | 143.4 | 7, 10 | 6, 10 |
| 9 | 6.53 dd (14.32, 11.45) | 129.4 | 8 | 23 | 6.69 dd (10.88, 14.32) | 128.3 | 7, 8 | 7, 23 |
| 10 | 6.28 d (11.45) | 128.9 | 12, 23 | 12 | 7.53 d (11.45) | 145.4 | 8, 12, 23 | 8, 13 |
| 11 | - | 135.2 | | | - | 134.4 | | |
| 12 | 4.66 s | 69.6 | 10, 11, 13, 23 | 10 | - | 198.9 | | |
| 13 | - | 61.9 | | | 4.37 dd (7.45, 2.3) | 49.2 | 15, 17 | 14, 10 |
| 14 | 3.89 s | 61.1 | 15 | | 2.35 m | 39.9 | 12, 15, 17 | 13, 18 |
| 15 | - | 83.9 | | | - | 86.7 | | |
| 16 | Not detected | | | | 6.72 brs | - | 13, 14 | |
| 17 | - | 172.4 | | | - | 171.1 | | |
| 18 | 1.96 m | 37.3 | 15, 19 | 19 | 2.03 m | 41.6 | | 19 |
| 19a | 3.80 m | 57.2 | 15 | 18 | 3.85 m | 58.8 | | 18 |
| 19b | 3.80 m | 57.2 | 15 | 18 | 4.06 m | 58.8 | | 18 |
| 20 | - | 168.0 | | | - | 167.6 | | |
| 21 | 3.70 s | 51.0 | 20 | | 3.74 s | 52.1 | 20 | |
| 22 | 1.66 d (1.15) | 13.2 | 3, 4, 5 | 7 | 1.71 s | 14.4 | 4, 5, 6 | 7 |
| 23 | 1.86 s | 12.2 | 10, 11, 12 | 9 | 1.98 s | 12.0 | 10, 11 | 9 |

## 5.   Mechanism of dihydroNG391 induction

Identified compound **1** is the reduced form of NG391. Thus, we proposed three potential mechanisms of NPD938's involvement in this reduction process. The first one is the direct interaction between NPD938 and NG391, causing chemical reduction. This possibility was excluded by incubation of NPD938 (30 µM) with a similar concentration of NG391/393 in YG media, followed by UPLC-MS analysis, which failed to detect **1** (Fig. S31). Involvement of the KR domain in the polyketide synthase of PKS-NRPS during the reduction process or indirect activation of another enzyme to catalyze this reduction are two other possibilities for NPD938's involvement. To explore the precise mechanism, NG391/393 and lucilactaene were separately fed to a PKS-NRPS knockout strain (Δ*luc5*) in the presence or absence of NPD938. Despite PKS-NRPS knockout, the Δ*luc5* strain was able to convert NG391 into **1**, only in the presence of NPD938, in a concentration-dependent manner (Fig. 12), however it failed to convert lucilactaene into compound **2** (data not shown). This proves that the KR domain is not involved in the reduction process and suggests that NPD938 may activate another enzyme to reduce the C-12 position in NG391/393 into the corresponding alcohols. No predicted functional protein could be observed within *luc* gene cluster to catalyze this reduction step, so this NPD938-activated enzyme probably located outside the lucilactaene gene cluster. This

data also suggests that the relative stereochemistry of C-13 and C-14 positions in (1) is

similar to that reported for NG391 [104].
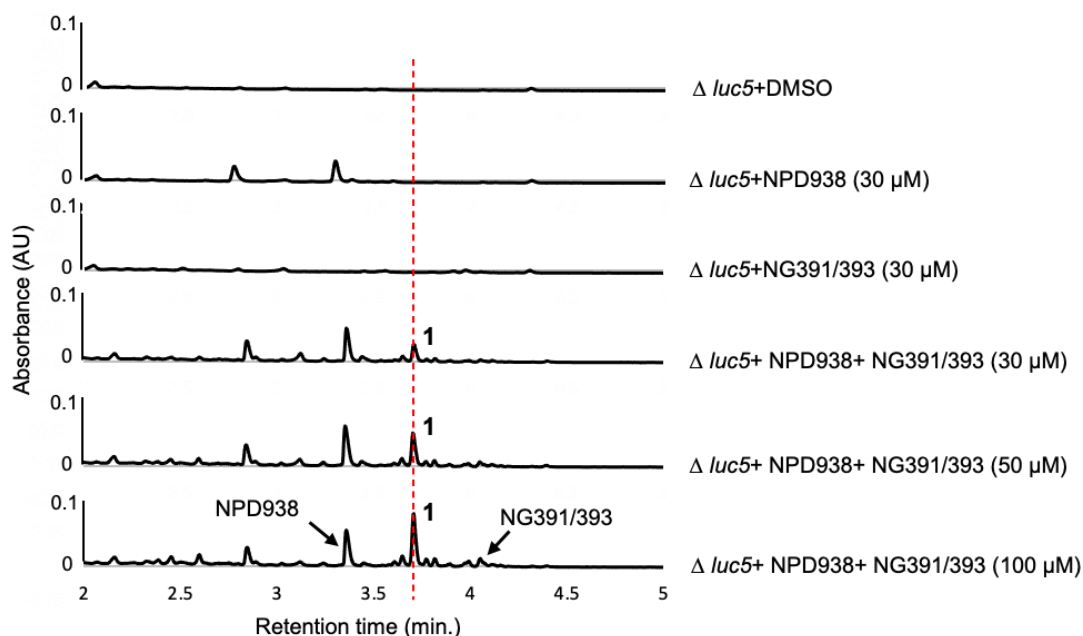


**Fig. 12.** UPLC chromatograms (at λ 320 nm) of Δ*luc5* strains treated with NG391/393 (30, 50, 100 µM) in the presence or absence of NPD938 (30 µM). Results indicate the induction of dihydroNG391 (**1**) only in the presence of NPD938, suggesting indirect enzymatic reduction of NG391/393 by another enzyme that was induced by NPD938.

## 6. Antimalarial activity

In a recently published article authored by our group, we reported that lucilactaene is

an effective antimalarial compound *in vitro* ($IC_{50} = 0.16$ µM), about 12 times more potent

than NG391 ($IC_{50} = 1.8$ µM), indicating that the tetrahydrofuran ring is important for

activity and its opening, similar to NG391/393, might be the cause of this marked

decrease in potency [99]. Therefore, compounds **1–3** were subjected to *in vitro*

antimalarial activity screening. Dihydrolucilactaene (**2**) displayed extremely potent

activity against wild-type (3D7) and chloroquine-resistant (K1) *P. falciparum* growth

($IC_{50}$ = 0.0015 µM for both 3D7 and K1), suggesting a different mode of action than

chloroquine. 13α-hydroxylucilactaene (**3**) showed strong but less potent activity than **2**,

with an $IC_{50}$ of 0.67 µM. DihydroNG391 (**1**) exhibited weak antimalarial activity ($IC_{50}$ =

62.1 µM) (Table 2). Based on these novel observations, along with previously reported

data [99], we provided insight into the structure-activity relationship of lucilactaenes as

promising antimalarial lead compounds.

## 7.   **Structure-activity relationship of lucilactaenes as antimalarial lead compounds**.

Thus far, only three lucilactaene analogues have been assayed against *P. falciparum*

[99]. Compounds **1–3** identified in this study enabled us to elucidate the important

features of the structure-activity relationship for lucilactaenes as antimalarial lead

compounds. Removal of the epoxide ring from NG391 to obtain **2** resulted in a 1200-fold

increase of antimalarial activity, suggesting that this epoxide ring is extremely detrimental

for activity (Fig. 13). Previous studies assumed that the fused tetrahydrofuran and

pyrrolidone rings in lucilactaene are important for activity [99]; However, opening of the

tetrahydrofuran ring to form **2** resulted in a 100-fold increase of activity, confirming that

the tetrahydrofuran ring is not more important for activity than the intact pyrrolidone ring

and removal of epoxide. This was supported by 13α-hydroxylucilactaene (**3**) data, in which an intact tetrahydrofuran ring is present but hydroxylation at C-13 resulted in a 4-fold decrease in activity. This means that C-13 and C-14 positions of pyrrolidone ring are essential for activity, and epoxidation or hydroxylation at these centers markedly decreases antimalarial activity. Furthermore, reduction of the C-12 carbonyl group of NG391/393 to its corresponding alcohol in **1** resulted in a 34-fold decrease in antimalarial activity. Finally, demethylation of the lucilactaene methyl ester and formation of the free carboxylic acid group resulted in a ca 300-fold decrease in activity that might be attributable to the increased polarity that hinders its intracellular accumulation to a sufficient extent, for producing antimalarial activity.



Lucilactaene
$IC_{50}$ 0.15 μM
*$IC_{50}$ 17.4 μM

Dihydrolucilactaene (**2**)
$IC_{50}$ 0.0015 μM
*$IC_{50}$ 37.7 μM

NG391
$IC_{50}$ 1.8 μM
*$IC_{50}$ 15.8 μM

13α-hydroxylucilactaene (**3**)
$IC_{50}$ 0.67 μM
*$IC_{50}$ > 70 μM

Demethyllucilactaene
$IC_{50}$ 43.9 μM
*$IC_{50}$ > 70 μM

DihydroNG391 (**1**)
$IC_{50}$ 62.1 μM
*$IC_{50}$ > 70 μM
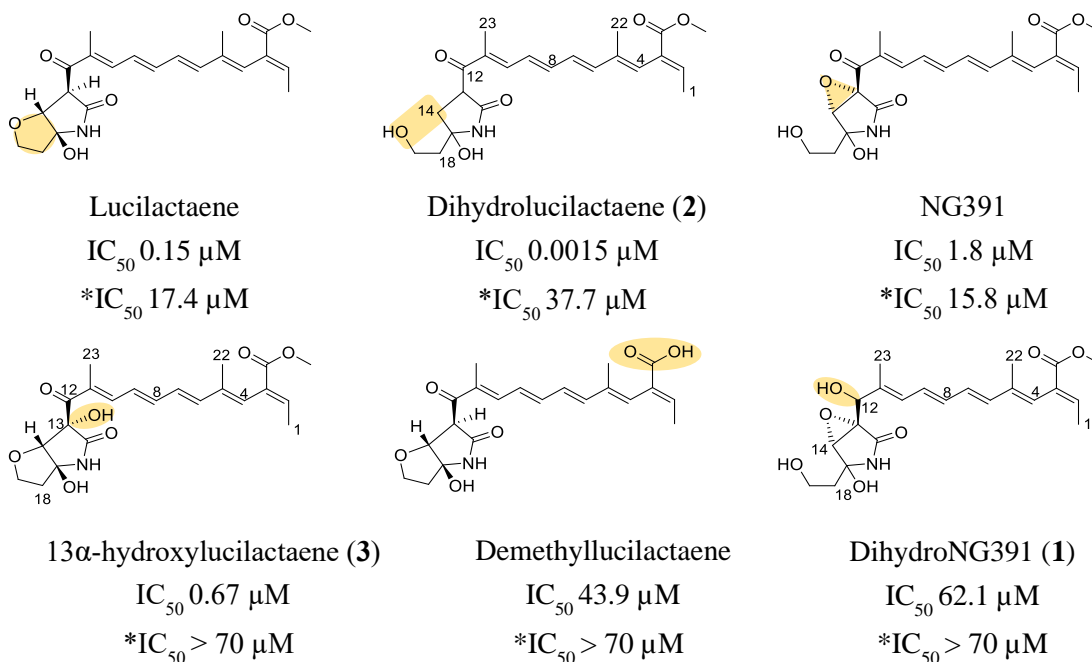
**Fig. 13.** Structure-activity relationship of lucilactaene and its derivatives as potential antimalarial lead compounds showing its weak cytotoxicity profile (*$IC_{50}$). Highlighting indicates altered positions from another derivative that responsible for increase or decrease in antimalarial activity ($IC_{50}$).

## 8.   Other biological activities

The previously reported cytotoxicity of lucilactaene also motivated us to screen compounds **1–3** against different cell lines (HeLa, HL-60, MKN74, and T98G) [98, 99]. Compounds **1** and **3** exhibited no cytotoxic activity at concentrations up to 70 µM. However, dihydrolucilactaene (**2**) exhibited weak cytotoxic activity against HeLa and HL-60 cells ($IC_{50}$ of 21 and 37 µM, respectively), (Table 2). This demonstrates a high selectivity of **2** against *P. falciparum* without marked cytotoxicity suggesting a promising drug candidate for malaria treatment.

The antibacterial activity against *S. aureus* and *E. coli*, and antifungal activity against *A. fumigatus*, *P. oryzae*, and *C. albicans*, were assessed. Dihydrolucilactaene (**2**) exhibited only weak inhibition of *P. oryzae* growth, with an $IC_{50}$ value of 6.7 µM. However, dihydroNG391 (**1**) exhibited no biological activity against any of the tested strains, at concentrations of up to 70 µM (Table 2).

**Table 2.** Growth inhibitory concentrations (IC$_{50}$, µM) of **1-3**, compared with those reported for lucilactaene derivatives [99].

| Type | Cell line/ Strain | 1 | 2 | 3 | Lucilactaene | NG391 | Demethyl lucilactaene | Positive controls |
|---|---|---|---|---|---|---|---|---|
| Cancer cells | HeLa | >70 | 21.5 | >70 | 24.9 | 14.1 | >70 | 4.3 |
| | HL60 | >70 | 37.7 | >70 | 17.4 | 15.8 | >70 | 2.2 |
| | MKN74 | >70 | >70 | NA | NA | NA | NA | |
| | T98G | >70 | >70 | NA | NA | NA | NA | 8.7 |
| Bacteria | *Staphylococcus aureus* | >70 | >70 | NA | >70 | >70 | >70 | 5.4 |
| | *Escherichia coli* | >70 | >70 | NA | >70 | >70 | >70 | 4.6 |
| Fungi | *Aspergillus fumigatus* | >70 | >70 | NA | >70 | >70 | >70 | 0.21 |
| | *Pyricularia oryzae* | >70 | 6.7 | NA | >70 | >70 | >70 | 0.16 |
| | *Candida albicans* | >70 | >70 | NA | >70 | >70 | >70 | 0.03 |
| *Plasmodium falciparum* | 3D7 (WT) | 62.1 | 0.0015 | 0.67 | 0.15 | 1.8 | 43.9 | 0.019 |
| | K1 (Chloroquine resistant) | NA | 0.0015 | NA | NA | NA | NA | NA |

Positive controls: paclitaxel (nM) for HeLa and HL-60; chloramphenicol (µM) for *Staphylococcus aureus* & *Escherichia coli*; amphotericin B (µM) for *Candida albicans*; artemisinin (µM) for *Plasmodium falciparum*.

NA: not assayed

## 9. Conclusion

In this study, we sought to induce/alter secondary metabolites production in filamentous fungi using NPD938 in order to discover new bioactive natural products. We successfully purified and identified two new and one known lucilactaene derivatives from *Fusarium* sp. RK97-94 culture treated with NPD938. Of these compounds, only dihydroNG391 **(1)** was proved to be induced by NPD938 via an indirect reduction process catalyzed by an enzyme probably outside the lucilactaene gene cluster. Dihydrolucilactaene **(2)** exhibited extremely potent and selective antimalarial activity (IC$_{50}$ = 0.0015 µM). We also investigated the structure-activity relationships between six different lucilactaene derivatives as antimalarial lead compounds. Both epoxide and tetrahydrofuran rings are not necessary for antimalarial activity. In contrast, pyrrolidone ring seems to be important and is retained in compounds with strong activity as **2**, **3**, and lucilactaene. These insights may enable chemical synthesis of new derivatives with enhanced bioactivity and chemical stability in the future, highlighting the merit of chemical induction and/or alteration of microbial secondary metabolism, for activating a silent biosynthetic pathway or modifying an existing one to generate new bioactive drug candidates.

## 10. Material and Methods

### 10.1. General Experimental Procedures

Solvents and reagents of analytical quality were obtained from their commercial suppliers. LC/MS and MS/MS analyses were performed on a Waters UPLC H-Class system (Waters, Milford, MA, USA), connected to an AB Sciex API3200 by an ESI probe (AB Sciex, Framingham, MA, USA), on a Waters Acquity UPLC BEH $C_{18}$ column (1.7 μm, 2.1 mm i.d. × 50 mm) with an acetonitrile−0.05% aqueous formic acid gradient system. HRMS data was acquired using a Waters Vion IMS QTof system. Preparative HPLC was performed using a Waters 600E pump system with a Senshu Pak Pegasil ODS column (20 mm i.d. × 250 mm or 10 mm i.d. × 250 mm, 5 μm) (Senshu Scientific Co., Ltd, Tokyo, Japan). Optical rotations were determined with a HORIBA SEPA-300 high-sensitive polarimeter (HORIBA, Kyoto, Japan). The $^1$H-NMR data were acquired at 500 MHz and the $^{13}$C-NMR data were acquired at 125 MHz using a JEOL JNM-ECA-500 spectrometer (JEOL, Tokyo, Japan).

### 10.2. Fungal strains and culture conditions

*Fusarium* sp. RK97-94 [26], and a PKS-NRPS knockout strain (Δ*luc5*) [25] were used. To optimize culture conditions, strains were grown on six culture media including CYA medium [3.5% Czapek-Dox Broth (Difco Co.), 0.5% yeast extract, 0.0005% $CuSO_4$,

0.001% ZnSO$_4$•7H$_2$O], YES medium (2% yeast extract, 15% sucrose, 0.05% MgSO$_4$•7H$_2$O, 0.0005% CuSO$_4$, 0.001% ZnSO$_4$•7H$_2$O), FDY medium (1.5% glucose, 1.5% soluble starch, 1% corn steep liquor, 1% dried yeast, 0.3% malt extract, 0.03% MgSO$_4$•7H$_2$O, 0.1% KH$_2$PO$_4$, 0.1% agar, pH 6.0), OM medium (6% oatmeal, 0.1% agar), YG media (0.5% yeast extract, 2% glucose) and PDB+0.1% agar medium [2.4% potato dextrose broth (Difco Co.), 0.1% agar], and screened compounds were compared against different NPD938 concentrations (3, 10, 30, 50, and 100 µM) for secondary metabolite induction within 4, 7, 10 and 14 d in a 24-well plate at 28 °C.

## 10.3. Extraction and LC-MS analysis

Each well was harvested using 2 mL ethanol, transferred to a centrifugation tube, and kept at a refrigerator overnight. The tubes were then centrifuged, and the supernatant was transferred to glass tubes and evaporated under nitrogen gas. The residues were dissolved in 200 µL MeOH and filtered using a 0.2 µm filter. Filtrates were analyzed via ultra-performance liquid chromatography (UPLC)/mass spectrometry (MS) using a Waters Acquity UPLC H-Class system (Waters, Milford, MA, USA) equipped with a mass spectrometer (API 3200, Applied Biosystems). A reversed-phase column (BEH C18, 2.1 × 50 mm, 1.7 µm, Waters) was used at a flow rate of 0.6 mL/min. Two gradient systems were used as follows: first method, MeCN (solvent B) in 0.05% formic acid/H$_2$O (solvent

A), with 5 to 100% B from 0 to 3 min, 100% B from 3 to 5 min, and re-equilibration with

5% B from 5 to 6.5 min; second method, MeCN (solvent B) in 0.05% formic acid/$H_2O$

(solvent A), with 5 to 50% B from 0 to 4 min, 50 to 65% B from 4 to 5 min, 65 to 100%

B from 5 to 5.5 min, 100% B from 5.5 to 7 min, and re-equilibration with 5% B from 7

to 8.5 min. Conditions for MS included an ion spray voltage of 5.0 kV, a curtain gas

pressure of 15 psi, a nebulizer gas pressure of 40 psi, an auxiliary gas pressure of 50 psi,

and an ion source temperature of 400 °C.

## 10.4. Isolation of 1-3

Five liters of *Fusarium* sp. RK97-94 culture was prepared using twelve bottles of 2 L

flasks. Each flask contained ~ 425 mL culture (416 mL media + 8 mL fungal preculture

+ 400 µL of 30 mM NPD938) and was statically incubated for 10 d at 28 °C (Fig. S4).

Flasks were extracted with equal volumes of acetone overnight, followed by filtration and

evaporation of the acetone layer. The aqueous phase was then partitioned three times with

a similar volume of anhydrous EtOAc, followed by evaporation of the EtOAc to yield a

dark reddish brown oily residue of 2.77 g. This extract was subjected to fractionation via

normal-phase MPLC (RediSep Rf Gold® Silica Gel disposable flash columns, Teledyne

Isco, U.S., 40 g) using a gradient elution of hexane (solvent A) and EtOAc (solvent B) as

follows: 10% B for 3 CV, 20% B for 3 CV, 20–50% in 15 CV, 50–100% in 15 CV, and

washing with 100% EtOAc (3 CV) and 100% MeOH (5 CV) (Fig. S5). MPLC fraction

tubes 64–72 were gathered (~400 mg), dissolved in 5 mL MeOH, and further fractionated

into four subfractions (I, II, III, and IV) via preparative high-performance liquid

chromatography (Fig. S3) using a reversed-phase column (PEGASIL ODS, $20 \times 250$ mm,

5 µm, Senshu Scientific Co. Ltd., Tokyo, Japan): mobile phase, A (0.05% formic acid in

$H_2O$), B (MeCN); gradient elution, B 40 to 60% (0 to 40 min), B 60 to 100% (40 to 50

min), B 100% (50 to 60 min); flow rate of 9 mL/min. Compound **1** accumulated in

subfraction I (52 mg), which was subjected to open silica column ($150 \times 25$ mm, 60 µm

and ~ 2.5 mL/min flow rate) using a gradient elution of chloroform and methanol (0, 2.5,

5, 10, 50% MeOH), followed by semi-preparative RP-HPLC (PEGASIL ODS, $10 \times 250$

mm, 5 µm, isocratic elution, 35% MeCN in water and 4 mL/min flow rate) to afford 3.5

mg of **(1)**. Compound **2** (2.7 mg) was purified from subfraction IV (32.5 mg) via

preparative RP-HPLC (PEGASIL ODS, $20 \times 250$ mm, 5 µM, Senshu Scientific Co. Ltd.,

Tokyo, Japan) using an isocratic elution of 55% MeCN in water at a flow rate of 8 mL/min.

Compound **3** (8.5 mg) was purified from subfraction II (26.5 mg) via preparative RP-

HPLC [mobile phase, A ($H_2O$), B (MeCN); gradient elution, B 40 to 60% (0 to 40 min),

B 60 to 100% (40 to 50 min), B 100% (50 to 60 min); flow rate of 8 mL/min].

**DihydroNG391 (1):** Yellow amorphous powder, $[\alpha]_D^{24}$ -7 (*c* 0.02, MeOH); LC-UV [MeCN-H$_2$O (0.05% HCOOH)] $\lambda_{max}$ 324 nm; IR: 3320, 2917, 2360, 2330, 1633 and 1540 cm$^{-1}$. $^1$H and $^{13}$C NMR data, see Table 1; HR-ESI-TOF/MS found *m/z* 418.1851 [M-H]$^-$ calculated for 418.1871 (C$_{22}$H$_{29}$NO$_7$).

**Dihydrolucilactaene (2):** Yellow amorphous powder, $[\alpha]_D^{24}$ +30 (*c* 0.02, MeOH); LC-UV [MeCN-H$_2$O (0.05% HCOOH)] $\lambda_{max}$ 368 nm; IR: 3384, 3010, 2921, 1635, 1436, 1014 and 948 cm$^{-1}$. $^1$H and $^{13}$C NMR data, see Table 1; HR-ESI-TOF/MS found *m/z* 402.1914 [M-H]$^-$ calculated for 402.1922 (C$_{22}$H$_{29}$NO$_6$).

**13α-hydroxylucilactaene (3):** Yellow amorphous powder, $[\alpha]_D^{24}$ -116 (*c* 0.11, MeOH); LC-UV [MeCN-H$_2$O (0.05% HCOOH)] $\lambda_{max}$ 360 nm; IR: 3259, 3031, 2950, 2360, 2339, 1698, 1243, 1043 and 989 cm$^{-1}$. $^1$H and $^{13}$C NMR data, see Table S1; HR-ESI-TOF/MS found *m/z* 418.1857 [M+H]$^+$ calculated for 418.1860 (C$_{22}$H$_{27}$NO$_7$).

**10.5. Cytotoxic, antimalarial, and antimicrobial activity tests**

The *in vitro* cytotoxicity assay method used herein has been previously described [105]. The antimalarial and antimicrobial assays against *Plasmodium falciparum* 3D7 and K1, *Staphylococcus aureus* 209, *Escherichia coli* HO141, *Aspergillus fumigatus* Af293, *Pyricularia oryzae* kita-1, and *Candida albicans* JCM1542 were also described in the previous report [106].

## Chapter 3

## Isolation of new lucilactaene derivatives from P450 monooxygenase and aldehyde dehydrogenase knockout *Fusarium* sp. RK97-94 strains and their biological activities

In this chapter we aimed at the isolation, identification and bioactivity evaluation of new lucilactaene derivatives from P450 monooxygenase and aldehyde dehydrogenase knockout strains Δ*luc2* and Δ*luc3,* respectively. We have succeeded to isolate prelucilactaene G (**4**), and prelucilactaene H (**5**) from the aldehyde dehydrogenase knockout strain (Δ*luc3*) culture broth, as well as prelucilactaene A (**6**), prelucilactaene B (**7**), and two isomeric mixtures of prelucilactaene E (**8**) and prelucilactaene F (**9**), from the P450 monooxygenase knockout strain (Δ*luc2*) culture broth. Our data suggest the involvement of the aldehyde dehydrogenase (Luc3) in lucilactaene biosynthesis, and support the involvement of the P450 monooxygenase (Luc2) in C-20 hydroxylation rather than C-13 – C-14 epoxidation or C-15 hydroxylation. Isolated compounds displayed moderate to strong antimalarial activities, and the structure-activity relationship of lucilactaene derivatives was examined.

## 1. Introduction

*Fusarium* sp. RK97-94 has been identified as a producing strain of lucilactaene and NG391. Lucilactaene was initially obtained from the same strain as a potent cell cycle inhibitor [98], whereas NG391 was initially isolated as a neuroprotective compound from *Fusarium* sp. TF-0452 [27]. Due to their novel structures and bioactivities, these molecules have sparked considerable interest in terms of biosynthetic research and total chemical synthesis [99,104,107,108].

More recently, we found that lucilactaene and NG391 demonstrated potent *in vitro* antimalarial activity ($IC_{50}$ 0.15 and 1.8 µM, respectively) [99]. In addition, chemical induction of secondary metabolism in *Fusarium* sp. RK97-94 resulted in the isolation of new lucilactaene derivatives, the most potent of which was dihydrolucilactaene ($IC_{50}$ 1.5 nM) [109]. The tetrahydrofuran ring was initially thought to be essential for lucilactaene's antimalarial activity. However, opening this tetrahydrofuran ring resulted in a 100-fold increase in antimalarial activity [109]. Furthermore, removing the epoxide from NG391 to form dihydrolucilactaene resulted in a 1200-fold increase in activity [109]. This research suggests that lucilactaene and its derivatives could be promising lead compounds for antimalarial drug development.

Despite their remarkable bioactivities, the biosynthesis of lucilactaene remains largely unknown. So far, the biosynthetic gene cluster of lucilactaene and NG391 has been recently discovered (Fig. S32) [99]. It harbors eight biosynthetic genes that are closely related to those in the gene cluster of fusarin C/A, the structural analogs of NG391 / lucilactaene, respectively [99]. One of these genes, *luc5*, encodes a PKS-NRPS, showed high similarity to *fus1*, and is involved in the formation of the core structure of lucilactaene and NG391 [110]. A similar product in *Fusarium fujikuroi*, prefusarin, was speculated based on LC-MS/MS analysis to be the Fus1 release product in fusarin C/A biosynthesis [110]. On the other hand, *luc1*, encodes a methyltransferase, is a homologue of *fus9*. *luc1* and *fus9* were proved to be involved in the final methylation step of the C-20 carboxyl derivatives into lucilactaene and fusarin C/A, respectively [99,110–112]. *Luc4*, *luc7*, and *luc8* encode a transporter, an elongation factor, and a protease, respectively, which are not commonly involved in the biosynthesis of secondary metabolites. Homologues of these genes (*fus6, fus3,* and *fus4,* respectively) were also reported to be not essential in the fusarin C biosynthesis [110]. Thus, we hypothesized that *luc2*, *luc3*, and *luc6* encoding a P450 monooxygenase, an aldehyde dehydrogenase, and a putative α/ß hydrolase, respectively, could be involved in the biosynthesis of lucilactaene and NG391. Individual disruption of these genes has the potential not only

to produce new lucilactaene derivatives with potent antimalarial activity, but also to uncover the secrets behind NG391 / lucilactaene biosynthesis. In this study, culturing of two mutants *Fusarium* sp. RK97-94 strains (Δ*luc2* and Δ*luc3*) has resulted in identification of several lucilactaene derivatives (Fig. 14), with moderate to strong antimalarial activity.
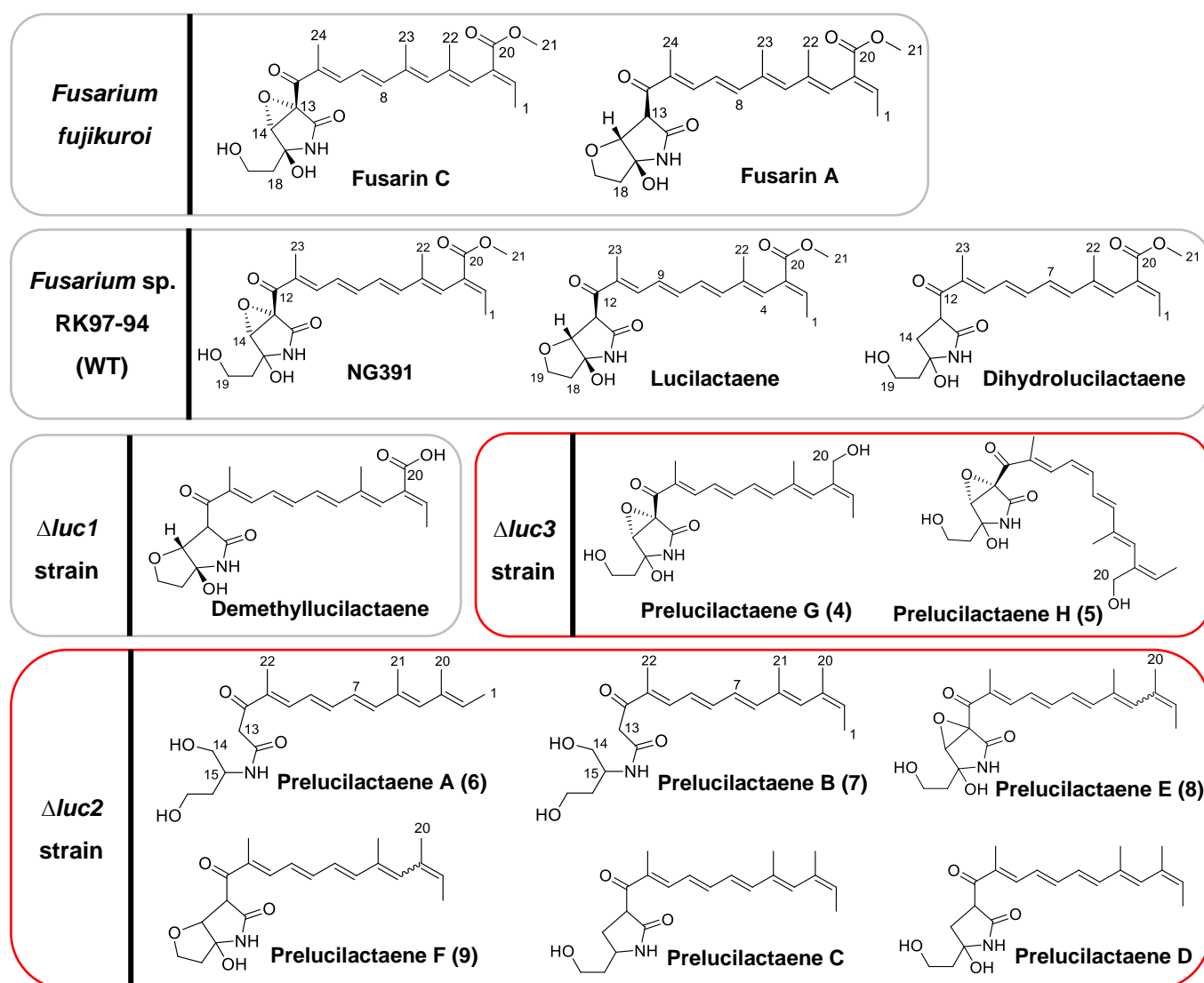


**Fig. 14.** Known and newly identified lucilactaene derivatives sorted by producing strain.

## 2. Results and Discussion

### 2.1. LC-MS analysis of *Δluc2* and *Δluc3* strains' cultures

Culture broths of the aldehyde dehydrogenase (Luc3) and P450 monooxygenase (Luc2) knockout strains (Δluc3 and Δluc2, respectively) were extracted and analyzed by LC-MS to detect any possible biosynthetic intermediates. Both Δluc2 and Δluc3 strains failed to produce lucilactaene and/or NG391, which confirms the involvement of *luc3* and *luc2* gene-products in lucilactaene and NG391 biosynthesis. This was not the case in fusarin C biosynthesis in *Fusarium fujikuroi*, in which *fus7*, a homologue of *luc3*, was not essential for biosynthesis, and its knocking out had no effect on fusarin C production [110]. The Δluc3 strain produced a major metabolite at a retention time of 3.3 min with *m/z* 390 [M+H]$^+$ and UV absorption at $\lambda_{max}$ 382 nm (Fig. 15). This suggested a compound with a retained polyene skeleton, but with higher polarity than lucilactaene or NG391, possibly via converting the C-20 ester group into corresponding alcohol or acid. On the other hand, the Δluc2 strain accumulated several metabolites with a major one at a retention time of 4.7 min, with *m/z* 362 [M+H]$^+$, and UV absorption at $\lambda_{max}$ 380 nm (Fig. 15). This mass is matching with the predicted release product of the PKS-NRPS in lucilactaene / NG391 biosynthesis that consists of a heptaketide connected to homoserine amino acid. The minor peaks detected in Δluc2 culture extract displayed [M+H]$^+$ at *m/z*

344 (MW343), 358 (MW357), 360 (MW359), and 374 (MW373), suggesting possible biosynthetic intermediates of lucilactaene / NG391 (Fig. 15). Knocking out the homologous gene in fusarin C gene cluster, *fus8*, has produced similar structural analogs that were speculated by LC-MS/MS analysis only [110]. Interestingly, this mass is matching our speculation to be the early release product of the PKS-NRPS in lucilactaene / NG391 biosynthesis that consists of a heptaketide connected to homoserine amino acid. On the other hand, Δ*luc3* produced another major metabolite at 3.3 min with expected [M+H]$^+$ 390.3 *m/z* and UV$_{max}$ 382 nm (Fig. 15). MPLC fractionation followed by HPLC purification were used to isolate the target metabolites **4**-**9** (Fig. S33 and Fig. S34), that were elucidated by NMR and mass spectrometry.
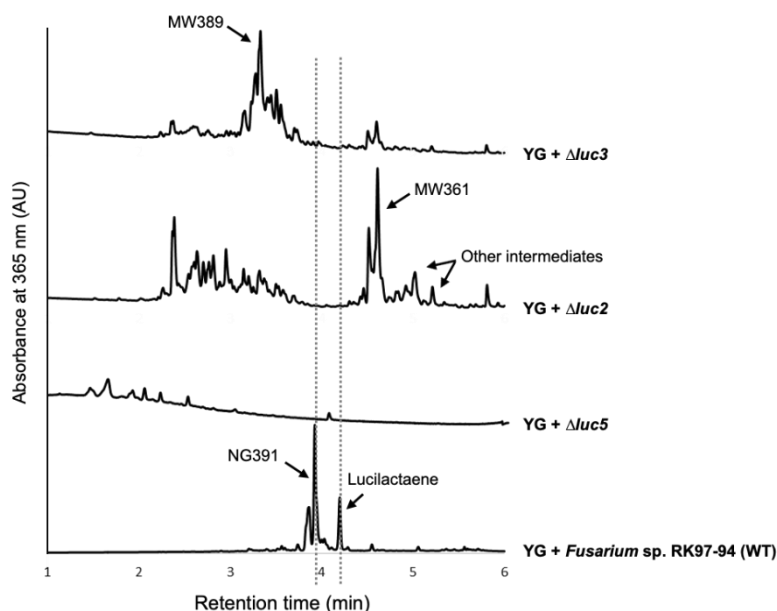


**Fig. 15.** Metabolic profiling of culture broths extracts of PKS-NRPS (Δ*luc5*), P450 monooxygenase (Δ*luc2*), and aldehyde dehydrogenase (Δ*luc3*) knockout strains in comparison with *Fusarium* sp. RK97-94 (WT). Both Δ*luc2* and Δ*luc3* strains failed to produce final products lucilactaene or NG391, however, they accumulated MW361 and MW389 intermediates, respectively.

## 2.2. Structure elucidation of isolated compounds 4-9

Compound **4** was isolated as yellow amorphous powder upon freeze drying. It displayed a molecular formula of $C_{21}H_{27}NO_6$ as determined by HR-ESI-TOF/MS (found $m/z$ 388.1763 $[M - H]^-$, calculated for $C_{21}H_{26}NO_6$, 388.1766) (Fig. S35). The IR spectrum implied the presence of hydroxyl (3410 cm$^{-1}$) and carbonyl groups (1698 and 1716 cm$^{-1}$) (Fig. S36). This compound carries nine double bond equivalents (DBE), compared with eight DBEs detected in NG391 / lucilactaene. $^1$H-NMR showed seven olefinic proton signals ranging from $\delta_H$ 5.69 to 7.47; three shielded methyl signals at $\delta_H$ 1.57 (d, $J$ = 6.87 Hz), 1.80 (s), 1.95 (s); one methine signal at $\delta_H$ 4.13, (s), and three methylene signals at $\delta_H$ 2.00 (m), 3.84 (m), and 4.02 (s) (Table 3, Fig. S37-S43). This spectroscopic pattern was highly comparable with that of NG391/393 [102], with few key structural differences. The main differences in $^1$H-NMR spectrum of **4** were the disappearance of the methyl ester protons signal, the appearance of a proton signal at $\delta_H$ 4.02 (2H, s, H-20) due to a hydroxylated methylene group, and the upfield shift of H-2 at $\delta_H$ 5.69 (1H, q, $J$ = 6.87 Hz). $^{13}$C-NMR data revealed the presence of only two carbonyl signals at $\delta_C$ 191.7 and 172.4, assigned for C-12 and C-17, respectively, and the disappearance of the 3$^{rd}$ carbonyl signal of the ester group at C-20, usually present in NG391. This supported the nine DBE observed after analysis of the HR-ESI-TOF/MS

data compared to the ten DBE observed in NG391/393. DEPT-135 data revealed the presence of three methylene groups at $\delta_C$ 38.6 (C-18), 58.3 (C-19), and new signal at $\delta_C$ 67.0 suggesting the C-20 functionality has been changed from $COOCH_3$ into $CH_2OH$. HMBC correlations from H-2 to $\delta_C$ 67.1 (C-20), $\delta_C$ 132.8 (C-4), and from H-20 to $\delta_C$ 139.2 (C-3), 132.8 (C-4) confirmed the $CH_2OH$ substitution at C-3. Detailed COSY, HSQC, and HMBC data confirmed the presence of a pentaene skeleton attached to the substituted pyrrolidone ring in similar way to NG391 (Fig. 16). Large coupling constant values of 14.89 Hz between $J_{H6-H7}$ and $J_{H8-H9}$ combined with strong NOESY correlations between H-9 and H-22, H-4 and H-6, and H-7 and H-21 indicated an *E* configuration of the polyene skeleton and identify the compound as 20-hydroxyNG391 derivative, named prelucilactaene G (**4**) (Fig. 16). Compound **5** had the identical molecular formula calculated by HR-ESI-TOF/MS to that of **4** (Fig. S44), IR data (Fig. S45), and similar ^{1}H and ^{13}C NMR spectra, except for the chemical shifts of the polyene protons from H-7 to H-10 and their corresponding ^{13}C signals (Table 3, Fig. S46-S52). Relatively small coupling constant value of 11.45 Hz between $J_{H8-H9}$ combined with strong NOESY correlation between H-7 and H-10, and H-8 and H-9 indicate a *Z* configuration of the polyene skeleton at C-8 and identify the compound as 20-hydroxyNG393 derivative, named prelucilactaene H (**5**) (Fig. 16). Compounds **4** and **5** were previously isolated by

another group as a mixture [100], and this is the first report for its single isomer

purification.

**Table 3.** NMR spectroscopic data of **4** and **5** (CD$_3$OD, $^1$H 500 MHz, $^{13}$C 125 MHz).

| | Prelucilactaene G (4) | | | Prelucilactaene H (5) | | |
|---|---|---|---|---|---|---|
| **No.** | $\delta_C$, type | $\delta_H$ (Multiplicity, $J$ Hz) | HMBC | $\delta_C$, type | $\delta_H$ (Multiplicity, $J$ Hz) | HMBC |
| 1 | 15.3, CH$_3$ | 1.57, d (6.87) | 2, 3 | 15.3, CH$_3$ | 1.58, dd (6.87, 1.15) | 2, 3 |
| 2 | 125.1, CH | 5.69, q (6.87) | 1, 4, 20 | 124.4, CH | 5.69, q (6.87) | 1, 4, 20 |
| 3 | 139.2, C | - | | 139.2, C | - | |
| 4 | 132.8, CH | 6.11, brs | 2, 6, 21 | 132.7, CH | 6.11, brs | 2, 6, 21 |
| 5 | 138.5, C | - | | 139.0, C | - | |
| 6 | 144.0, CH | 6.64, d (14.89) | 4, 7, 8, 21 | 144.7, CH | 6.61, d (14.89) | 4, 8, 21 |
| 7 | 129.1, CH | 6.52, dd (10.31, 14.89) | 5 | 125.0, CH | 7.02, dd (12.03, 14.89) | 5 |
| 8 | 145.0, CH | 6.81, dd (10.31, 14,89) | 7, 10 | 141.1, CH | 6.57, dd (11.45) | 6, 10 |
| 9 | 128.6, CH | 6.75, dd (10.31, 14.32) | 7 | 124.2, CH | 6.42, dd (11.45, 10.88) | 7 |
| 10 | 146.1, CH | 7.47, d (10.31) | 8, 12, 22 | 139.8, CH | 7.94, d (12.03) | 12, 22 |
| 11 | 134.6, C | - | | 135.0, C | - | |
| 12 | 191.7, C | - | | 191.8, C | - | |
| 13 | 63.7, C | - | | 63.6, C | - | |
| 14 | 65.3, CH | 4.13, s | 15 | 65.5, CH | 4.21, s | 15 |
| 15 | 85.9, C | - | | 86.4, C | - | |
| 16 (NH) | - | - | | - | - | |
| 17 | 172.4, C | - | | 172.6, C | - | |
| 18 | 38.6, CH$_2$ | 2.00, m | 15, 19 | 38.3, CH$_2$ | 2.05, m | 15, 19 |
| 19a | 58.4, CH$_2$ | 3.84, m | 15 | 58.5, CH$_2$ | 3.85, m | 15 |
| 19b | 58.4, CH$_2$ | 3.84, m | 15 | 58.5, CH$_2$ | 3.85, m | 15 |
| 20 | 67.1, CH$_2$ | 4.02, s | 2, 3, 4 | 67.1, CH$_2$ | 4.02, s | 2, 3, 4 |
| 21 | 14.5, CH$_3$ | 1.80, s | 4, 5, 6 | 15.0, CH$_3$ | 1.85, d (1.15) | 4, 5, 6 |
| 22 | 11.3, CH$_3$ | 1.95, s | 10, 11, 12 | 11.0, CH$_3$ | 1.95, s | 10, 11, 12 |

Compound **6** was also isolated as yellow amorphous powder upon freeze drying, with UV absorption at $\lambda_{max}$ 380 nm, and a molecular formula of $C_{21}H_{31}NO_4$ as determined by HR-ESI-TOF/MS analysis (found: *m/z* 360.2167 [M-H]$^-$, calculated for $C_{21}H_{30}NO_4$, 360.2180) (Fig. S53). IR data indicated the presence of hydroxyl and carbonyl groups (Fig. S54). This compound carries three DBEs less than that in lucilactaene or NG391. These data are consistent with the predicted structure of the early PKS-NRPS release product consisting of a heptaketide skeleton attached to homoserine amino acid without cyclization. To confirm this structure, compound **6** was subjected to extensive 1D and 2D-NMR analysis (Table 4, Fig. S55-S62). $^1$H-NMR displayed the characteristic pattern of the pentaene skeleton of lucilactaene and NG391, however the substituted pyrrolidone signals were different. $^{13}$C-NMR and DEPT135 suggested the presence of four $CH_3$ groups, four $CH_2$, and two carbonyl groups. The fourth methyl group newly detected in this structure appeared at $\delta_C$ 16.5 and assigned for the C-20 which usually converted to carboxymethyl ester ($COOCH_3$) in later steps in lucilactaene and NGs biosynthesis. The two additional methylene groups were detected at $\delta_C$ 44.2 and 65.2, assigned for C-13 and C-14, respectively, which confirm the de-epoxidation and opening of the pyrrolidone ring at C13-C14 linkage. This was furtherly confirmed by the strong HMBC correlation from H-13 at $\delta_H$ 3.72 to both carbons of the carbonyl groups at C-12 and C-17. The

connection of the carbon skeleton of homoserine moiety was confirmed by COSY and HSQC (Fig. 16). Large coupling constant values of 14.89 Hz between $J_{H6-H7}$ and $J_{H8-H9}$ combined with strong NOESY correlation between H-9 and H-22, H-4 and H-6, and H-7 and H-21 indicate an *E* configuration of the polyene skeleton and identify the compound as prelucilactaene A (**6**) (Fig. 16). Compound **7** had the identical molecular formula calculated by HR-ESI-TOF/MS to that of **6** (Fig. S63), IR data (Fig. S64), and matched NMR data except for the chemical shifts form H-1 to H-4 and their corresponding $^{13}$C signals as well as in C-20 chemical shift (Table 4, Fig. S65-S71), indicating that the difference between these two isomers should be at the level of the first double bond of the polyene skeleton. This was confirmed by the chemical shift of C-20 ($\delta_C$ 23.6) in **7** compared with the corresponding carbon in **6** at $\delta_C$ 16.5, indicating a 2Z configuration of **7** which named prelucilactaene B (Fig. 16).

**Table 4.** NMR spectroscopic data of **6** and **7** (CDCl$_3$, $^1$H 500 MHz, $^{13}$C 125 MHz).

| No. | Prelucilactaene A (6) $\delta_C$, Type | $\delta_H$ (Multiplicity, $J$ Hz) | HMBC | Prelucilactaene B (7) $\delta_C$, Type | $\delta_H$ (Multiplicity, $J$ Hz) | HMBC |
|---|---|---|---|---|---|---|
| 1 | 13.9, CH$_3$ | 1.74, d (6.87) | 2,3 | 15.1, CH$_3$ | 1.54, d (6.87) | 2, 3 |
| 2 | 128.3, CH | 5.58, q (6.87) | 20 | 124.5, CH | 5.43, q (6.87) | 20 |
| 3 | 133.8, C | - | | 133.2, C | - | |
| 4 | 140.0, CH | 6.10, brs | 2, 6, 21 | 134.9, CH | 6.11, brs | 2, 6, 21 |
| 5 | 132.5, C | - | | 134.7, C | - | |
| 6 | 144.7, CH | 6.51, d (14.89) | 4, 7, 8, 21 | 143.4, CH | 6.56, d (15.46) | 4, 8, 21 |
| 7 | 126.6, CH | 6.35, dd (10.31, 14.89) | 6 | 127.0, CH | 6.38, dd (10.88, 14.89) | 6 |
| 8 | 143.3, CH | 6.71, dd (11.45, 14,89) | 10 | 143.0, CH | 6.72, dd (10.88, 14.32) | 7, 9, 10 |
| 9 | 126.7, CH | 6.58, dd (10.88, 14.32) | 8 | 127.0, CH | 6.60, dd (11.45, 14.32) | 11 |
| 10 | 142.1, CH | 7.22, d (11.45) | 12, 22 | 141.9, CH | 7.23, d (11.45) | 8, 22 |
| 11 | 134.0, C | - | | 134.3, C | - | |
| 12 | 196.3, C | - | | 196.4, C | - | |
| 13 | 44.2, CH$_2$ | 3.72, s | 12, 17 | 44.2, CH$_2$ | 3.73, s | 12, 17 |
| 14 | 65.2, CH$_2$ | 3.68, m | | 65.2, CH$_2$ | 3.70, m | 15 |
| 15 | 48.9, CH | 4.18, m | | 48.9, CH | 4.18, m | 14 |
| 16 (NH) | - | 7.38, d (7.44) | | - | 7.38, (6.87) | |
| 17 | 167.9, C | - | | 167.9, C | - | |
| 18a | 34.3, CH$_2$ | 1.67, m | | 34.3, CH$_2$ | 1.67, m | |
| 18b | 34.4, CH$_2$ | 1.85, m | | 34.3, CH$_2$ | 1.84, m | |
| 19 | 58.7, CH$_2$ | 3.61, m | 15 | 58.7, CH$_2$ | 3.60, m | |
| 20 | 16.5, CH$_3$ | 1.83, s | 2, 3, 4 | 23.6, CH$_3$ | 1.82, s | 2, 3 |
| 21 | 14.1, CH$_3$ | 1.97, s | 4, 5 | 14.0, CH$_3$ | 1.80, s | 5, 6 |
| 22 | 11.6, CH$_3$ | 1.93, s | 10, 11, 12 | 11.6, CH$_3$ | 1.93, s | 10, 11, 12 |

Compound **8** was isolated as an isomeric mixture, giving yellow amorphous powder upon freeze drying. The molecular formula was determined by HR-ESI-TOF/MS analysis to be C$_{21}$H$_{27}$NO$_5$ (found: *m/z* 396.1781 [M+Na]$^+$, calculated for C$_{21}$H$_{27}$NO$_5$Na, 396.1787) (Fig. S72). IR data confirmed the presence of hydroxyl and carbonyl groups (Fig. S73).

This compound lacks an oxygen atom compared to **4**, but it retains equal unsaturation number which excluded ring opening or double bond reduction possibilities, suggesting that the $CH_2OH$ in **4** might be converted into $CH_3$. This was confirmed by NMR analysis of **8** (Table 5, Fig. S74-S80) that showed two methylene carbons only in DEPT NMR at $\delta_C$ 58.4 (C-19) and 38.6 (C-18), while missing the hydroxylated methylene carbon signal of C-20 usually appears at $\delta_C$ 67.1, which was replaced by a new methyl carbon signal at $\delta_C$ 16.8. Thus, the planar structure of **8** was identified as decarboxyNG391 derivative, named prelucilactaene E (Fig. 16). The *E* configuration of the polyene skeleton in one isomer was indicated by the strong NOESY correlations between H-9 and H-22, H-8 and H-10, H-7 and H-21, and H-4 and H-6 (Fig. S80). The *E/Z* isomerization at C-4 was confirmed by the difference in chemical shifts of C-21 ($\delta_C$ 20.9) in the *E*-isomer compared with the corresponding carbon in the *Z*-isomer at $\delta_C$ 14.5, respectively. The absolute stereochemistry of the epoxide ring in **8** was not determined, however it should be identical to NG391 final product because both compounds carry the same epoxidated 2-pyrrolidone ring moiety that is biosynthesized by the same enzyme, Luc6.

**Table 5.** NMR spectroscopic data of **8** (CDCl₃, ¹H 500 MHz, ¹³C 125 MHz).

| No. | Prelucilactaene E (8) | | |
|---|---|---|---|
| | $\delta_H$ (Multiplicity, J Hz) | $\delta_C$, Type | HMBC |
| 1 | 1.73, d (6.87) <br> 1.76, d (6.87) | 14.1, CH₃ <br> 16.6, CH₃ | 2, 3 |
| 2 | 5.57, q (6.87) <br> 5.43, q (6.87) | 128.2, CH <br> 127.9, CH | 1, 4 |
| 3 | - | 135.1, C <br> 134.7, C | |
| 4 | 6.11, s <br> 6.00, s | 140.9, CH <br> 138.6, CH | 2, 6, 21 |
| 5 | - | 134.0, C <br> 133.1, C | |
| 6 | 6.56, d (14.89) <br> 7.03, d (15.46) | 146.0, CH <br> 138.8, CH | 8, 21 |
| 7 | 6.46, m <br> 6.52, m | 128.3, CH <br> 129.9, CH | 5 |
| 8 | 6.80, m | 145.5, CH | 10 |
| 9 | 6.72, m <br> 6.77, m | 128.0, CH <br> 128.9, CH | 7 |
| 10 | 7.473, d (10.31) <br> 7.466, d (10.31) | 146.5, CH <br> 146.2, CH | 8, 12, 22 |
| 11 | - | 134.4, C <br> 134.1, C | |
| 12 | - | 191.6, C | |
| 13 | - | 63.7, C <br> 61.6, C | |
| 14 | 4.12, s <br> 4.13, s | 65.29, CH <br> 65.33, CH | 15, 17 |
| 15 | - | 85.9, C | |
| 16 (NH) | - | - | |
| 17 | - | 172.4, C | |
| 18 | 2.00, m | 38.6, CH₂ | 15, 19 |
| 19 | 3.83, m | 58.5, CH₂ | 15 |
| 20 | 1.82, s | 16.8, CH₃ | 2, 3, 4 |
| 21 | 1.92, s <br> 1.96, s | 20.9, CH₃ <br> 14.5, CH₃ | 4, 5, 6 |
| 22 | 1.94, s | 11.3, CH₃ | 10, 11, 12 |

Compound **9** (MW357) was obtained as an isomeric mixture, giving yellow amorphous powder after freeze drying. It displayed a high resolution mass of *m/z* 380.1837 [M+Na]⁺ calculated for C₂₁H₂₇NO₄Na, 380.1838 (Fig. S81). IR data implied

the presence of hydroxyl and carbonyl groups in the structure (Fig. S82). $^1$H-NMR data

displayed similar pattern of the furano-pyrrolidone ring detected in lucilactaene (Fig. S83).

Disappearance of the methyl proton's signal of the ester group and appearance of new

methyl signal at $\delta_H$ 1.82 suggested a decarboxylated lucilactaene derivative, which was

confirmed by $^1$H-$^1$H COSY, HSQC, and DEPT NMR analysis (Fig. S84-S86). The

structure elucidation was supported by MS/MS analysis which produced a product ion

peak at *m/z* 274.1062 calculated for $C_{13}H_{17}NO_4Na$, 274.1055, like that detected in

lucilactaene indicating similar furano-pyrriolidone ring structure (Fig. S87 and Fig. S89).

Detection of this fragment suggests a neutral loss of $[C_8H_{10}]$ proving that the polyene

skeleton is not oxygenated, and C-20 is a methyl group. Thus, the planar structure of **9**

was identified as prelucilactaene F (Fig. 16). Similar to compound **8**, The *E/Z*

isomerization at C-4 was confirmed by the difference in chemical shifts of C-21 ($\delta_C$ 20.8)

in the *E*-isomer compared with the corresponding carbon in the *Z*-isomer at $\delta_C$ 14.2,

respectively.
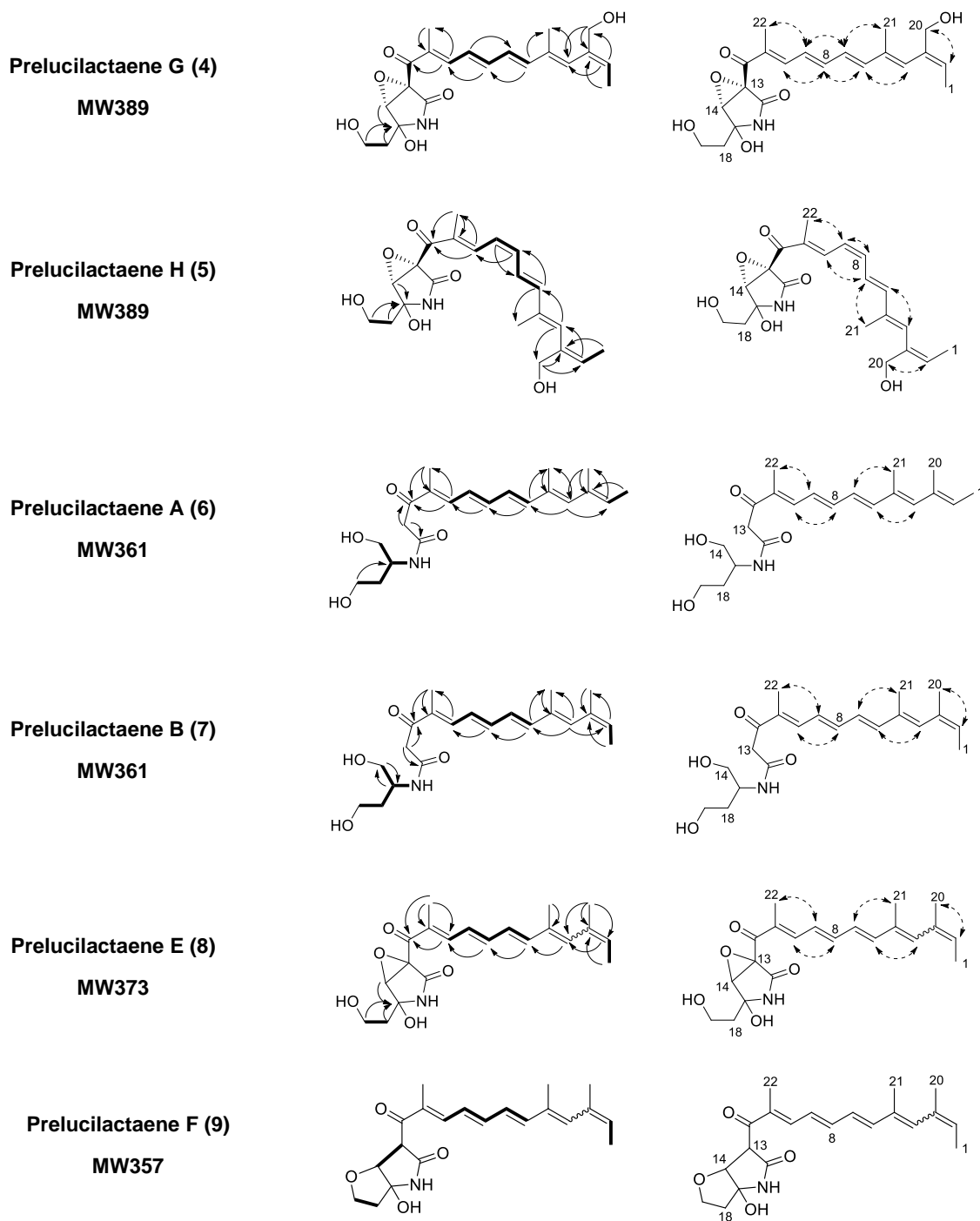
**Fig. 16.** Chemical structures of compounds **4-9** showing the 2D-NMR correlations.

COSY: bold line, HMBC: one sided arrows, NOESY: double sided arrows.

## 2.3. LC-MS/MS analysis of isolated compounds

The isolated compounds are structural analogues to fusarin C and its derivatives that were previously determined by LC-MS/MS based on the characteristic fragmentation pattern of the polyene skeleton (Fig. S88) [110]. Thus, all compounds including those with low amounts (MW343 and MW359), that couldn't be analyzed by NMR, were subjected to HR-LC-MS/MS analysis to support elucidating their structures. To validate this fragmentation pattern, additional five known lucilactaene derivatives were also subjected to LC-MS/MS and the reported fragmentation pattern was confirmed (Fig. S89-S93). Comparing the accurate mass of the sodium adduct of the isolated compounds and their product ion spectra with those of NG391 or lucilactaene could give evidence about C-20 substitution and the chemistry of the substituted pyrrolidone moiety. Thus, fragments of already identified or predicted structures were theoretically speculated based on the characteristic polyene fragmentation pattern reported [110], and compared with the corresponding experimental data (Fig. S94-S98). For instance, compound **4** displayed a high resolution mass of *m/z* 384.2182 [M+Na]$^+$ calculated for $C_{21}H_{31}NO_4Na$, 384.2151. This compound gave a product ion peak at *m/z* 278.1382 calculated for $C_{13}H_{21}NO_4Na$, 278.1368 (Fig. S95). This fragment has 4 DBEs that assigned for two carbonyls and two double bonds of the polyene skeleton, which confirm that the pyrrolidone and epoxide

rings must be opened. In addition, this data also suggests the neutral loss of $[C_8H_{10}]$ indicating that C-20 is a methyl group, and the polyene skeleton is devoid from any oxygenations. MW359 showed a product ion peak at *m/z* 276.1210 calculated for $C_{13}H_{19}NO_4Na$, 276.1212, like that detected in dihydrolucilactaene, suggesting a mono-hydroxylated 2-pyrrolidone ring structure (Fig. S90 and Fig. S98). However, MW343 displayed a product ion peak at *m/z* 260.1258 calculated for $C_{13}H_{19}NO_3Na$, 260.1263, suggesting a deoxy derivative of MW359 (Fig. S97). This data also suggested the neutral loss of $[C_8H_{10}]$ in both compounds, indicating polyene skeletons free from any oxygens. Thus, structures of these compounds were speculated and named as prelucilactaene C (MW343) and prelucilactaene D (MW359) (Fig. 14).

## 2.4. Biological activities and structure activity relationship of lucilactaene derivatives

We have recently discovered that lucilactaene and its derivatives, particularly dihydrolucilactaene, are highly effective antimalarial compounds [12]. Thus, isolated compounds in this study were assessed *in vitro* for antimalarial activity against *P. falciparum* 3D7 and other biological activities as well. Prelucilactaene E (**8**) and F (**9**) displayed relatively strong antimalarial activity ($IC_{50}$ = 3.5 and 4.3 µM, respectively). Prelucilactaene G (**4**) and H (**5**) showed almost similar antimalarial activity with $IC_{50}$ of

13.3 and 15.6 µM, respectively. Compounds **4**, **5**, and **8** exhibited weak antiproliferative activity only against HL-60 cell lines with $IC_{50}$ of ~ 46, 48, and 54 µM, respectively. Prelucilactaene A (**6**) and prelucilactaene B (**7**) exhibited weak antimalarial activity ($IC_{50}$ = 15.2 and 26.9 µM, respectively) without any cytotoxicity (Table 6). Note that all compounds were not active against other microorganisms, such as bacteria and fungi. Using these new data, we updated our previously reported structure-activity relationship (SAR) of lucilactaene derivatives as potent antimalarial lead compounds (Fig. 17).

As shown in Fig. 17, the one-way ANOVA revealed that different functional groups at C-20 account for statistically significant difference in mean antimalarial activity of lucilactaene derivatives as follows; lucilactaene / NG391 ($COOCH_3$) > prelucilactaene E / F ($CH_3$) > prelucilactaene G / H ($CH_2OH$) > demethyllucilactaene (COOH) (Tables S1). This suggested that functional groups with increased polarity at C-20 is not desirable for antimalarial activity. The 8*E* and 8*Z* configuration in **4** and **5**, respectively, displayed similar antimalarial potency. In addition, the 2*Z* configuration in prelucilactaene B (**7**, $IC_{50}$ 15.2 µM) displayed no significant changes in activity from the 2*E* isomer prelucilactaene A (**6**, $IC_{50}$ 26.9 µM). Thus, it seems that the *E* or *Z* configuration of the polyene skeleton have no significant effect on the antimalarial activity. Additionally, all

the lucilactaene derivatives that displayed an $IC_{50}$ less than 5 µM retained the pyrrolidone

ring in its structure, which might be important for the antimalarial activity.

**Table. 6.** Biological activity of identified compounds **4-9**.

| # | Compound | HeLa growth | HL-60 growth | *S. aureus.* growth | *E. coli.* growth | *A. fumigatus* growth | *P. oryzae* growth | *C. albicans* growth | *P. f.* growth 3D7 |
|---|---|---|---|---|---|---|---|---|---|
| | | Inhibitory concentration ($IC_{50}$, µM) | | | | | | | |
| 1 | **Prelucilactaene G (4)** | >70 | 46.3 | >70 | >70 | >70 | >70 | >70 | 10.9 |
| 2 | **Prelucilactaene H (5)** | >70 | 48.8 | >70 | >70 | >70 | >70 | >70 | 12.1 |
| 3 | **Prelucilactaene A (6)** | >70 | >70 | >70 | >70 | >70 | >70 | >70 | 15.2 |
| 4 | **Prelucilactaene B (7)** | >70 | >70 | >70 | >70 | >70 | >70 | >70 | 24.9 |
| 5 | **Prelucilactaene E (8)** | >70 | 53.6 | >70 | >70 | >70 | >70 | >70 | 3.9 |
| 6 | **Prelucilactaene F (9)** | NA | NA | NA | NA | NA | NA | NA | 4.5 |

NA: not assayed
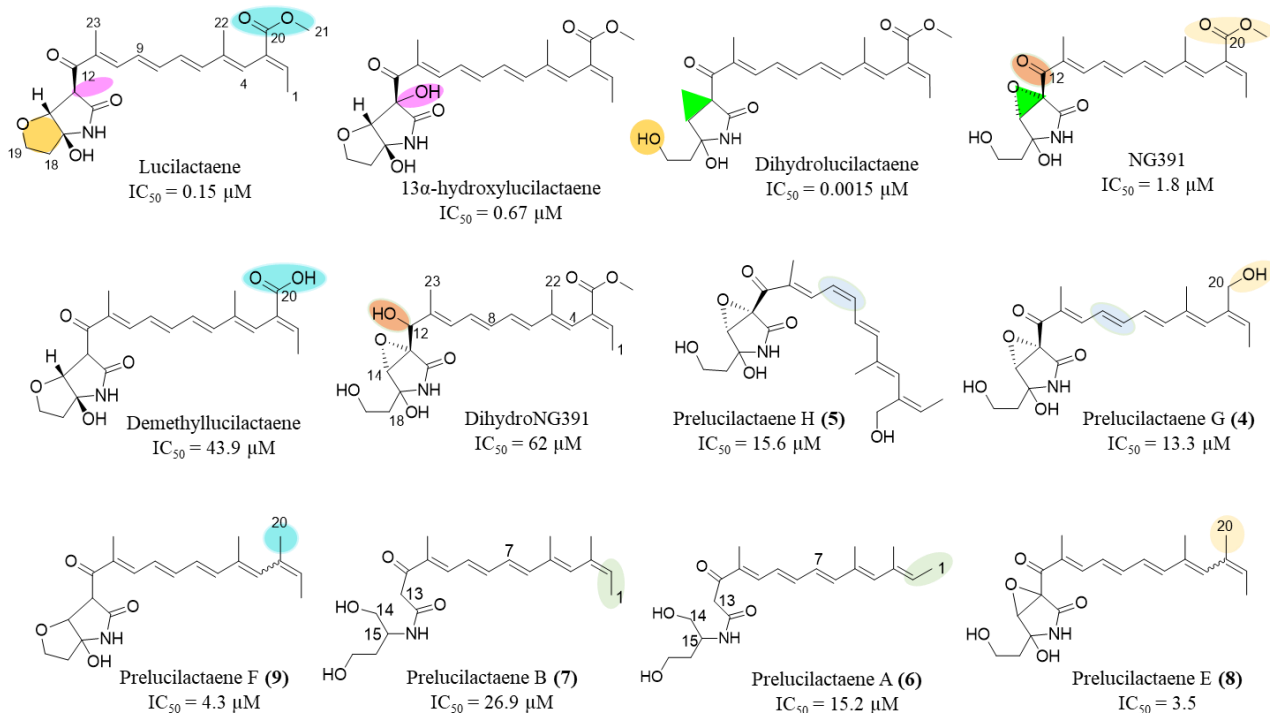


**Fig. 17.** Updates on Structure activity relationship of lucilactaene and its derivatives as potential antimalarial lead compounds.

67

## 2.5. Feeding compounds 4, 7, and 8 to Δ*luc5* strain

LC-MS analysis and comparison with NG391/393 authentic sample confirmed that the PKS-NRPS knockout strain (Δ*luc5*) successfully converted the fed compound **4** into NG391/393, but not to lucilactaene (Fig. 18). This suggested that **4** could be a biosynthetic intermediate of NG391, that possesses similar C-13 and C-14 relative stereochemistry. However, compounds **7** and **8** displayed significant instability within 24 hours of incubation in the production medium (YG), impeding their conversion into the final products (Fig. S99). This suggests that hydroxylation of C-20 significantly improves the chemical stability of these compounds.
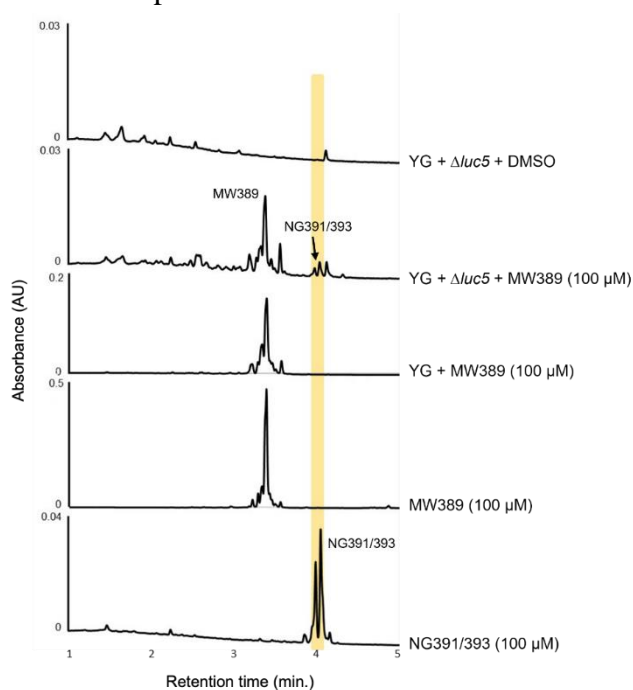


**Fig. 18.** LC-MS analysis of ethanolic extract of PKS-NRPS knockout strain (Δ*luc5*) after feeding with prelucilactaene G (MW389, **4**). Δ*luc5* strain successfully converted **1** into final product NG391. YG + MW389 mean that MW389 compound was incubated with YG medium without fungal strains for 7 days at 28 °C to confirm its stability and exclude any false positive peaks. MW389 stock is the stock of feeding compound dissolved in MeOH that was kept in -80 °C.

## 2.6. Putative biosynthetic pathway of NG391 and lucilactaene

Although some of the isolated compounds were unstable in the production media which precluded a successful feeding experiment, their chemical structures (Fig. 14) have enabled us to predict the roles of Luc2 and Luc3 and to speculate the putative biosynthetic pathway of NG391 and lucilactaene (Fig. 19). We predicted a pathway closely related to that proposed in fusarin C/A [110,112], but having a main difference which is the involvement of the aldehyde dehydrogenase (Luc3) in NG391 / lucilactaene biosynthesis. Initially, the multifunctional PKS-NRPS (Luc5) condenses one acetyl-CoA unit with six malonyl-CoA units and a homoserine, followed by a reductive release of an alcohol intermediate, prelucilactaene B (**7**), from the hybrid PKS-NRPS assembly line (Fig. 19). From the Δ*luc2* strain, we identified 6 compounds (**6-9**, prelucilactaene C, and prelucilactaene D). All these compounds were C-20 methyl derivatives, and some of them have a completely modified 2-pyrrolidone ring structure (**8** and **9**), suggesting that Luc2 is involved in C-20 hydroxylation rather that 2-pyrrolidone ring formation and its subsequent modifications. Luc6, a putative α/ß hydrolase, may be involved in these steps because a homologous hydrolase enzyme, Fus2, was predicted to be involved in the corresponding reactions in the fusarin C biosynthesis [110]. Based on the identified structures, it seems that both Luc2 and Luc6 function in parallel in modification of

prelucilactaene B (**7**). In the absence of Luc2 (Fig. S100), Luc6 may firstly catalyze the 2-pyrrolidone ring formation to form prelucilactaene C from **7**, followed by C-15 hydroxylation by the same enzyme to give prelucilactaene D, then converted to prelucilactaene E by epoxidation, and finally can be converted to prelucilactaene F by cyclization. Prelucilactane D, prelucilactaene E, and prelucilactaene F can be converted into dihydrolucilactaene, NG391, and lucilactaene, respectively, by C-20 modification. In the presence of Luc2, Luc2 may hydroxylate C-20 methyl group of some of the intermediates shown in Fig. S100. The Δ*luc3* strain accumulated the C-20 alcoholic analogs (**4** and **5**) as major metabolites and could not produce NG391 or lucilactaene. This proved that the aldehyde dehydrogenase (Luc3) is involved in the biosynthesis, and the P450 monooxygenase (Luc2), unlike Fus8 in fusarin C biosynthesis, is not enough for the full oxidation of the C-20 methyl group into carboxylic acid, which is a prerequisite for the final methylation step. Thus, we speculated that Luc3 is involved in the biosynthesis by further oxidation of the C-20 alcoholic analog (**4**) into a carboxylic derivative, which we have not identified. This unidentified carboxylic derivative may be converted to demethyllucilactaene, another carboxylic derivative, because Δ*luc1* strain accumulated demethyllucilactaene as a major metabolite [99]. These carboxylic

derivatives will be subsequently methylated by a methyltransferase (Luc1) as a final step

in the biosynthesis as previously reported [99].
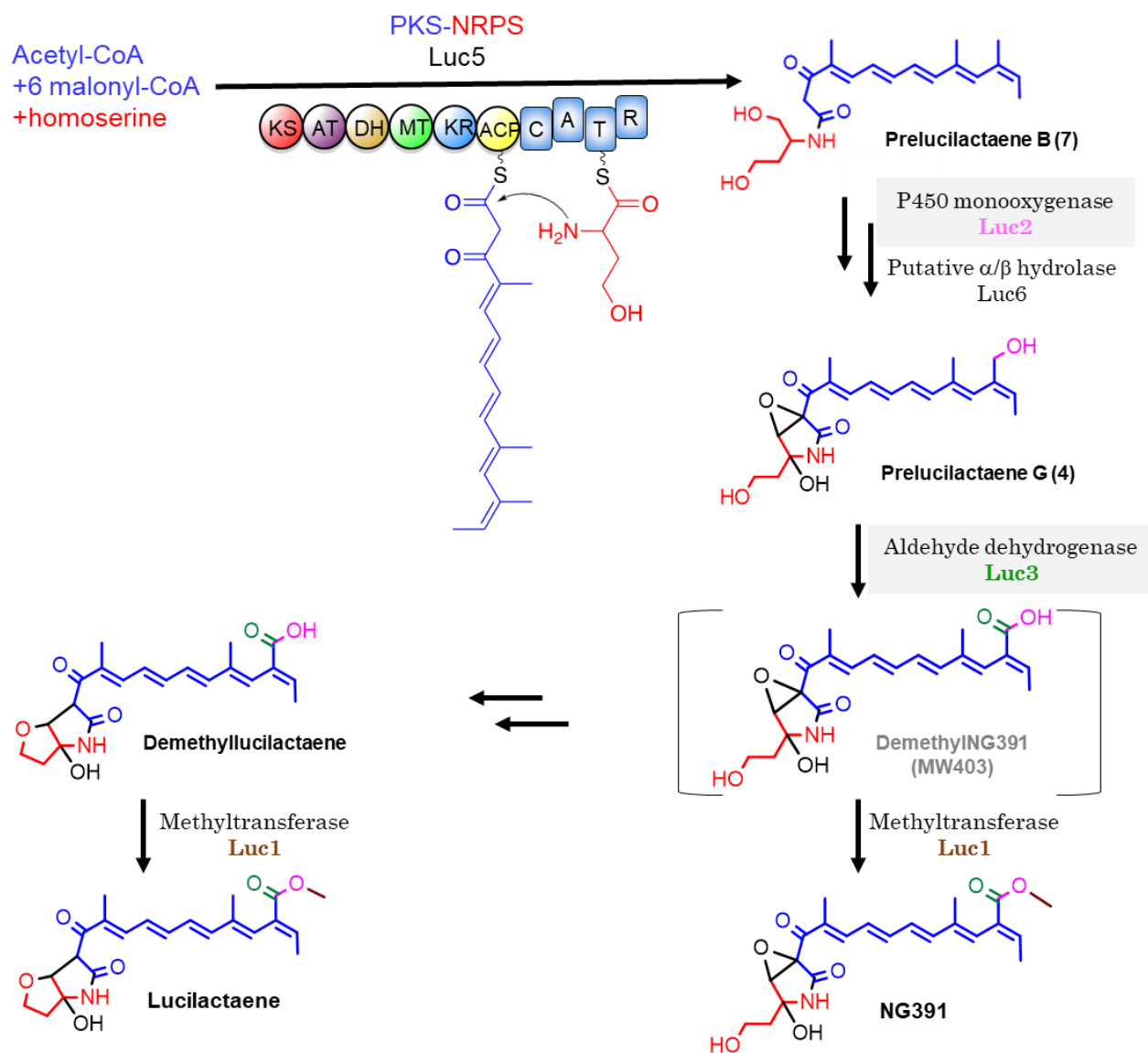


**Fig. 19.** Putative biosynthetic pathway of NG391 and lucilactaene.

**Conclusion**

Culturing of *Fusarium* sp. RK97-94 disruption mutants (Δ*luc2*) or (Δ*luc3*) has the potential not only to produce new bioactive lucilactaene derivatives, but also to uncover the mysterious biosynthetic mechanisms of NG391 and lucilactaene. Herein, we demonstrated that culturing of the P450 monooxygenase knockout strain (Δ*luc2*) has resulted in isolation and identification of C-20 methyl analogues of NG391 and lucilactaene (**6-9**, prelucilactaene C, and prelucilactaene D), suggesting that Luc2 might be involved in C-20 hydroxylation. On the other hand, C-20 hydroxylated derivatives (**4-5**) were isolated from the aldehyde dehydrogenase knockout strain (Δ*luc3*) which is probably responsible for further oxidation of **4** and **5** into corresponding carboxylic acids. The PKS-NRPS knockout strain (Δ*luc5*) successfully converted prelucilactaene G (**4**) into NG391, however instability of the C-20 methylated analogues precluded successful feeding experiment. Structures of isolated compounds enabled us to predict the putative biosynthetic pathway of NG391 and lucilactaene. Isolated compounds displayed moderate antimalarial activity except for prelucilactaene E (**8**) and F (**9**) that were relatively strong inhibitors to malaria parasite growth (IC$_{50}$ 3.9 and 4.5 µM, respectively). The impact of C-20 substitutions, *E/Z* configuration, as well as pyrrolidone ring opening on antimalarial activity was also demonstrated.

## 3. Materials and Methods

### 3.1. General Experimental Procedures

Solvents and reagents of analytical quality were obtained from their commercial suppliers. LC/MS and MS/MS analyses were performed on a Waters UPLC H-Class system (Waters, Milford, MA, USA), connected to an AB Sciex API3200 by an ESI probe (AB Sciex, Framingham, MA, USA) or Waters Synapt G2, respectively, using a Waters Acquity UPLC BEH $C_{18}$ column (1.7 μm, 2.1 mm i.d. × 50 mm) with an acetonitrile−0.05% aqueous formic acid gradient system. HRMS data was acquired using a Waters Vion IMS QTof system and Waters Synapt G2. Preparative HPLC was performed using a Waters 600E pump system with a Senshu Pak Pegasil ODS column (20 mm i.d. × 250 mm or 10 mm i.d. × 250 mm, 5 μm) (Senshu Scientific Co., Ltd, Tokyo, Japan). Optical rotations were recorded with a HORIBA SEPA-300 high-sensitive polarimeter (HORIBA, Kyoto, Japan). The $^1$H-NMR data were acquired at 500 MHz and the $^{13}$C-NMR data were acquired at 125 MHz using a JEOL JNM-ECA-500 spectrometer (JEOL, Tokyo, Japan). Chemical shifts were referenced to a residual solvent signal (methanol-$d_4$ $^1$H $\delta_H$ 3.31, $^{13}$C $\delta_C$ 49.0) and (CDCl$_3$ $^1$H $\delta_H$ 7.26, $^{13}$C $\delta_C$ 77.1). The UV absorption was recorded on a JASCO V-630 BIO spectrophotometer whereas the IR spectrum was recorded on a HORIBA FT720 with a DuraSample IR II ATR instrument.

## 3.2. Fungal strains, culture conditions, and feeding experiment

PKS-NRPS knockout *Fusarium* sp. RK97-94 strain (Δ*luc5*) was constructed previously [99]. Strains were firstly precultured in PDB+0.1% agar medium [2.4% potato dextrose broth (Difco Co.), 0.1% agar], for 72-96 hrs at 28 °C, followed by static culturing in 50 mL YG liquid media (0.5% yeast extract, 2% glucose) for 7 days at 28 °C to detect possible biosynthetic intermediates. In feeding experiment, 0.5 mL cultures in YG media were prepared in 24-well plate and inoculated in day 1 with 10 µL preculture and fed compounds **4**, **7**, and **8** (final conc. was 100 µM) and kept at 28 °C for 7days. DMSO was used as negative control. Fed compounds were also separately incubated in YG media at 28 °C for 7 days without Δ*luc5* strain to check its stability in the production medium.

## 3.3. DNA manipulations

Total DNA was purified from *Fusarium* sp. RK97-94 using the DNeasy plant total DNA isolation kit (QIAGEN KK, Tokyo, Japan). PCR amplifications were done using a thermal cycler (Model PTC-200, Bio-Rad Laboratories, Inc., Hercules, CA) and either KOD Plus Neo (Toyobo, Tokyo, Japan) or KOD FX Neo (Toyobo) DNA polymerases. KOD Plus Neo, a proofreading DNA polymerase, was used for plasmid construction, and KOD FX Neo was used for routine PCR. The PCR products were cloned by using the InFusion system (Takara Shuzo, Kyoto, Japan) and sequenced, where necessary.

Plasmids were amplified in *Escherichia coli* DH5α [113]. The sequencing reactions were performed using the BigDye Terminator version 3.1 cycle sequencing kit (Amersham-Pharmacia Biotech, Piscataway, NJ). Reaction products were analyzed using an Applied Biosystems 3730xl DNA analyzer (Perkin Elmer/Applied Biosystems, Foster City, CA). Nucleotide and amino acid sequence data were analyzed using Serial Cloner software (http://serialbasics.free.fr/Serial_Cloner.html), and open reading frames were predicted by FGENESH and FGENESH+ software (Softberry, Inc, NY) or by AUGUSTUS (http://bioinf.uni-greifswald.de/webaugustus/).

## 3.4. Fungal transformation

*Fusarium* sp. RK97-94 was transformed using the *Agrobacterium tumefaciens*-mediated transformation (ATMT) method [114], as described previously [115,116]. *A. tumefaciens* strain C58 was cultured with a conidial suspension of *Fusarium* sp. RK97-94. Transformants were selected with 200 or 500 µg/mL hygromycin B (Wako Pure Chemical Co., Osaka, Japan). In subsequent cultures of *Fusarium* sp. RK97-94 transformants, the appropriate selection reagent (200 µg/mL hygromycin B) was added as needed.

## 3.5. Construction of recombinant strains

The PCR primers used for plasmid construction are listed in Table S5.

*Luc2* disruptants were constructed as follows. The 1.5-kb sequence upstream of *luc2* was PCR amplified from the *Fusarium* sp. RK97-94 genomic DNA using IF_LB-*luc2*-5F and IF_5HPH-*luc2*-5R primers (fragment 1). The 1.6-kb hygromycin B-resistance gene expression unit was PCR amplified from pCSN45 with 5HPH and 3HPH primers (fragment 2). The 1.5-kb sequence downstream of *luc2* was PCR amplified from the genomic DNA of *Fusarium* sp. RK97-94 with IF_3HPH-*luc2*-3F and IF_RB-*luc2*-3R primers (fragment 3). The 8.7-kb vector sequence of pBI121 between the right and left borders was PCR amplified from pBI121 with RB and LB primers (fragment 4). The four fragments were joined by the InFusion system to yield a gene disruption vector, pBI-*luc2*::HPH. The *A. tumefaciens* strain transformed with this plasmid was used for ATMT. The *luc2* disruptants were selected by PCR with 5HPH and *luc2*-check-R primers, which hybridize the upstream region of the 1.6-kb hygromycin B-resistance gene expression unit and the 1.5-kb downstream of the deleted *luc2* ORF. This primer set amplifies the 3.1-kb fragment from the *luc2* disruptants.

*Luc3* disruptants were constructed as follows. The 1.5-kb sequence upstream of *luc3* was PCR amplified from the *Fusarium* sp. RK97-94 genomic DNA using IF_LB-*luc3*-5F and IF_5HPH-*luc3*-5R primers (fragment 1). The 1.6-kb hygromycin B-resistance gene expression unit was PCR amplified from pCSN45 [117] with 5HPH and 3HPH

primers (fragment 2). The 1.5-kb sequence downstream of *luc3* was PCR amplified from the genomic DNA of *Fusarium* sp. RK97-94 with IF_3HPH-*luc3*-3F and IF_RB-*luc3*-3R primers (fragment 3). The 8.7-kb vector sequence of pBI121 between the right and left borders was PCR amplified from pBI121 with RB and LB primers (fragment 4). The four fragments were joined by the InFusion system to yield a gene disruption vector, pBI-*luc3*::HPH. The *A. tumefaciens* strain transformed with this plasmid was used for ATMT. The *luc2* disruptants were selected by PCR with 5HPH and *luc3*-check-R primers, which hybridize the upstream region of the 1.6-kb hygromycin B-resistance gene expression unit and the 1.5-kb downstream of the deleted *luc3* ORF. This primer set amplifies the 3.1-kb fragment from the *luc3* disruptants.

## 3.6. Extraction and LC-MS analysis

Fifty milliliters of cultures of Δ*luc2* and Δ*luc3* were extracted with similar volume of acetone followed by its evaporation. The aqueous phase was then partitioned with equal volumes EtOAc 3 times and the collected EtOAc extract was concentrated by rotary evaporator under vacuum. Concentrated residues were dissolved in 5 mL MeOH and subjected to LC-MS analysis. In case of 24-well plate culture, each well was harvested using 2 mL ethanol, vortexed, centrifuged then the supernatant was dried up under nitrogen gas. The residues were re-dissolved in 200 µL methanol and filtered using a 0.2

micro-filter. Filtrates were analyzed by LC-MS using a reversed-phase column (BEH $C_{18}$, $2.1 \times 50$ mm, 1.7 µm, Waters), with a gradient solvent system as follows: MeCN (solvent B) in 0.05% formic acid/$H_2O$ (solvent A), with 5 to 50% B from 0 to 4 min, 50 to 65% B from 4 to 5 min, 65 to 100% B from 5 to 5.5 min, 100% B from 5.5 to 7 min, and re-equilibration with 5% B from 7 to 8.5 min, at a flow rate of 0.6 mL/min. Conditions for MS included an ion spray voltage of 5.0 kV, a curtain gas pressure of 15 psi, a nebulizer gas pressure of 40 psi, an auxiliary gas pressure of 50 psi, and an ion source temperature of 400 °C.

### 3.7. Isolation of 4-9

The aldehyde dehydrogenase knockout strain (Δ*luc3*) and the P450 monooxygenase disruption mutant (Δ*luc2*) were cultured in 2L flasks for purification of the target compounds (5 and 7.5 liters, respectively). Each flask contained ~ 410 mL culture (400 mL media + 10 mL fungal preculture) and was statically incubated for 7 days at 28 °C. Flasks were extracted with equal volumes of acetone overnight, followed by filtration and evaporation of the acetone layer. The aqueous phase was then partitioned three times with a similar volume of EtOAc, followed by evaporation of the EtOAc to yield dark reddish brown oily residues of 0.96 g and 1.4 g from Δ*luc3 and* Δ*luc2* cultures, respectively. These extracts were subjected to normal phase MPLC fractionation (RediSep Rf Gold®

Silica Gel disposable flash column, Teledyne Isco, U.S., 40 g) using a stepwise gradient elution of CHCl₃ (solvent A) and MeOH (solvent B) as follows: Δ*luc3*, 0, 1, 2, 3, 5, 7.5, 10, 20, 50, and 100 % B for 5 column volumes (CV) each; Δ*luc2*, 1% B for 2 CV, 3% B for 5 CV, 5% B for 7 CV, 7.5% B for 7 CV, 10% B for 7 CV, 20% B for 5 CV and 100% B for 5 CV. All the collected tubes from MPLC fractionation were analyzed by LC-MS, and fraction tubes from F52–63, eluted by 7.5% B from Δ*luc3*'s extract fractionation, were gathered (128 mg) (Fig. S33). Half of this fraction was subjected to HPLC purification (PEGASIL ODS, 20 × 250 mm, 5 µm, Senshu Scientific Co. Ltd., Tokyo, Japan), using isocratic elution of 30% acetonitrile in water at a flow rate of 15 mL/min to obtain isomeric mixtures of **4** and **5** (8 mg). This mixture subjected to another round of HPLC purification using the same isocratic method with flow rate of 1 mL/min to obtain the two pure isomers, **4** (2.4 mg) and **5** (2.6 mg).

After MPLC fractionation of the Δ*luc2* culture extract, all collected fraction tubes were analyzed by LC-MS. F14-16 (50 mg, **9**), F18-19 (28 mg, MW359), F23-26 (153 mg, MW343 and **8**), and F28-29 (58 mg, **6** and **7**) were separately collected (Fig. S34). Compounds **6** (0.9 mg) and **7** (0.7 mg) were purified from F28-29 by preparative HPLC using isocratic elution of 45% acetonitrile in water at a flow rate of 15 mL/min. Compound **8** (1.5 mg) was purified using 50% acetonitrile in water at a flow rate of 15

mL/min; Compound **9** (1 mg) was purified using 55% acetonitrile in water at a flow rate of 4 mL/min. MW343 and MW359 were purified by HPLC using isocratic elution of 50% acetonitrile in water at a flow rate of 4 mL/min that were subsequently subjected to LC-MS/MS analysis for structural elucidation.

**Prelucilactaene G (4):** Yellow amorphous powder, $[\alpha]_D^{24}$ +72 (*c* 0.1, MeOH); UV (MeOH) $\lambda_{max}$ (log ε) 366 (4.6) 266 (4.0) nm; IR $\nu_{max}$ (ATR): 3282, 2922, 1716, 1699, 1558, and 985 cm$^{-1}$.$^1$H and $^{13}$C-NMR data, see Table 3; HR-ESI-TOF/MS (found *m/z* 388.1763 [M - H]$^-$, calculated for $C_{21}H_{26}NO_6$, 388.1766).

**Prelucilactaene H (5):** Yellow amorphous powder, $[\alpha]_D^{24}$ +143 (*c* 0.1, MeOH); UV (MeOH) $\lambda_{max}$ (log ε) 368.5 (4.5) 230 (3.8) nm; IR $\nu_{max}$ (ATR): 3275, 2922, 1716, 1697, 1558, and 991 cm$^{-1}$. $^1$H and $^{13}$C-NMR data, see Table 3; HR-ESI-TOF/MS (found *m/z* 388.1761 [M - H]$^-$, calculated for $C_{21}H_{26}NO_6$, 388.1766).

**Prelucilactaene A (6):** Yellow amorphous powder, $[\alpha]_D^{24}$ - 18 (*c* 0.03, MeOH); UV (MeOH) $\lambda_{max}$ (log ε) 363 (3.0) nm; IR $\nu_{max}$ (ATR): 3365, 2956, 1685, 1652, 1558, and 1016 cm$^{-1}$. $^1$H and $^{13}$C-NMR data, see Table 4; HR-ESI-TOF/MS (found *m/z* 360.2167 [M - H]$^-$, calculated for $C_{21}H_{30}NO_4$, 360.2180).

**Prelucilactaene B (7):** Yellow amorphous powder, $[\alpha]_D^{24}$ -10 (*c* 0.05, MeOH); UV (MeOH) $\lambda_{max}$ (log ε) 362 (3.4) nm; IR $\nu_{max}$ (ATR): 3267, 2951, 1684, 1653, 1558, and

1014 cm$^{-1}$. $^1$H and $^{13}$C-NMR data, see Table 4; HR-ESI-TOF/MS (found *m/z* 360.2175 [M - H]$^-$, calculated for $C_{21}H_{30}NO_4$, 360.2180).

**Prelucilactaene E (8):** Yellow amorphous powder, $[\alpha]_D^{24}$ +79 (*c* 0.1, MeOH); UV (MeOH) $\lambda_{max}$ (log ε) 377 (4.4) nm; IR $\nu_{max}$ (ATR): 3363, 2922, 1716, 1684, 1558, and 1087 cm$^{-1}$.$^1$H and $^{13}$C-NMR data, see Table 5; HR-ESI-TOF/MS (found *m/z* 396.1781 [M+Na]$^+$, calculated for $C_{21}H_{27}NO_5Na$, 396.1787).

**Prelucilactaene F (9):** Yellow amorphous powder, UV (MeOH) $\lambda_{max}$ (log ε) 365.5 (3.2) nm; IR $\nu_{max}$ (ATR): 3365, 2918, 1684, 1653, 1558, and 1018 cm$^{-1}$. $^1$H and $^{13}$C-NMR data, see Fig. S83-S86; HR-ESI-TOF/MS (found *m/z* 380.1837 [M+Na]$^+$, calculated for $C_{21}H_{29}NO_4Na$, 380.1838).

### 3.8. Cytotoxic, antimalarial, and antimicrobial activity tests

The method for *in vitro* cytotoxicity assessment employed in this study was previously described [105]. The antimalarial and antimicrobial assays against *Plasmodium falciparum* 3D7, *Staphylococcus aureus* 209, *Escherichia coli* HO141, *Aspergillus fumigatus* Af293, *Pyricularia oryzae* kita-1, and *Candida albicans* JCM1542 were previously reported [106]. Briefly, *P. falciparum* 3D7 was cultured at 37°C under 5% $CO_2$ in human erythrocytes (3% hematocrit) (blood type A, provided by the Japanese Red Cross Society) in RPMI1640 (Invitrogen/Life Technologies, pre-added with 25 mM

HEPES, and 0.03% L-glutamine). The RPMI1640 was then supplemented with glucose (200 g/L) and hypoxanthine (0.002 mg/mL). To perform the *Pf* 3D7growth assay, 0.5 µl of test sample was pipetted into a 96-well plate. Next, 100 µl of 0.3% parasitized red blood cells, and 2% hematocrit were dispensed. Following 72-h exposures at 37°C to test sample, plates were frozen at -70°C overnight and then thawed at room temperature for at least 1 h. To evaluate lactate dehydrogenase (LDH) activity, 150 µl of freshly made reaction mixture (166 µM 3-acetyl pyridine adenine dinucleotide (APAD), 166 mM sodium L-lactate, 208 µM Nitro Blue tetrazolium chloride, 150 µg/ml diaphorase (22.5 U/ml), 0.8% Tween 20, 116 mM Tris-HCl, pH 8.0) was added. Plates were shaken to ensure mixing, and absorbance was monitored in a plate reader (PerkinElmer) at 650 nm after 10 min of incubation at room temperature in the dark.
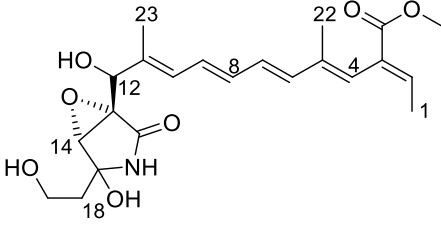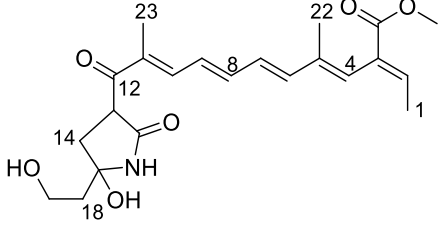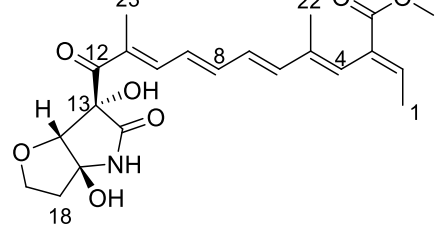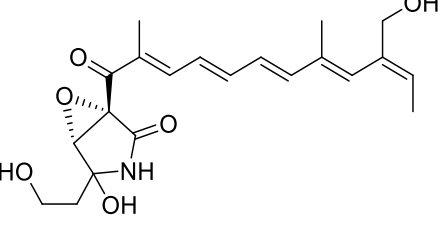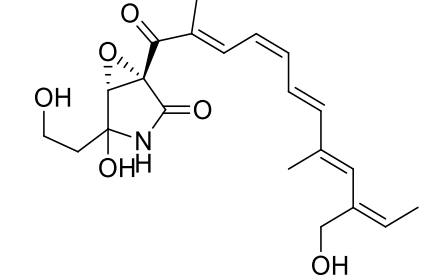
# **Summary and Conclusion**
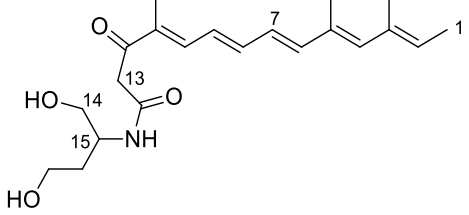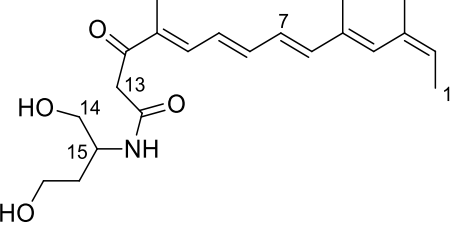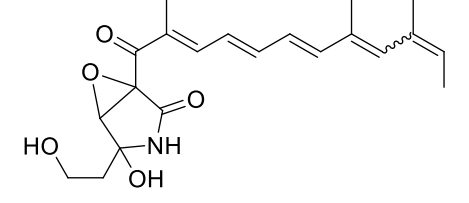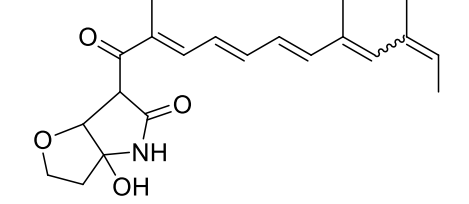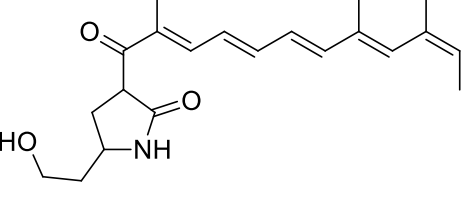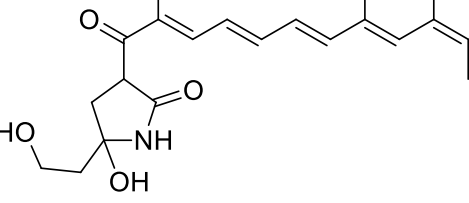
The continuous discovery of novel drugs for the treatment of life-threatening diseases such as cancer, resistant bacterial infections, and malaria is of great importance. Natural products and their derivatives, especially those from microbial origins, always play a key role in drug discovery and development. Recently, microbial genome sequencing and bioinformatics tools revealed that the majority of secondary metabolite biosynthetic gene clusters are silent under usual laboratory conditions. This suggests the existence of a great number of novel metabolites yet to be discovered via the activation of such silent gene clusters. Genetic-based approaches were widely exploited for targeted activation of specific gene clusters. However, in this study we applied the chemical induction approach to activate fungal secondary metabolism by using a recently discovered fungal metabolism regulator, NPD938. At first, we have succeeded to isolate and identify two new and one known lucilactaene derivatives from *Fusarium* sp. RK97-94 culture treated with NPD938 (30 µM). Of these compounds, we have proved that dihydroNG391 (**1**) is strongly induced by NPD938 via indirect mechanism. As of bioactivity, dihydrolucilactaene (**2**) displayed extremely potent antimalarial activity with $IC_{50}$ of 1.5 nM, whereas 13α-hydroxylucilactaene (**3**) exhibited potent antimalarial activity with $IC_{50}$ of 0.67 µM. The superb antimalarial activity of lucilactaene and dihydrolucilactaene

83

1    motivated us to isolate and identify more lucilactaene derivatives and to study the

2    structure-activity relationship (SAR) of lucilactaene and its derivatives as potent

3    antimalarial lead compounds. The biosynthetic gene cluster of lucilactaene was recently

4    identified by our group; however, only a knockout mutant of methyltransferase (*luc1*)

5    was reported to be involved in the final methylation step in lucilactaene biosynthesis. We

6    hypothesized that *luc2* and *luc3* encode for P450 monooxygenase and aldehyde

7    dehydrogenase, respectively, and they could be involved in the biosynthesis of

8    lucilactaene and NG391. Knocking out these genes has the potential to not only produce

9    new lucilactaene derivative with potent antimalarial activity, but also uncover the hidden

10    secrets behind lucilactaene biosynthetic pathway. We have succeeded to isolate and

11    identify prelucilactaene G (**4**), and prelucilactaene H (**5**) from aldehyde dehydrogenase

12    knockout strain (Δ*luc3*) culture broth, as well as prelucilactaene A (**6**), prelucilactaene B

13    (**7**), two isomeric mixtures of prelucilactaene E (**8**) and prelucilactaene F (**9**), from P450

14    monooxygenase knockout strain (Δ*luc2*) culture broth. Isolated compounds displayed

15    moderate to strong antimalarial activity and the structure-activity relationship of

16    lucilactaene derivatives was investigated. In contrast to the previous report,

17    tetrahydrofuran ring is not essential for lucilactaene antimalarial activity, and its opening

18    resulted in 100-fold increase in activity. Interestingly, de-epoxidation of NG391

1  compound into dihydrolucilactaene (**2**) has resulted in 1200-fold increase in antimalarial

2  activity, which reflects the dramatic effect of epoxide group in decreasing this activity.

3  We have also demonstrated that reduction of C-12 carbonyl group, increasing the polarity

4  of C-20 position by $CH_2OH$ or COOH, or opening the pyrrolidone ring was not good for

5  antimalarial activity. Additionally, we argued that *E* and *Z* configurations of the polyene

6  skeleton of this class of compounds have no significant impact on antimalarial activity.

7  Based on these isolated compounds, we speculated the biosynthetic pathway of

8  lucilactaene and NG391. It was interesting that all the isolated lucilactaene derivatives

9  from P450 monooxygenase knockout strain (Δ*luc2*) were C-20 methylated analogues,

10 suggesting that Luc2 might be involved in C-20 hydroxylation. This was supported by

11 identification of the C-20 hydroxylated analogue as a major metabolite from the culture

12 broth of the Δ*luc3* strain where *luc2* was normally expressed. On the other hand, we

13 speculated that aldehyde dehyderogenase (Luc2) might be involved in further oxidation

14 of the C-20 hydroxylated analogue into its carboxylic acid derivatives. This could be

15 explained by the accumulation of this hydroxylated analogue as a main product in Δ*luc3*

16 strain.

17

18

## 1    List of identified compounds

| Name / Source | Structure | Remarks |
|---|---|---|
| **DihydroNG391 (1)**<br><br>*Fusarium* sp. RK97-94 (WT) |  | ■ New compound.<br>■ Induced by NPD938.<br>■ Weak antimalarial activity |
| **Dihydrolucilactaene (2)**<br><br>*Fusarium* sp. RK97-94 (WT) |  | ■ New compound.<br>■ NPD938 independent.<br>■ Exptremely potent antimalarial activity (IC$_{50}$ 1.5 nM) |
| **13α-hydroxylucilactaene (3)**<br><br>*Fusarium* sp. RK97-94 (WT) |  | ■ Known compound.<br>■ NPD938 independent.<br>■ Potent antimalarial activity. (IC$_{50}$ 0.67 µM) |
| **Prelucilactaene G (4)**<br><br>Δ*luc3* strain |  | ■ Firstly isolated as single pure isomer.<br>■ Biosynthetic intermediate.<br>■ Moderate antimalarial activity |
| **Prelucilactaene H (5)**<br><br>Δ*luc3* strain |  | ■ Firstly isolated as single pure isomer.<br>■ Biosynthetic intermediate.<br>■ Moderate antimalarial activity |

| Name / Source | Structure | Remarks |
|---|---|---|
| **Prelucilactaene A (6)**<br><br>Δ*luc2* strain |  | ▪ New compound.<br>▪ Biosynthetic intermediate.<br>▪ Moderate antimalarial activity |
| **Prelucilactaene B (7)**<br><br>Δ*luc2* strain |  | ▪ New compound.<br>▪ Biosynthetic intermediate.<br>▪ Moderate antimalarial activity |
| **Prelucilactaene E (8)**<br><br>Δ*luc2* strain |  | ▪ New compound.<br>▪ Biosynthetic intermediate.<br>▪ Strong antimalarial activity |
| **Prelucilactaene F (9)**<br><br>Δ*luc2* strain |  | ▪ New compound.<br>▪ Biosynthetic intermediate.<br>▪ Strong antimalarial activity |
| **Prelucilactaene C**<br><br>Δ*luc2* strain |  | ▪ Structure proposed by MS/MS fragmentation.<br>▪ Biosynthetic intermediate. |
| **Prelucilactaene D**<br><br>Δ*luc2* strain |  | ▪ Structure proposed by MS/MS fragmentation.<br>▪ Biosynthetic intermediate. |

1

# Future prospective

In this study, we evidenced the very strong antimalarial potential of lucilactaene and its derivatives by isolating and identifying dihydrolucilactaene along with other analogues. We were also able to identify key structural properties of this class of compounds that are critical for robust antimalarial activity. These findings could pave the way for synthetic chemists to create novel lucilactaene compounds with improved stability and bioactivity.

Dihydrolucilactaene exhibited very powerful antimalarial activity against both wild-type (3D7) and chloroquine resistant (K1) *Plasmodium falciparum* strains, indicating a distinct mechanism of action. We are currently collaborating with biologists in our group to identify the target of dihydrolucilactaene.

Inspecting the *in vivo* antimalarial activity of dihydrolucilactaene is very important step in drug development process. Thus, large scale production of dihydrolucilactaene is necessary. Deep understanding of biosynthetic mechanism of dihydrolucilactaene could enable us to boost the yield via genetic modification of its biosynthetic machinery.

**References**

1.  Bennett JW. From molecular genetics and secondary metabolism to molecular metabolites and secondary genetics. Can J Bot. 1995; 73 (S1): 917-924.

2.  Alexander F. On the Antibacterial action of cultures of a *Penicillium*, with special reference to their use in the isolation of *B. influenzae*. Br J Exp Pathol. 1929; 10 (3): 226.

3.  Comroe JH. Pay dirt - The story of Streptomycin. Part 1. From Waksman to Waksman. Am Rev Respir Dis. 1978; 117 (4), 773-781.

4.  Davies J. Where have all the antibiotics gone?. Can J Infect Dis Med Microbiol 2006; 17 (5), 287-290.

5.  Davies J and Davies D. Origins and evolution of antibiotic resistance. Microbiol Mol Biol Rev. 2010; 74 (3), 417-433.

6.  Buhaescu I, Izzedine H. Mevalonate pathway: A review of clinical and therapeutical implications. Clin Biochem. 2007; 40 (9-10), 575-584.

7.  Caputi L, Aprea E. Use of terpenoids as natural flavouring compounds in food industry. Recent Pat food Nutr Agric. 2012; 3 (1), 9-16.

8.  Tu Y. The discovery of artemisinin (qinghaosu) and gifts from Chinese medicine. Nat Med. 2011; 17 (10), 1217-1220.

9.  Nicolaou KC, Dai W -M, Guy RK. Chemistry and biology of taxol. Angew Chem. 1994; 33 (1), 15-44.

10. Roberts MF. Alkaloids: biochemistry, ecology, and medicinal applications. Springer Science & Business Media; 2013.

11. Fischbach MA, Walsh CT. Assembly-line enzymology for polyketide and nonribosomal peptide antibiotics: Logic machinery, and mechanisms. Chem Rev. 2006; 106 (8), 3468-3496.

12. Jenke-Kodama H, Sandmann A, Müller R, Dittmann E. Evolutionary implications of bacterial polyketide synthases. Mol Biol Evol. 2005; 22 (10), 2027-2039.

13. Klaus M, Grininger M. Engineering strategies for rational polyketide synthase design. Nat Prod Rep. 2018; 35 (10), 1070-1081.

14. Till M, Race PR. The assembly line enzymology of polyketide biosynthesis. Methods Mol Biol. 2016; 31-49.

15. Atanasov AG, Waltenberger B, Pferschy-Wenzig EM, Linder T, Wawrosch C, Uhrin P, *et al*. Discovery and resupply of pharmacologically active plant-derived natural products: A review. Biotechnol Adv. 2015; 33 (8), 1582-1614.

16. Harvey AL, Edrada-Ebel R, Quinn RJ. The re-emergence of natural products for drug discovery in the genomics era. Nat Rev Drug Discov. 2015; 14 (2), 111-129.

17. Newman DJ, Cragg GM. Natural products as sources of new drugs over the nearly four decades from 01/1981 to 09/2019. J Nat Prod. 2020; 83 (3), 770-803.

18. Tintore M, Vidal-Jordana A, Sastre-Garriga J. Treatment of multiple sclerosis — success from bench to bedside. Nat Rev Neurol. 2019; 15 (1), 53-58.

19. Waltenberger B, Mocan A, Šmejkal K, Heiss EH, Atanasov AG. Natural products to counteract the epidemic of cardiovascular and metabolic disorders. Molecules. 2016; 21 (6), 807.

20. Cragg GM, Pezzuto JM. Natural products as a vital source for the discovery of cancer chemotherapeutic and chemopreventive agents. Med Princ Pract. 2016; 25 (2), 41-59.

21. Campbell WC, Fisher MH, Stapley EO, Albers-Schönberg G, Jacob TA. Ivermectin: A potent new antiparasitic agent. Science. 1983; 221 (4613), 823-828.

22. Keller NP. Fungal secondary metabolism: regulation, function and drug discovery. Nat Rev Microbiol. 2019; 17 (3), 167-180.

23. Díez B, Gutiérrez S, Barredo JL, Van Solingen P, Van Der Voort LHM, Martín JF. The cluster of penicillin biosynthetic genes: Identification and characterization of the *pcbAB* gene encoding the α-aminoadipyl-cysteinyl-valine synthetase and linkage to the *pcbC* and *penDE* genes. J Biol Chem. 1990; 265 (27), 16358-16365

24. Reen FJ, Romano S, Dobson ADW, O'Gara F. The sound of silence: Activating silent biosynthetic gene clusters in marine microorganisms. Mar Drugs. 2015; 13 (8), 4754-4783.

25. Netzker T, Fischer J, Weber J, Mattern DJ, König CC, Valiante V, *et al*. Microbial communication leading to the activation of silent fungal secondary metabolite gene clusters. Front Microbiol. 2015; 6, 299.

26. Baral B, Akhgari A, Metsä-Ketelä M. Activation of microbial secondary metabolic pathways: Avenues and challenges. Synth. Syst. Biotechnol. 2018; 3 (3), 163-178.

27. Bode HB, Bethe B, Höfs R, Zeeck A. Big effects from small changes: Possible ways to explore nature's chemical diversity. ChemBioChem. 2002; 3 (7), 619-627.

28. Lopez JA V., Nogawa T, Futamura Y, Shimizu T, Osada H. Nocardamin glucuronide, a new member of the ferrioxamine siderophores isolated from the ascamycin-producing strain *Streptomyces* sp. 80H647. J Antibiot. 2019; 72 (12), 991-995.

29. Rawa MSA, Nogawa T, Okano A, Futamura Y, Nakamura T, Wahab HA, *et al*. A new peptaibol, RK-026A, from the soil fungus *Trichoderma* sp. RK10-F026 by culture condition-dependent screening. Biosci Biotechnol Biochem. 2021; 85 (1), 69-76.

30. Scherlach K, Hertweck C. Triggering cryptic natural product biosynthesis in microorganisms. Org Biomol Chem. 2009; 7 (9), 1753-1760.

31. Christian OE, Compton J, Christian KR, Mooberry SL, Valeriote FA, Crews P. Using jasplakinolide to turn on pathways that enable the isolation of new chaetoglobosins from *Phomospis asparagi*. J Nat Prod. 2005; 68 (11), 1592-1597.

32. Strobel G, Daisy B, Castillo U, Harper J. Natural products from endophytic microorganisms. J Nat Prod. 2004; 67 (2), 257-268.

33. Schroeckh V, Scherlach K, Nützmann HW, Shelest E, Schmidt-Heck W, Schuemann J, *et al*. Intimate bacterial-fungal interaction triggers biosynthesis of archetypal polyketides in *Aspergillus nidulans*. Proc Natl Acad Sci U S A. 2009; 106 (34), 14558-14563.

34. Charusanti P, Fong NL, Nagarajan H, Pereira AR, Li HJ, Abate EA, *et al*. Exploiting adaptive laboratory evolution of *Streptomyces clavuligerus* for antibiotic discovery and overproduction. PLoS One. 2012; 7 (3), e33727.

35. Ochi K, Okamoto S, Tozawa Y, Inaoka T, Hosaka T, Xu J, *et al*. Ribosome engineering and secondary metabolite production. Adv Appl Microbiol. 2004; 56 (56), 155-179.

36. Ochi K, Hosaka T. New strategies for drug discovery: Activation of silent or weakly expressed microbial gene clusters. Appl Microbiol Biotechnol. 2013; 97 (1), 87-98.

37. Chai YJ, Cui C Bin, Li CW, Wu CJ, Tian CK, Hua W. Activation of the dormant derived *Penicillium purpurogenum* G59. Mar Drugs. 2012; 10 (3), 559-582.

38. González A, Jiménez A, Vázquez D, Davies JE, Schindler D. Studies on the mode of action of hygromycin B, an inhibitor of translocation in eukaryotes. Biochim Biophys Acta. 1978; 521 (2), 459-469.

39. Whitehouse I, Rando OJ, Delrow J, Tsukiyama T. Chromatin remodelling at promoters suppresses antisense transcription. Nature. 2007; 450 (7172), 1031-1035.

40. Bednar J, Horowitz RA, Grigoryev SA, Carruthers LM, Hansen JC, Koster AJ, *et al*. Nucleosomes, linker DNA, and linker histone form a unique structural motif that directs the higher-order folding and compaction of chromatin. Proc Natl Acad Sci U S A. 1998; 95 (24), 14173-14178.

41. Saha A, Wittmeyer J, Cairns BR. Chromatin remodelling: The industrial revolution of DNA around histones. Nat. Rev. Mol. Cell Biol. 2006; 7 (6), 437-447.

42. Marks PA, Richon VM, Breslow R, Rifkind RA. Histone deacetylase inhibitors as new cancer drugs. Curr Opin Oncol. 2001. 13 (6), 477-483.

43. Cichewicz R. Epigenetic regulation of secondary metabolite biosynthetic genes in fungi-Biocommunication of Fungi. Springer Netherlands; 2012; 57-69.

44. Chiang YM, Chang SL, Oakley BR, Wang CCC. Recent advances in awakening silent biosynthetic gene clusters and linking orphan clusters to natural products in microorganisms. Curr Opin Chem Biol. 2011; 15 (1), 137-143.

45. Shwab EK, Jin WB, Tribus M, Galehr J, Graessle S, Keller NP. Histone deacetylase activity regulates chemical diversity in *Aspergillus*. Eukaryot Cell. 2007; 6 (9), 1656-1664.

46. Szewczyk E, Chiang YM, Oakley CE, Davidson AD, Wang CCC, Oakley BR. Identification and characterization of the asperthecin gene cluster of *Aspergillus nidulans*. Appl Environ Microbiol. 2008; 74 (24), 7607-7612.

47. Van Der Heul HU, Bilyk BL, McDowall KJ, Seipke RF, Van Wezel GP. Regulation of antibiotic production in Actinobacteria: New perspectives from the post-genomic era. Nat Prodt Rep. 2018; 35 (6), 575-604.

48. Tilburn J, Sarkar S, Widdick DA, Espeso A, Orejas M, Mungroo J, *et al*. The *Aspergillus* PacC zinc finger transcription factor mediates regulation of both acid- and alkaline-expressed genes by ambient pH. EMBO J. 1995; 14 (4), 779-790.

49. Hortschansky P, Eisendle M, Al-Abdallah Q, Schmidt AD, Bergmann S, Thön M, *et al*. Interaction of HapX with the CCAAT-binding complex - A novel mechanism of gene regulation by iron. EMBO J. 2007; 26 (13), 3157-3168.

50. Caddick MX, Arst Jr HN. Deletion of the 389 N-terminal residues of the transcriptional activator AREA does not result in nitrogen metabolite derepression in *Aspergillus nidulans*. J Bacteriol. 1998;180 (21):5762–4.

51. Bayram Ö, Braus GH. Coordination of secondary metabolism and development in fungi: The velvet family of regulatory proteins. FEMS Microbiol Rev. 2012; 36 (1),1-24.

52. Dowzer CE, Kelly JM. Analysis of the *creA* gene, a regulator of carbon catabolite repression in *Aspergillus nidulans*. Mol Cell Biol. 1991; 11 (11), 5701-5709.

53. Brakhage AA. Molecular regulation of β-lactam biosynthesis in filamentous fungi. Microbiol Mol Biol Rev. 1998; 62 (3), 547-585.

54. Keller NP, Nesbitt C, Sarr B, Phillips TD, Burow GB. pH regulation of sterigmatocystin and aflatoxin biosynthesis in *Aspergillus* spp. Phytopathology. 1997; 87 (6), 643-648.

55. Bok JW, Keller NP. LaeA, a regulator of secondary metabolism in *Aspergillus* spp. Eukaryot Cell. 2004; 3 (2), 527-535.

56. Olano C, García I, González A, Rodriguez M, Rozas D, Rubio J, *et al*. Activation and identification of five clusters for secondary metabolites in *Streptomyces albus* J 1074. Microb Biotechnol. 2014;7 (3):242–56.

57. Kennedy J, Turner G. δ(L-α-Aminoadipyl)-L-cysteinyl-D-valin synthetase is a rate limiting enzyme for penicillin production in *Aspergillus nidulans*. Mol Gen Genet. 1996; 253 (1), 189-197.

58. Xu G, Wang J, Wang L, Tian X, Yang H, Fan K, *et al*. "Pseudo" γ-butyrolactone receptors respond to antibiotic signals to coordinate antibiotic biosynthesis. J Biol Chem. 2010; 285 (35), 27440-27448.

59. Zhang YY, Zou ZZ, Niu GQ, Tan HR. *jadR** and *jadR2* act synergistically to repress jadomycin biosynthesis. Sci China Life Sci. 2013; 56 (7), 584-590.

60. Bunet R, Song L, Mendes MV, Corre C, Hotel L, Rouhier N, *et al*. Characterization and manipulation of the pathway-specific late regulator AlpW reveals *Streptomyces ambofaciens* as a new producer of kinamycins. J Bacteriol. 2011; 193 (5), 1142-1153.

61. Lee HN, Huang J, Im JH, Kim SH, Noh JH, Cohen SN, *et al*. Putative TetR family transcriptional regulator SCO1712 encodes an antibiotic downregulator in *Streptomyces coelicolor*. Appl Environ Microbiol. 2010; 76 (9), 3039-3043.

62. Takano E, Kinoshita H, Mersinias V, Bucca G, Hotchkiss G, Nihira T, *et al*. A bacterial hormone (the SCB1) directly controls the expression of a pathway-specific regulatory gene in the cryptic type I polyketide biosynthetic gene cluster of *Streptomyces coelicolor*. Mol Microbiol. 2005; 56 (2), 465-479.

63. Gomez-Escribano JP, Song L, Fox DJ, Yeo V, Bibb MJ, Challis GL. Structure and biosynthesis of the unusual polyketide alkaloid coelimycin P1, a metabolic product of the *cpk* gene cluster of *Streptomyces coelicolor* M145. Chem Sci. 2012; 3 (9), 2716-2720.

64. Martínez-Burgo Y, Santos-Aberturas J, Rodríguez-García A, Barreales EG, Tormo JR, Truman AW, *et al*. Activation of secondary metabolite gene clusters in *Streptomyces clavuligerusby* the PimM regulator of *streptomyces natalensis*. Front Microbiol. 2019; 10, 580.

65. Wu Q Bin, Chen XA, Lv ZY, Zhang XY, Liu Y, Li YQ. Activation and discovery of tsukubarubicin from *Streptomyces tsukubaensis* through overexpressing SARPs. Appl Microbiol Biotechnol. 2021; 1-11.

66. Krause J, Handayani I, Blin K, Kulik A, Mast Y. Disclosing the potential of the SARP-type regulator Papr2 for the activation of antibiotic gene clusters in streptomycetes. Front Microbiol. 2020; 11, 225.

67. Wilkinson B, Micklefield J. Mining and engineering natural-product biosynthetic pathways. Nat Chem Biol. 2007; 3 (7), 379-386.

68. Liu T, Mazmouz R, Ongley SE, Chau R, Pickford R, Woodhouse JN, *et al*. Directing the heterologous production of specific cyanobacterial toxin variants. ACS Chem Biol. 2017; 12 (8), 2021-2029.

69. Ongley SE, Bian X, Zhang Y, Chau R, Gerwick WH, Müller R, *et al*. High-titer heterologous production in *E. coli* of lyngbyatoxin, a protein kinase C activator from an uncultured marine *Cyanobacterium*. ACS Chem Biol. 2013; 8 (9), 1888-1893.

70. Wendt-Pienkowski E, Huang Y, Zhang J, Li B, Jiang H, Kwon H, *et al*. Cloning, sequencing, analysis, and heterologous expression of the fredericamycin biosynthetic gene cluster from *Streptomyces griseus*. J Am Chem Soc. 2005; 127 (47), 16442-16452.

71. Young TS, Walsh CT. Identification of the thiazolyl peptide GE37468 gene cluster from *Streptomyces* ATCC 55365 and heterologous expression in *Streptomyces lividans*. Proc Natl Acad Sci U S A. 2011; 108 (32), 13053-13058.

72. Smith DJ, Burnham MKR, Edwards J, Earl AJ, Turner G. Cloning and heterologous expression of the penicillin biosynthetic gene cluster from *Penicillium chrysogenum*. Biotechnol. J. 1990; 8 (1), 39-41.

73. Nielsen MT, Nielsen JB, Anyaogu DC, Holm DK, Nielsen KF, Larsen TO, *et al*. Heterologous reconstitution of the intact geodin gene cluster in *Aspergillus nidulans* through a simple and versatile PCR based approach. PLoS One. 2013; (8), e72871.

74. Alberti F, Foster GD, Bailey AM. Natural products from filamentous fungi and production by heterologous expression. Appl Microbiol Biotechnol. 2017; 101 (2), 493-500.

75. Craney A, Ozimok C, Pimentel-Elardo SM, Capretta A, Nodwell JR. Chemical perturbation of secondary metabolism demonstrates important links to primary metabolism. Chem Biol. 2012; 19 (8), 1020-1027.

76. Seyedsayamdost MR. High-Throughput platform for the discovery of elicitors of silent bacterial gene clusters. Proc Natl Acad Sci U S A. 2014; 111 (20), 7266-7271.

77. Panthee S, Takahashi S, Hayashi T, Shimizu T, Osada H. β-carboline biomediators induce reveromycin production in *Streptomyces* sp. SN-593. Sci Rep. 2019; (1), 1-8.

78. Umetsu N, Kaji J, Tamari K. Investigation on the toxin production by several blast fungus strains and isolation of tenuazonic acid as a novel toxin. Agric Biol Chem. 1972; 36 (5), 859-866.

79. Aver'yanov AA, Lapikova VP, Lebrun MH. Tenuazonic acid, toxin of rice blast fungus, induces disease resistance and reactive oxygen production in plants. Russ J Plant Physiol. 2007; 54 (6), 749-754.

80. Motoyama T, Ishii T, Kamakura T, Osada H. Screening of tenuazonic acid production-inducing compounds and identification of NPD938 as a regulator of fungal secondary metabolism. Biosci Biotechnol Biochem. 2021; 85 (10), 2200-2208.

81. Yun CS, Motoyama T, Osada H. Biosynthesis of the mycotoxin tenuazonic acid by a fungal NRPS-PKS hybrid enzyme. Nat Commun. 2015; 6 (1), 1-9.

82. Meyer V, Andersen MR, Brakhage AA, Braus GH, Caddick MX, Cairns TC, *et al*. Current challenges of research on filamentous fungi in relation to human welfare and a sustainable bio-economy: a white paper. Fungal Biol Biotechnol. 2016; 3 (1), 1-17.

83. Brakhage AA. Regulation of fungal secondary metabolism. Nat Rev Microbiol. 2013; 11 (1), 21–32.

84. Hertweck C. Hidden biosynthetic treasures brought to light. Nat Chem Biol. 2009; 5 (7), 450-452.

85. Bergmann S, Schümann J, Scherlach K, Lange C, Brakhage AA, Hertweck C. Genomics-driven discovery of PKS-NRPS hybrid metabolites from *Aspergillus nidulans*. Nat Chem Biol. 2007; 3 (4), 213-217.

86. Motoyama T, Nogawa T, Hayashi T, Hirota H, Osada H. Induction of nectriapyrone biosynthesis in the rice blast fungus *Pyricularia oryzae* by disturbance of the two-component signal transduction system. ChemBioChem. 2019; 20 (5), 693-700.

87. Biggins JB, Liu X, Feng Z, Brady SF. Metabolites from the induced expression of cryptic single operons found in the genome of *Burkholderia pseudomallei*. J Am Chem Soc. 2011; 133 (6), 1638-1641.

88. Bok JW, Hoffmeister D, Maggio-Hall LA, Murillo R, Glasner JD, Keller NP. Genomic mining for *Aspergillus* natural products. Chem Biol. 2006; 13 (1), 31-37.

89. Nogawa T, Terai A, Amagai K, Hashimoto J, Futamura Y, Okano A, *et al*. Heterologous expression of the biosynthetic gene cluster for verticilactam and identification of analogues. J Nat Prod. 2020; 83 (12), 3598-3605.

90. Takao R, Sakai K, Koshino H, Osada H, Takahashi S. Identification of the kinanthraquinone biosynthetic gene cluster by expression of an atypical response regulator. Biosci Biotechnol Biochem. 2021; 85 (3), 714-721.

91. Panthee S, Takahashi S, Takagi H, Nogawa T, Oowada E, Uramoto M, *et al*. Furaquinocins I and J: Novel polyketide isoprenoid hybrid compounds from *Streptomyces reveromyceticus* SN-593. J Antibiot. 2011; 64 (7), 509-513.

92. Yun CS, Motoyama T, Osada H. Regulatory mechanism of mycotoxin tenuazonic acid production in *Pyricularia oryzae*. ACS Chem Biol. 2017; 12 (9), 2270-2274.

93. Bok JW, Chung DW, Balajee SA, Marr KA, Andes D, Nielsen KF, *et al*. GliZ, a transcriptional regulator of gliotoxin biosynthesis, contributes to *Aspergillus fumigatus* virulence. Infect Immun. 2006; 74 (12), 6761-6768.

94. Panthee S, Kito N, Hayashi T, Shimizu T, Ishikawa J, Hamamoto H, *et al*. β-carboline chemical signals induce reveromycin production through a LuxR family regulator in *Streptomyces* sp. SN-593. Sci Rep. 2020; 10 (1), 1-10.

95. Osada H. Introduction of new tools for chemical biology research on microbial metabolites. Bioscience, Biotechnology and Biochemistry. 2010; 74 (6), 1135-1140.

96. Kato N, Takahashi S, Nogawa T, Saito T, Osada H. Construction of a microbial natural product library for chemical biology studies. Curr Opin Chem Biol. 2012; 16 (1-2), 101-108.

97. Bashyal BP, Faeth SH, Gunatilaka AAL. 13α–Hydroxylucilactaene and other metabolites of an endophytic strain of *Fusarium acuminatum*. Nat Prod Commun. 2007; 2 (5), 547-550.

98. Kakeya H, Kageyama SI, Nie L, Onose R, Okada G, Beppu T, *et al*. Lucilactaene, a new cell cycle inhibitor in p53-transfected cancer cells, produced by a *Fusarium* sp. J Antibiot. 2001; 54 (10), 850-854.

99. Kato S, Motoyama T, Futamura Y, Uramoto M, Nogawa T, Hayashi T, *et al*. Biosynthetic gene cluster identification and biological activity of lucilactaene from *Fusarium* sp. RK97-94. Biosci Biotechnol Biochem. 2020; 84 (6), 1303-1307.

100. Kyekyeku JO, Kusari S, Adosraku RK, Bullach A, Golz C, Strohmann C, *et al*. Antibacterial secondary metabolites from an endophytic fungus, *Fusarium solani* JK10. Fitoterapia. 2017; 119, 108-114.

101. Maharjan S, Lee SB, Kim GJ, Cho SJ, Nam JW, Chin J, *et al*. Isolation of unstable isomers of lucilactaene and evaluation of anti-inflammatory activity of secondary metabolites produced by the endophytic fungus *Fusarium* sp. QF001 from the roots of *Scutellaria baicalensis*. Molecules. 2020; 25 (4), 923.

102. Krasnoff SB, Sommers CH, Moon Y-S, Donzelli BGG, Vandenberg JD, Churchill ACL, *et al*. Production of mutagenic metabolites by *Metarhizium anisopliae*. J Agric Food Chem. 2006; 54 (19), 7083-7088.

103. Kleigrewe K, Aydin F, Hogrefe K, Piecuch P, Bergander K, Würthwein EU, *et al*. Structure elucidation of new fusarins revealing insights in the rearrangement mechanisms of the *Fusarium* mycotoxin fusarin C. J Agric Food Chem. 2012; 60 (21), 5497-5505.

104. Hayashi Y, Yamaguchi J, Shoji M. The diastereoselective asymmetric total synthesis of NG-391, a neuronal cell-protecting molecule. Tetrahedron. 2002; 58 (49), 9839-9846.

105. Lim CL, Nogawa T, Uramoto M, Okano A, Hongo Y, Nakamura T, *et al*. RK-1355A and B, novel quinomycin derivatives isolated from a microbial metabolites fraction library based on NPPlot screening. J Antibiot. 2014; 67 (4), 323-329.

106. Nogawa T, Okano A, Lim CL, Futamura Y, Shimizu T, Takahashi S, *et al*. Opantimycin A, a new metabolite isolated from *Streptomyces* sp. RK88-1355. J Antibiot. 2017; 70 (2), 222-225.

107. Coleman RS, Walczak MC, Campbell EL. Total synthesis of Lucilactaene, a cell cycle inhibitor active in p53-inactive cells. J Am Chem Soc. 2005; 127 (46), 16038-16039.

108. Yamaguchi J, Kakeya H, Uno T, Shoji M, Osada H, Hayashi Y. Determination by asymmetric total synthesis of the absolute configuration of lucilactaene, a cell-cycle inhibitor in p53-transfected cancer cells. Angew Chemie. 2005; 44 (20), 3110-3115.

109. A. Abdelhakim I, Bin Mahmud F, Motoyama T, Futamura Y, Takahashi S, Osada H. Dihydrolucilactaene, a Potent Antimalarial Compound from Fusarium sp. RK97-94. J Nat Prod. 2022; 85(1), 63–69.

110. Niehaus EM, Kleigrewe K, Wiemann P, Studt L, Sieber CMK, Connolly LR, *et al*. Genetic manipulation of the *Fusarium fujikuroi* fusarin gene cluster yields insight into the complex regulation and fusarin biosynthetic pathway. Chem Biol. 2013; 20 (8), 1055-1066.

111. Kleigrewe K, Niehaus EM, Wiemann P, Tudzynski B, Humpf HU. New approach via gene knockout and single-step chemical reaction for the synthesis of isotopically labeled fusarin C as an internal standard for the analysis of this fusarium mycotoxin in food and feed samples. J Agric Food Chem. 2012; 60(34), 8350-8355.

112. Yang Q, Wang W, Lin Y, Lin Y, Tang Z, Wang J, *et al*. Characterization of a carboxyl methyltransferase in Fusarium graminearum provides insights into the biosynthesis of fusarin A. Org Biomol Chem. 2021; 19(30), 6638–6643.

113. Sambrook J, Fritsch EF, Maniatis T. Molecular cloning: A laboratory manual, 2nd edn by Cold Spring Harbor Laboratory Press, 1989. Trends Biotechnol. 1991.

114. De Groot MJA, Bundock P, Hooykaas PJJ, Beijersbergen AGM, Chapman JW. *Agrobacterium tumefaciens*-mediated transformation of filamentous fungi. Nat Biotechnol. 1998; 16 (9), 839-842.

115. Motoyama T, Ochiai N, Morita M, Iida Y, Usami R, Kudo T. Involvement of putative response regulator genes of the rice blast fungus *Magnaporthe oryzae* in

osmotic stress response, fungicide action, and pathogenicity. Current Genetics. 2008; 54 (4), 185-195.

116. Motoyama T, Hayashi T, Hirota H, Ueki M, Osada H. Terpendole E, a kinesin Eg5 inhibitor, is a key biosynthetic intermediate of indole-diterpenes in the producing fungus *Chaunopycnis alba*. Chem Biol. 2012; 19 (12), 1611-1619.

117. Motoyama T, Kadokura K, Ohira T, Ichiishi A, Fujimura M, Yamaguchi I, *et al*. A two-component histidine kinase of the rice blast fungus is involved in osmotic stress response and fungicide action. Fungal Genet Biol. 2005; 42 (3), 200-212.

**Supporting information**

Contents

**Table S1.** NMR spectroscopic data (500 MHz, CDCl$_3$) for compound **3** compared with 13α-hydroxylucilactaene from literature.

**Table S2.** PCR primers used in Δ*luc2* and Δ*luc3* mutants' construction.

**Table. S3.** List of cell lines and fungal strains used in this study.

**Fig. S1.** Structure of NPD938.

**Fig. S2.** UPLC chromatograms of *Fusarium* sp. RK97-94 WT and Δ*luc5* strains induced with NPD938 30 μM, showing disappearance of lucilactaene, NGs and induced compound peaks in Δ*luc5* culture proving that the induced compound is lucilactaene analogue.

**Fig. S3.** Fractionation scheme of EtOAc extract using normal phase MPLC followed by RP-HPLC to give subfractions (I-IV), from which compounds **1-3** were isolated.

**Fig. S4.** Static culture of *Fusarium* sp. RK97-94 in YG media induced by NPD938 (30 μM) for 10 days at 28 °C.

**Fig. S5.** MPLC fractionation of EtOAc extract (2.77 g) of *Fusarium* sp. RK97-94 using Hexane: EtOAc gradient elution.

**Fig. S6.** HR-ESI-TOF/MS of DihydroNG391 (**1**).

**Fig. S7.** $^1$H-NMR spectrum of DihydroNG391 (**1**) (CD$_3$OD, 500 MHz).

**Fig. S8.** $^{13}$C-NMR spectrum of DihydroNG391 (**1**) (CD$_3$OD, 125 MHz).

**Fig. S9.** DEPT135 spectrum of DihydroNG391 (**1**) (CD$_3$OD, 125 MHz).

**Fig. S10.** $^1$H-$^1$H COSY spectrum of DihydroNG391 (**1**) (CD$_3$OD, 500 MHz).

**Fig. S11.** HSQC spectrum of DihydroNG391 (**1**) (CD$_3$OD, 500/125 MHz).

**Fig. S12.** HMBC spectrum of DihydroNG391 (**1**) (CD$_3$OD, 500/125 MHz).

**Fig. S13.** NOESY spectrum of DihydroNG391 (**1**) (CD$_3$OD, 500 MHz).

**Fig. S14.** HR-ESI-TOF/MS of Dihydrolucilactaene (**2**).

**Fig. S15.** $^1$H-NMR spectrum of Dihydrolucilactaene (**2**) (CDCl$_3$, 500 MHz).

**Fig. S16.** $^{13}$C-NMR spectrum of Dihydrolucilactaene (**2**) (CDCl$_3$, 125 MHz).

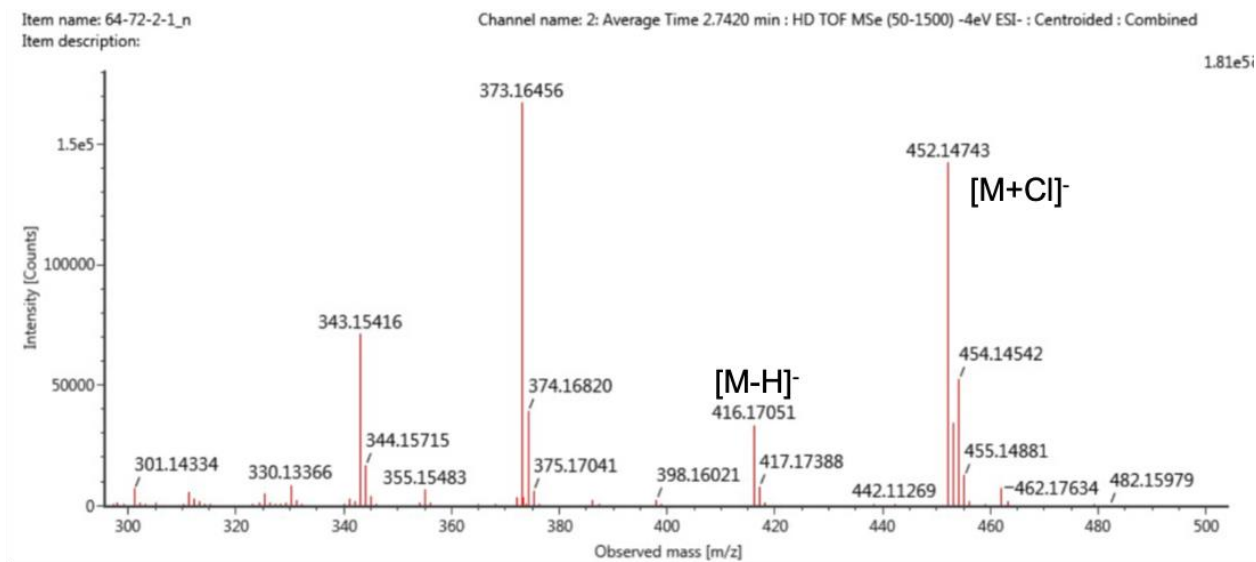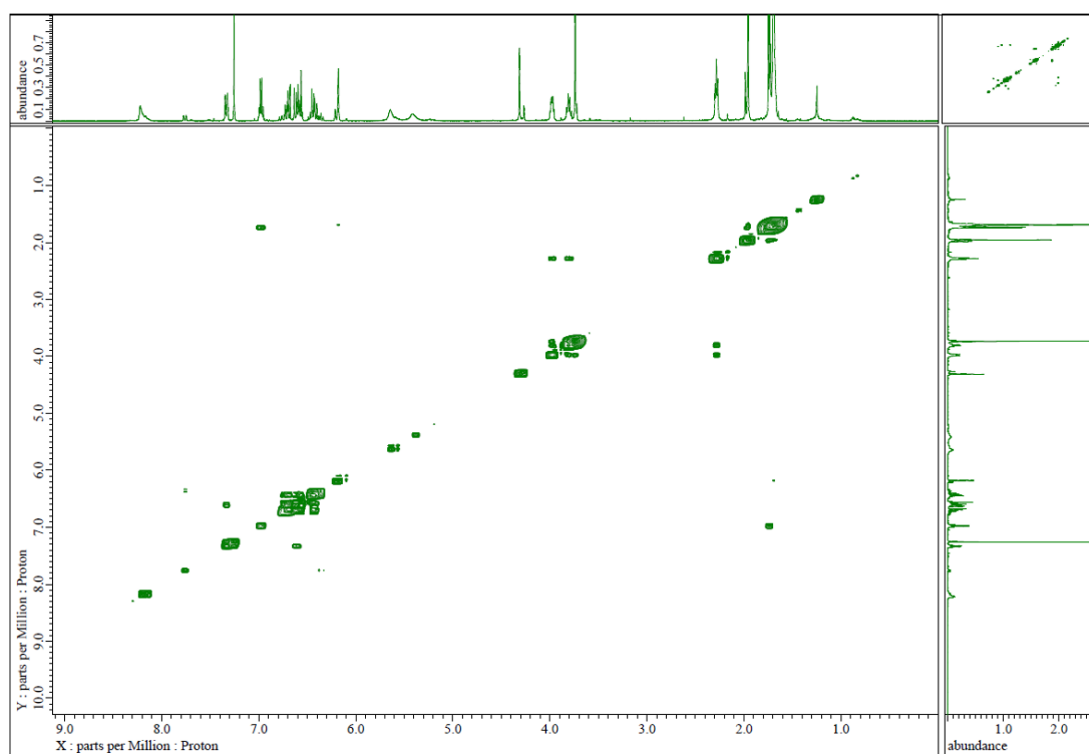**Fig. S17.** DEPT135 spectrum of Dihydrolucilactaene (**2**) (CDCl$_3$, 125 MHz).

**Fig. S18.** $^1$H-$^1$H COSY spectrum of Dihydrolucilactaene (**2**) (CDCl$_3$, 500 MHz).

**Fig. S19.** HSQC spectrum of Dihydrolucilactaene (**2**) (CDCl$_3$, 500/125 MHz).

**Fig. S20.** HMBC spectrum of Dihydrolucilactaene (**2**) (CDCl$_3$, 500/125 MHz).

**Fig. S21.** NOESY spectrum of Dihydrolucilactaene (**2**) (CDCl$_3$, 500 MHz).

**Fig. S22.** HR-ESI-TOF/MS of 13α-hydroxylucilactaene (**3**).

**Fig. S23.** $^1$H-NMR spectrum of 13α-hydroxylucilactaene (**3**) (CDCl$_3$, 500 MHz).

**Fig. S24.** $^{13}$C-NMR spectrum of 13α-hydroxylucilactaene (**3**) (CDCl$_3$, 125 MHz).

**Fig. S25.** DEPT135 spectrum of 13α-hydroxylucilactaene (**3**) (CDCl$_3$, 125 MHz).

**Fig. S26.** $^1$H-$^1$H COSY spectrum of 13α-hydroxylucilactaene (**3**) (CDCl$_3$, 500 MHz).

**Fig. S27.** HSQC spectrum of 13α-hydroxylucilactaene (**3**) (CDCl$_3$, 500/125 MHz).

**Fig. S28.** HMBC spectrum of 13α-hydroxylucilactaene (**3**) (CDCl$_3$, 500/125 MHz).
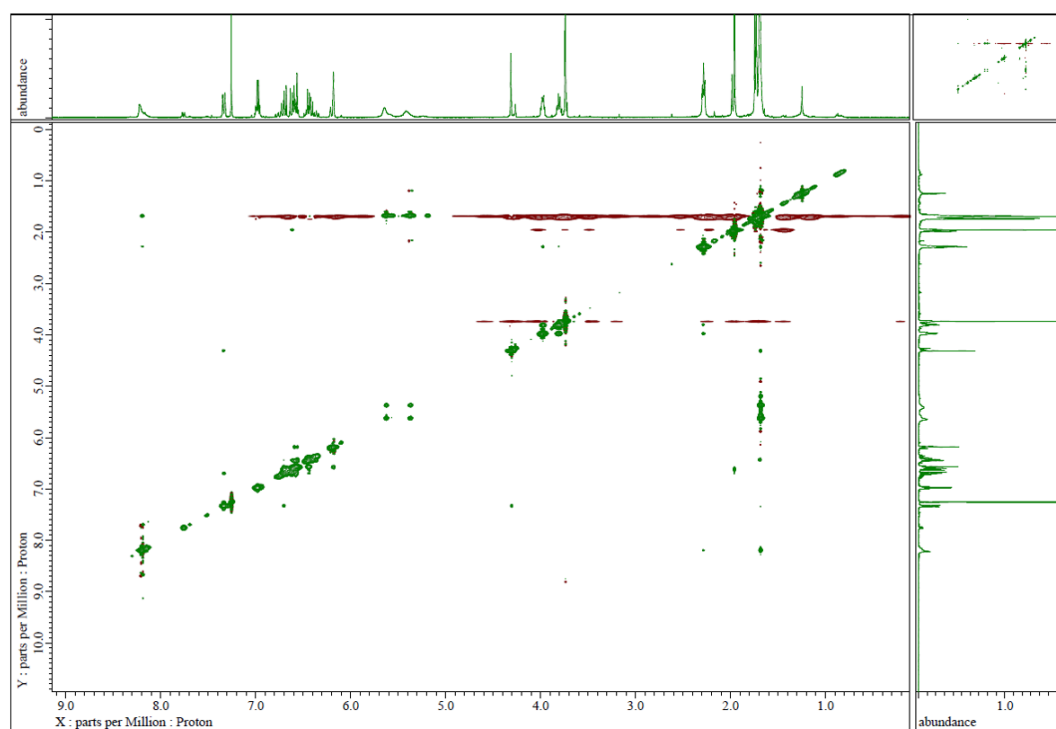
**Fig. S29.** NOESY spectrum of 13α-hydroxylucilactaene (**3**) (CDCl$_3$, 500 MHz).
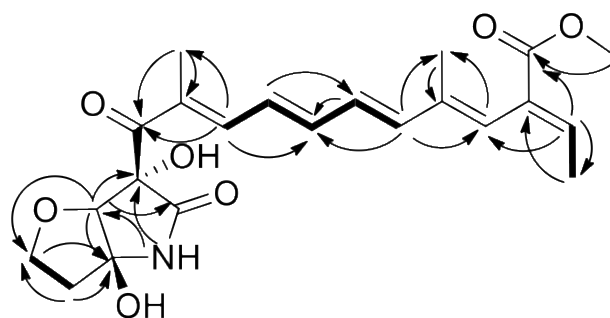
**Fig. S30.** 2D-NMR correlations of 13α-hydroxylucilactaene (**3**). COSY: bold line, HMBC: arrows
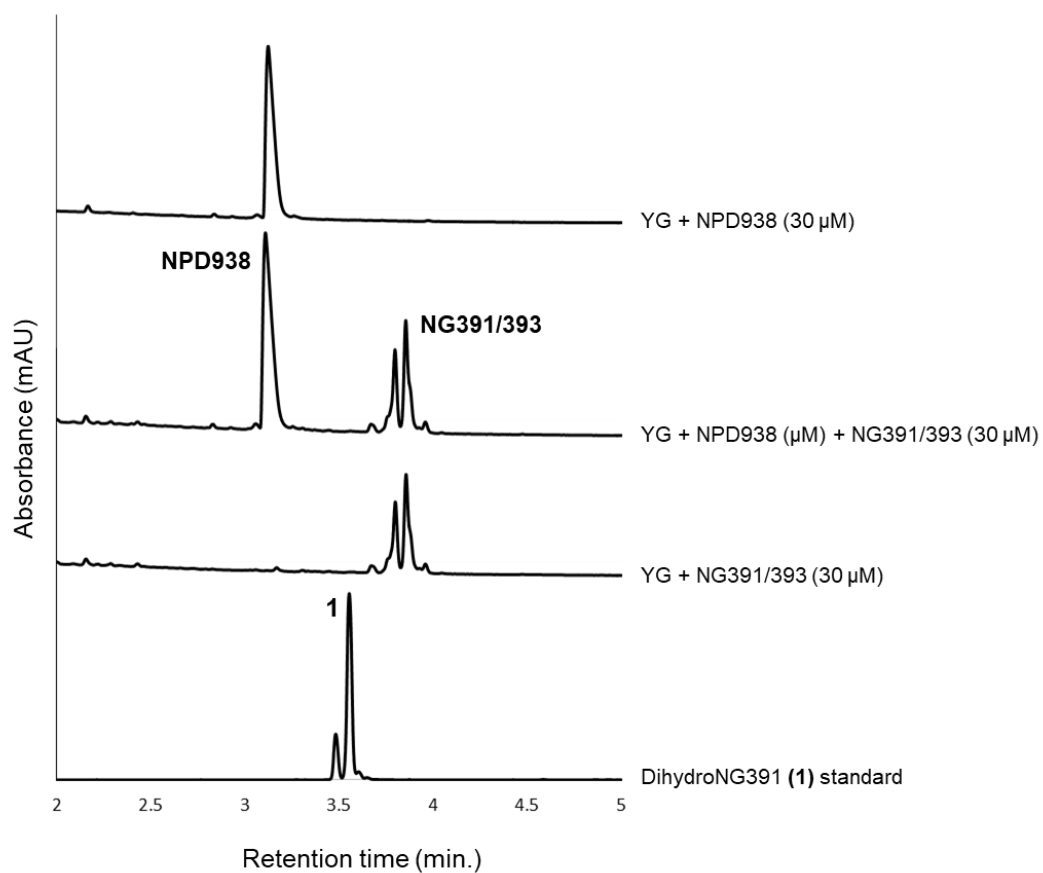
**Fig. S31.** UPLC-MS analysis after incubation of NPD938 (30 μM) with NG391/393 (30 μm) for 7 days resulted in no direct interaction between both compounds.

**Fig. S32.** Biosynthetic gene cluster of lucilactaene with predicted functions of its genes.

**Fig. S33.** Purification scheme for compounds **4** and **5**.

**Fig. S34.** Purification scheme for compounds **6-9**.

**Fig. S79.** HMBC spectrum of prelucilactaene E (**8**) (CD$_3$OD, 500/125 MHz).

**Fig. S80.** NOESY spectrum of prelucilactaene E (**8**) (CD$_3$OD, 500 MHz).

**Fig. S81.** HR-ESI-TOF/MS of prelucilactaene F (**9**).

**Fig. S82.** IR spectrum of prelucilactaene F (**9**).

**Fig. S83.** $^1$H-NMR of prelucilactaene F (**9**), compared with lucilactaene (CDCl$_3$, 500 MHz).

**Fig. S84.** $^1$H-$^1$H COSY spectrum of prelucilactaene F (**9**) (CDCl$_3$, 500 MHz).

**Fig. S85.** DEPT135 NMR of prelucilactaene F (**9**) (CDCl$_3$, 125 MHz).

**Fig. S86.** HSQC spectrum of prelucilactaene F (**9**) (CDCl$_3$, 500/125 MHz).

**Fig. S87.** MSMS fragmentation of prelucilactaene F (**9**).

**Fig. S88.** Reported MSMS fragmentations of Fusarin C and its derivatives.

**Fig. S89.** MSMS fragmentation of Lucilactaene.

**Fig. S90.** MSMS fragmentation of Dihydrolucilactaene (**2**).

**Fig. S91.** MSMS fragmentation of NG391.

**Fig. S92.** MSMS fragmentation of 13α-hydroxylucilactaene (**3**).

**Fig. S93.** MSMS fragmentation of DihydroNG391 (**1**).

**Fig. S94.** MSMS fragmentation of MW361 compound (prelucilactaene G, **4**).

**Fig. S95.** MSMS fragmentation of MW361 compound (prelucilactaene B, **7**).

**Fig. S96.** MSMS fragmentation of MW373 compound (prelucilactaene E, **8**).

**Fig. S97.** MSMS fragmentation of MW343 (prelucilactaene C).

**Fig. S98.** MSMS fragmentation of MW359 (prelucilactaene D).

**Fig. S99.** LC-MS analysis of ethanolic extract of PKS-NRPS knockout strain (Δ*luc5*) after feeding with:

**A.** Prelucilactaene B (MW361, **7**) and **B.** Prelucilactaene E (MW373, **8**). Fed compounds

displayed significant instability in the production medium within the first 24 hours which

prevent its conversion to the final products.

**Fig. S100.** Possible conversion mechanism of compounds isolated from the Δ*luc2* strain.

**Table S1.** NMR data (500 MHz, CDCl$_3$) for compound **3** compared with 13α-

hydroxylucilactaene from literature [97].

| No. | Compound (3) | | | 13α-hydroxylucilactaene | |
|-----|--------------|--------|------|-------------------------|--------|
|     | δ$_H$ (Multiplicity, $J$ Hz) | δ$_C$ | HMBC | δ$_H$ (Multiplicity, $J$ Hz) | δ$_C$ |
| 1 | 1.73 dd (6.87, 1.15) | 16.1 | 2, 3 | 1.72 d (7.0) | 16.0 |
| 2 | 6.97 q (6.87) | 140.5 | 1, 4, 20 | 6.96 q (7.0) | 140.4 |
| 3 | - | 130.4 | | - | 130.4 |
| 4 | 6.18 brs | 127.5 | 2, 22 | 6.16 s | 127.4 |
| 5 | - | 138.2 | | - | 138.1 |
| 6 | 6.56 d (15.46) | 141.2 | 4, 8, 22 | 6.55 d (14.5) | 141.1 |
| 7 | 6.68 dd (10.88, 14.89) | 142.1 | 8 | 6.69 dd (14.5, 10.8) | 142.0 |
| 8 | 6.42 dd (10.31, 14.89) | 128.7 | 9 | 6.41 dd (15.2, 10.8) | 128.7 |
| 9 | 6.61 dd (10.88, 14.89) | 128.4 | 7 | 6.58 dd (15.2, 11.4) | 128.3 |
| 10 | 7.32 d (11.46) | 143.2 | 8, 12, 23 | 7.36 d (11.4) | 143.1 |
| 11 | - | 133.0 | | - | 133.0 |
| 12 | - | 196.8 | | - | 197.0 |
| 13 | - | 85.2 | | - | 85.4 |
| 14 | 4.31 s | 91.3 | 13, 17, 19 | 4.33 s | 91.2 |
| 15 | - | 95.4 | | - | 95.3 |
| 16 | 8.22 | | 13, 14 | 8.22 brs | - |
| 17 | - | 175.5 | | - | 175.5 |
| 18 | 2.28 t (6.87) | 38.0 | 15, 19 | 2.26 m | 38.0 |
| 19a | 3.79 m | 68.9 | 15 | 3.74 m | 68.8 |
| 19b | 3.97 m | 68.9 | | 3.94 m | 68.8 |
| 20 | - | 167.6 | | - | 167.5 |
| 21 | 3.74 s | 52.0 | 20 | 3.72 s | 51.9 |
| 22 | 1.69 s | 14.4 | 4, 5 | 1.68 s | 14.3 |
| 23 | 1.95 s | 12.6 | 11, 12 | 1.93 s | 12.4 |

**Table S2.** PCR primers used in Δ*luc2* and Δ*luc3* mutants' construction.

| Target gene or vector | Primer | Sequence |
|---|---|---|
| *luc2* | IF_LB-luc2-5F | AACACATTGCGGACGTTGCTACTGGAAACTGCG TAATCCTCA |
| *luc2* | IF_5HPH-luc2-5R | GGTATCGATAAGCTTCGACTCGGGCAGCTTCAGG CGACCCAC |
| *luc2* | IF_3HPH-luc2-3F | CAAGAATAAAACGCGGTGTATCTGTGTAGCTGGC CAACATGA |
| *luc2* | IF_RB-luc2-3R | GGAAACGACAATCTGAACGACGATACATCCATGC TAGCTGCC |
| *luc3* | IF_LB-luc3-5F | AACACATTGCGGACGCTCGTCGCTTTGATCGTGT TCCTCAAG |
| *luc3* | IF_5HPH-luc3-5R | GGTATCGATAAGCTTCAGATGAGGTGAATAATCT CAGATTGA |
| *luc3* | IF_3HPH-luc3-3F | CAAGAATAAAACGCGTACAAAGGATGCGGCACA TGGGGATCT |
| *luc3* | IF_RB-luc3-3R | GGAAACGACAATCTGCGAGTTTCTTCATGACTTT GGGATTTT |
| pCSN45 | 5HPH | AAGCTTATCGATACCGTCGACAGAAGATG |
| pCSN45 | 3HPH | CGCGTTTTATTCTTGTTGACATGGAGC |
| pBI121 | LB | CGTCCCGCAATGTGTTATTAAGTTGTCTAAGC |
| pBI121 | RB | CAGATTGTCGTTTCCCGCCTTCAGTTT |
| *luc2* | luc2-check-R | GGTAATTTGTTAGGCCTTTTACGAAACC |
| *luc3* | luc3-check-R | AGGTGGATACCACTGGTCGACCTCATC |

**Table S3.** Cell lines and fungal strains used in this study.

| **Abbreviation** | **Definition** |
|---|---|
| 3D7 | Wild-type *Plasmodium falciparum* strain |
| HeLa | Hemi-elliptical Lens antenna cell line |
| HL-60 | Human promyelocytic Leukemic cell line |
| K1 | Chloroquine resistant *Plasmodium falciparum* strain |
| MKN-74 | Human stomach tumor cell line |
| T98G | Human glioblastoma tumor cell line |
| Δ*luc2* | P450 monooxygenase knockout *Fusarium* sp. RK97-94 strain |
| Δ*luc3* | Aldehyde dehydrogenase knockout *Fusarium* sp. RK97-94 strain |
| Δ*luc5* | PKS-NRPS knockout *Fusarium* sp. RK97-94 strain |
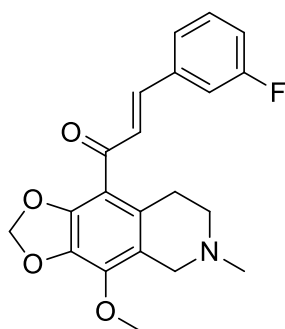
**Fig. S1.** Structure of NPD938.
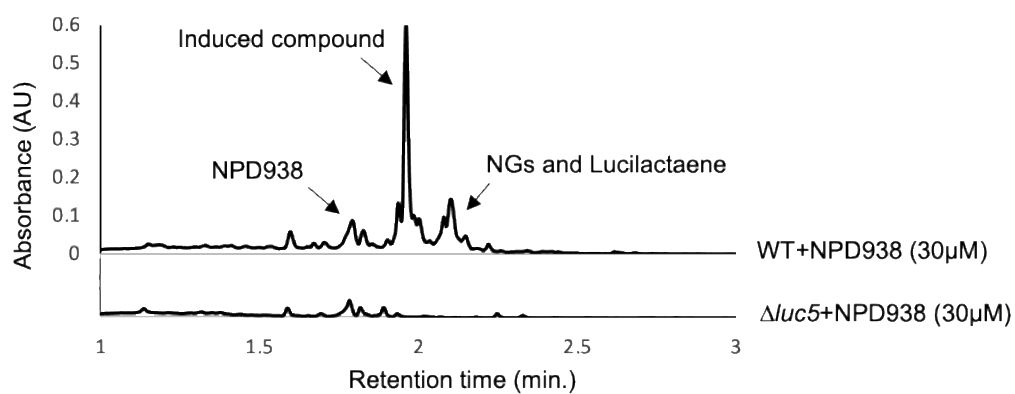


**Fig. S2.** UPLC chromatograms of *Fusarium* sp. RK97-94 WT and *Δluc5* strains induced with NPD938 30 μM, showing disappearance of lucilactaene, NGs and induced compound peaks in *Δluc5* culture proving that the induced compound is lucilactaene analogue.
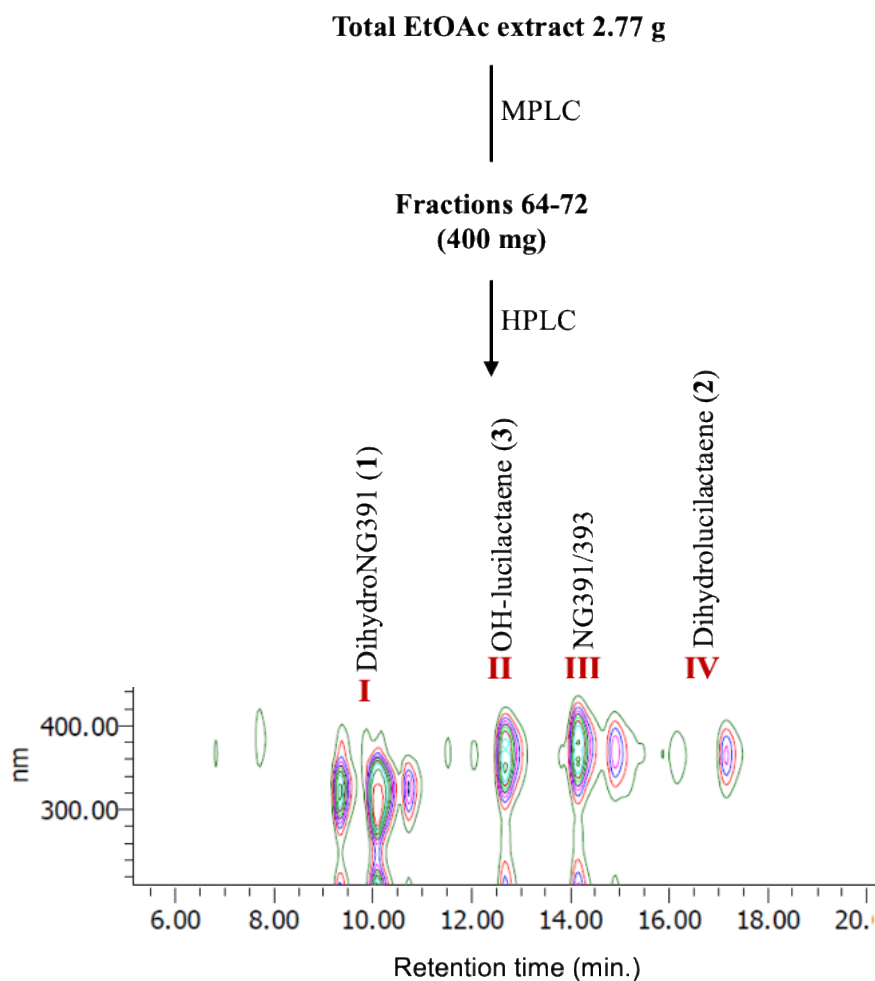
**Fig. S3.** Fractionation scheme of EtOAc extract using normal phase MPLC followed by RP-HPLC to give subfractions (I-IV), from which compounds **1-3** were isolated.

MPLC method: shown in Fig. S3

HPLC method: A (0.05% formic acid in $H_2O$), B (MeCN), gradient elution: B 40 to 60% (0 to 40 min), B 60 to 100% (40 to 50 min), B 100% (50 to 60 min); flow rate of 9 mL/min.

* Lower figure is the 2D PDA-UPLC chromatogram at multi-wavelengths showing lower UV absorption of **(1)** compared with other derivatives.
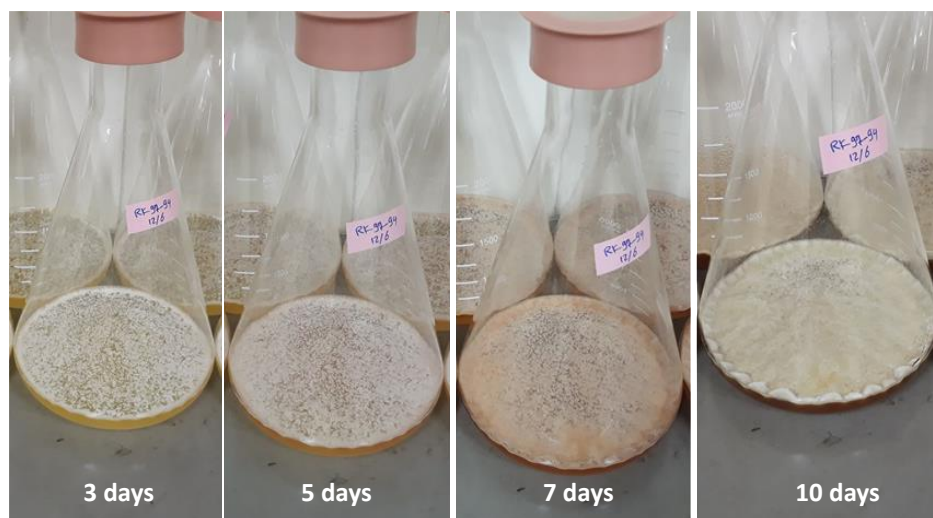
**Fig. S4.** Static culture of *Fusarium* sp. RK97-94 in YG media induced by NPD938 (30 μM)

for 10 days at 28 °C.
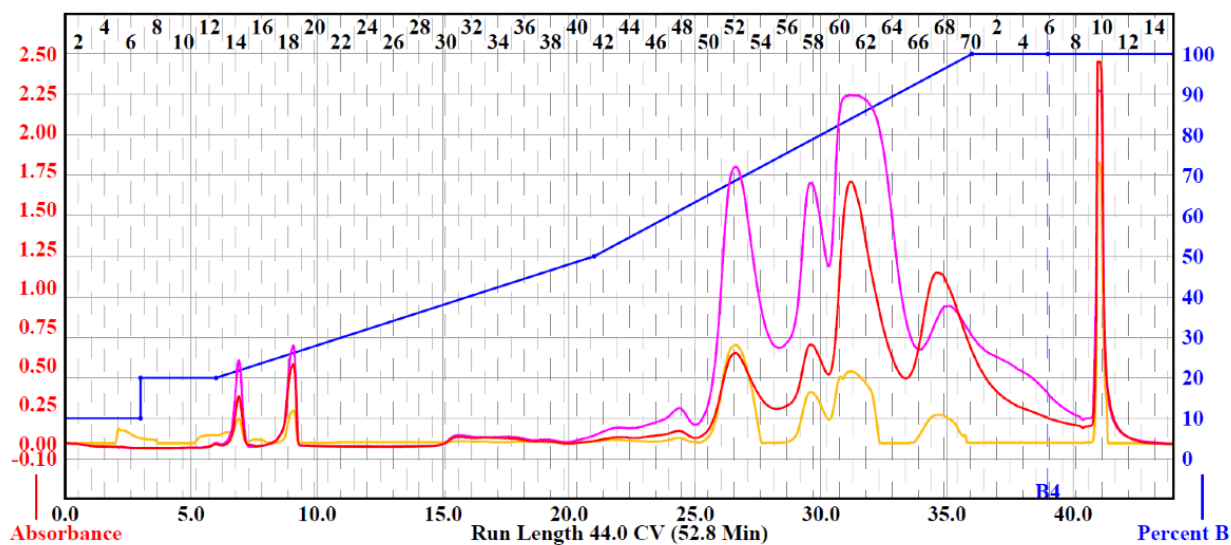


**Fig. S5.** MPLC fractionation of EtOAc extract (2.77 g) of *Fusarium* sp. RK97-94

using Hexane: EtOAc gradient elution.

MPLC method: A (hexane), B (EtOAc), gradient elution: 10% B for 3 CV, 20% B for

3 CV, 20-50 % in 15 CV, 50-100 % in 15 CV then washing with 100% EtOAc (3 CV)

and 100% methanol (5 CV) at 35 mL/min flow rate.
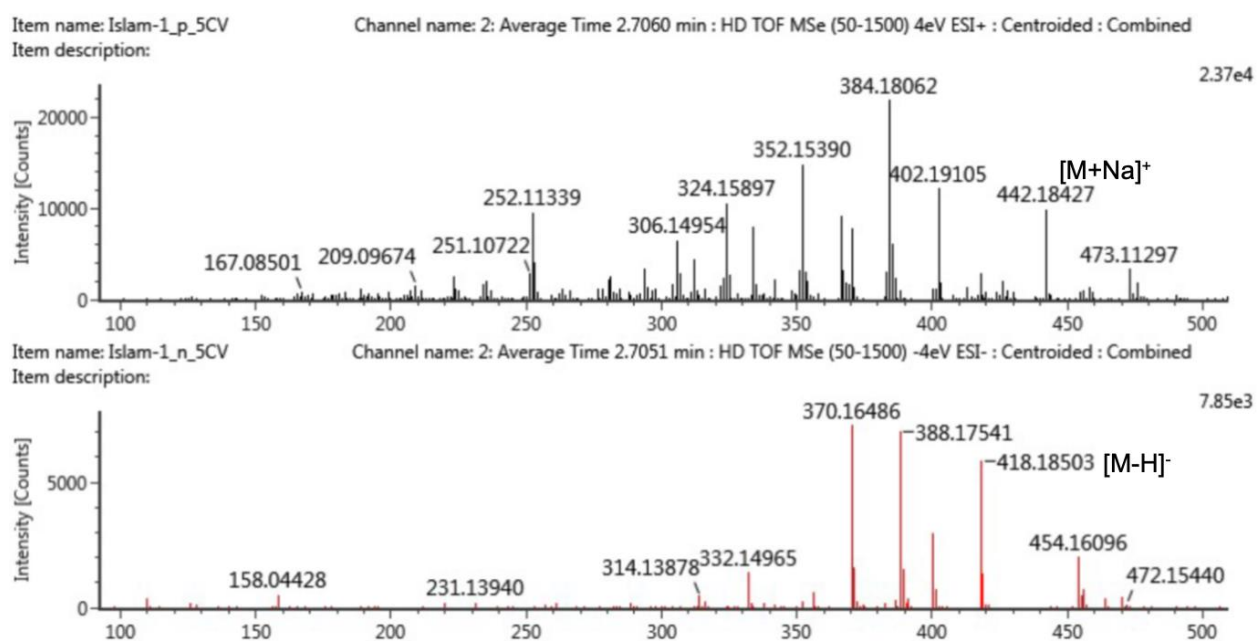
**Fig. S6.** HR-ESI-TOF/MS of dihydroNG391 (**1**).
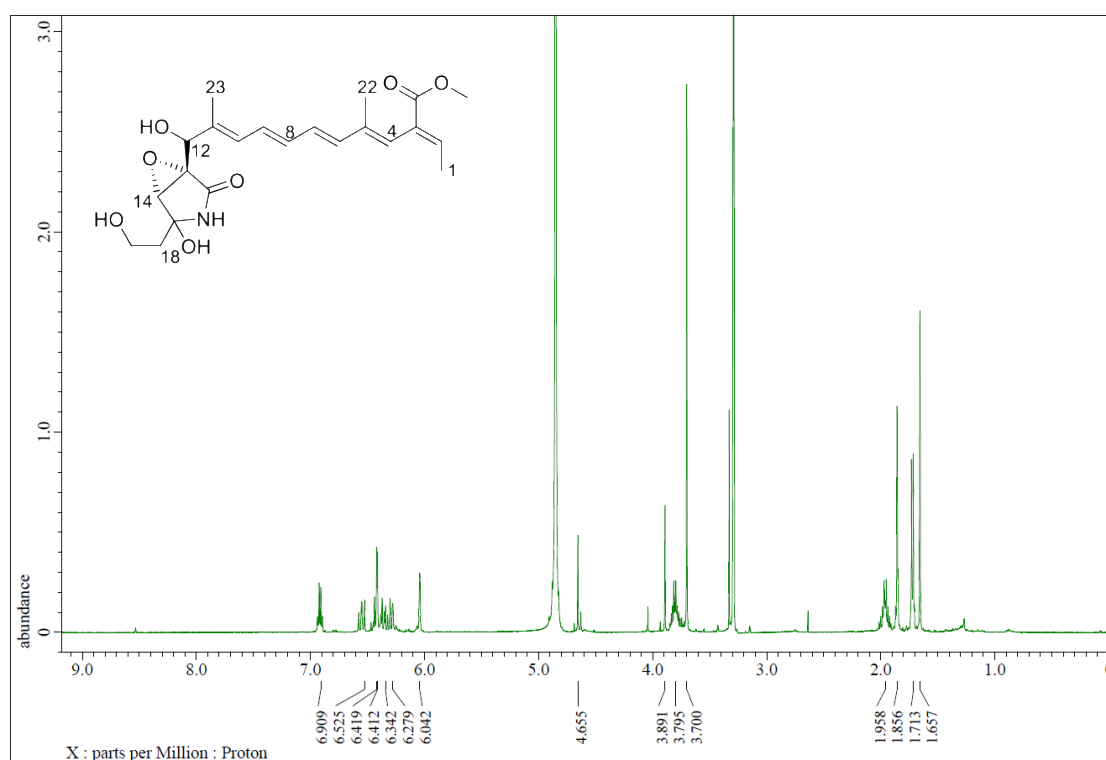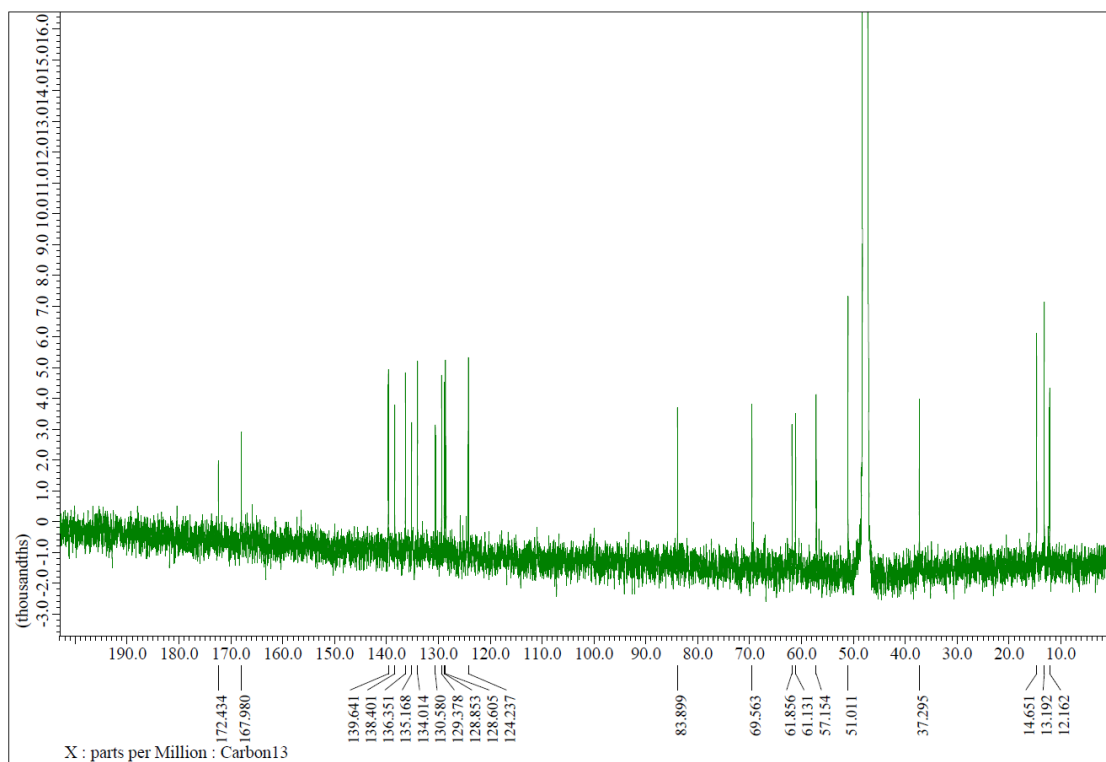
**Fig. S7.** $^1$H-NMR spectrum of DihydroNG391 (**1**) (CD$_3$OD, 500 MHz).



**Fig. S8.** $^{13}$C-NMR spectrum of DihydroNG391 (**1**) (CD$_3$OD, 125 MHz).
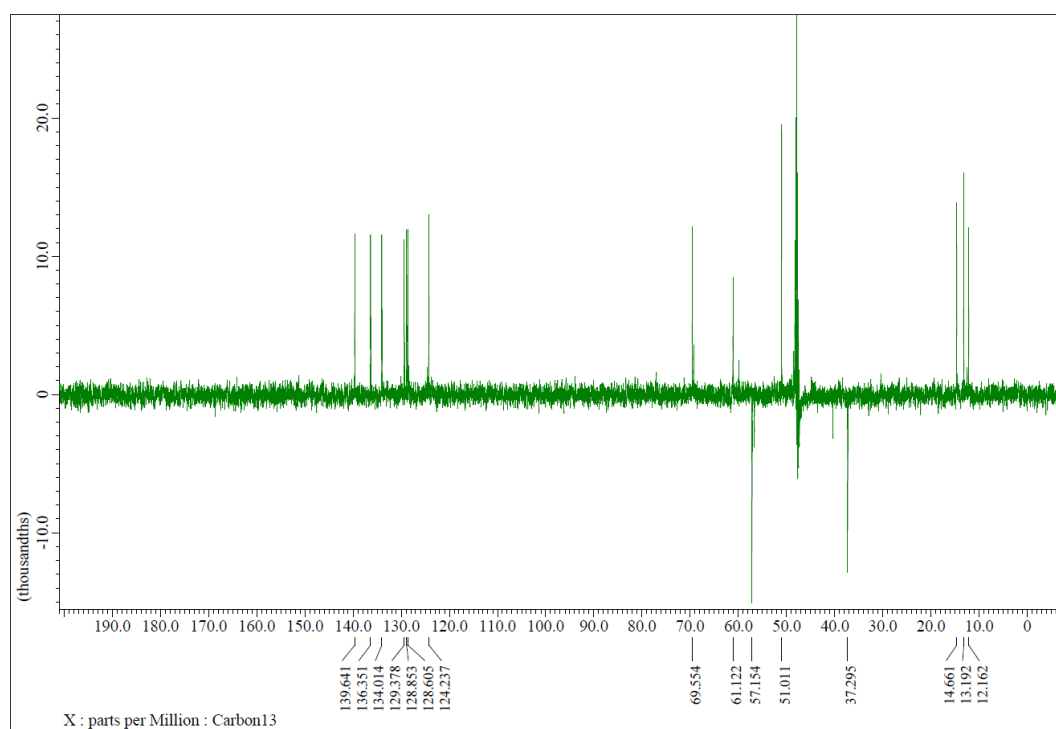
**Fig. S9.** DEPT135 spectrum of DihydroNG391 (**1**) (CD₃OD, 125 MHz).
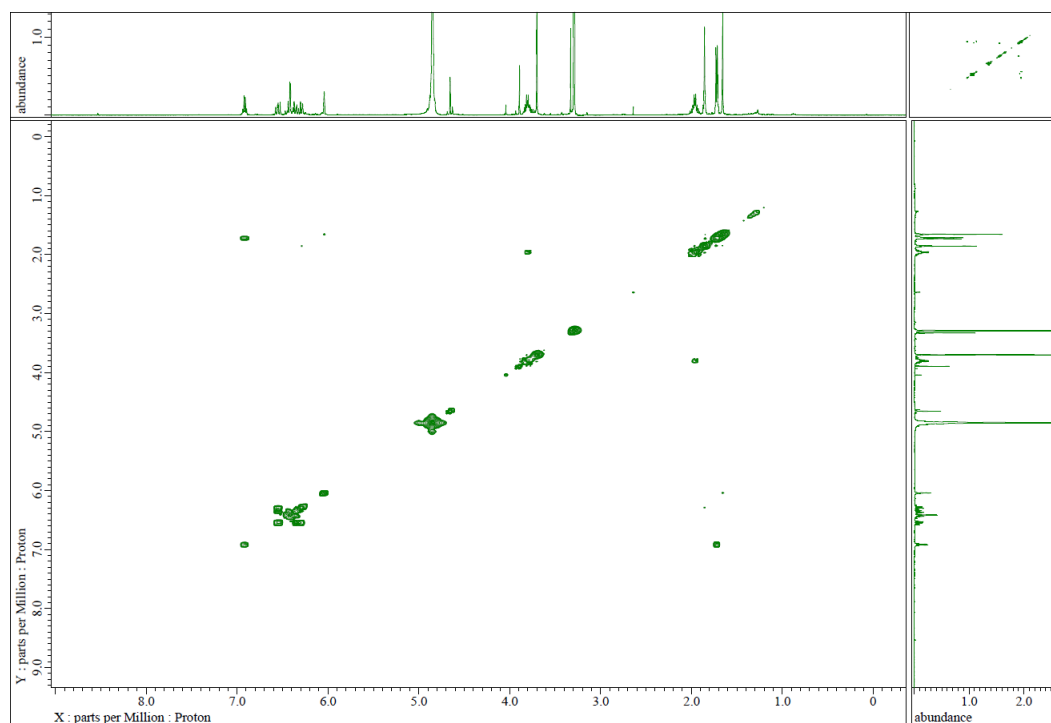


**Fig. S10.** ¹H-COSY spectrum of DihydroNG391 (**1**) (CD₃OD, 500 MHz).
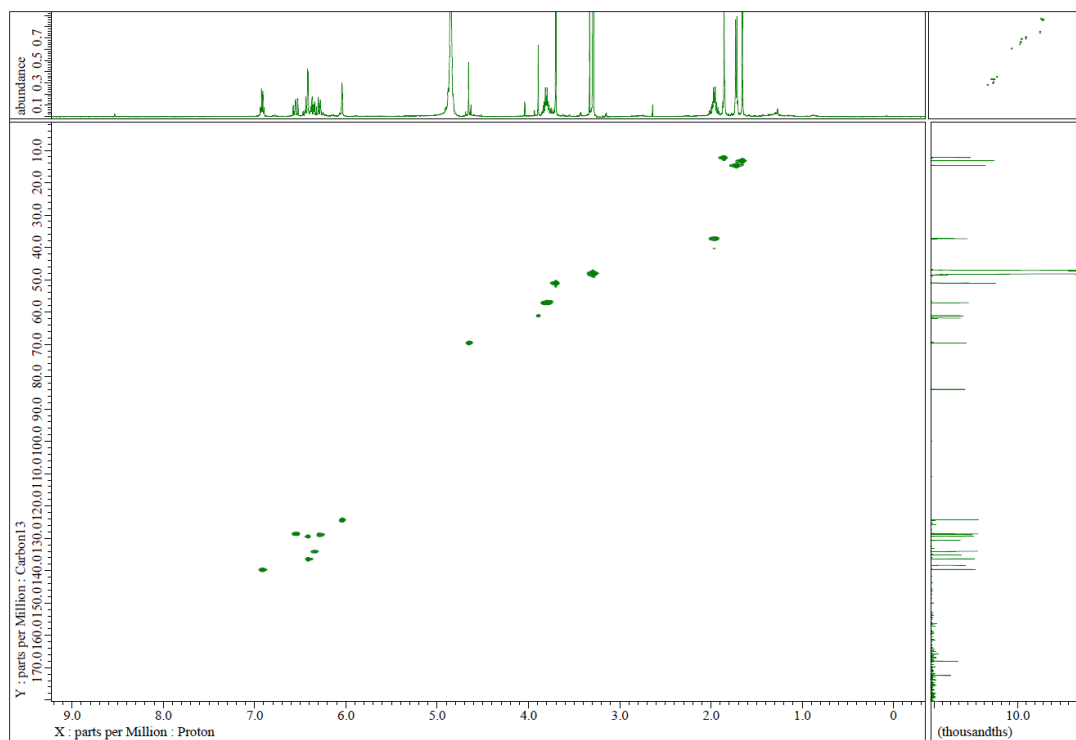
**Fig. S11.** HSQC spectrum of DihydroNG391 (**1**) (CD₃OD, 500/125 MHz).
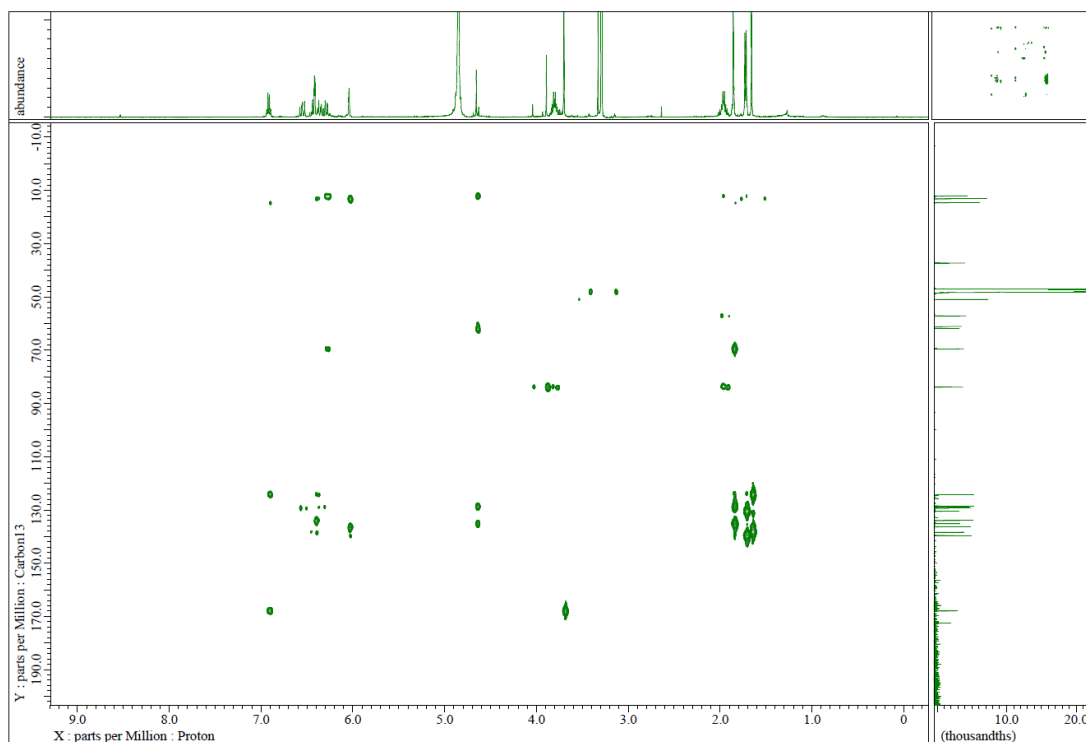


**Fig. S12.** HMBC spectrum of DihydroNG391 (**1**) (CD₃OD, 500/125 MHz).
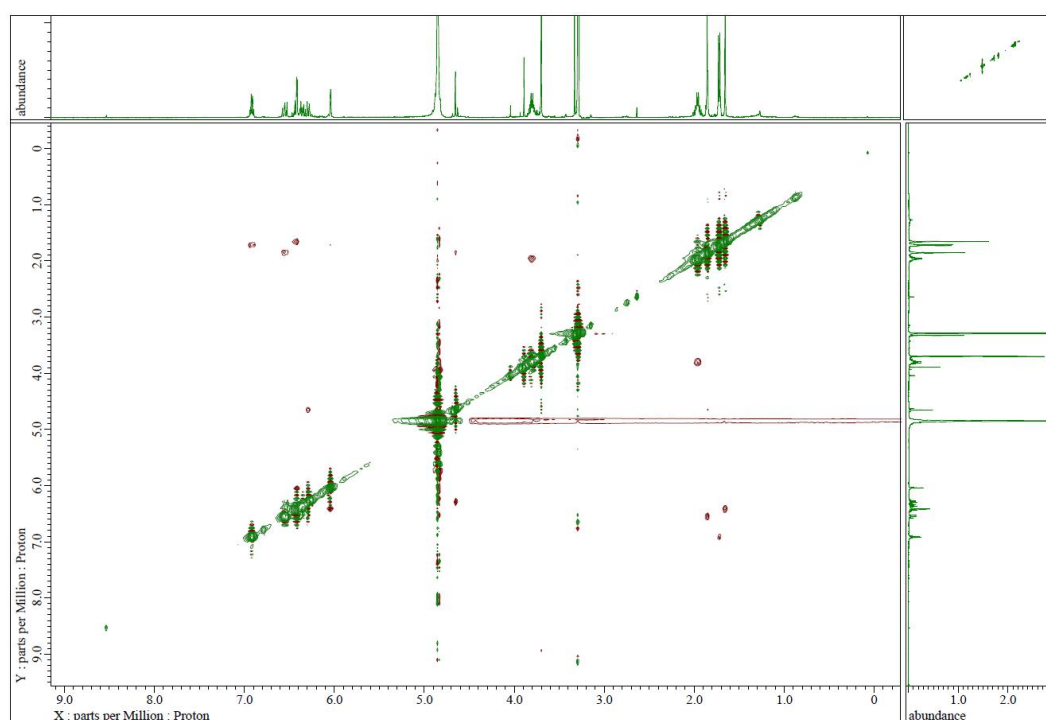
**Fig. S13.** NOESY spectrum of DihydroNG391 (**1**) (CD₃OD, 500 MHz).
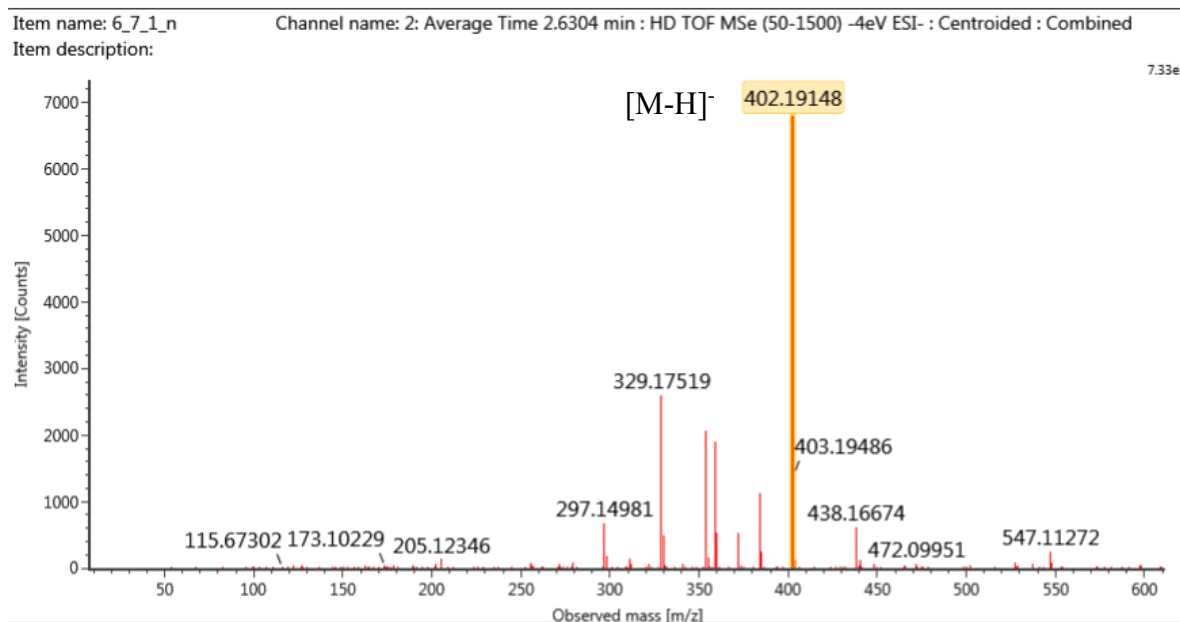


**Fig. S14.** HR-ESI-TOF/MS of Dihydrolucilactaene (**2**).
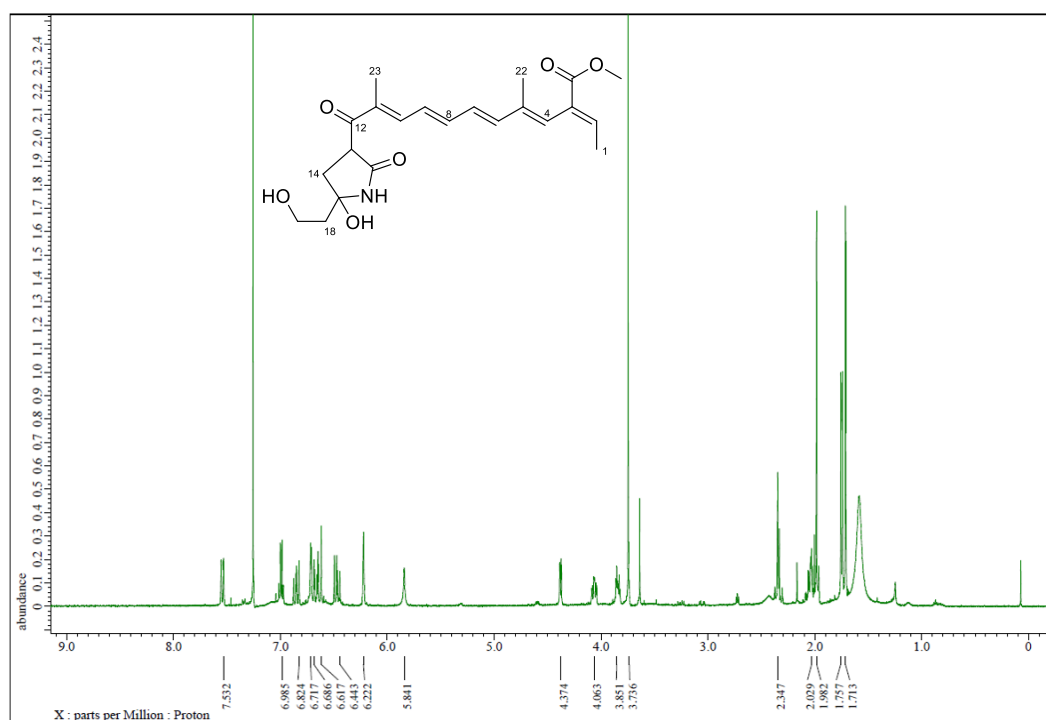
**Fig. S15.** ¹H-NMR spectrum of Dihydrolucilactaene (**2**) (CDCl₃, 500 MHz).
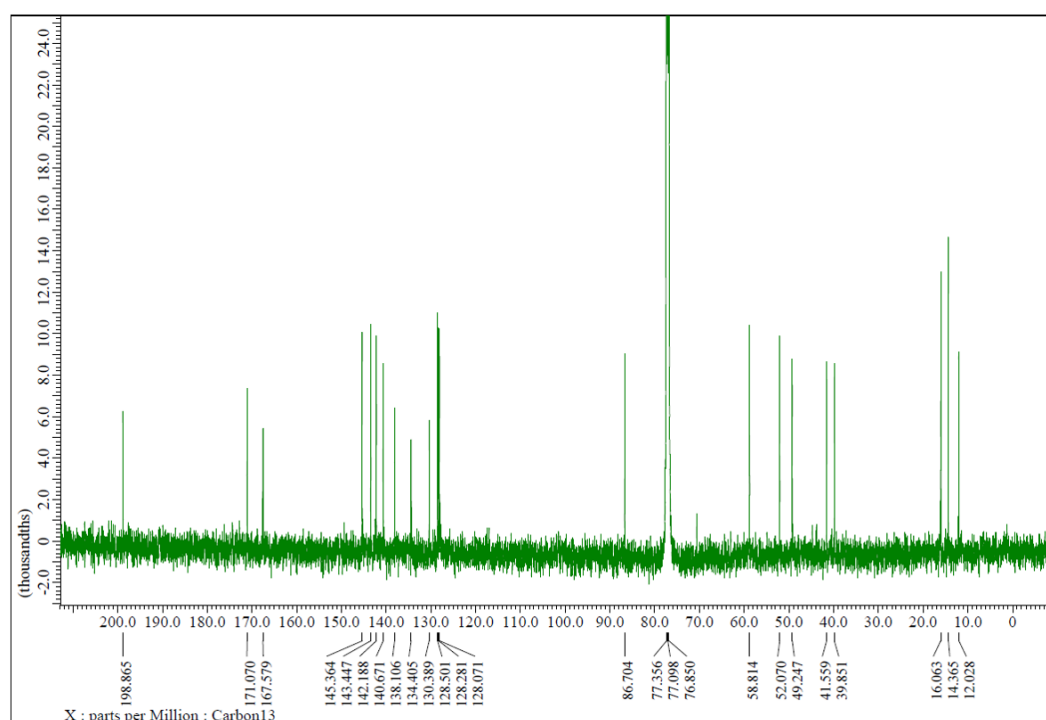


**Fig. S16.** ¹³C-NMR spectrum of Dihydrolucilactaene (**2**) (CDCl₃, 125 MHz).
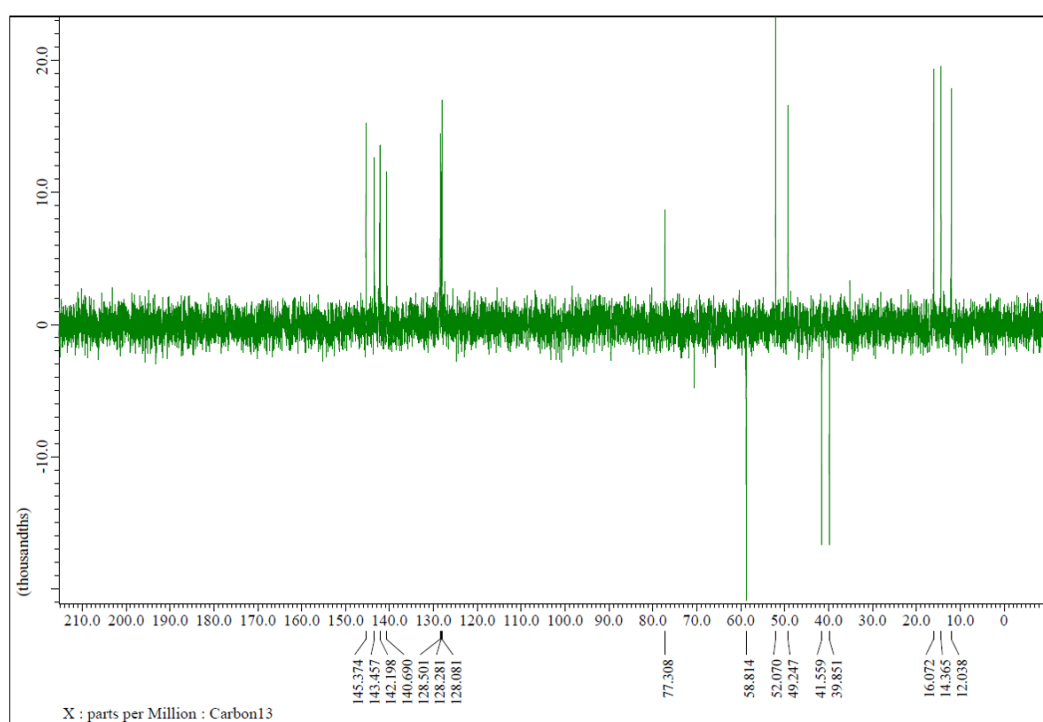
**Fig. S17.** DEPT135 spectrum of Dihydrolucilactaene (**2**) (CDCl₃, 125 MHz).



**Fig. S18.** ¹H-COSY spectrum of Dihydrolucilactaene (**2**) (CDCl₃, 500 MHz).

**Fig. S19.** HSQC spectrum of Dihydrolucilactaene (**2**) (CDCl₃, 125 MHz).



**Fig. S20.** HMBC spectrum of Dihydrolucilactaene (**2**) (CDCl₃, 500/125 MHz).
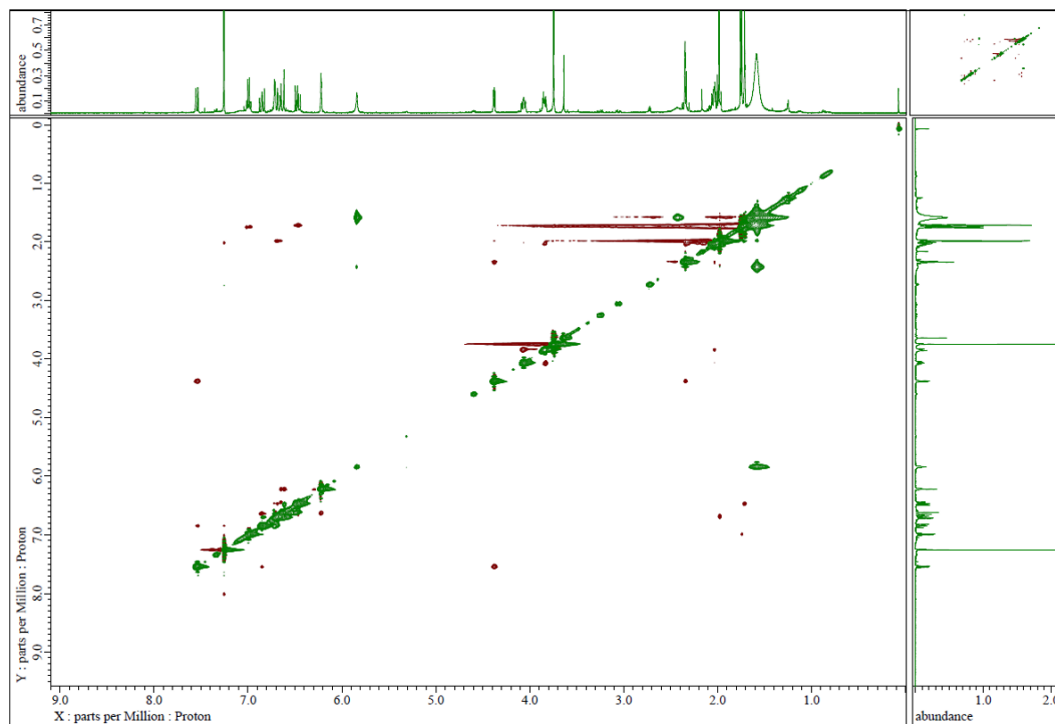
**Fig. S21.** NOESY spectrum of Dihydrolucilactaene (**2**) (CDCl₃, 500 MHz).



**Fig. S22.** HR-ESI-TOF/MS of 13α-hydroxylucilactaene (**3**).
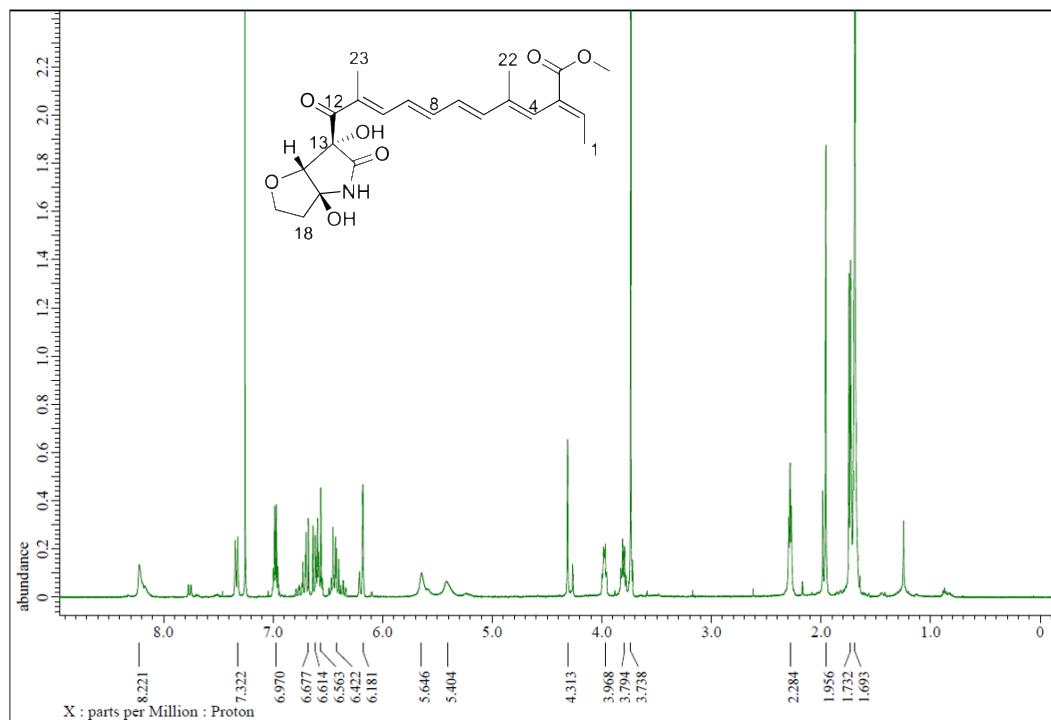
**Fig. S23.** $^1$H-NMR spectrum of 13α-hydroxylucilactaene (**3**) (CDCl$_3$, 500 MHz).
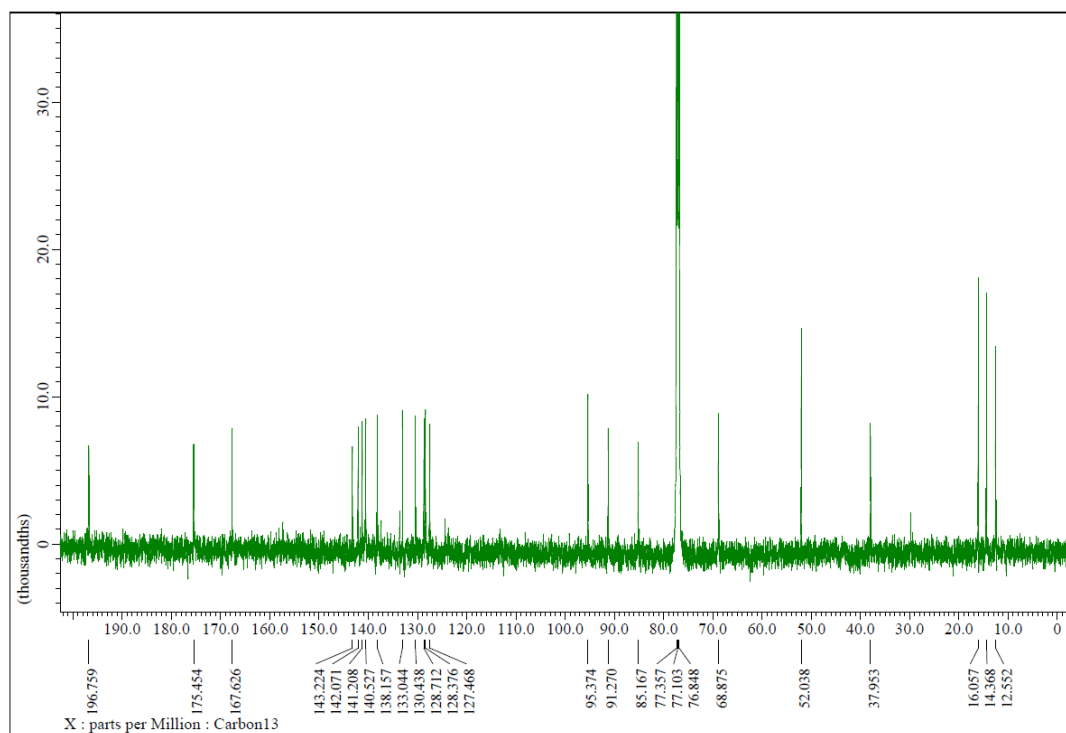


**Fig. S24.** $^{13}$C-NMR spectrum of 13α-hydroxylucilactaene (**3**) (CDCl$_3$, 125 MHz).
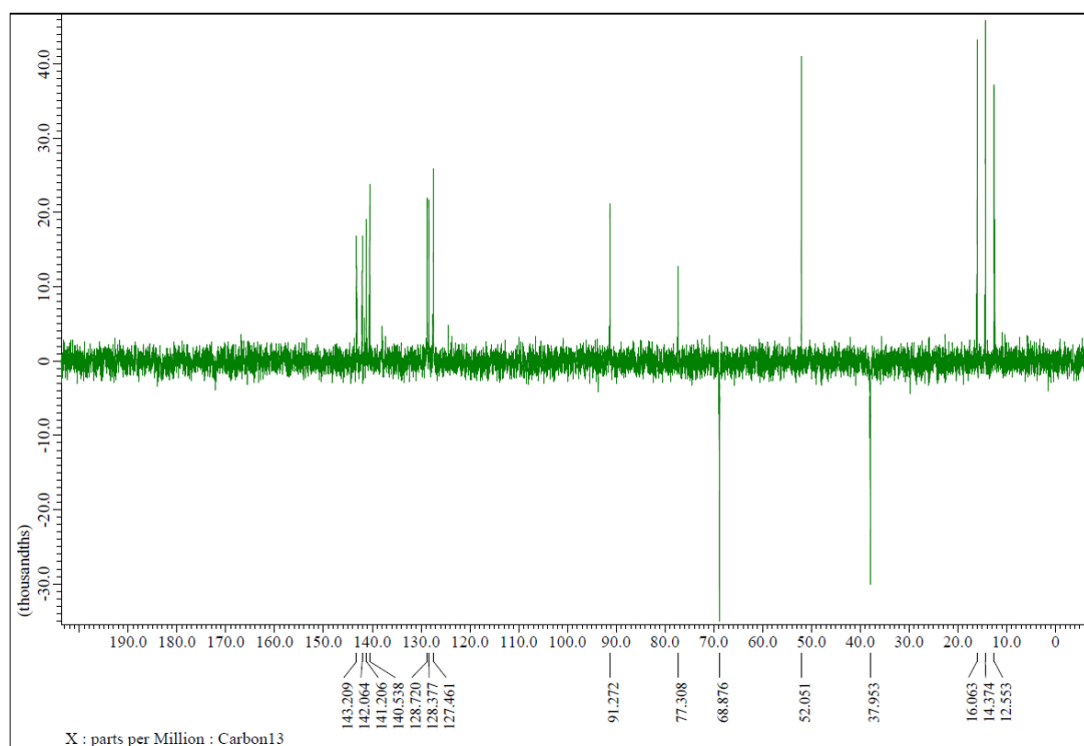
**Fig. S25.** DEPT135 spectrum of 13α-hydroxylucilactaene (**3**) (CDCl₃, 125 MHz).



**Fig. S26.** ¹H-COSY spectrum of 13α-hydroxylucilactaene (**3**) (CDCl₃, 500 MHz).
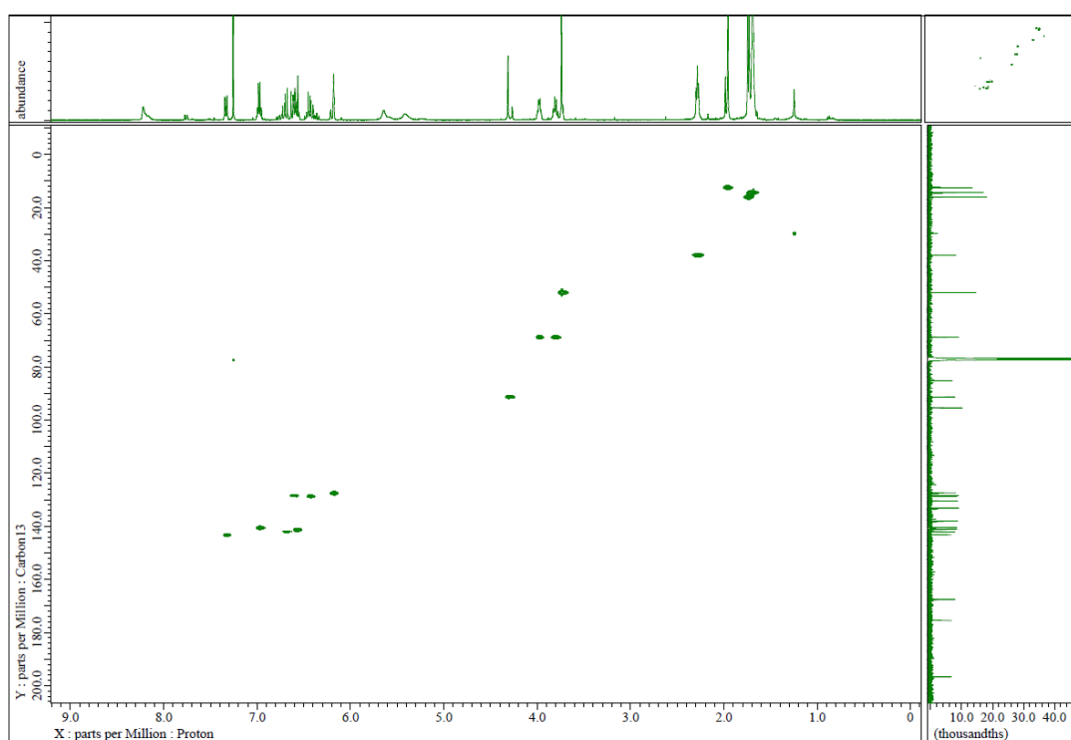
**Fig. S27.** HSQC spectrum of 13α-hydroxylucilactaene (**3**) (CDCl₃, 500/125 MHz).
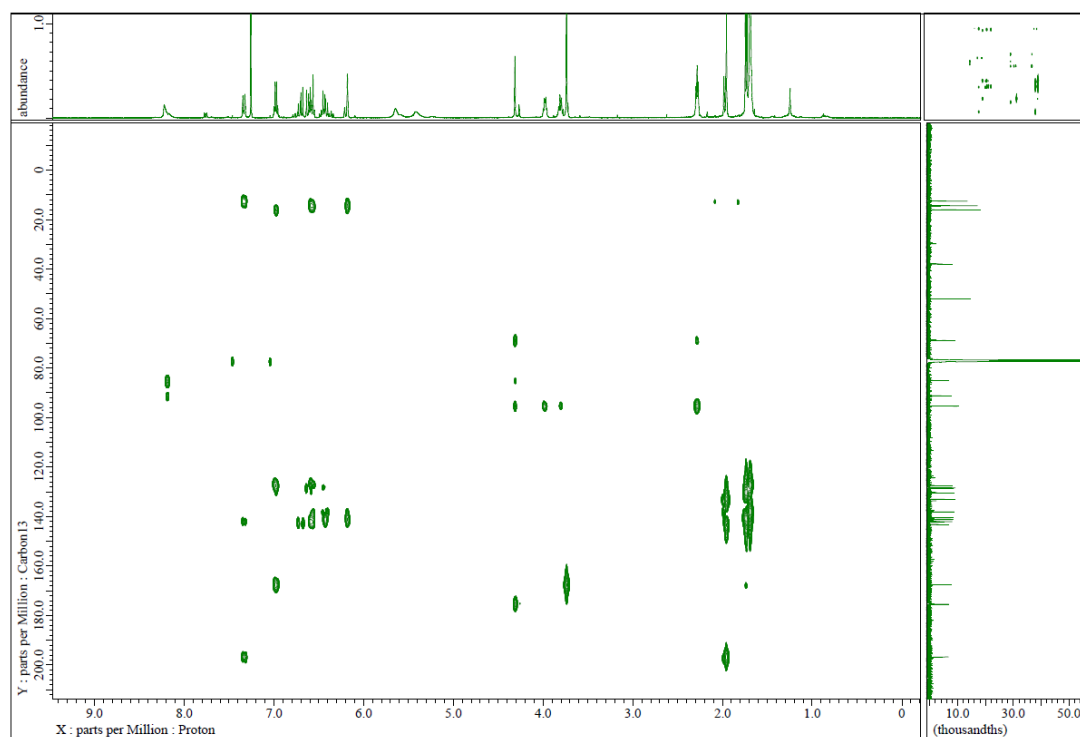


**Fig. S28.** HMBC spectrum of 13α-hydroxylucilactaene (**3**) (CDCl₃, 500/125 MHz).

**Fig. S29.** NOESY spectrum of 13α-hydroxylucilactaene (**3**) (CDCl₃, 500 MHz).



**Fig. S30.** 2D-NMR correlations of 13α-hydroxylucilactaene (**3**).

COSY: bold line,    HMBC: arrows.

**Fig. S31.** UPLC-MS analysis after incubation of NPD938 (30 µM) with NG391/393 (30 µM) for 7 days resulted in no direct interaction between both compounds.

| Gene name | Function | Gene name | Function |
|-----------|----------|-----------|----------|
| *luc1* | Methyl transferase | *luc5* | PKS-NRPS hybrid |
| *luc2* | Cytochrome P450 monooxygenase | *luc6* | Esterase |
| *luc3* | Aldehyde dehydrogenase | *luc7* | eEF-1B |
| *luc4* | Transporter | *luc8* | Protease |

**Fig. S32**. Biosynthetic gene cluster of lucilactaene with predicted functions of its genes

**5 L Δ*luc3* culture**

Extract with acetone

Evaporate acetone

Fractionate with EtOAc (3V)

**Aqueous layer**          **EtOAc extract (0.96 g)**

MPLC (CHCl$_3$:MeOH)
100 tubes. collected

**F52-63** (128 mg)
MS389

①    Isocratic elution of 30% acetonitrile in water at a flow rate of 15 ml/min.

Isomeric mixture (8 mg)

②    Isocratic elution of 30% acetonitrile in water at a flow rate of 1 ml/min.

Two pure E/Z isomers

**4** (2.4 mg), **5** (2.6 mg)

**Fig. S33**. Purification scheme for compounds **4** and **5**.

**7.5 L Δ*luc2* culture**

Extract with acetone

Evaporate acetone

Fractionate with EtOAc

**Aqueous layer**          **EtOAc extract (1.4 g)**

MPLC (CHCl₃:MeOH)
82 tubes. collected

**F14-16** (50 mg)    **F18-19** (28 mg)    **F23-26** (153 mg)    **F28-29** (58 mg)    **F30-31** (107 mg)
MS357              MS359                MS373 / MS343          MS361                MS361

⑤                                      ④                    ③

Mix. of *E/Z* isomers                   Mix. of *E/Z* isomers    Two pure *E/Z* isomers

**9** (1 mg)                            **8** (1.5 mg)          **6** (0.9 mg), **7** (0.7 mg)

③ Isocratic elution of 45% acetonitrile in water at a flow rate of 15 ml/min.

④ Isocratic elution of 50% acetonitrile in water at a flow rate of 15 ml/min.

⑤ Isocratic elution of 55% acetonitrile in water at a flow rate of 4 ml/min.

**Fig. S34.** Purification scheme for compounds **6-9**.
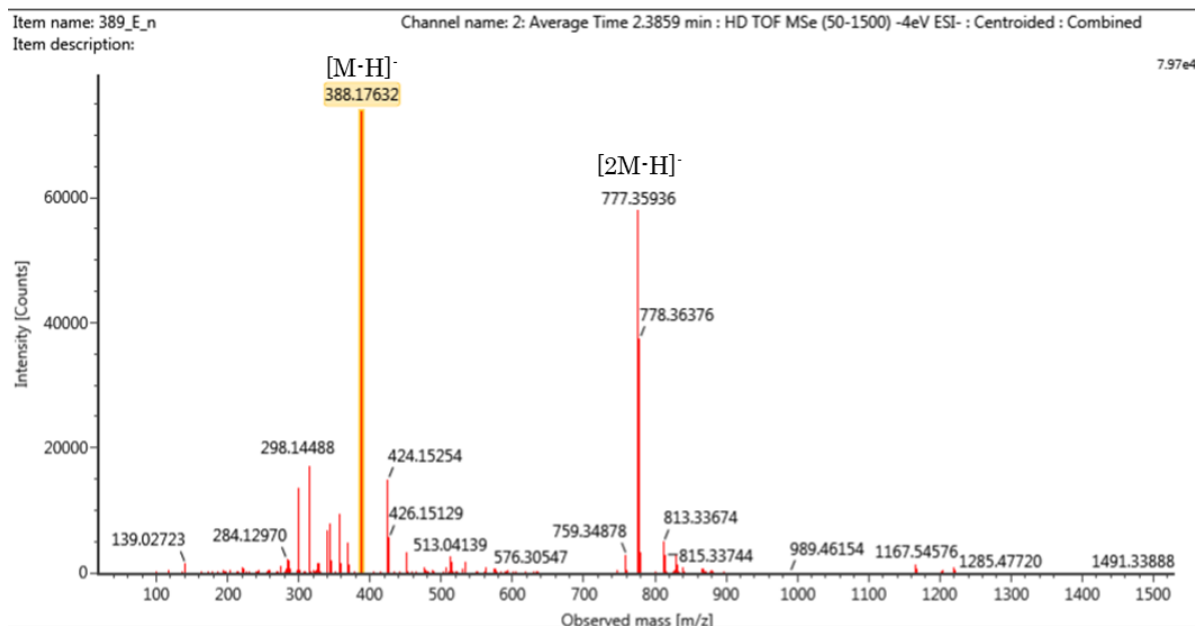
**Fig. S35.** HR-ESI-TOF/MS of prelucilactaene G (**4**)
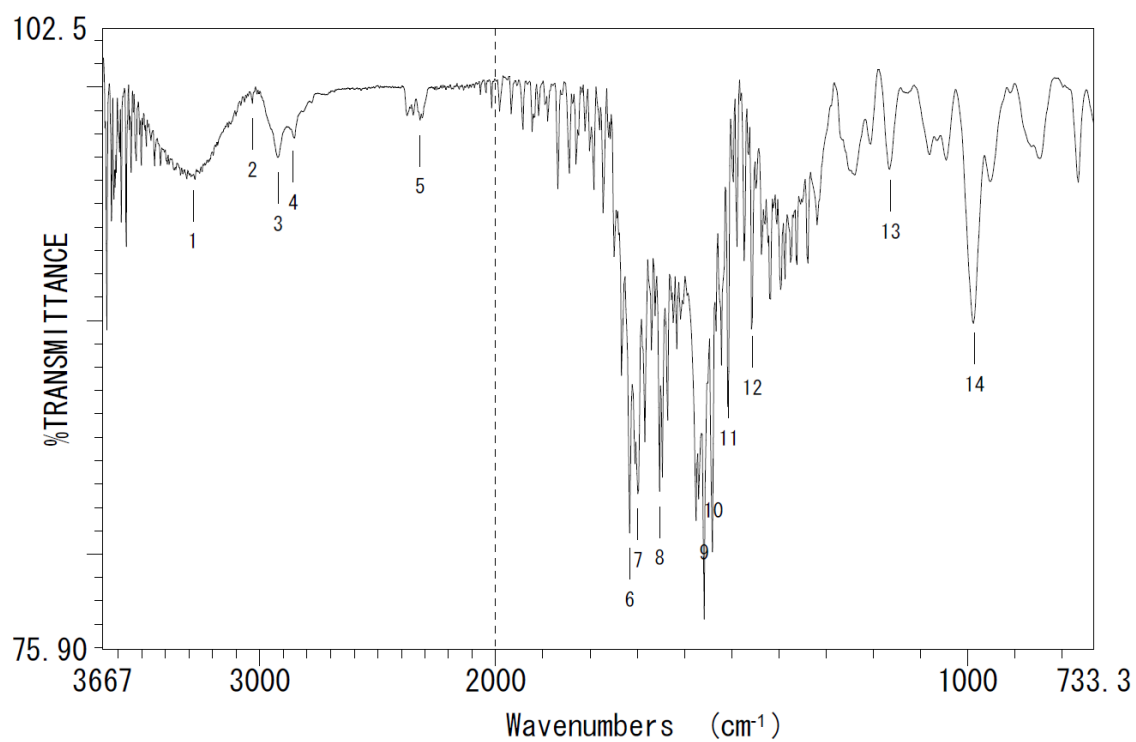


**Fig. S36.** IR spectrum of prelucilactaene G (**4**).
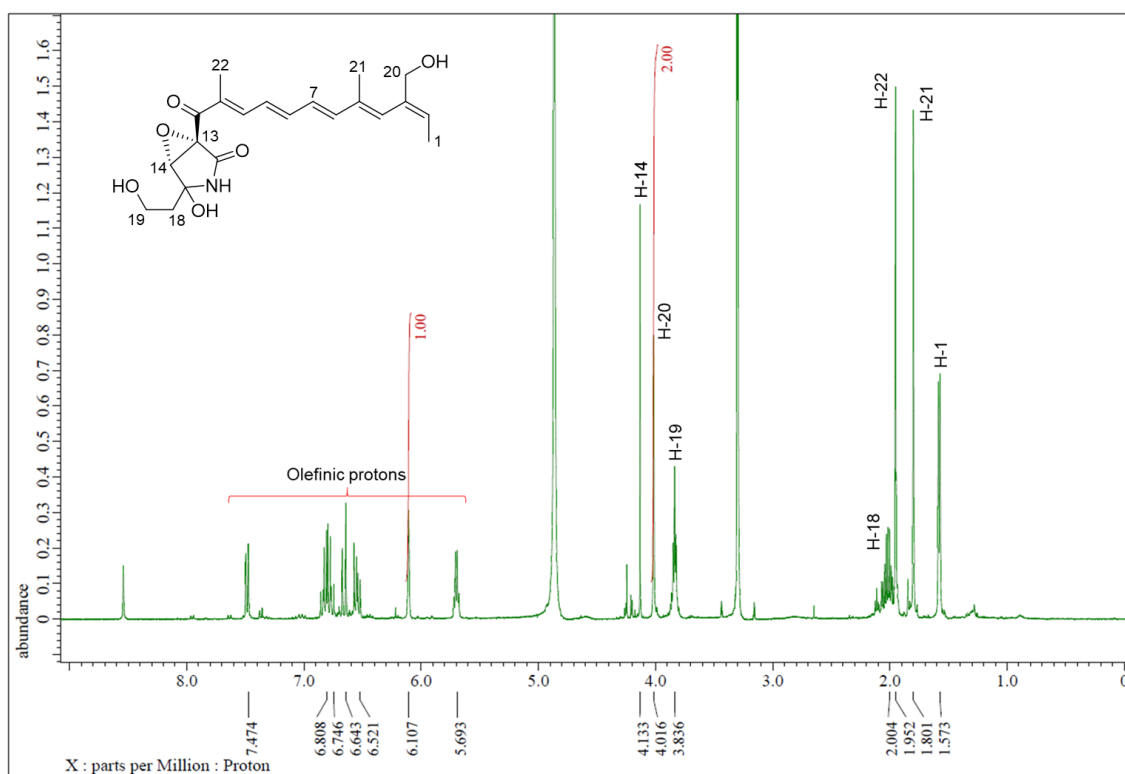
**Fig. S37.** $^1$H-NMR spectrum of prelucilactaene G (**4**) (CD$_3$OD, 500 MHz)
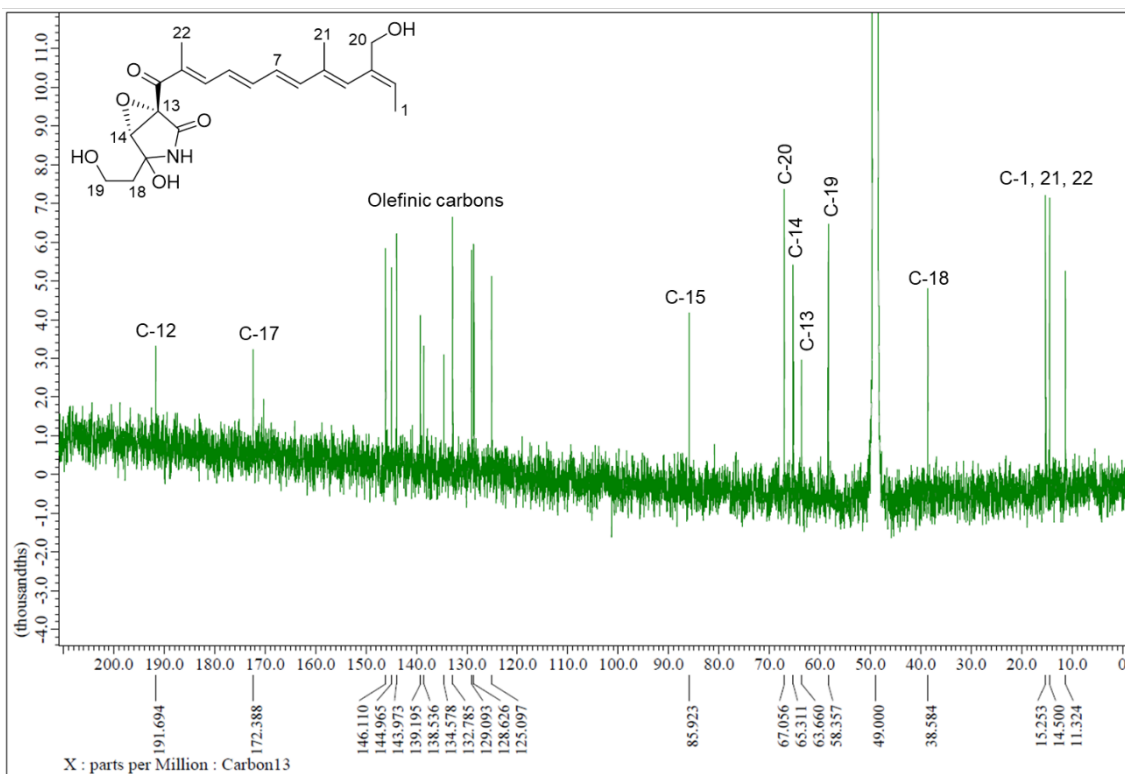


**Fig. S38.** $^{13}$C-NMR spectrum of prelucilactaene G (**4**) (CD$_3$OD, 125 MHz)
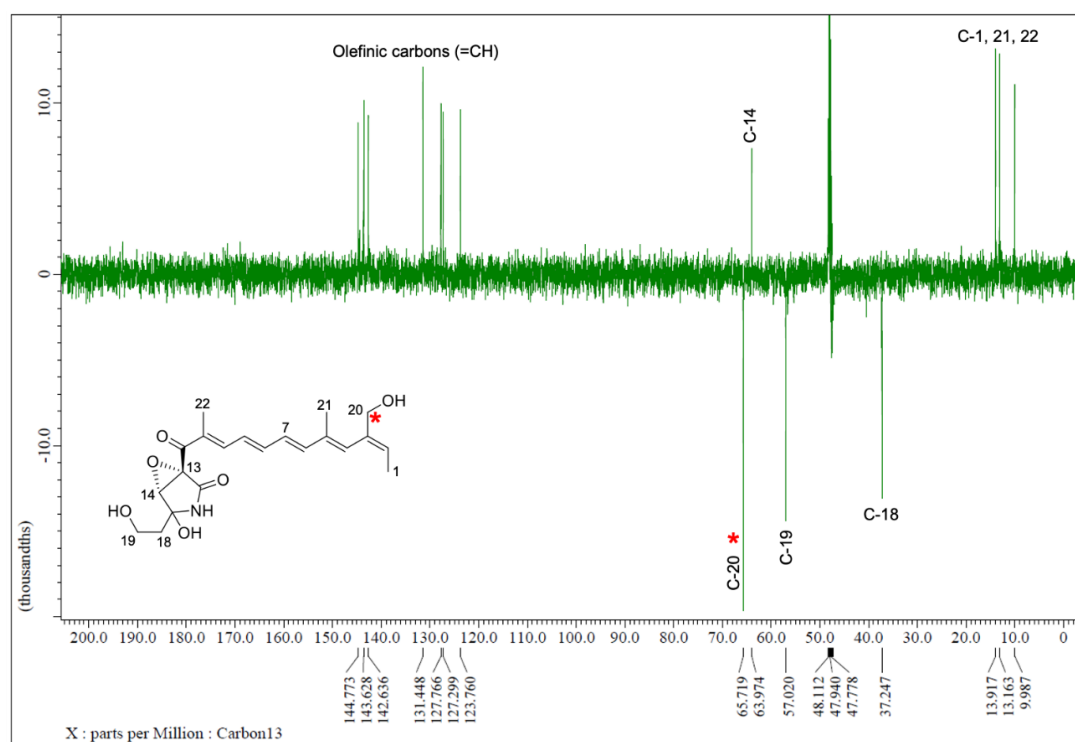
**Fig. S39.** DEPT135 spectrum of prelucilactaene G (**4**) (CD₃OD, 125 MHz)
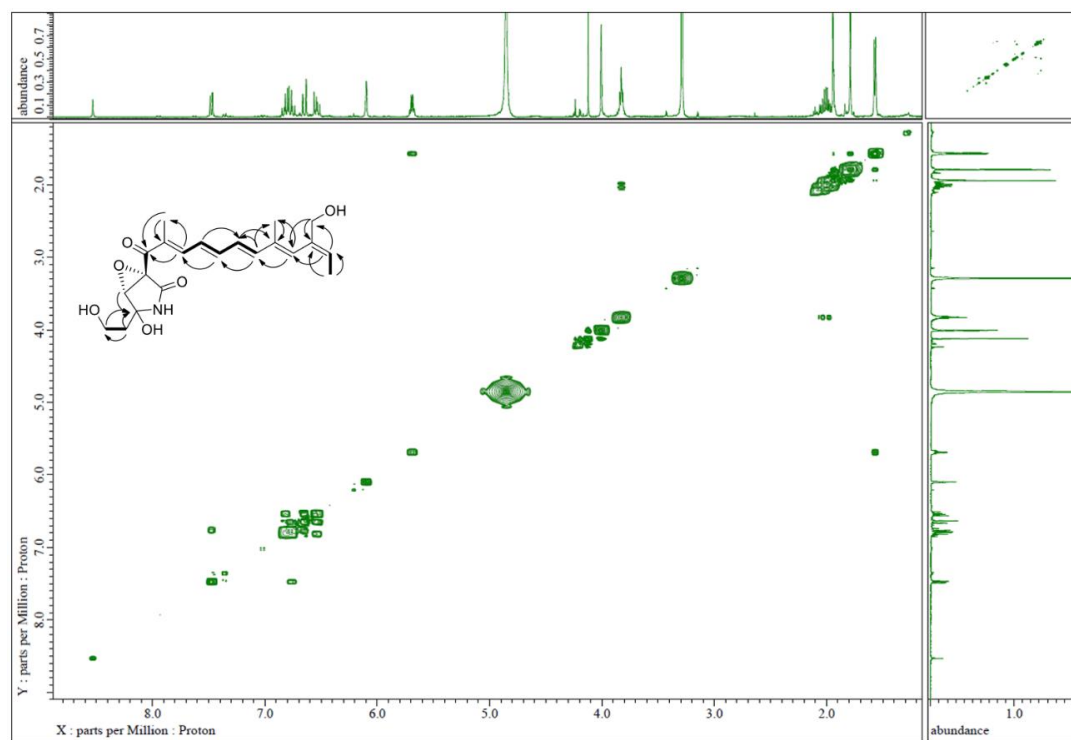


**Fig. S40.** ¹H-¹H COSY spectrum of prelucilactaene G (**4**) (CD₃OD, 500 MHz)
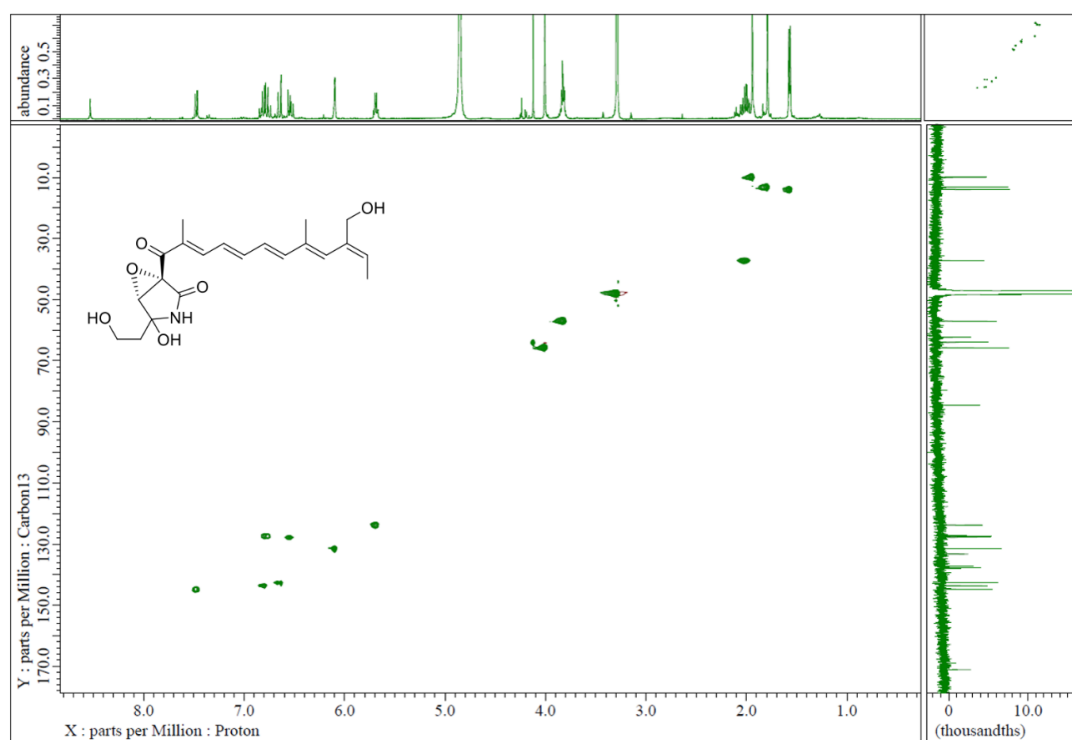
**Fig. S41.** HSQC spectrum of prelucilactaene G (**4**) (CD$_3$OD, 500/125 MHz)
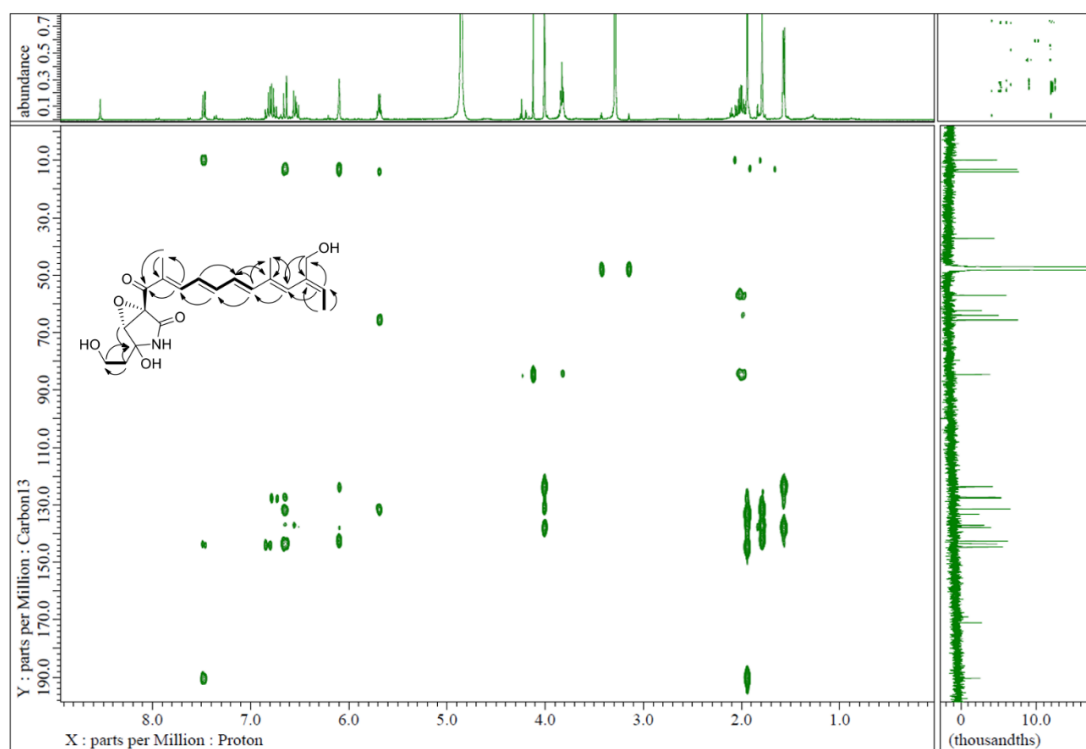


**Fig. S42.** HMBC spectrum of prelucilactaene G (**4**) (CD$_3$OD, 500/125 MHz)
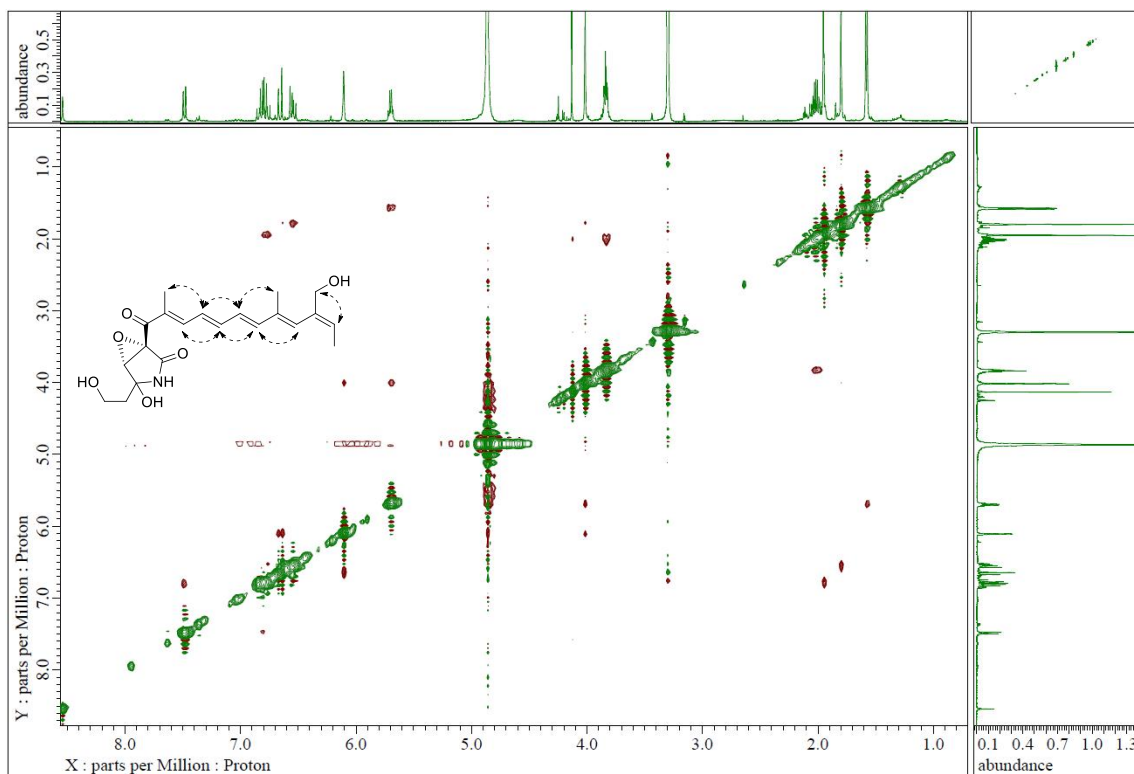
**Fig. S43.** NOESY spectrum of prelucilactaene G (**4**) (CD$_3$OD, 500 MHz)
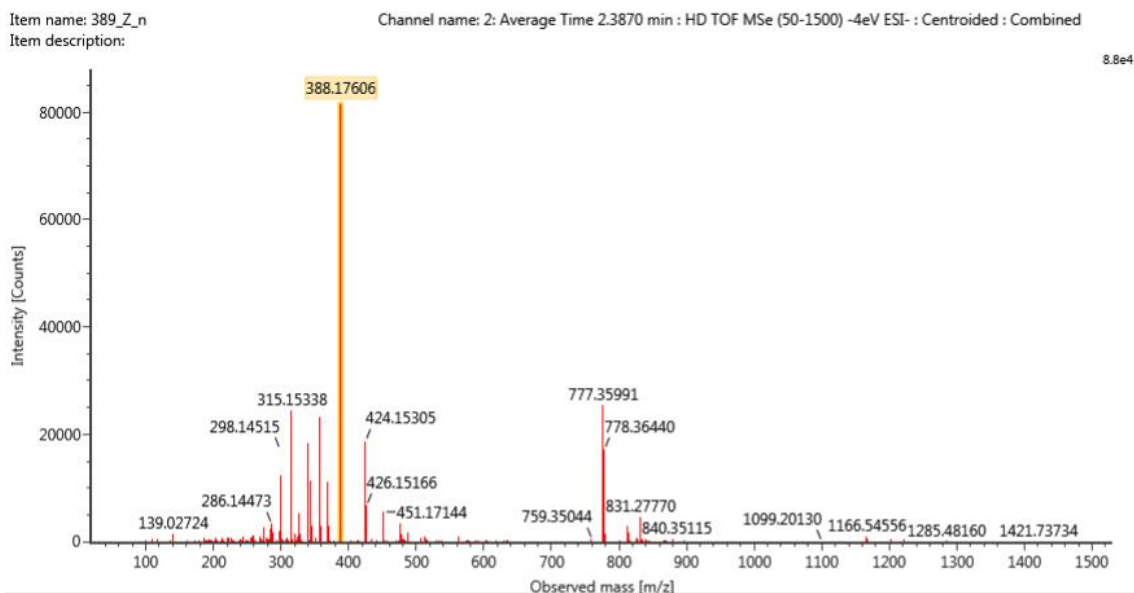


**Fig. S44.** HR-ESI-TOF/MS of prelucilactaene H (**5**)
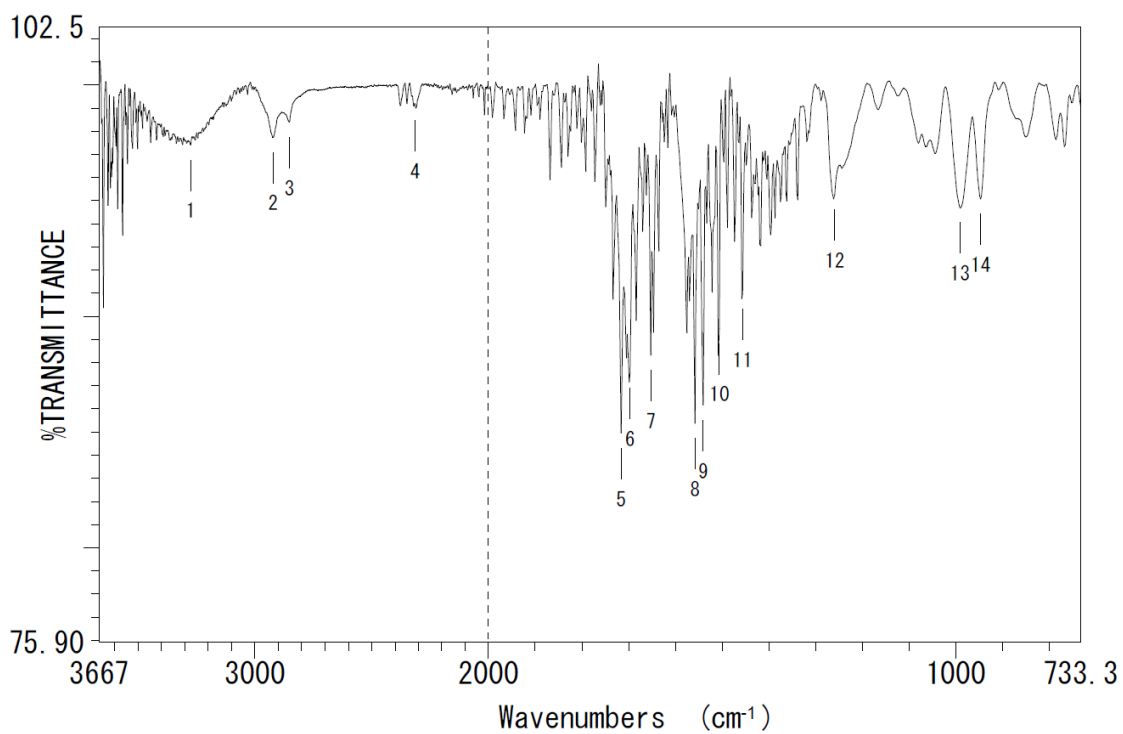
**Fig. S45.** IR spectrum of prelucilactaene H (**5**)
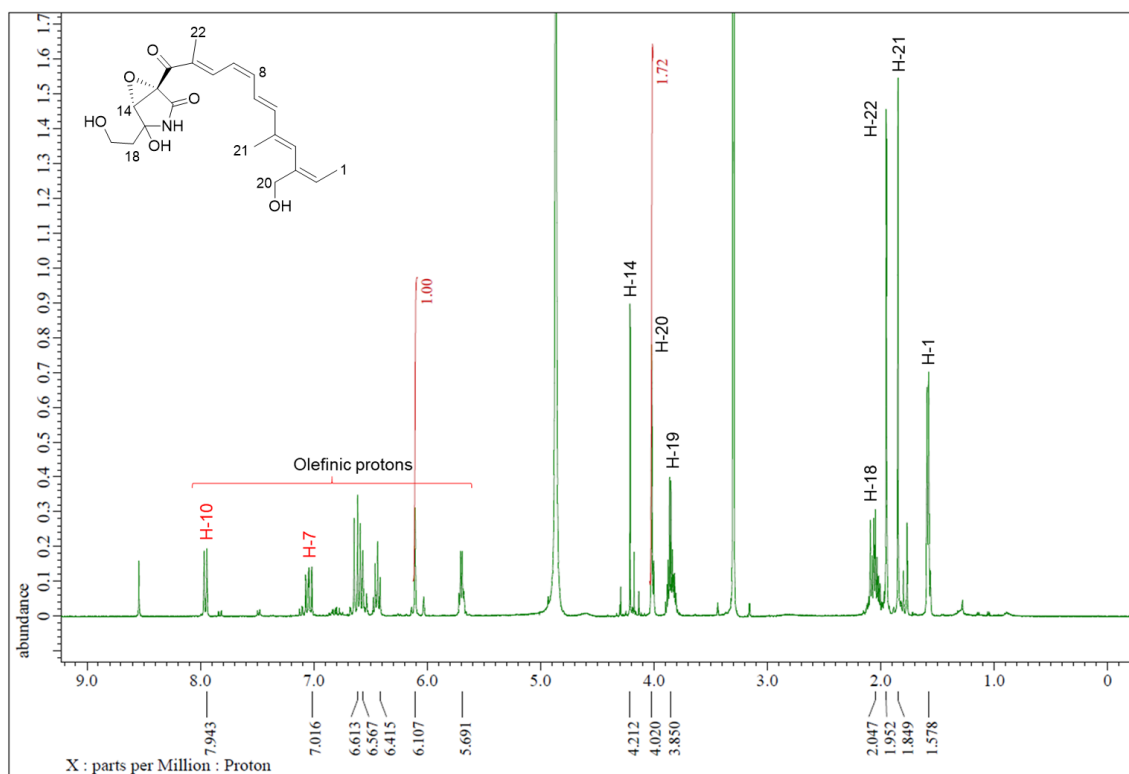


**Fig. S46.** ¹H-NMR spectrum of prelucilactaene H (**5**) (CD₃OD, 500 MHz)
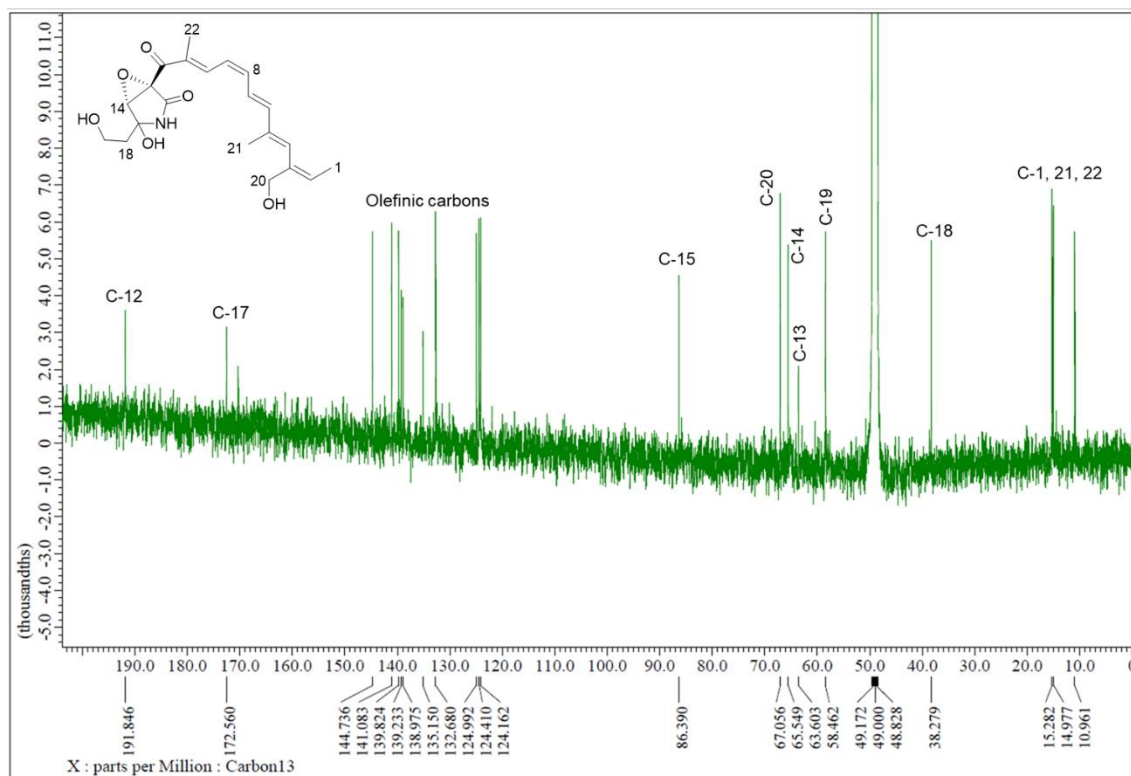
**Fig. S47.** ^{13}C-NMR spectrum of prelucilactaene H (**5**) (CD₃OD, 125 MHz)
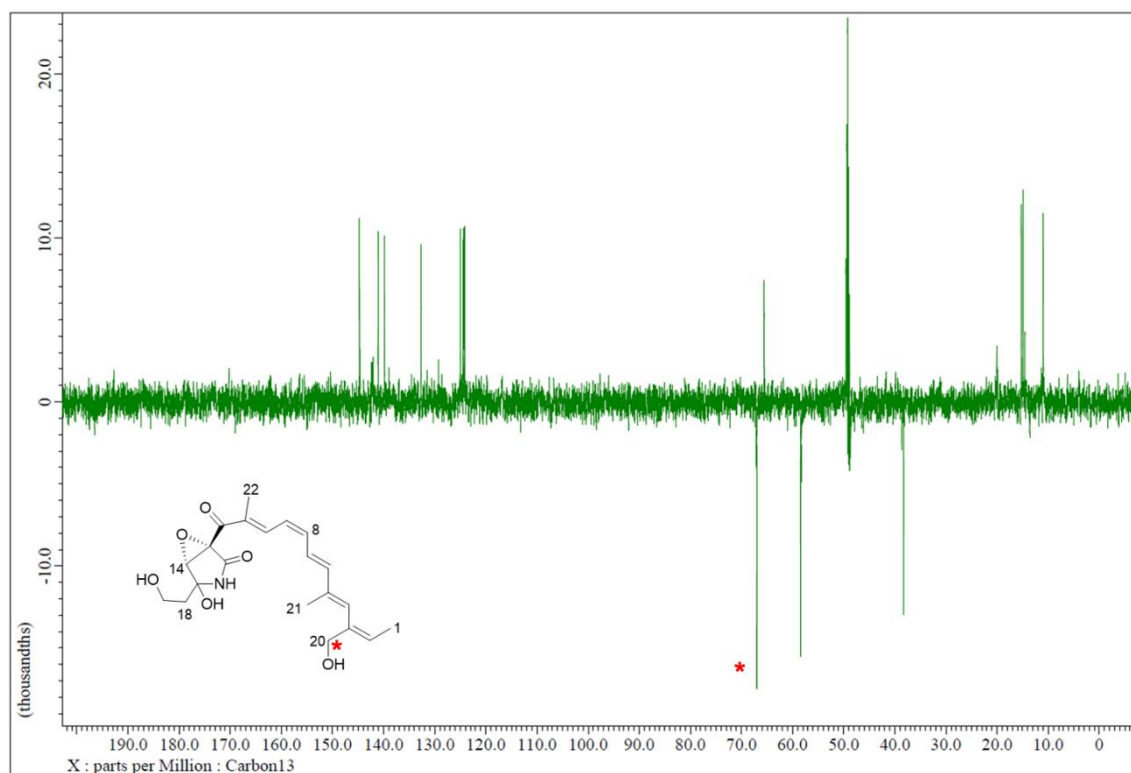


**Fig. S48.** DEPT135 spectrum of prelucilactaene H (**5**) (CD₃OD, 125 MHz)
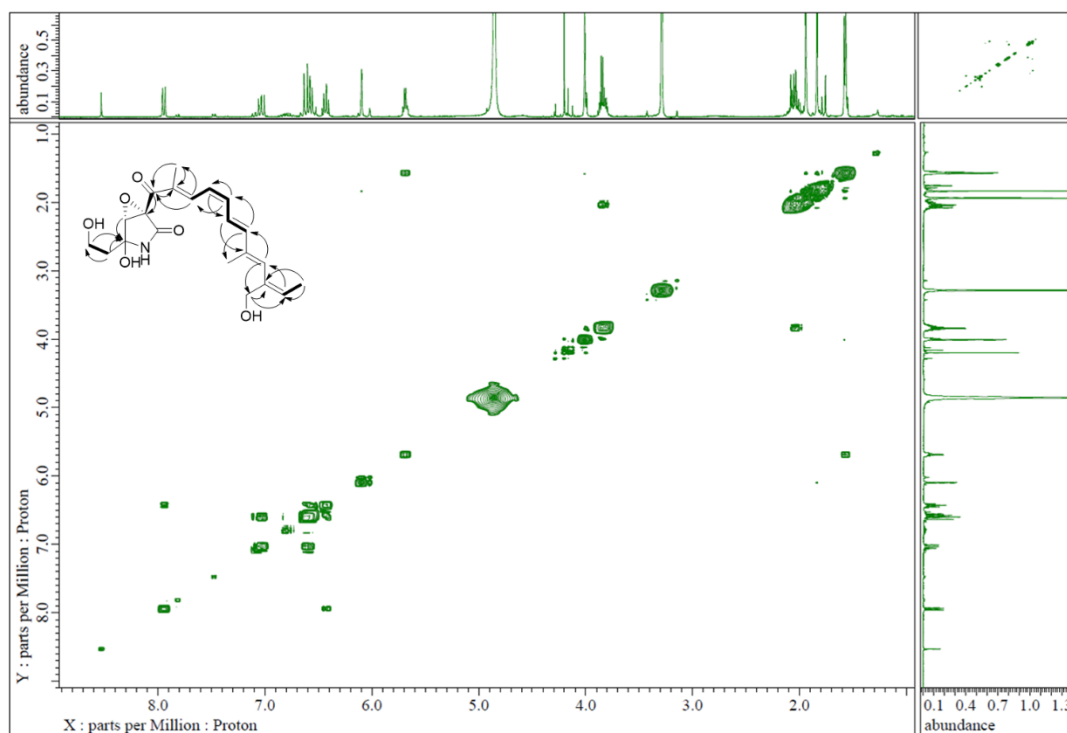
**Fig. S49.** $^1$H-$^1$H COSY spectrum of prelucilactaene H (**5**) (CD$_3$OD, 500 MHz)
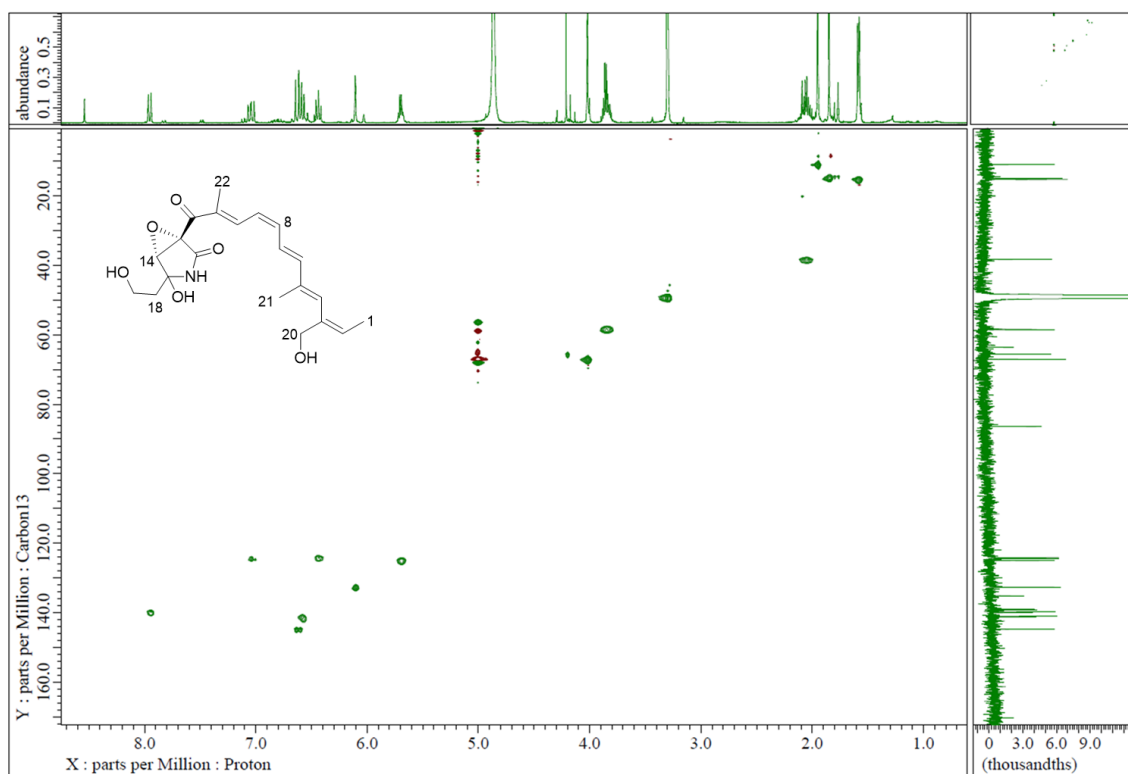


**Fig. S50.** HSQC spectrum of prelucilactaene H (**5**) (CD$_3$OD, 500/125 MHz)
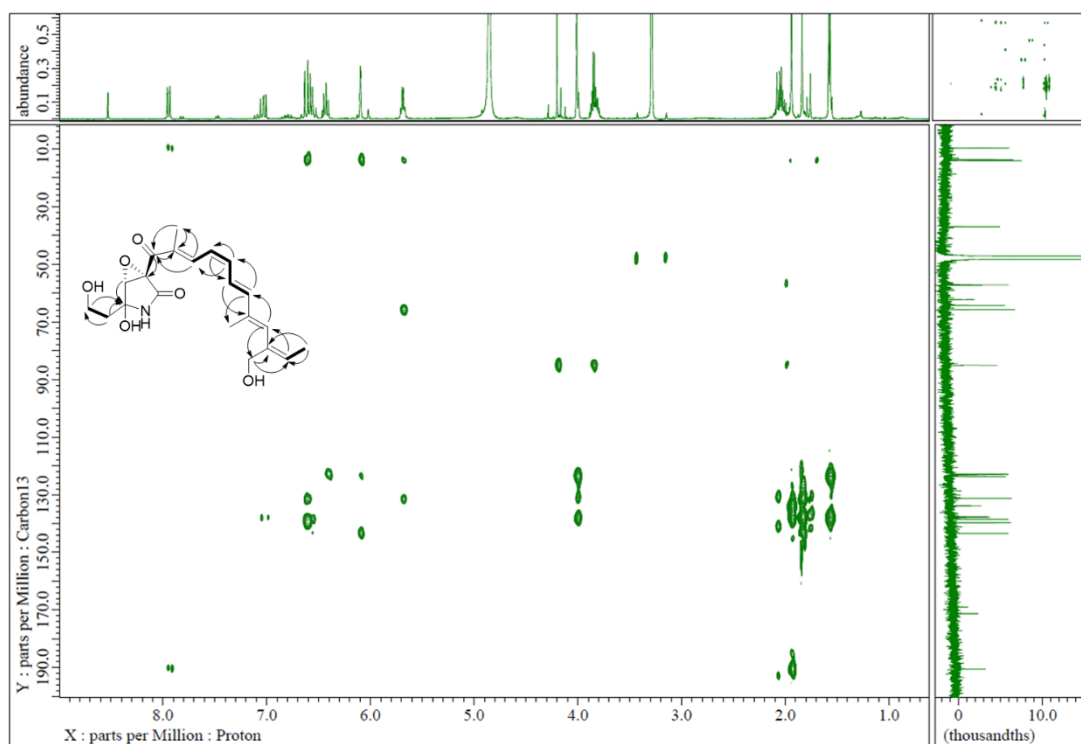
**Fig. S51.** HMBC spectrum of prelucilactaene H (**5**) (CD₃OD, 500/125 MHz)
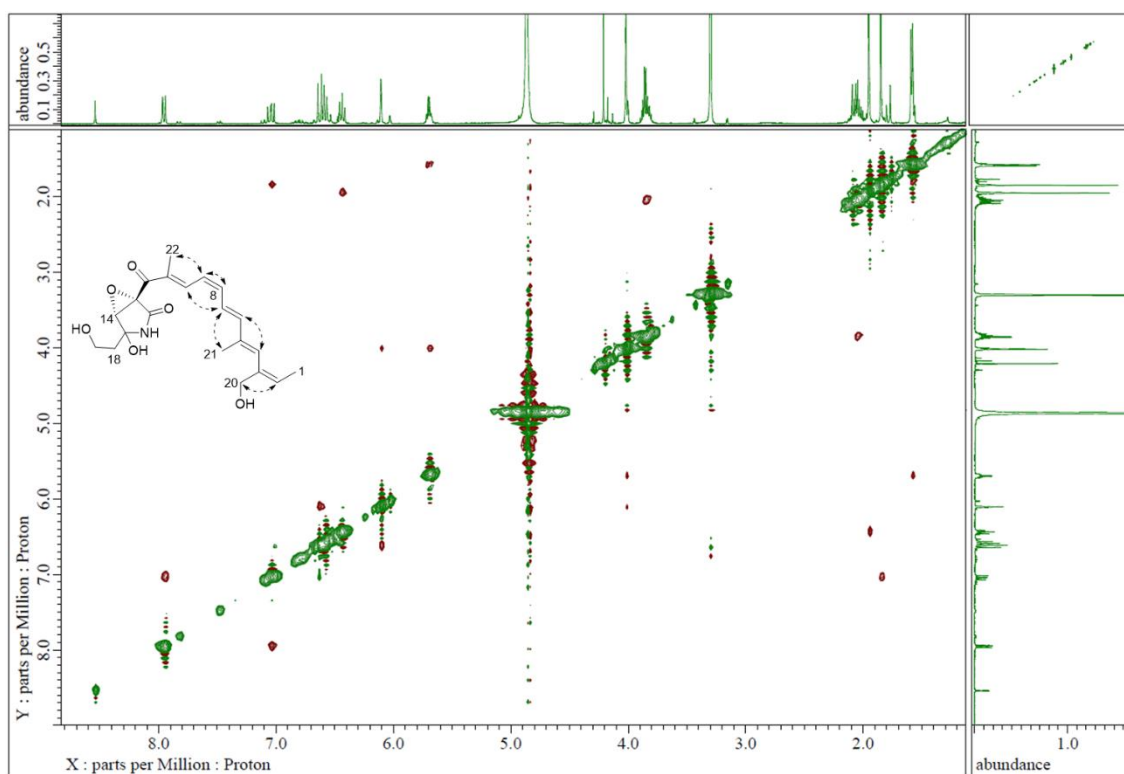


**Fig. S52.** NOESY spectrum of prelucilactaene H (**5**) (CD₃OD, 500 MHz)
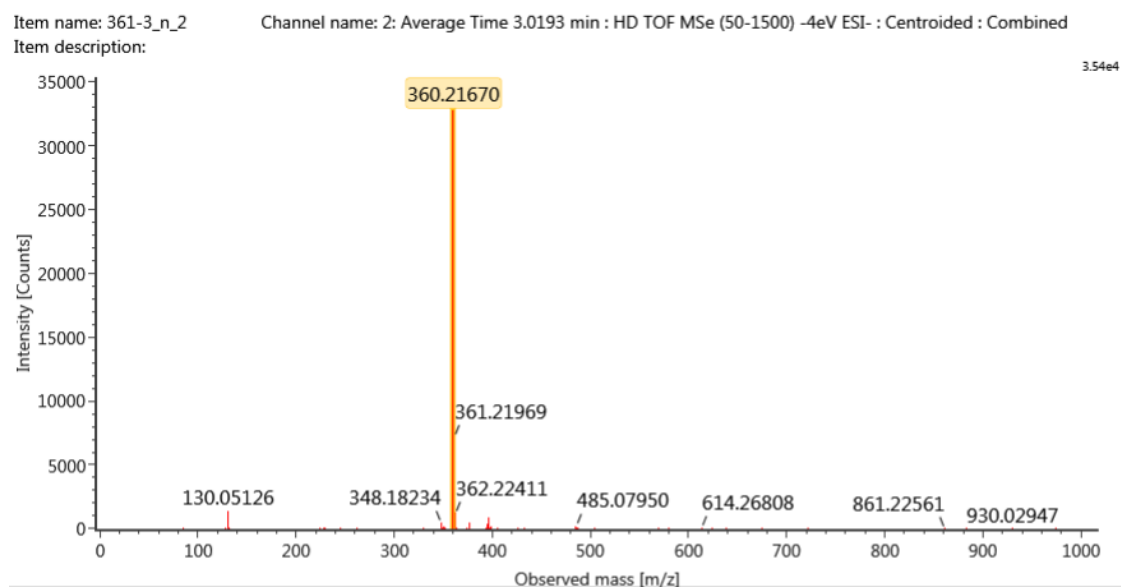
**Fig. S53.** HR-ESI-TOF/MS of prelucilactaene A (**6**)
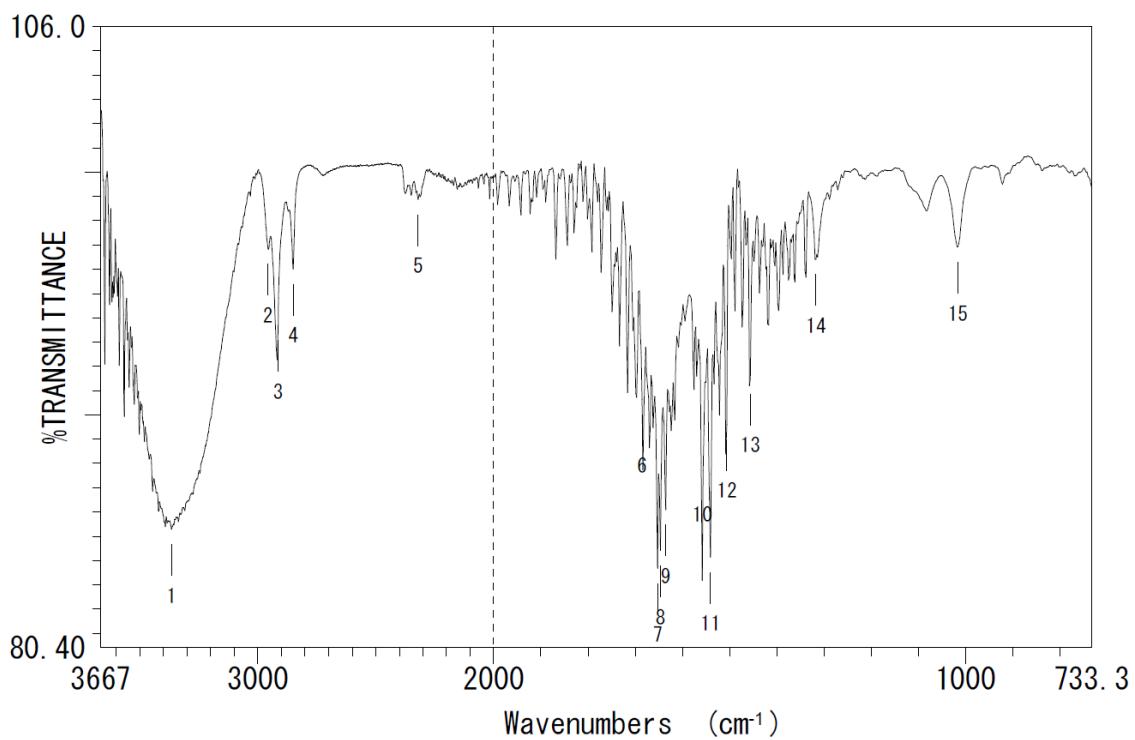


**Fig. S54**. IR spectrum of prelucilactaene A (**6**).
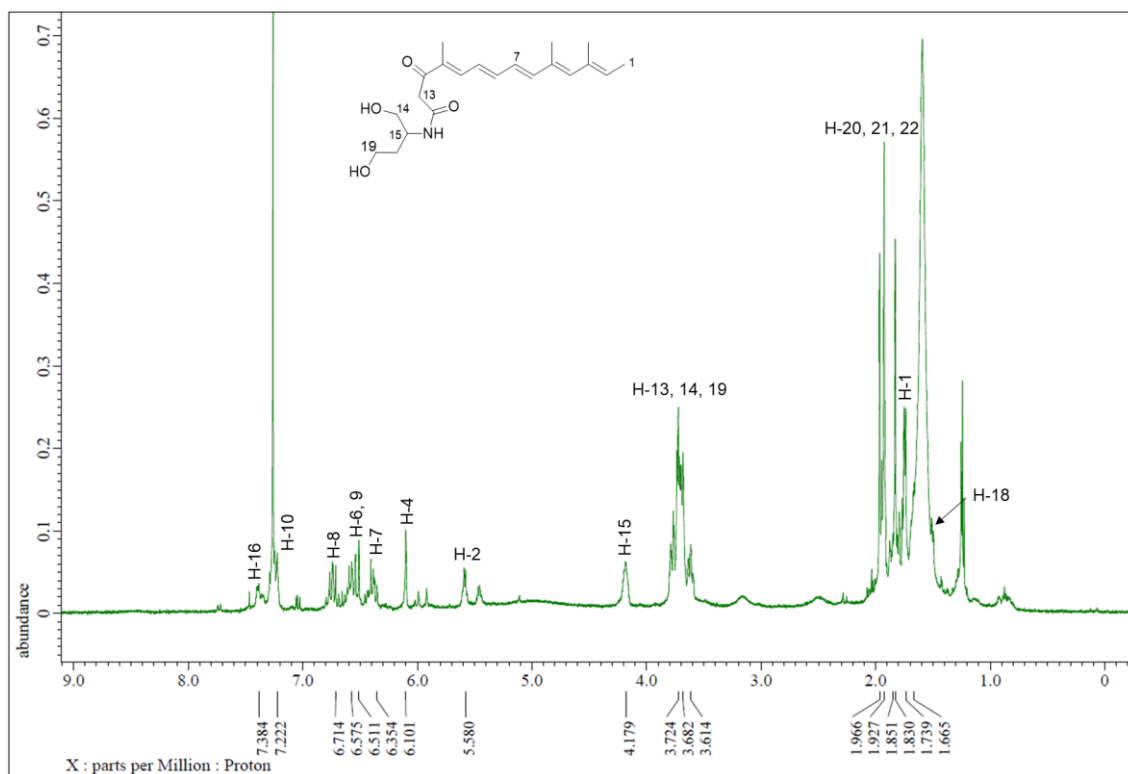
**Fig. S55.** $^1$H-NMR spectrum of prelucilactaene A (**6**) (CDCl$_3$, 500 MHz)
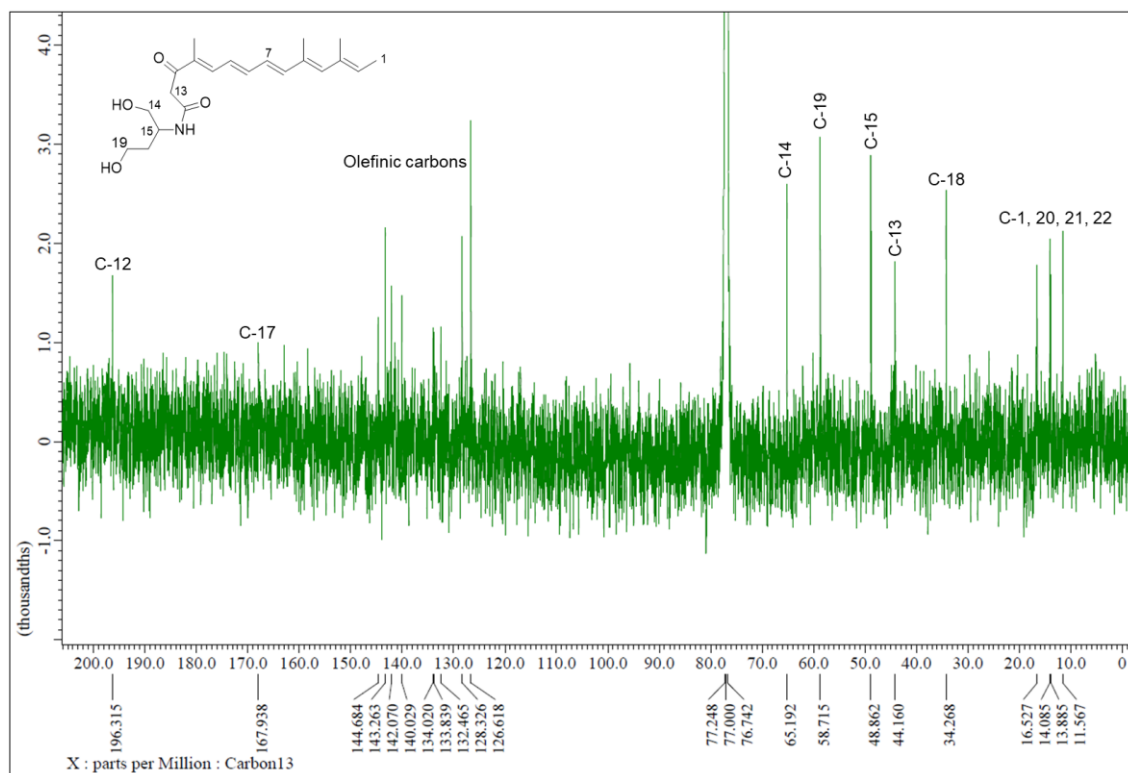


**Fig. S56.** $^{13}$C-NMR spectrum of prelucilactaene A (**6**) (CDCl$_3$, 125 MHz)
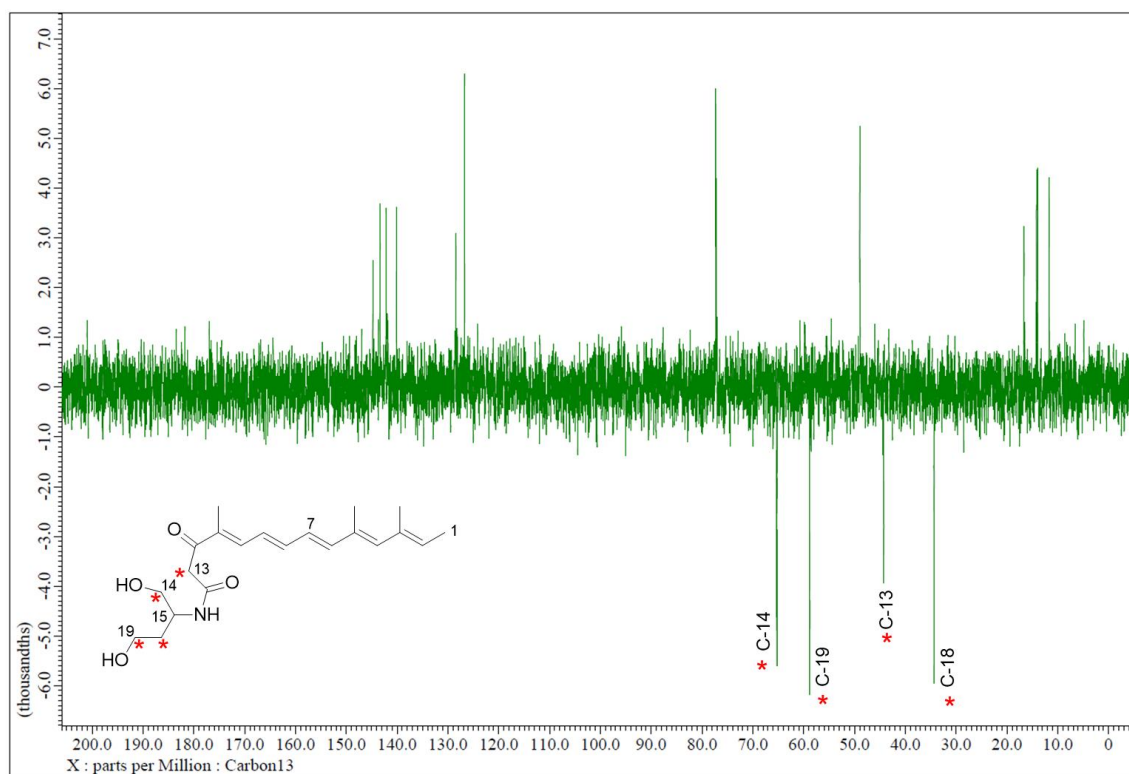
**Fig. S57.** DEPT135 spectrum of prelucilactaene A (**6**) (CDCl₃, 125 MHz)
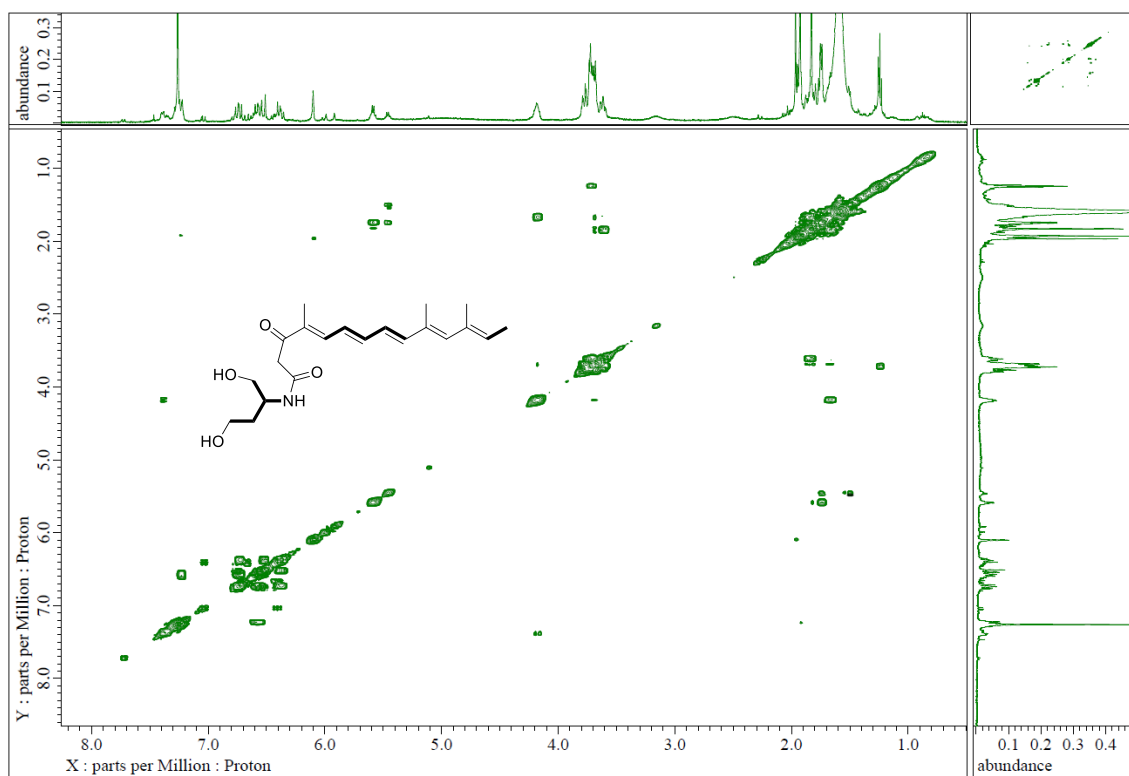


**Fig. S58.** ¹H-¹H COSY spectrum of prelucilactaene A (**6**) (CDCl₃, 500 MHz)
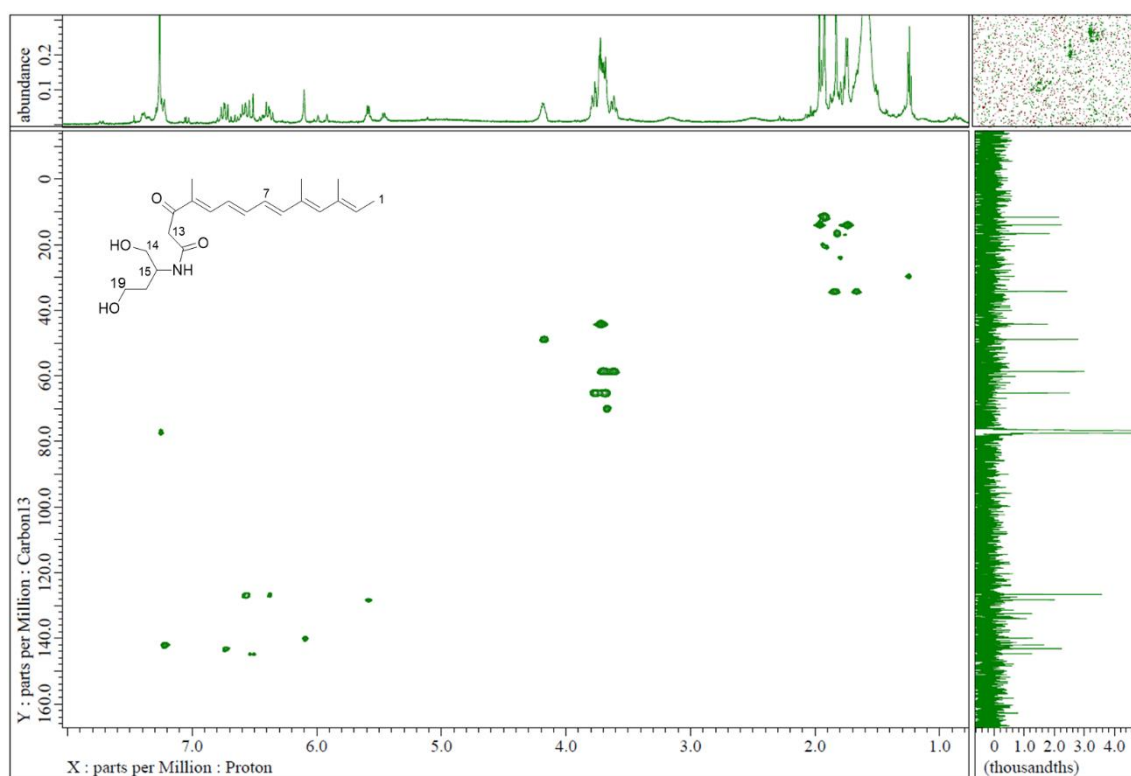
**Fig. S59.** HSQC spectrum of prelucilactaene A (**6**) (CDCl₃, 500/125 MHz)
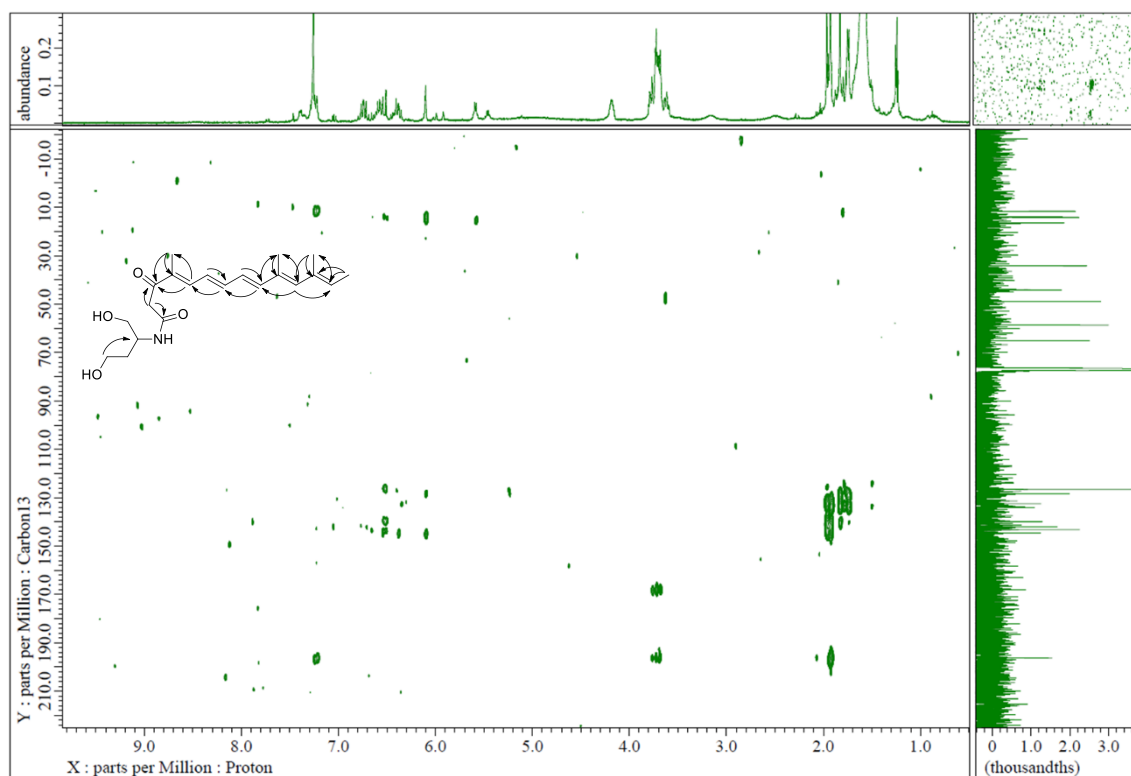


**Fig. S60.** HMBC spectrum of prelucilactaene A (**6**) (CDCl₃, 500/125 MHz)
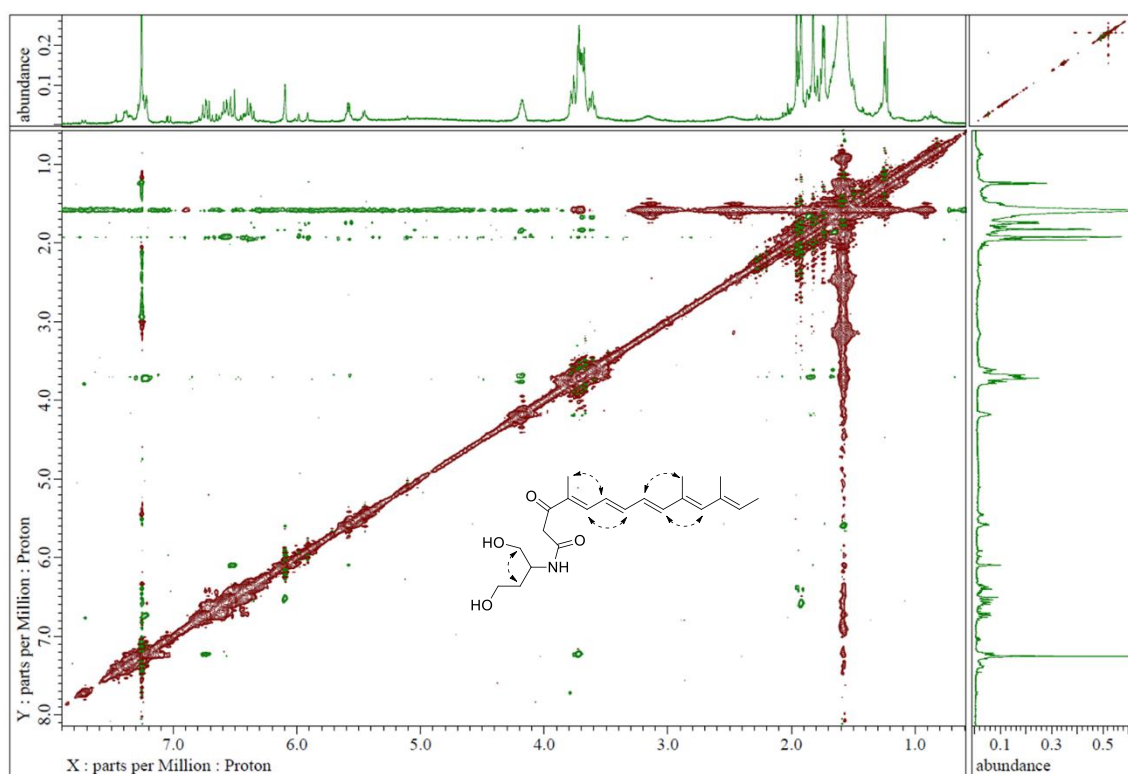
**Fig. S61.** NOESY spectrum of prelucilactaene A (**6**) (CDCl₃, 500 MHz)
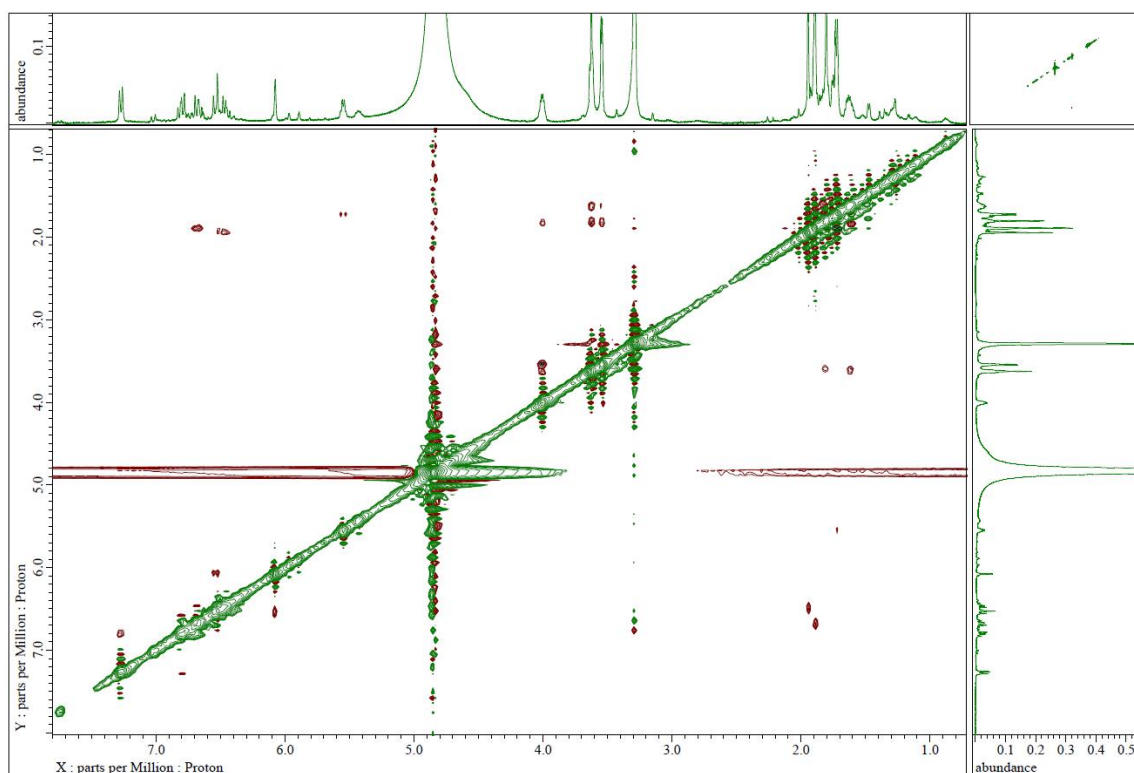


**Fig. S62.** NOESY spectrum of prelucilactaene A (**6**) (CD₃OD, 500 MHz)
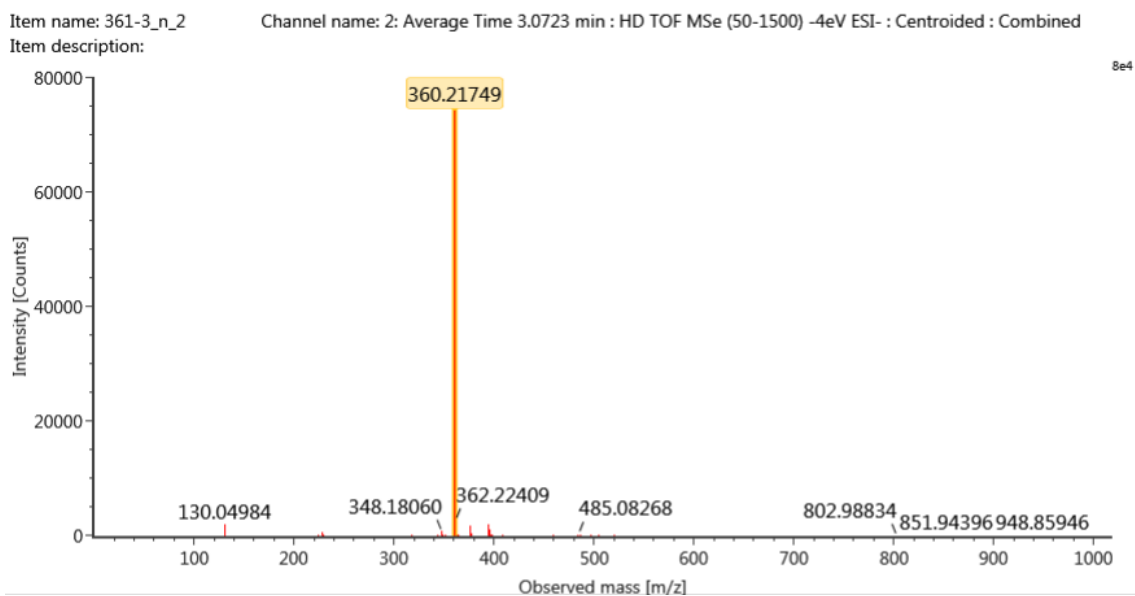
**Fig. S63.** HR-ESI-TOF/MS of prelucilactaene B (**7**)
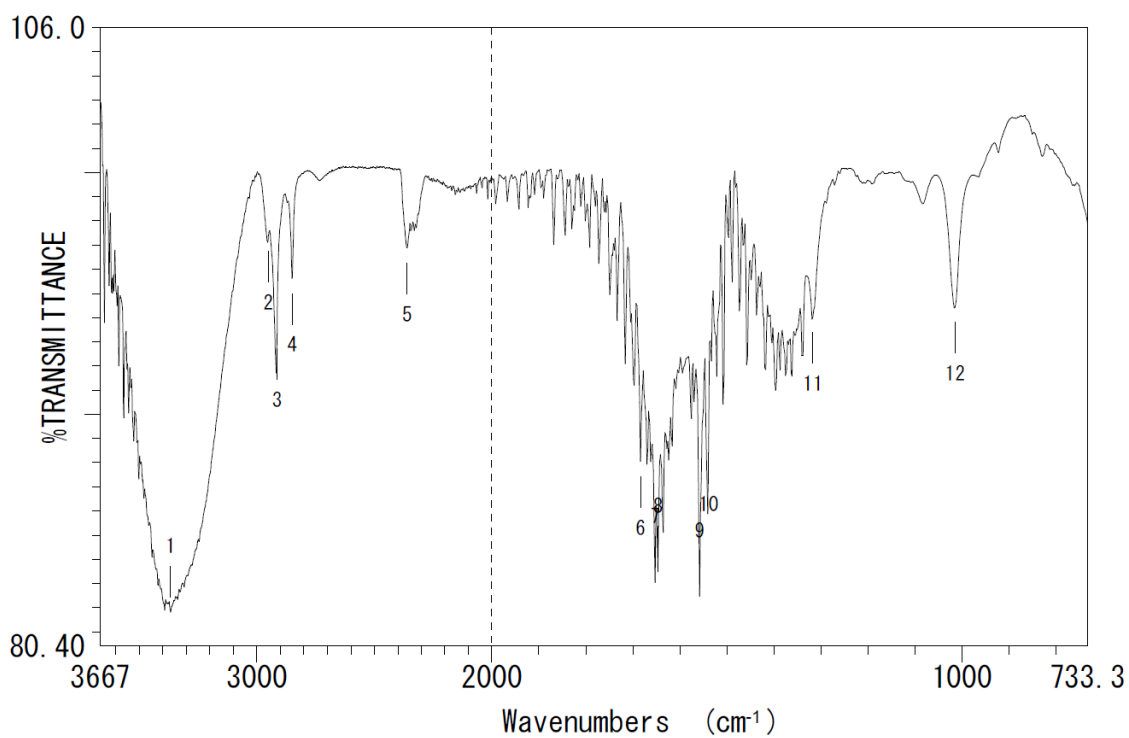


**Fig. S64.** IR spectrum of prelucilactaene B (**7**)
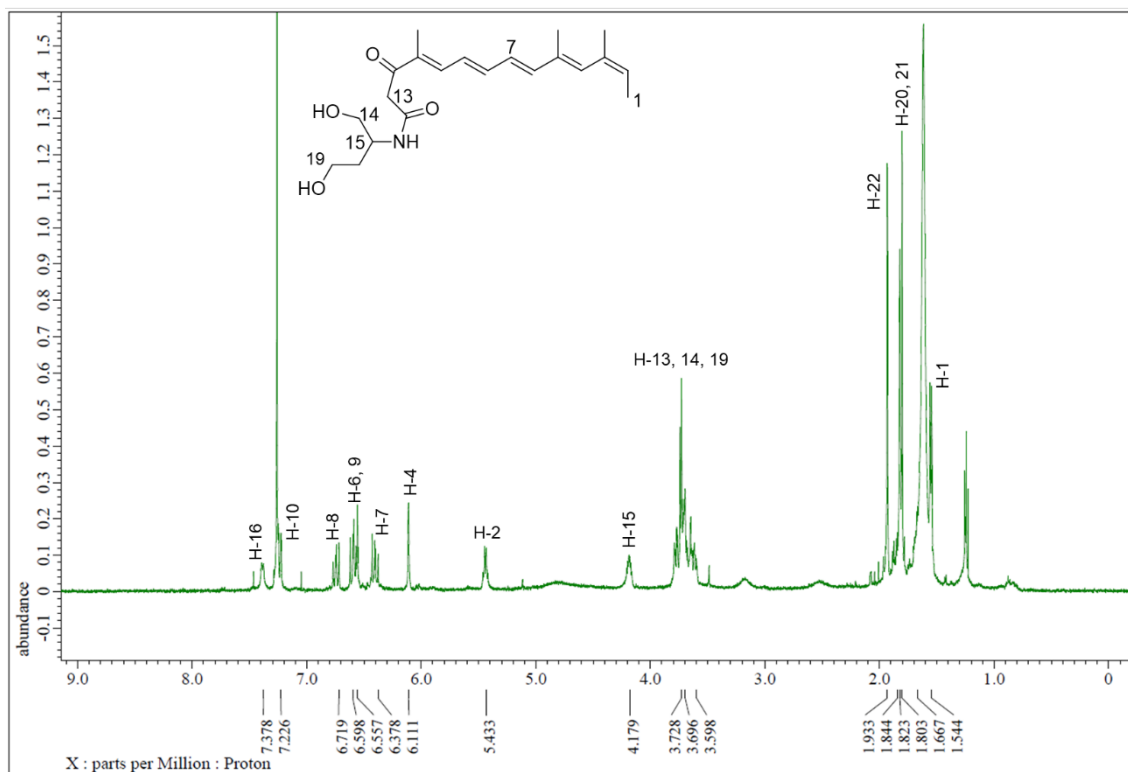
**Fig. S65.** ^{1}H-NMR spectrum of prelucilactaene B (**7**) (CDCl₃, 500 MHz)
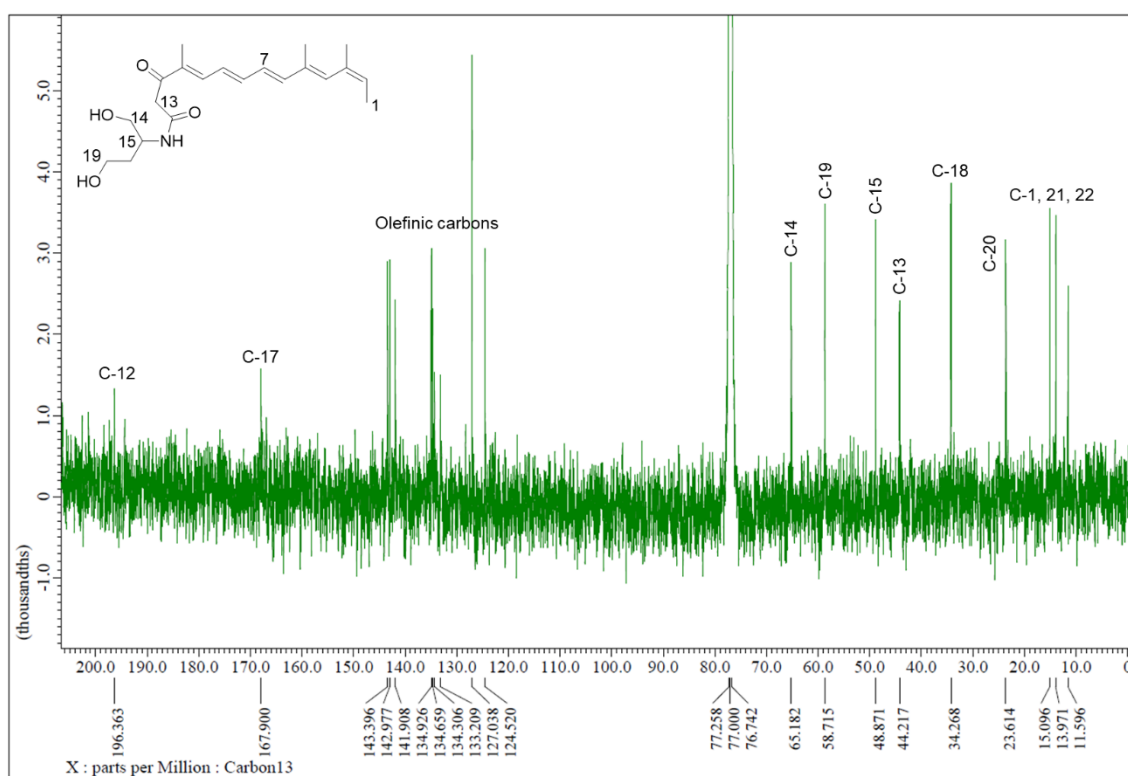


**Fig. S66.** ^{13}C-NMR spectrum of prelucilactaene B (**7**) (CDCl₃, 125 MHz)
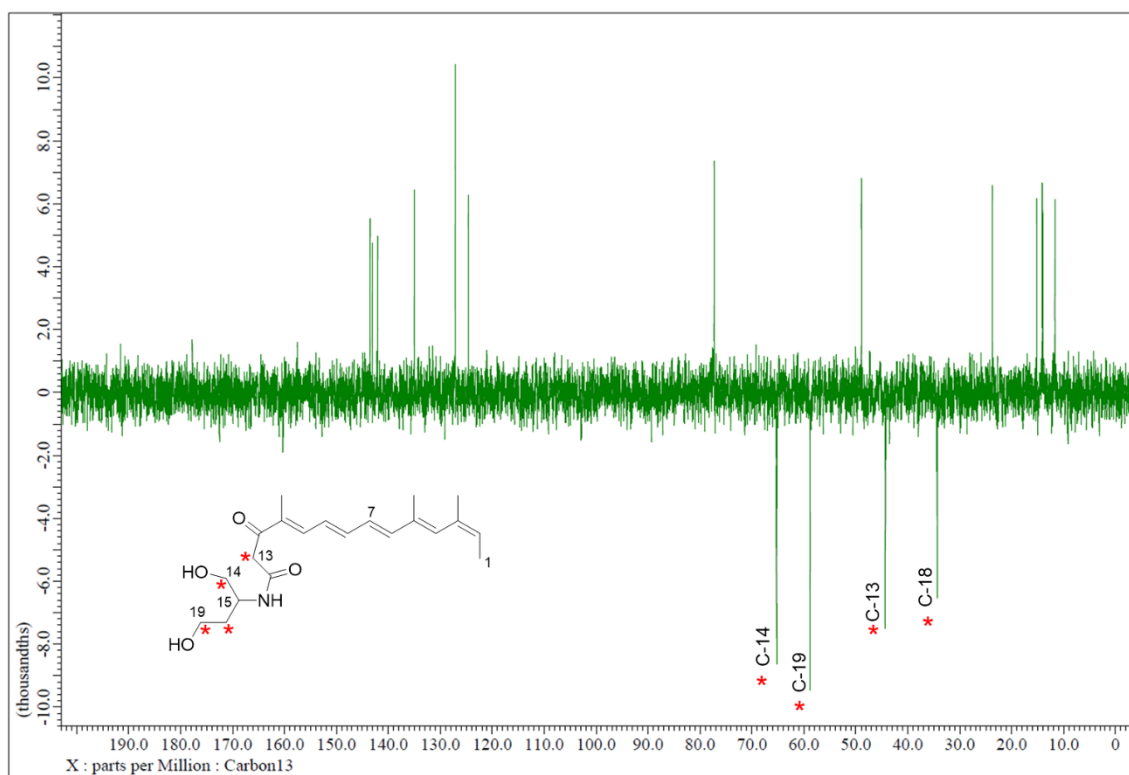
**Fig. S67.** DEPT135 spectrum of prelucilactaene B (**7**) (CDCl₃, 125 MHz)
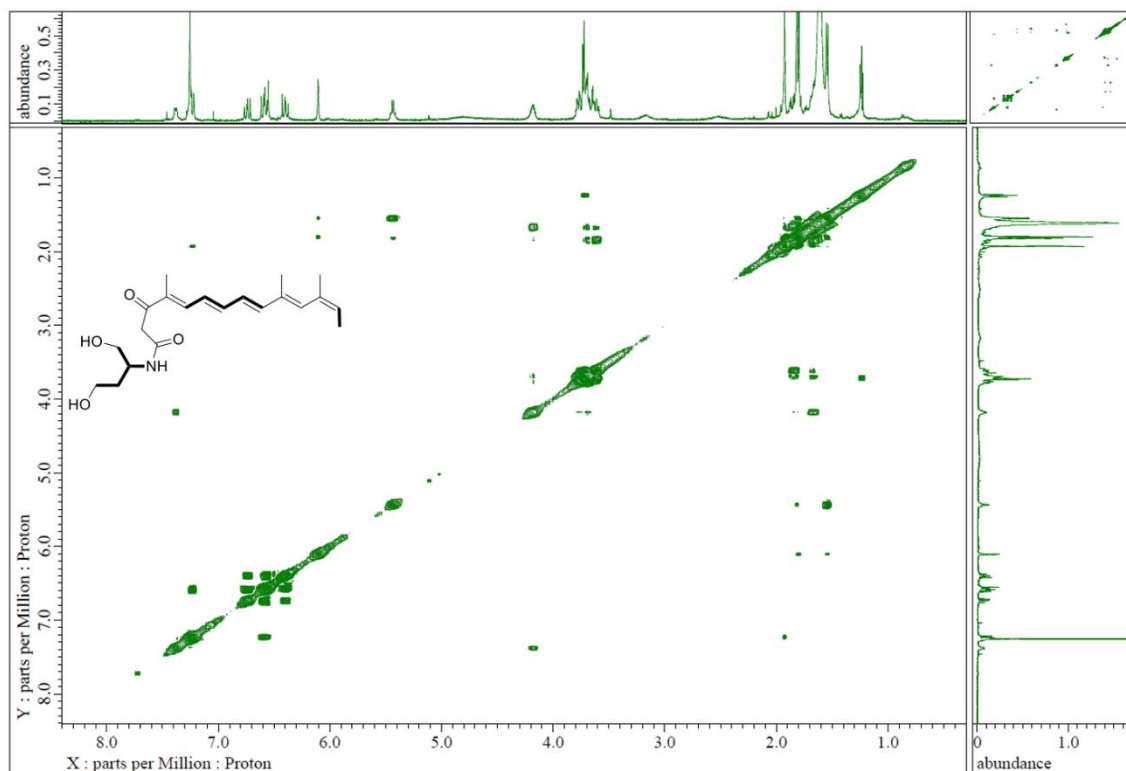


**Fig. S68.** ¹H-¹H COSY spectrum of prelucilactaene B (**7**) (CDCl₃, 500 MHz)
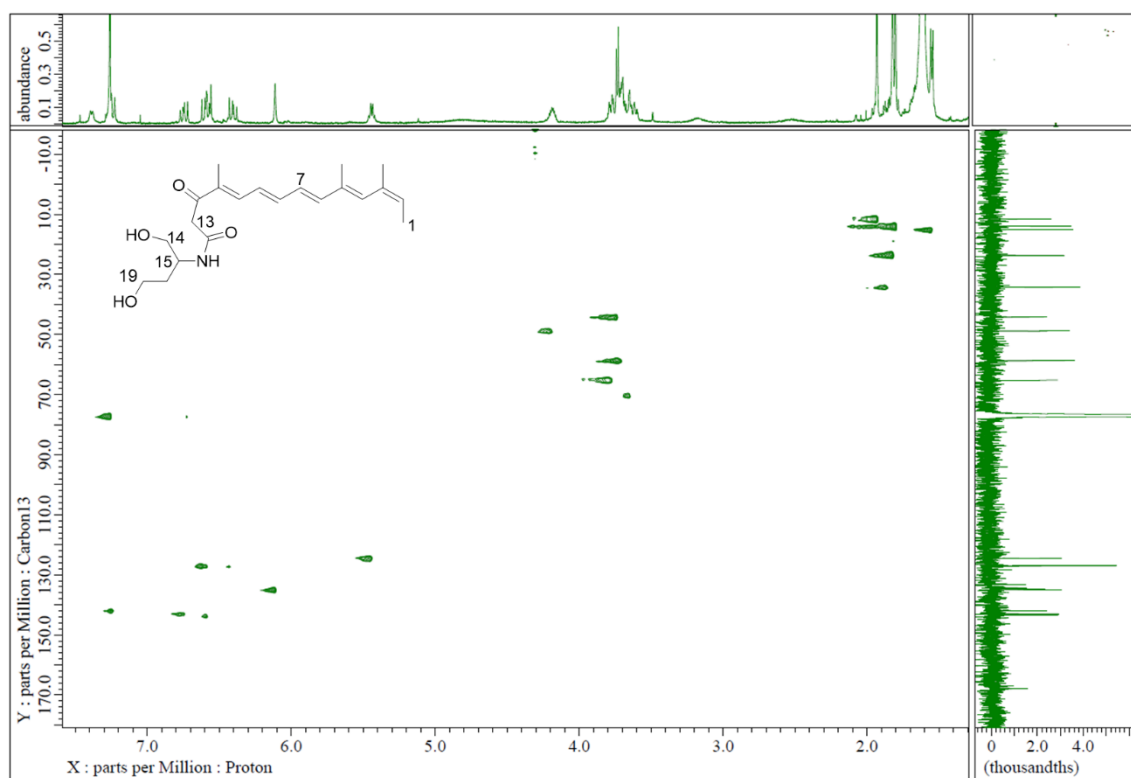
**Fig. S69.** HSQC spectrum of prelucilactaene B (**7**) (CDCl₃, 500/125 MHz)
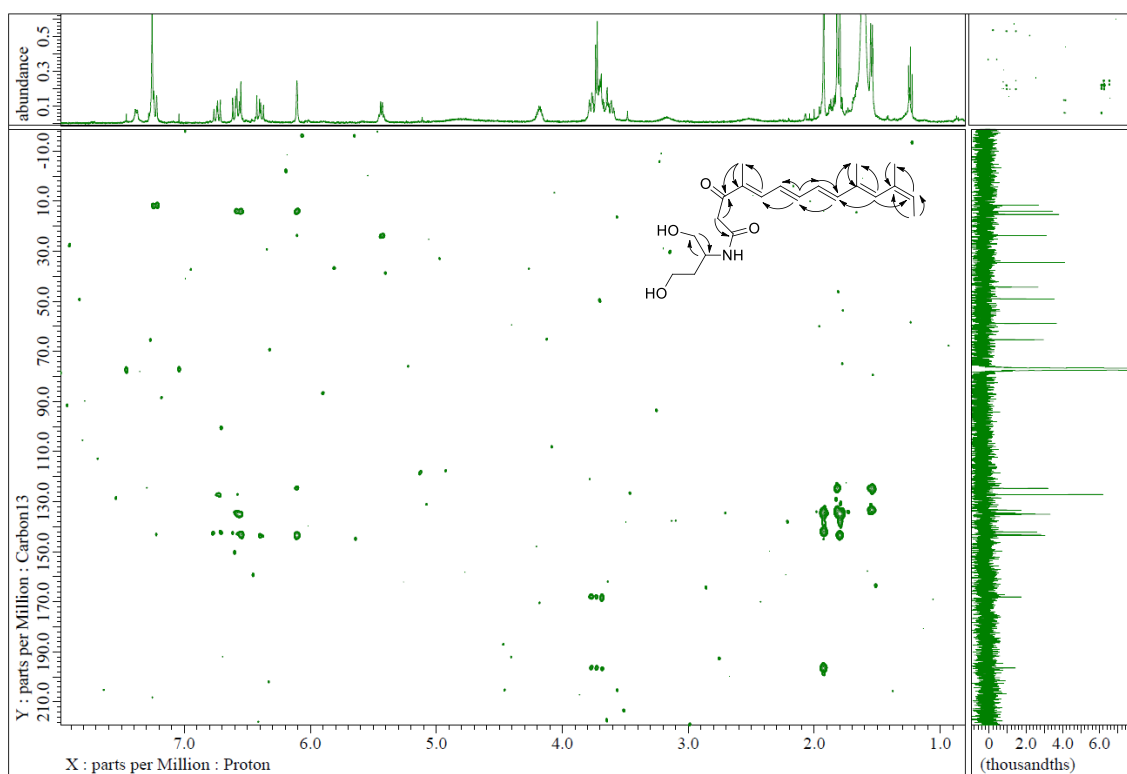


**Fig. S70.** HMBC spectrum of prelucilactaene B (**7**) (CDCl₃, 500/125 MHz)
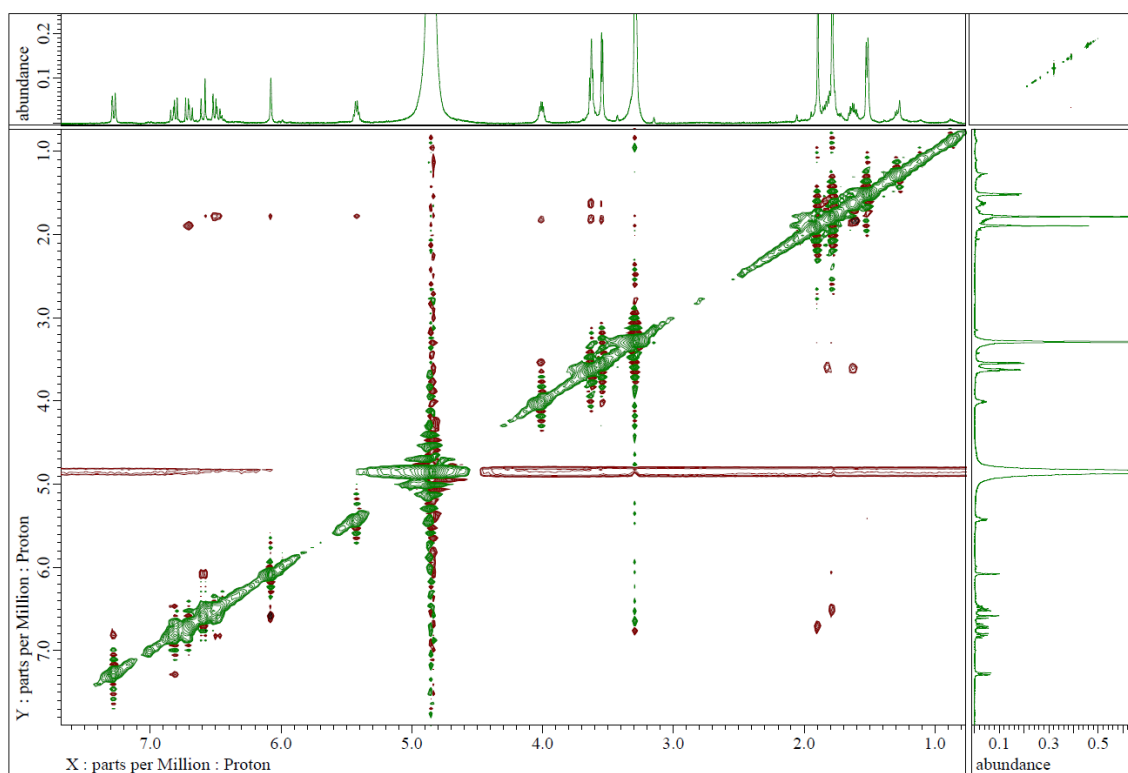
**Fig. S71.** NOESY spectrum of prelucilactaene B (**7**) (CD$_3$OD, 500 MHz)
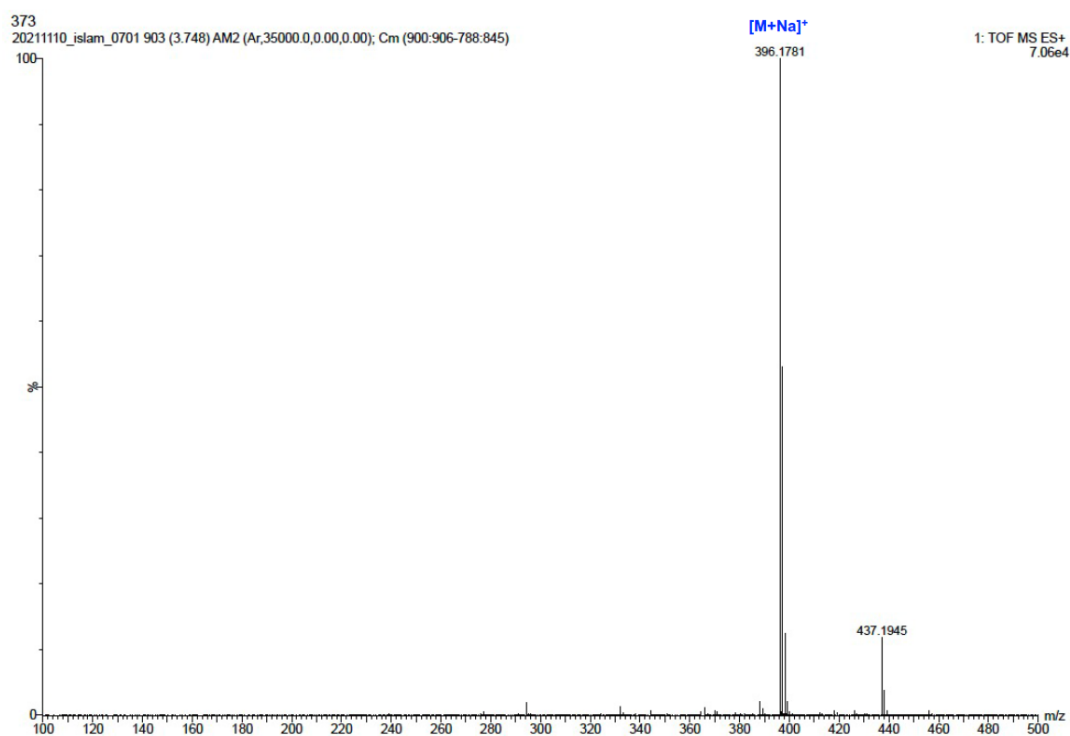


**Fig. S72.** HR-ESI-TOF/MS of prelucilactaene E (**8**)
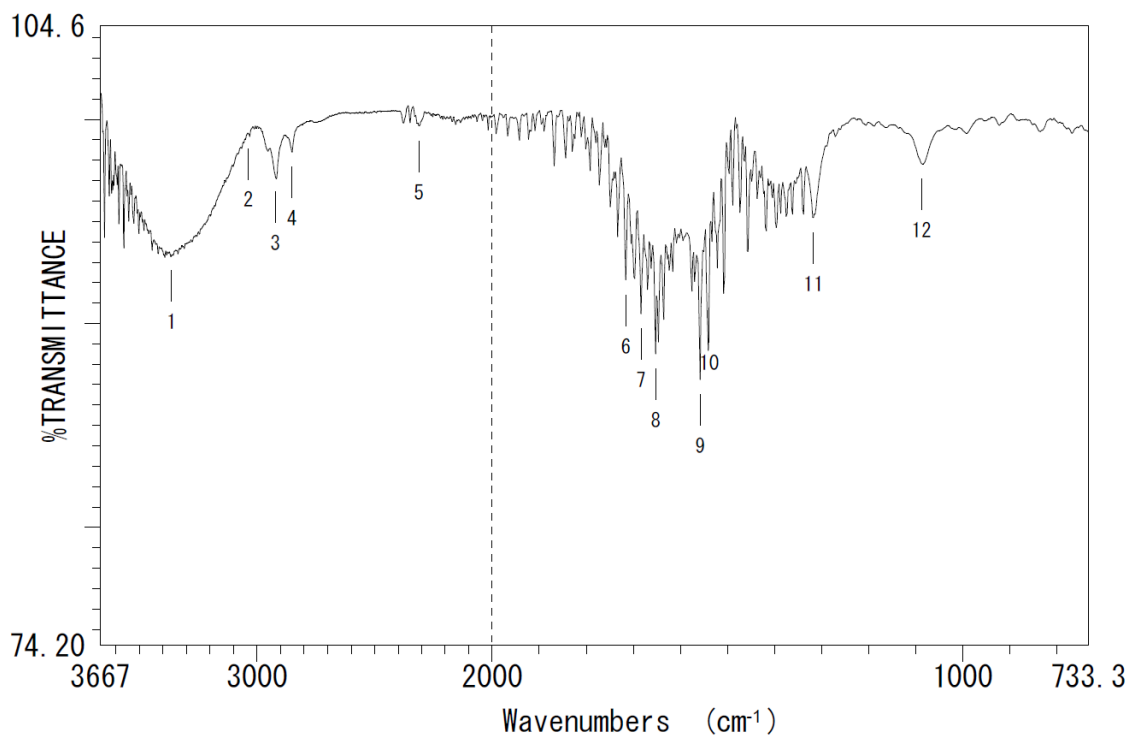
**Fig. S73.** IR spectrum of prelucilactaene E (**8**)
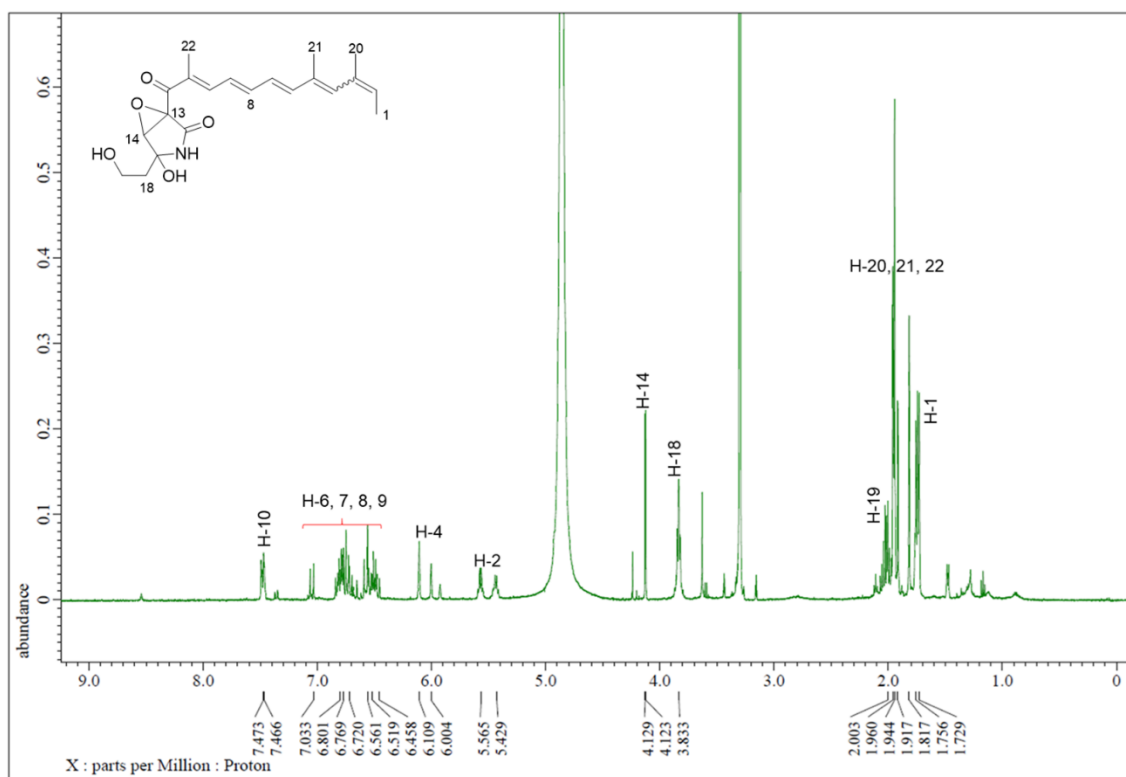


**Fig. S74.** $^1$H-NMR spectrum of prelucilactaene E (**8**) (CD$_3$OD, 500 MHz)
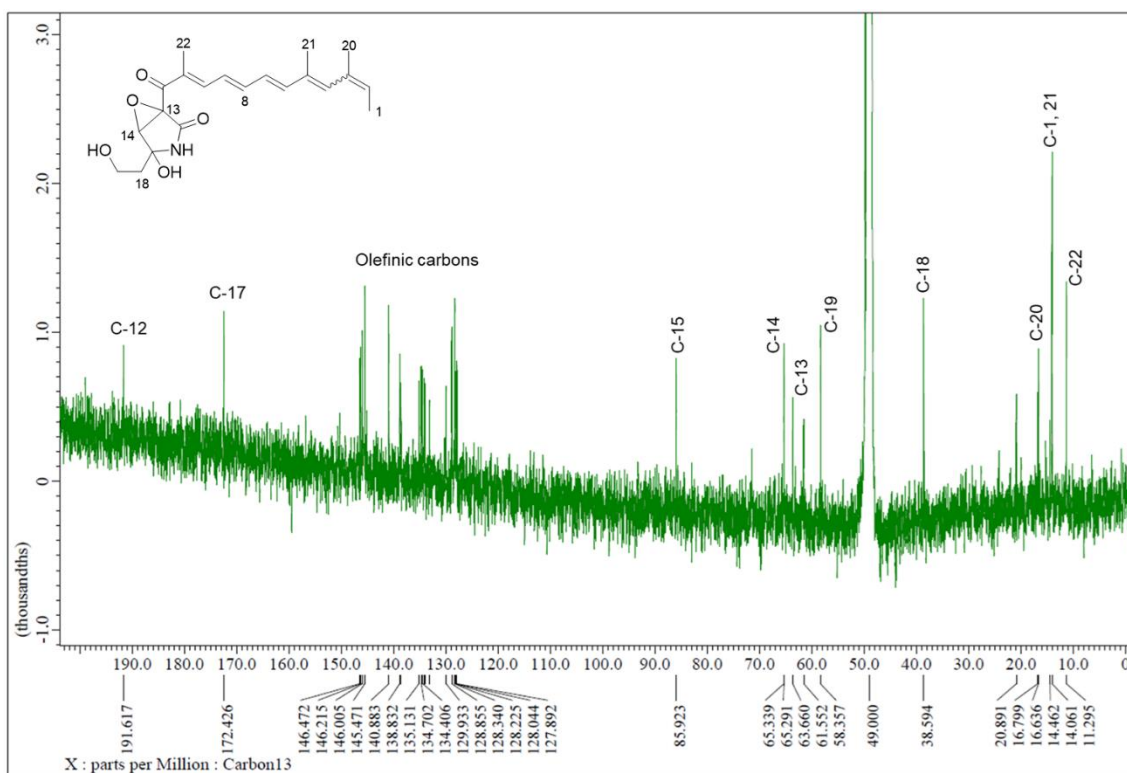
**Fig. S75.** $^{13}$C-NMR spectrum of prelucilactaene E (**8**) (CD$_3$OD, 125 MHz)
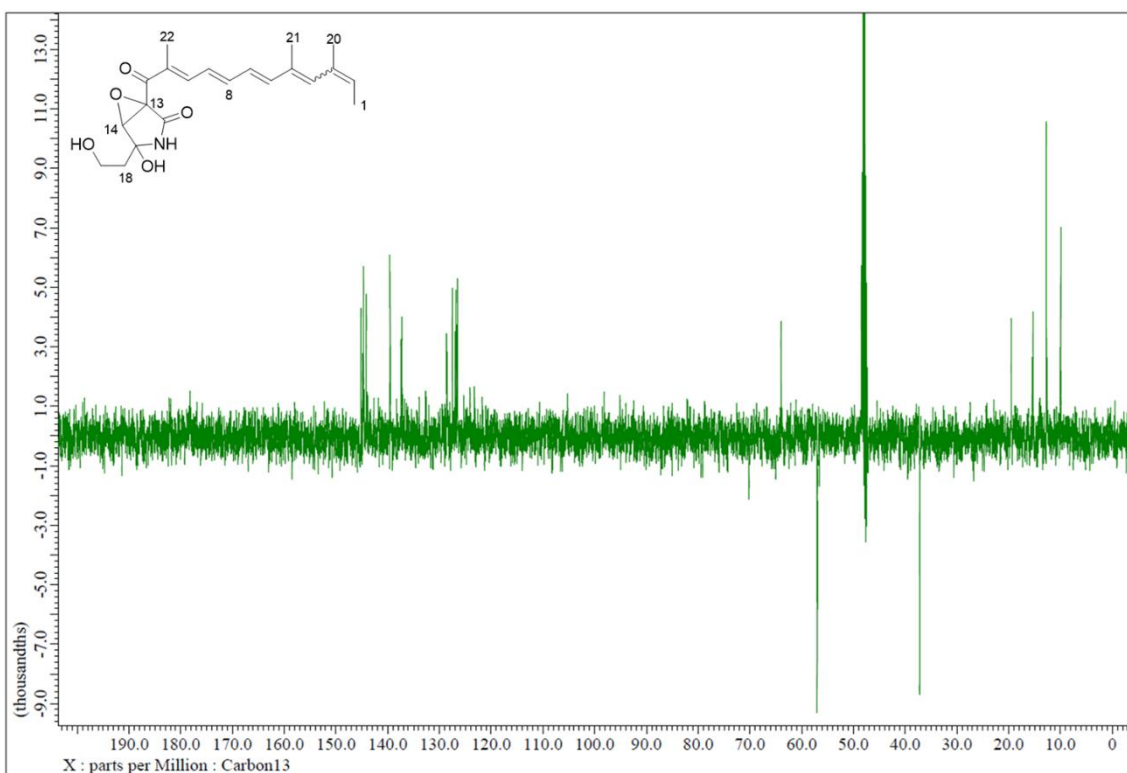


**Fig. S76.** DEPT135 spectrum of prelucilactaene E (**8**) (CD$_3$OD, 125 MHz)
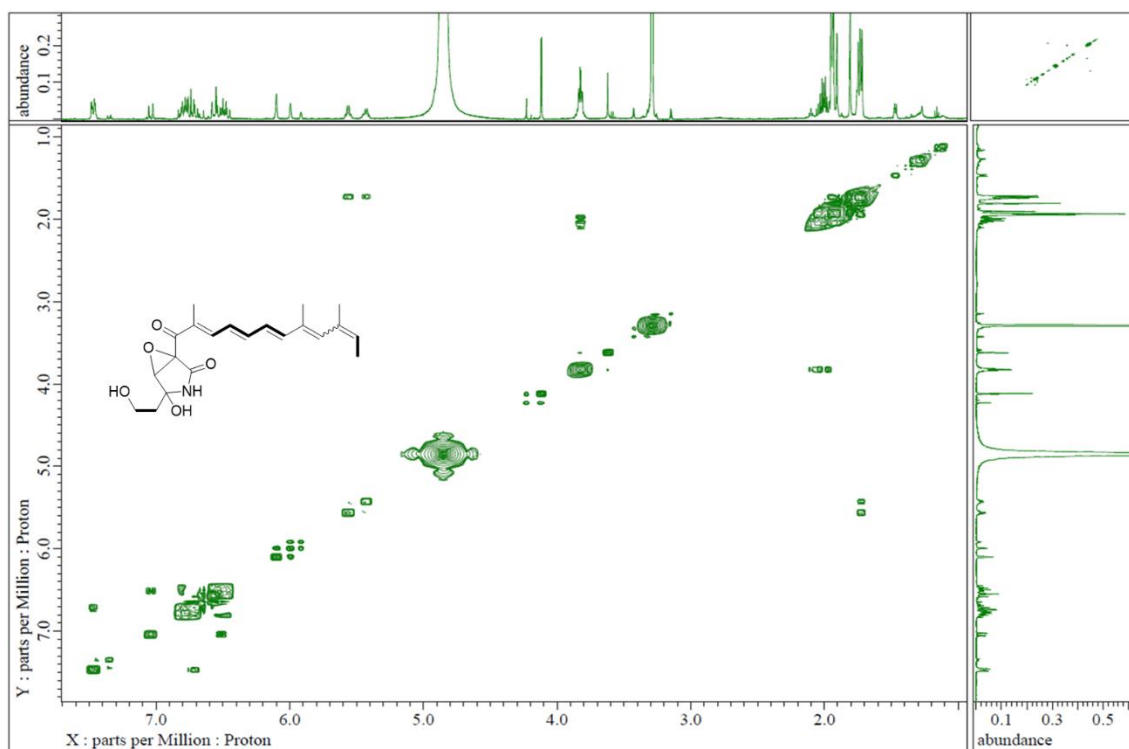
**Fig. S77.** $^1$H-$^1$H COSY spectrum of prelucilactaene E (**8**) (CD$_3$OD, 500 MHz)
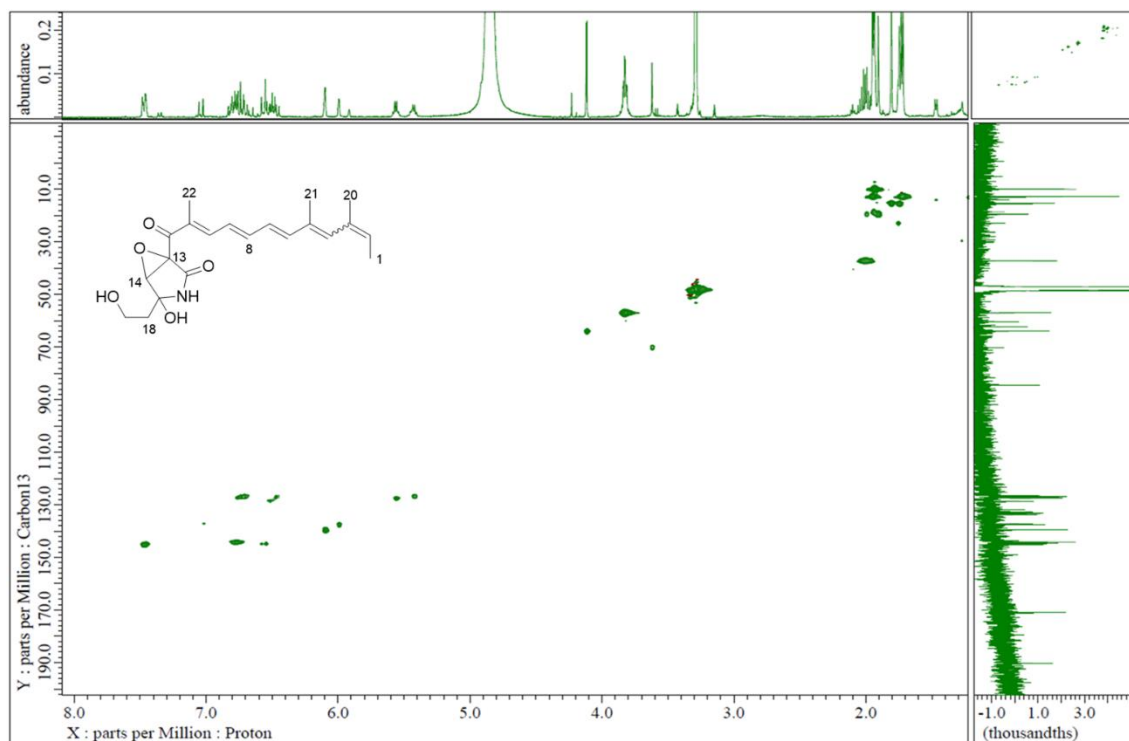


**Fig. S78.** HSQC spectrum of prelucilactaene E (**8**) (CD$_3$OD, 500/125 MHz)
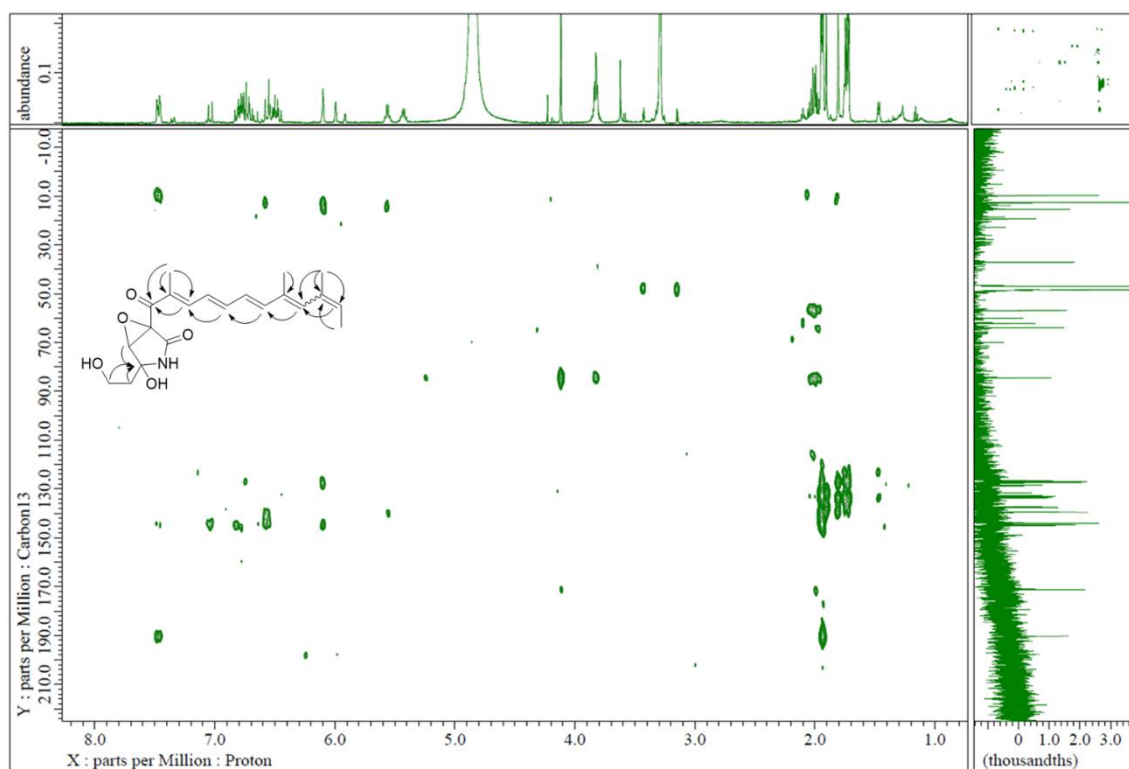
**Fig. S79.** HMBC spectrum of prelucilactaene E (**8**) (CD$_3$OD, 500/125 MHz)
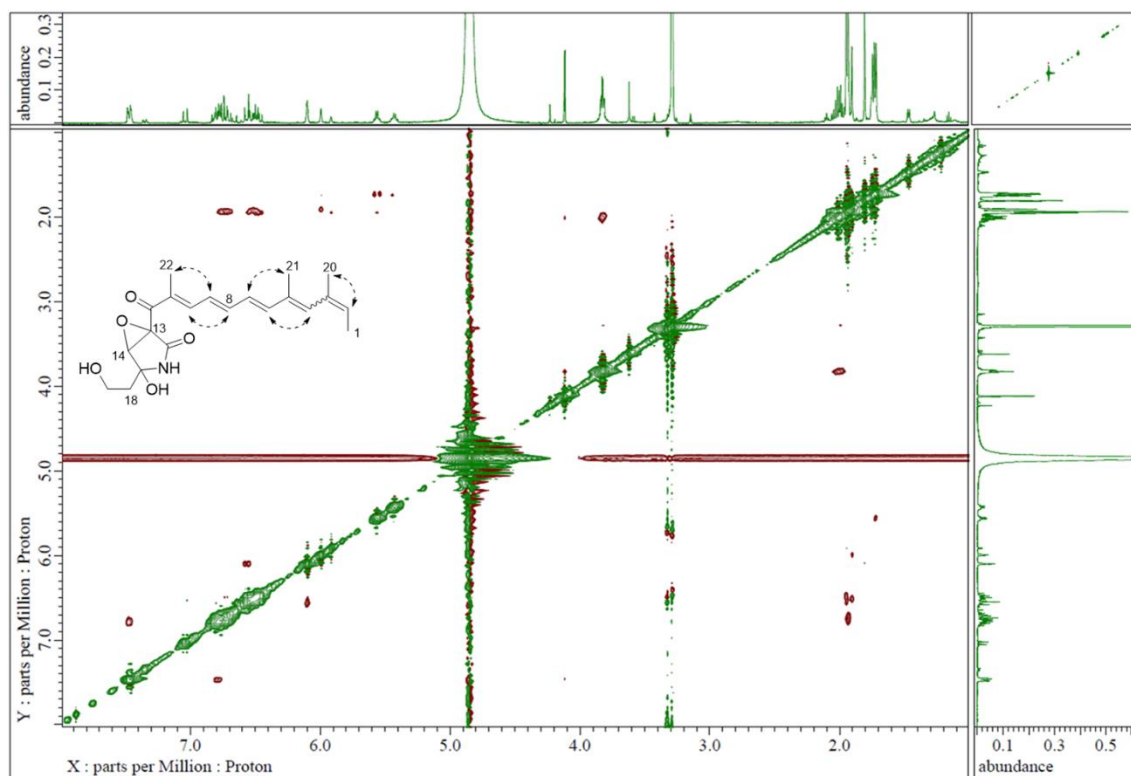


**Fig. S80.** NOESY spectrum of prelucilactaene E (**8**) (CD$_3$OD, 500 MHz)
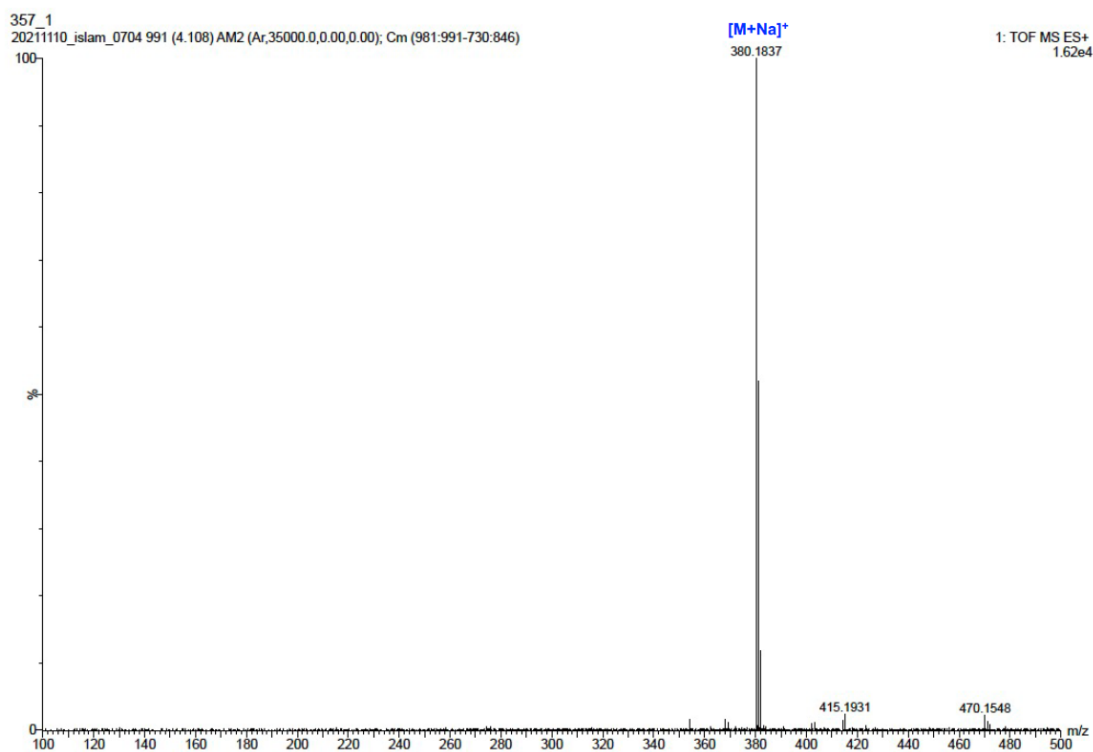
**Fig. S81.** HR-ESI-TOF/MS of prelucilactaene F (**9**)
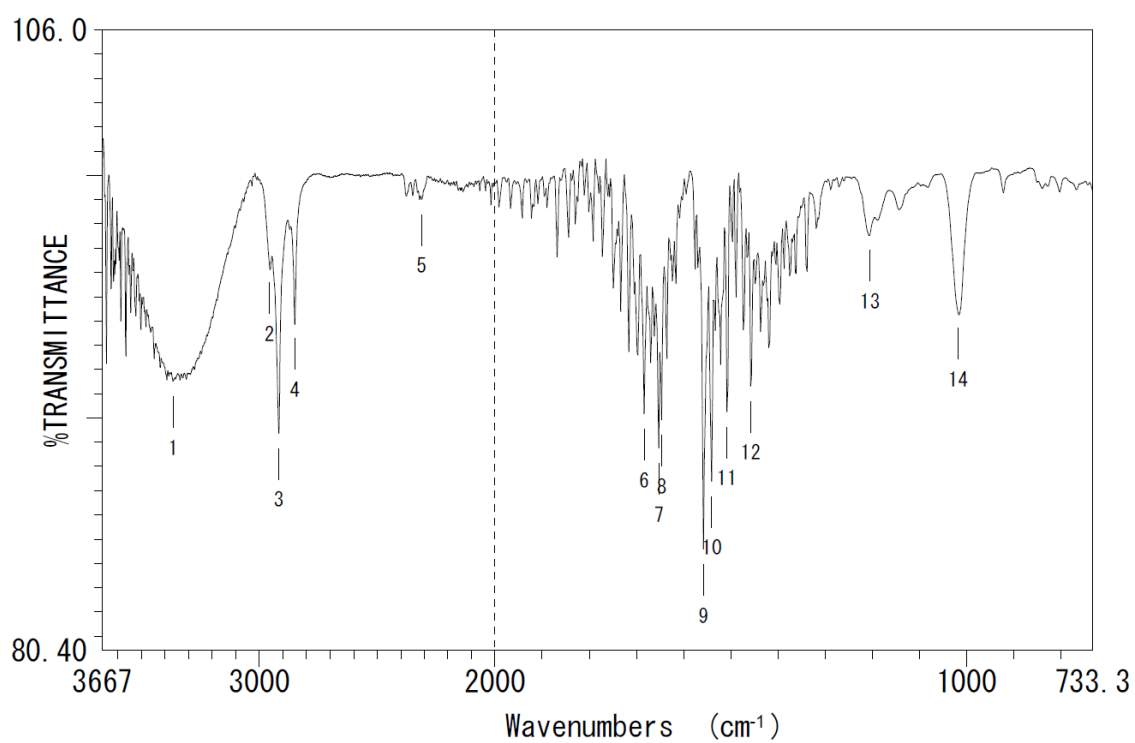


**Fig. S82.** IR spectrum of prelucilactaene E (**8**)
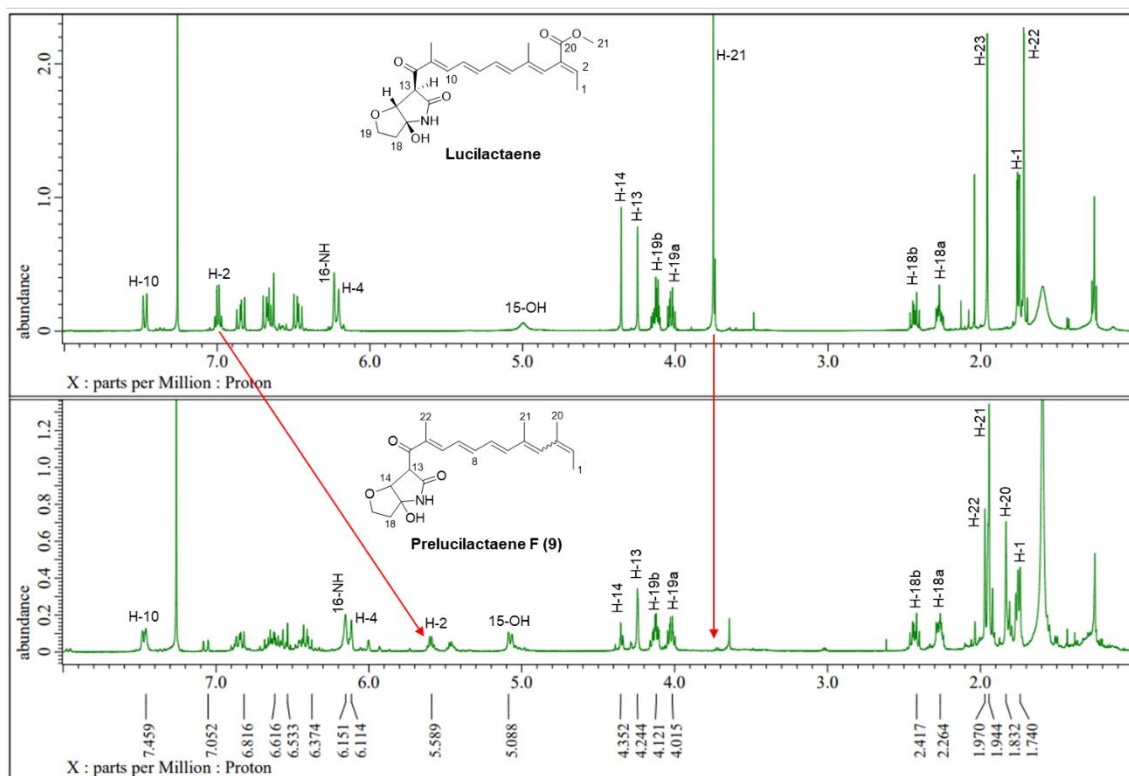
**Fig. S83.** ^{1}H-NMR of prelucilactaene F (**9**), compared with lucilactaene (CDCl$_3$, 500 MHz).
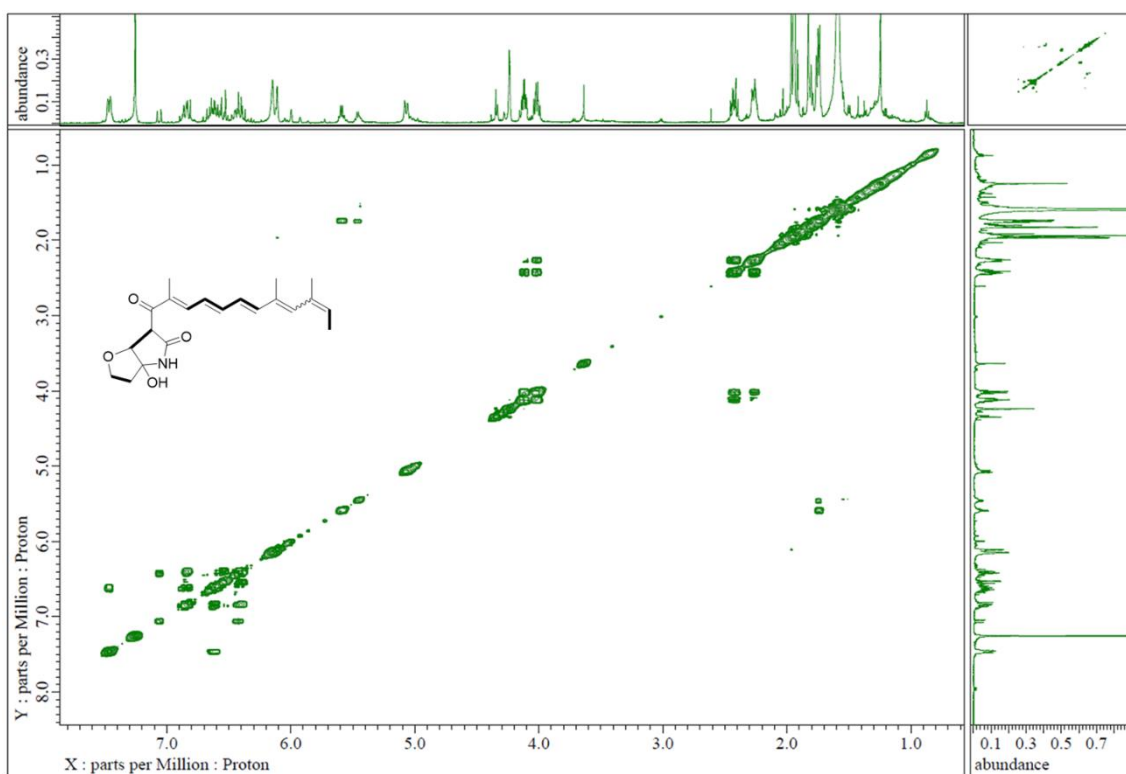


**Fig. S84.** ^{1}H-^{1}H COSY spectrum of prelucilactaene F (**9**) (CDCl$_3$, 500 MHz)
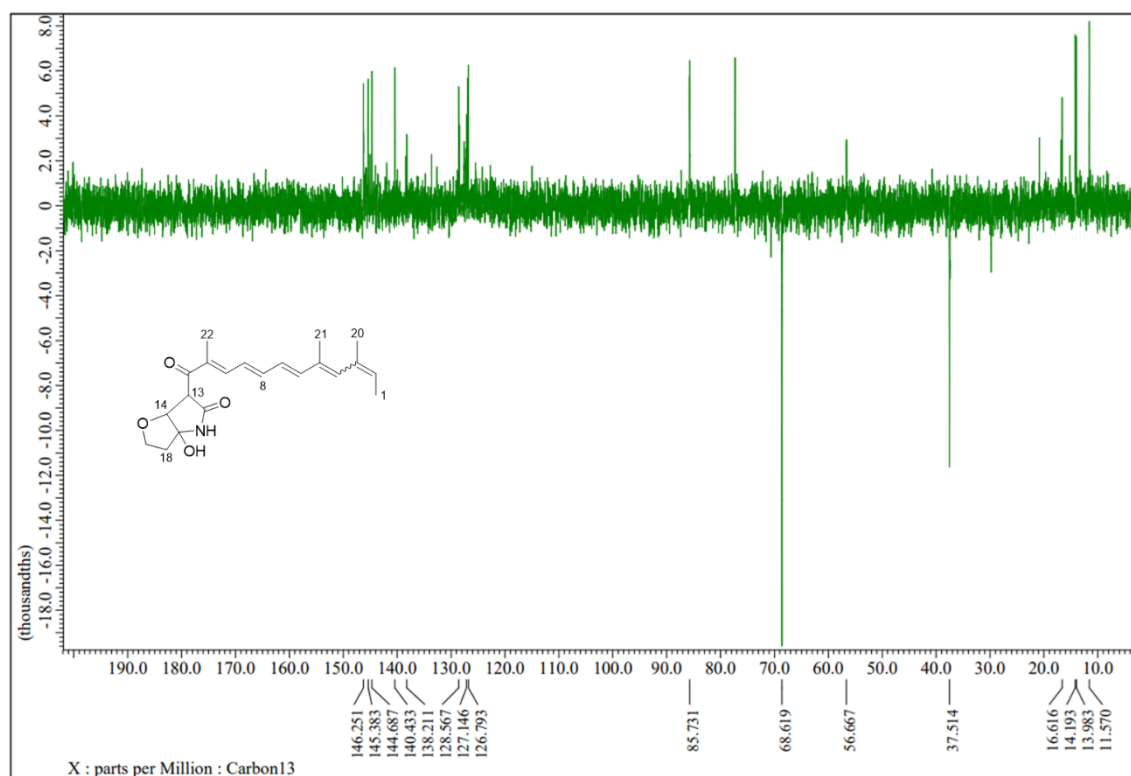
**Fig. S85.** DEPT135 NMR of prelucilactaene F (**9**) (CDCl$_3$, 125 MHz).
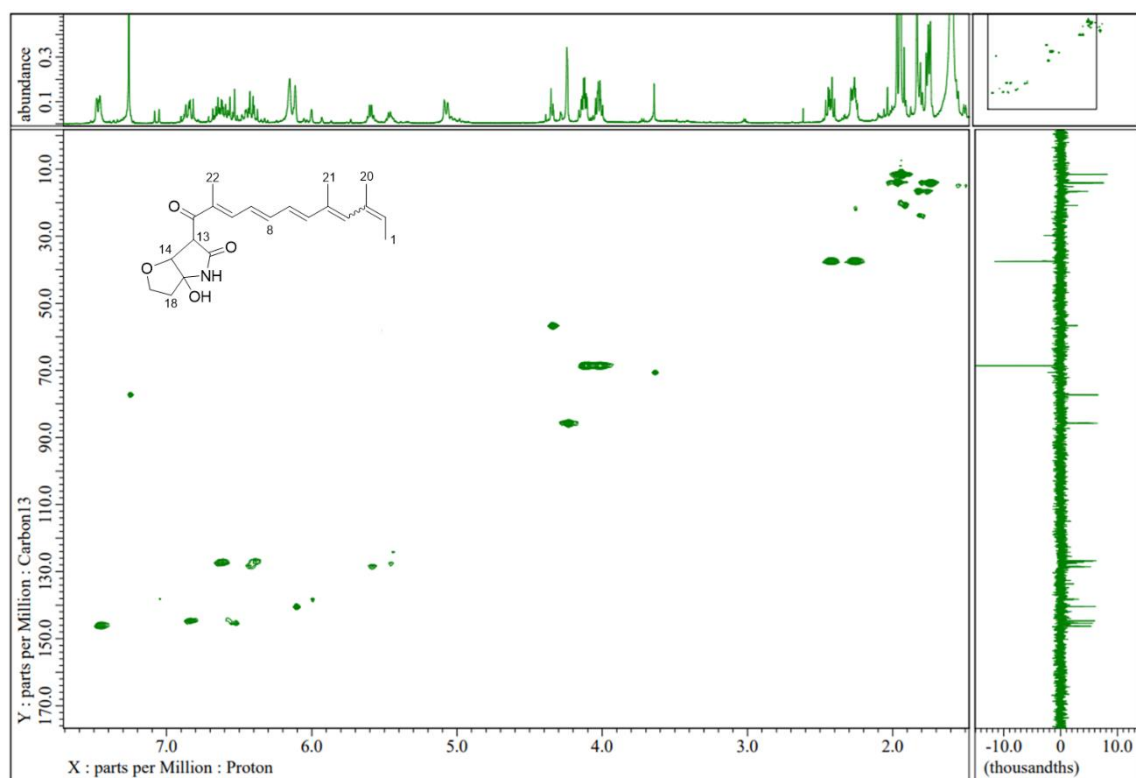


**Fig. S86.** HSQC spectrum of prelucilactaene F (**9**) (CDCl$_3$, 500/125 MHz)

## Prelucilactaene F (MW 357)
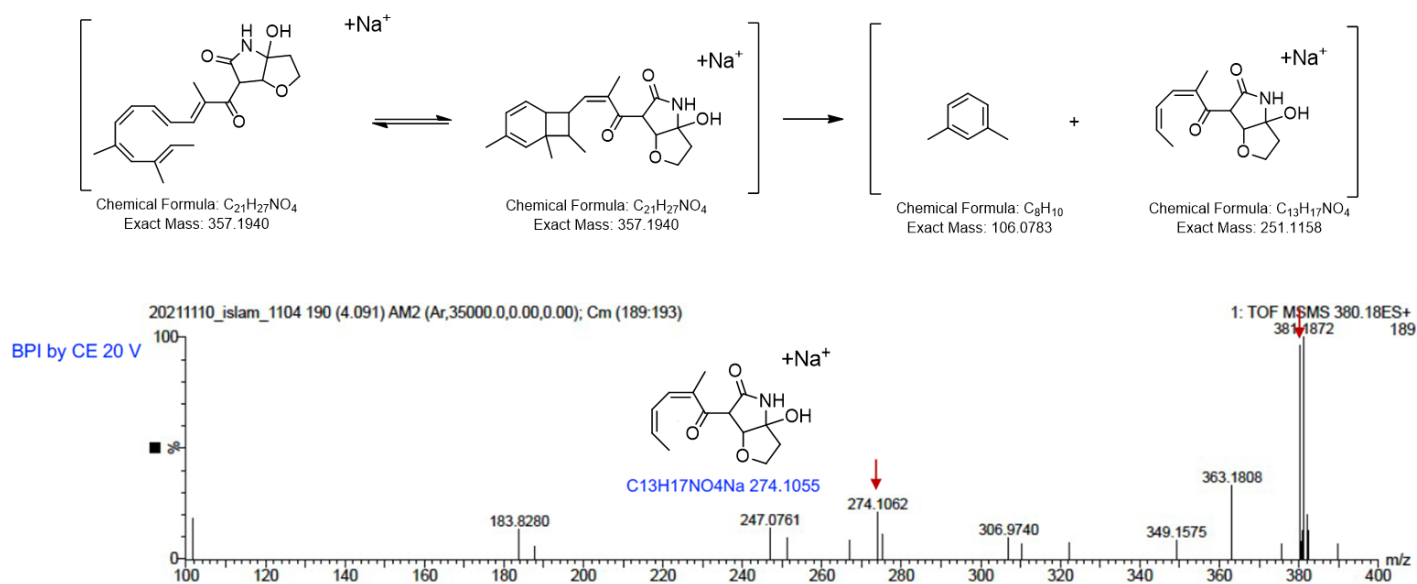




**Fig. S87.** MSMS fragmentation of MW357 compound (prelucilactaene F, **9**)



**Fig. S88.** Reported MSMS fragmentations of Fusarin C and its derivatives

Niehaus, Eva-Maria, et al. *Chemistry & Biology.* **2013,** 20(8): 1055-1066.
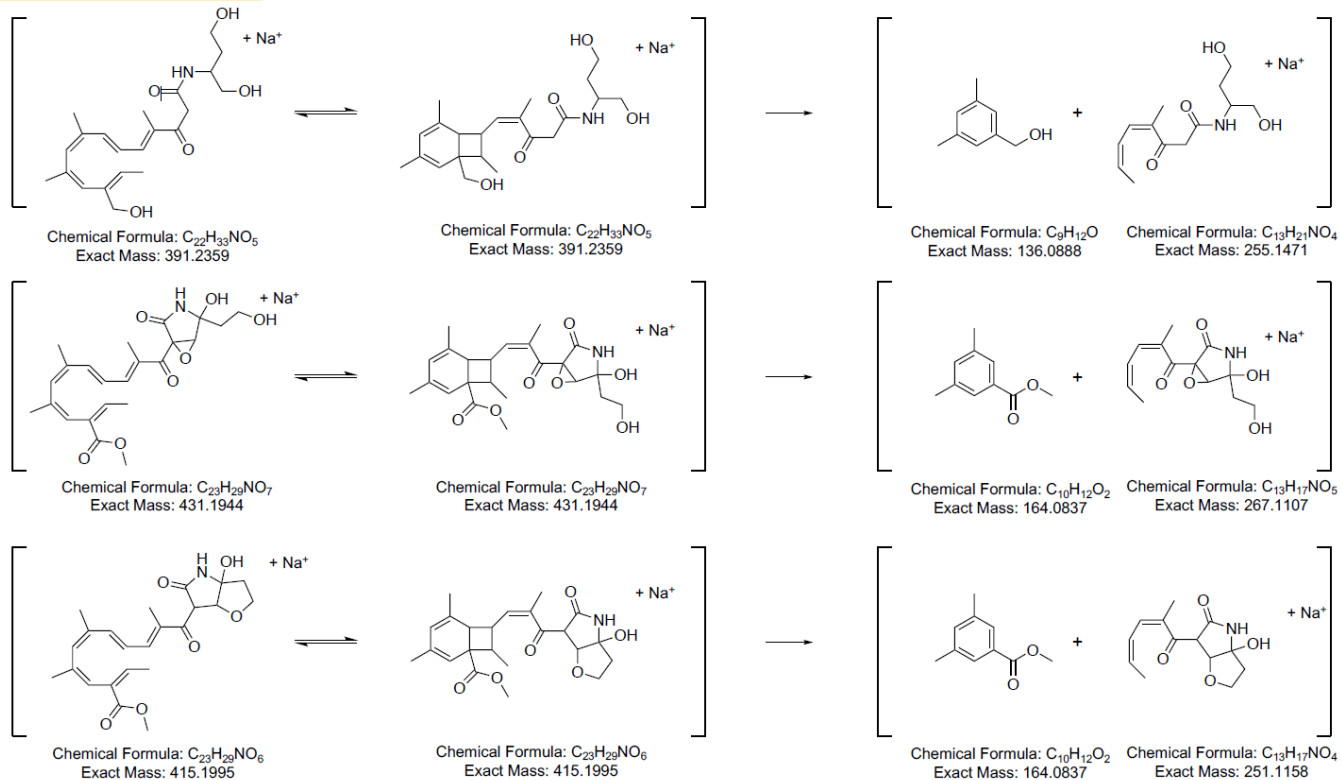
## Lucilactaene (MW 401)
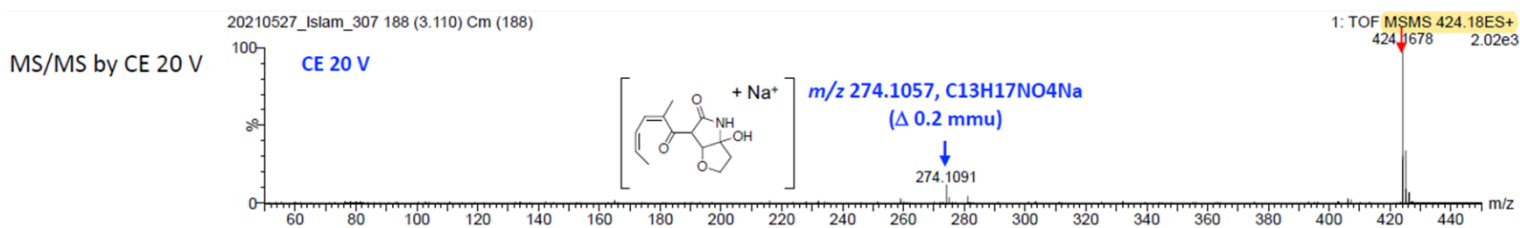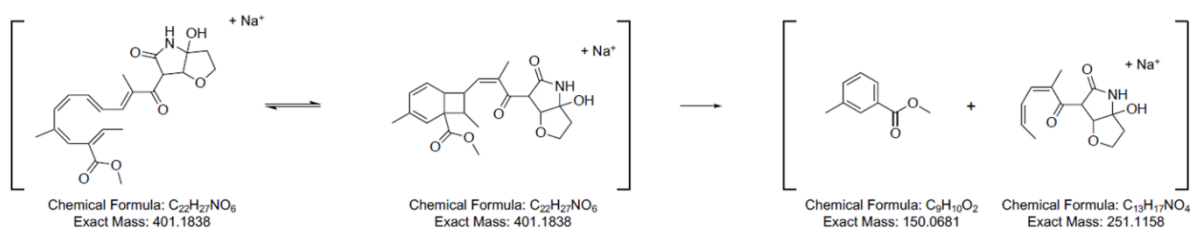


**Fig. S89.** MSMS fragmentation of Lucilactaene

## Dihydrolucilactaene (MW403)



**Fig. S90.** MSMS fragmentation of Dihydrolucilactaene

154
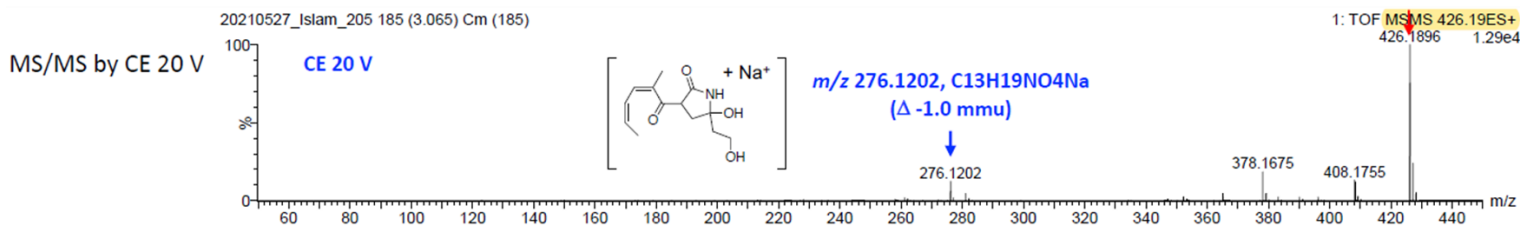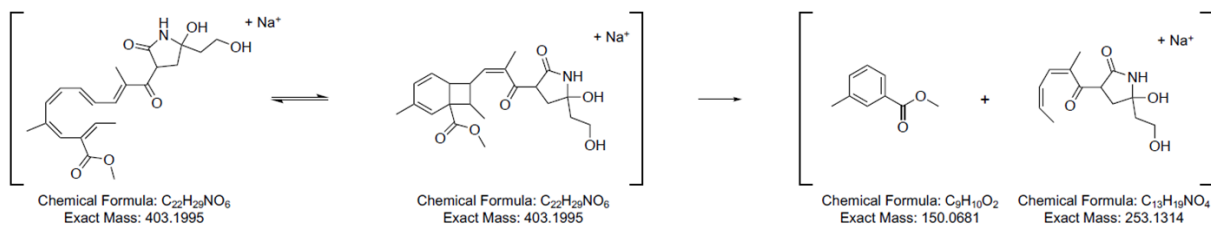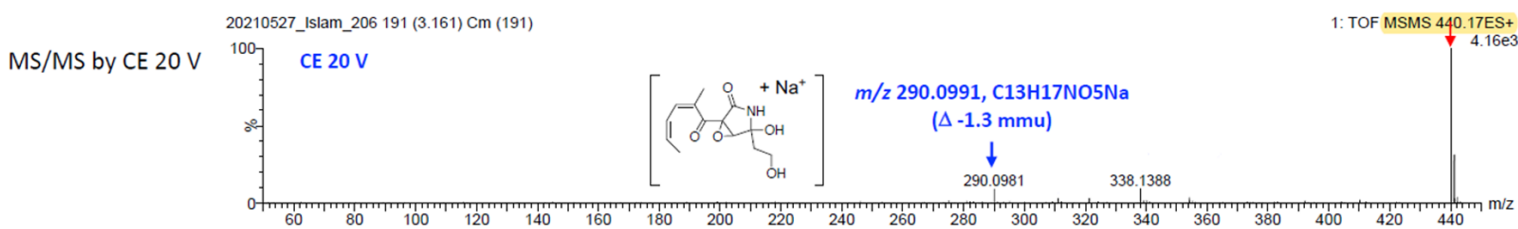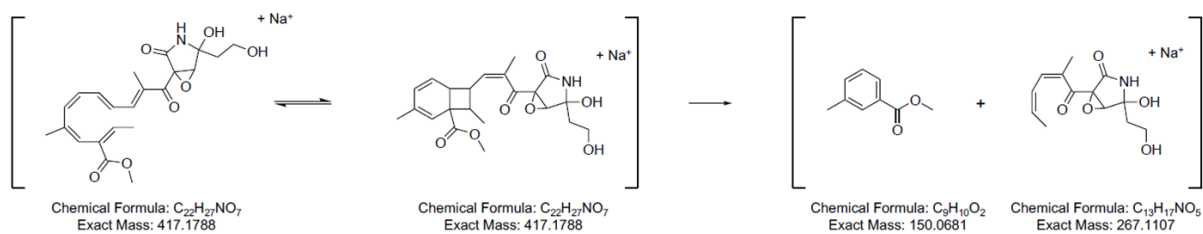
**NG391 (MW417)**



**Fig. S91.** MSMS fragmentation of NG391

**13α-hydroxylucilactaene (MW417)**
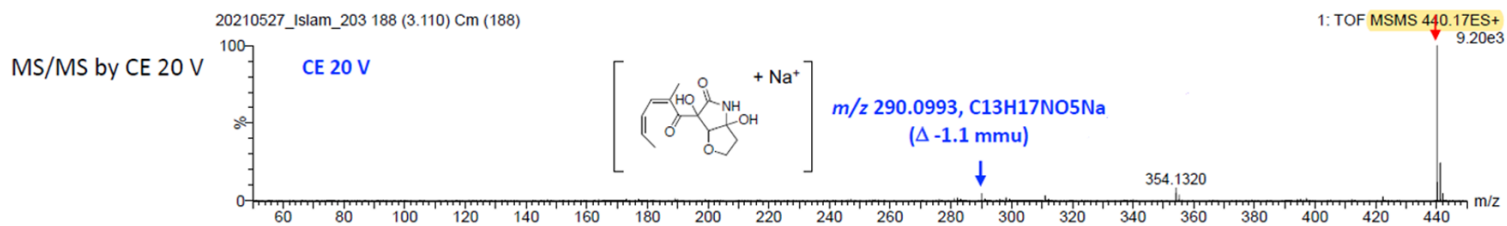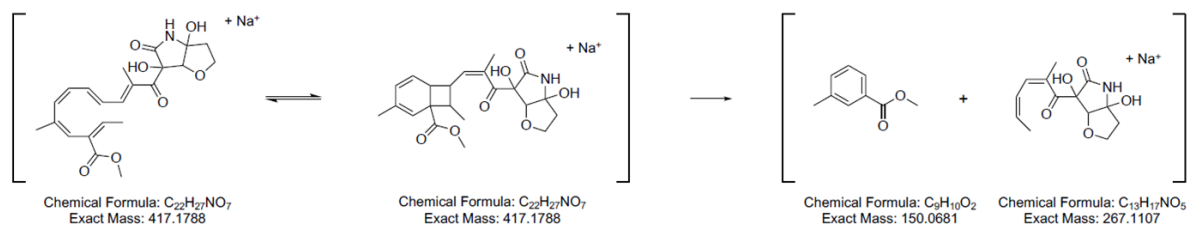


**Fig. S92.** MSMS fragmentation of 13-hydroxylucilactaene

## DihydroNG391 (MW419)
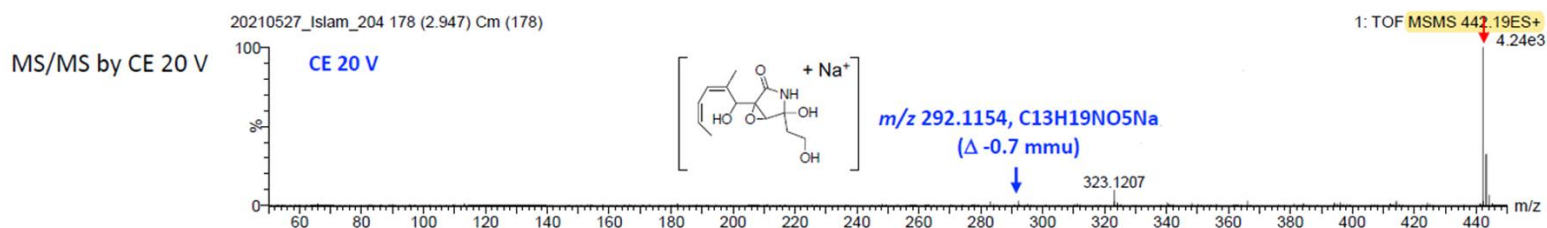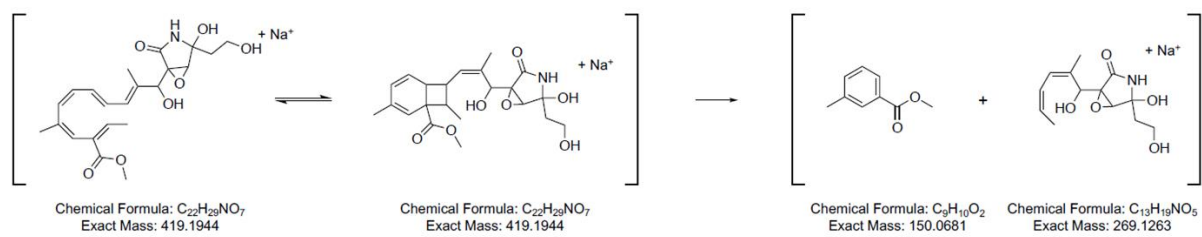


**Fig. S93.** MSMS fragmentation of DihydroNG391

## Prelucilactaene G (MW389)
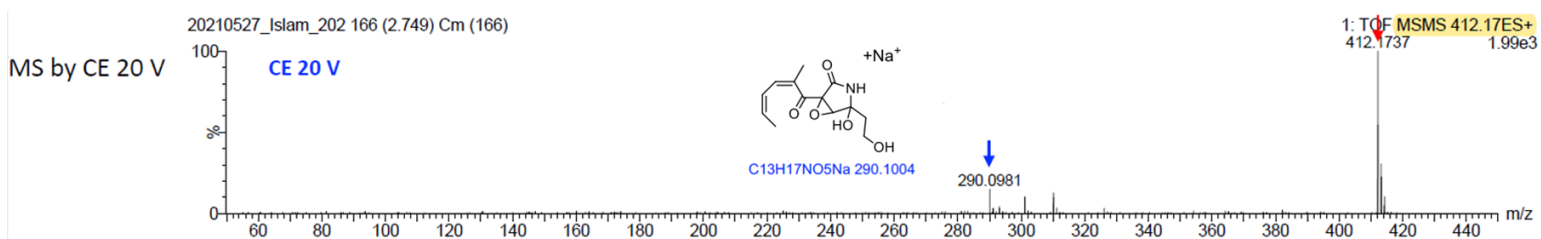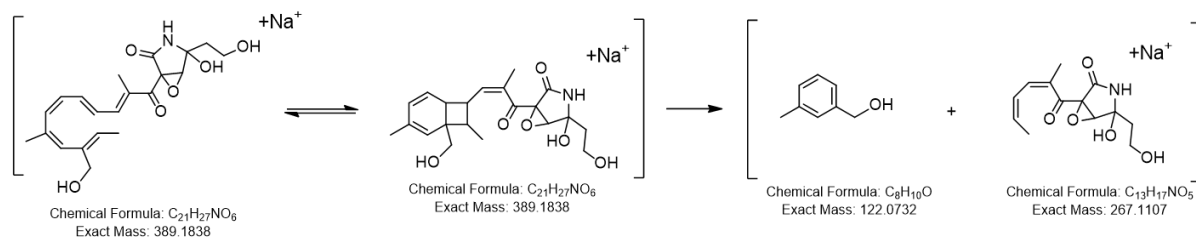


**Fig. S94.** MSMS fragmentation of MW361 compound (prelucilactaene G, **4**)

**Prelucilactaene B (MW361)**
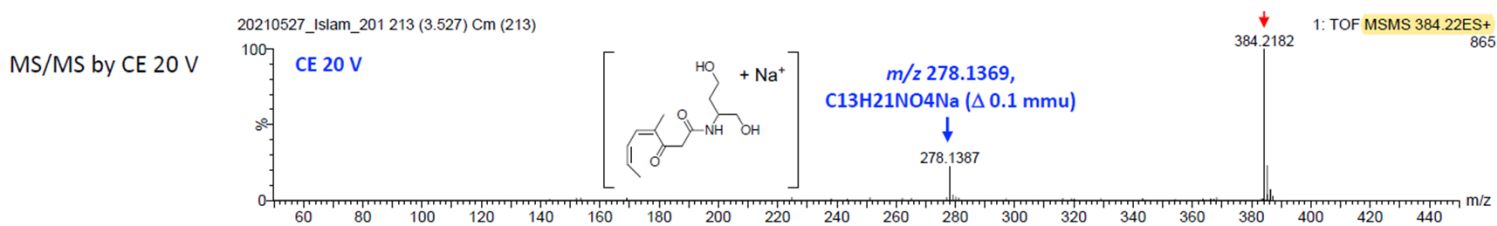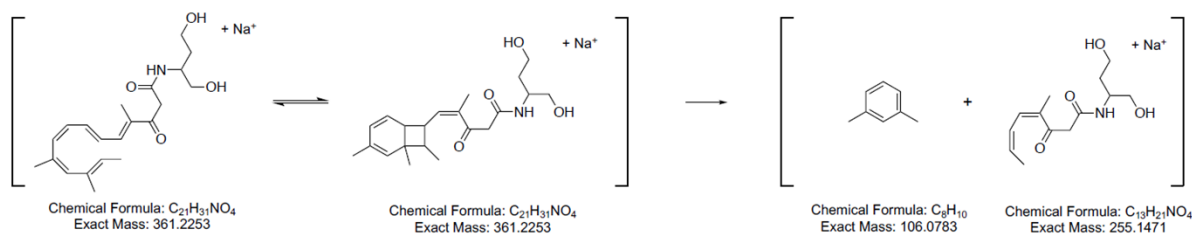


**Fig. S95.** MSMS fragmentation of MW361 compound (prelucilactaene B, **7**)

**Prelucilactaene E (MW373)**
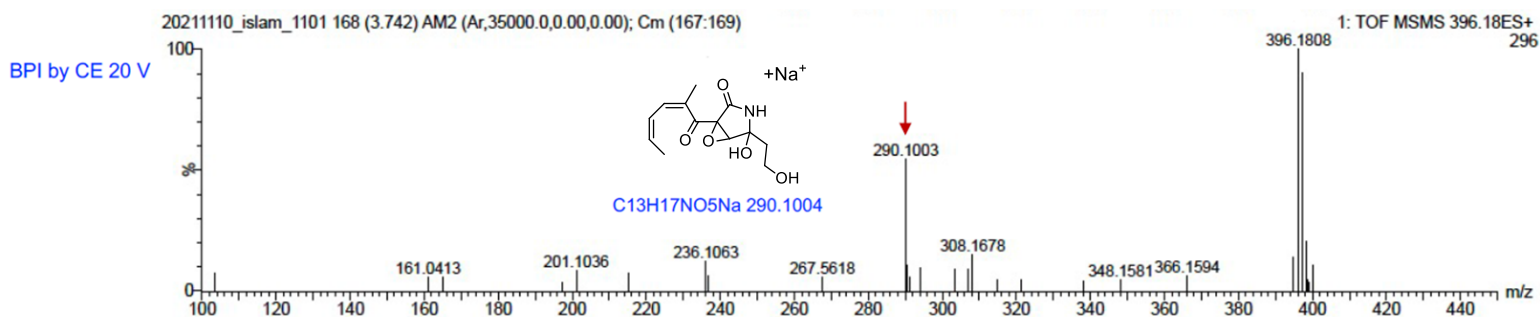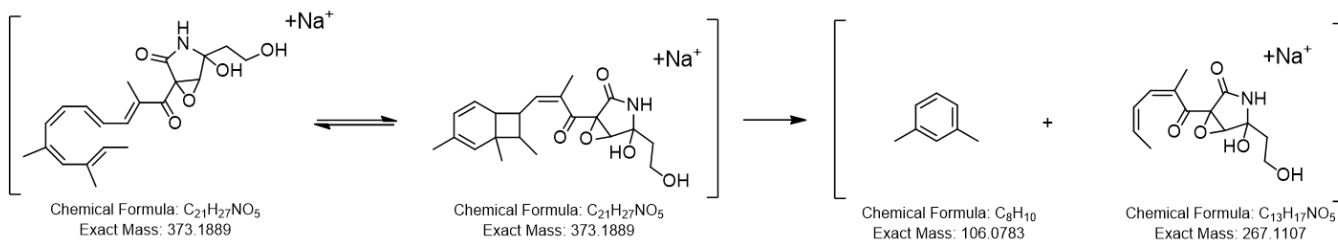


**Fig. S96.** MSMS fragmentation of MW373 compound (prelucilactaene E, **8**)

## Prelucilactaene C (MW343)
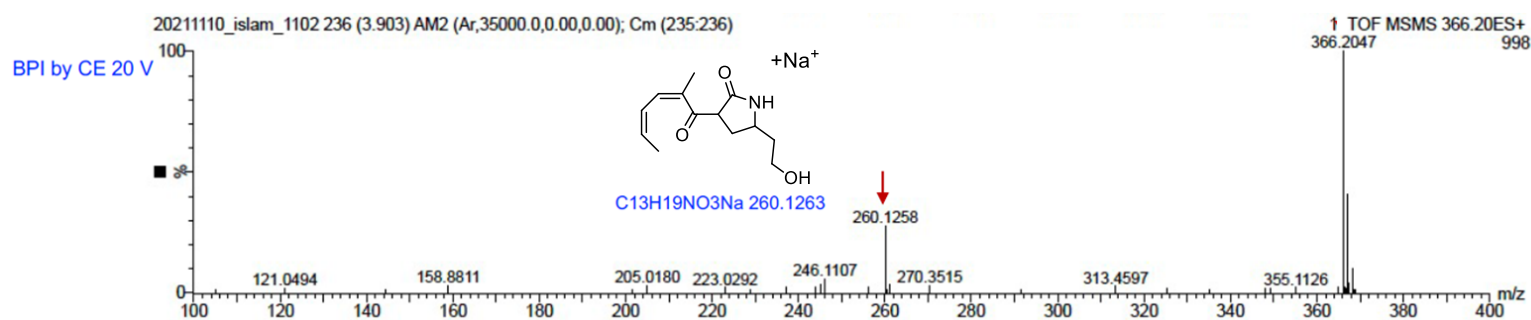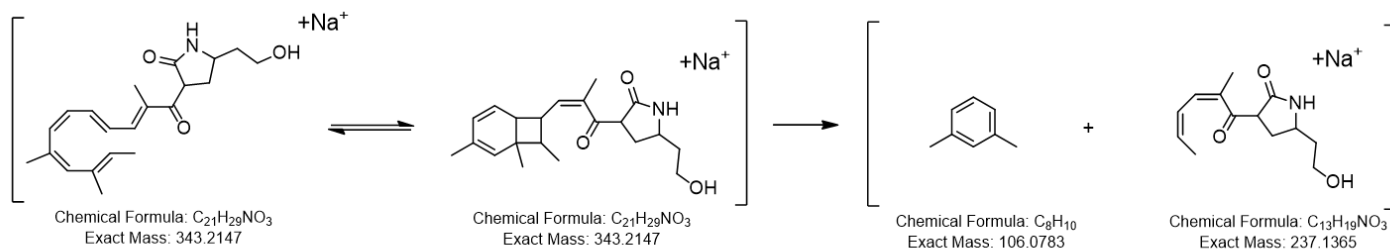


**Fig. S97.** MSMS fragmentation of MW343 (prelucilactaene C)

## Prelucilactaene D (MW359)
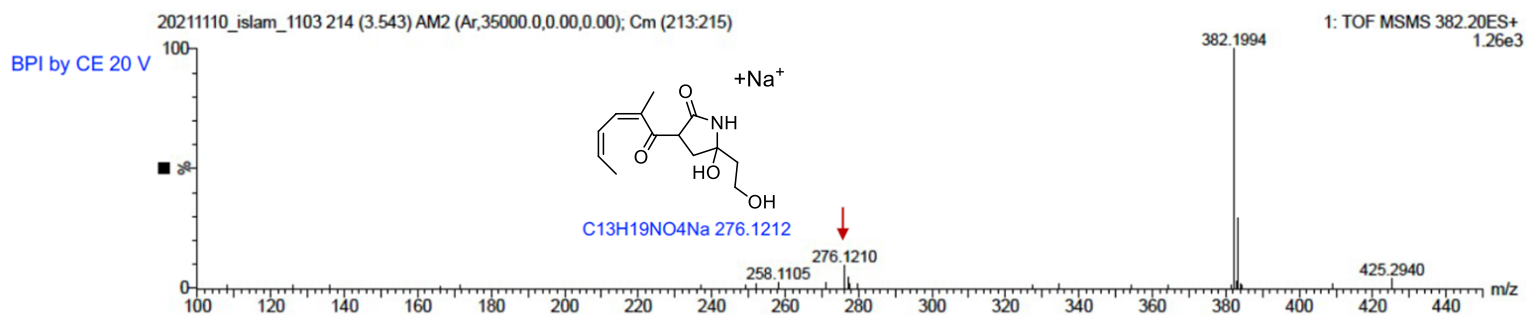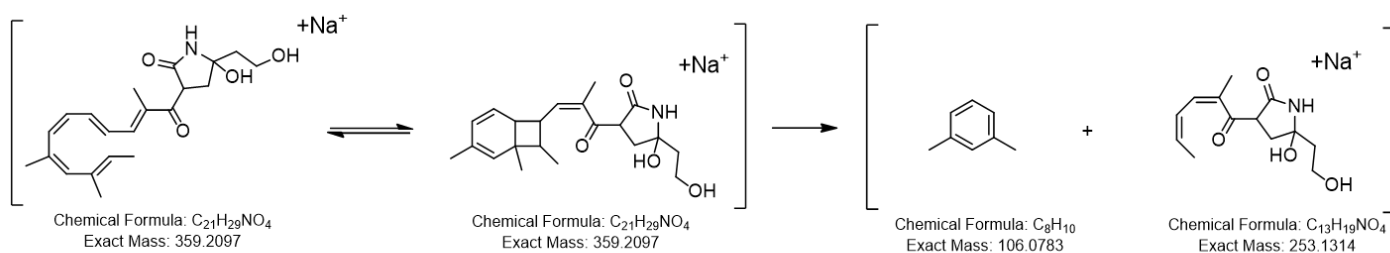


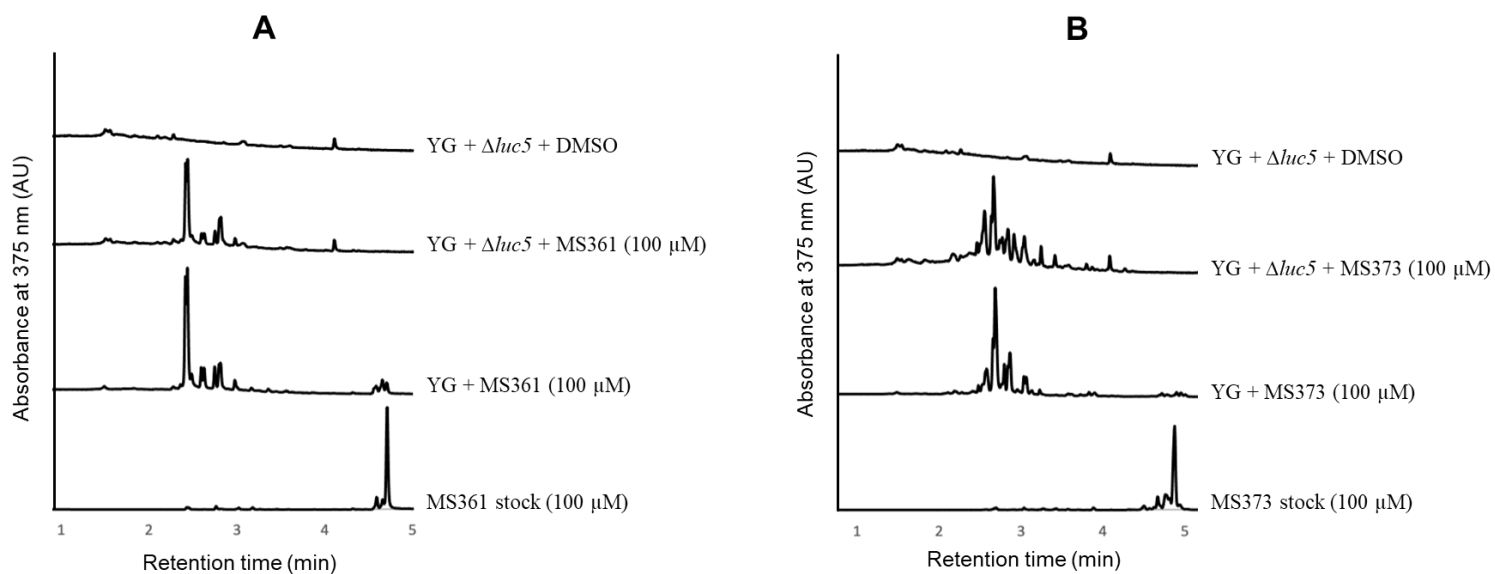**Fig. S98.** MSMS fragmentation of MW359 (prelucilactaene D)

**Fig. S99.** LC-MS analysis of ethanolic extract of PKS-NRPS knockout strain (Δ*luc5*) after feeding with:

**A.** Prelucilactaene B (MW361, **7**) and **B.** Prelucilactaene E (MW373, **8**). Fed compounds displayed significant

Instability in the production medium within the first 24 hours which prevent its conversion to the final products.
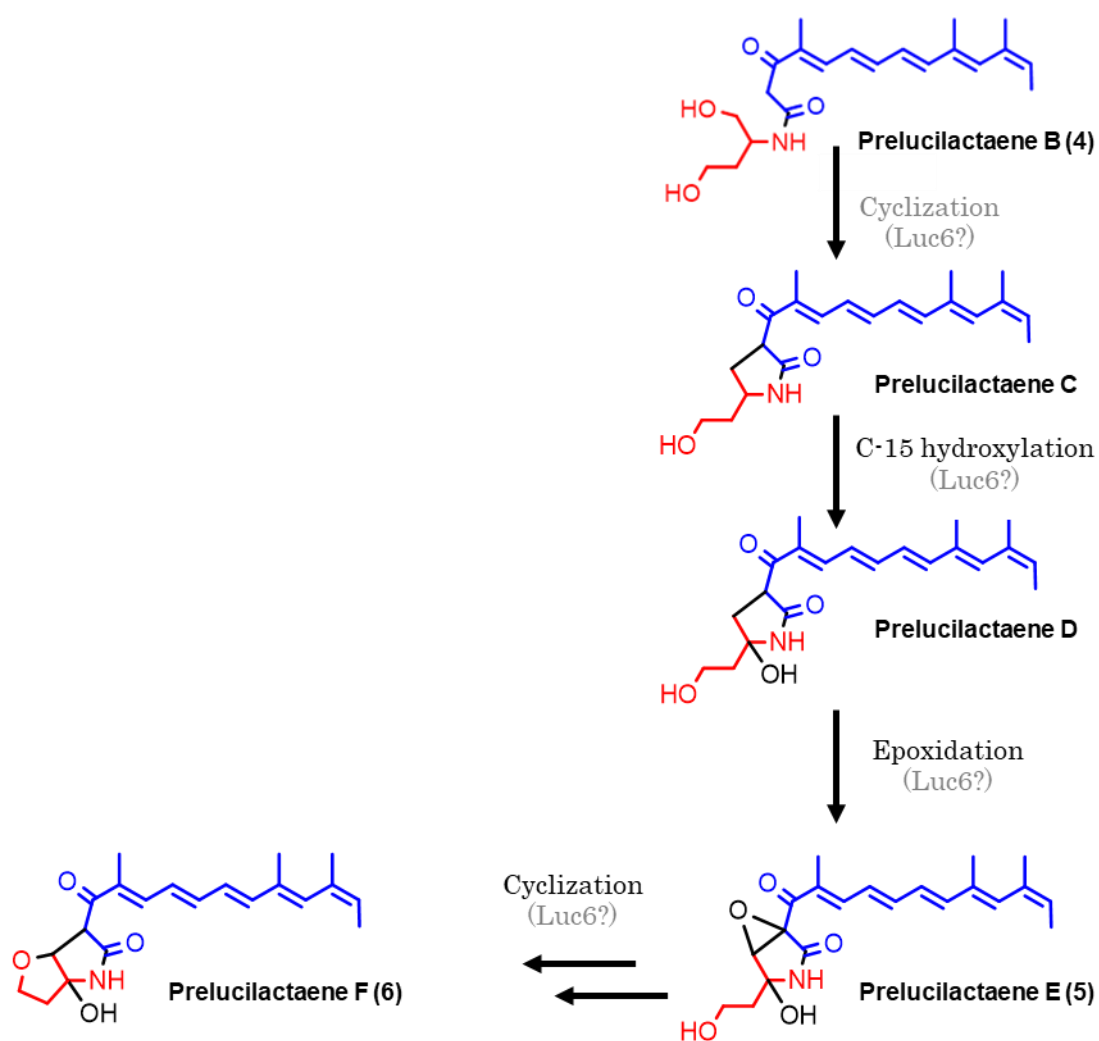
**Fig. S100.** Putative biosynthetic pathway of NG391 and lucilactaene.